CARLOTTA GIANNELLI

RATIONAL MOVING FRAMES ON POLYNOMIAL SPACE CURVES: THEORY AND APPLICATIONS

UNIVERSITÀ DEGLI STUDI DI FIRENZE
Dipartimento di Sistemi e Informatica
Dottorato di Ricerca in Informatica e Applicazioni
XXII Ciclo
Settore Disciplinare MAT/08

RATIONAL MOVING FRAMES ON POLYNOMIAL SPACE CURVES: THEORY AND APPLICATIONS

CARLOTTA GIANNELLI

Supervisors: *Rida T. Farouki* and *Alessandra Sestini*

PhD Coordinator: *Rocco De Nicola*

April, 2010

Carlotta Giannelli: *Rational moving frames on polynomial space curves: theory and applications,* Dottorato di Ricerca in Informatica e Applicazioni, © April, 2010

ABSTRACT

A moving frame along a space curve fixes a local coordinate system at any curve point which naturally identifies the orientation of an object moving along this trajectory. Frames that incorporate the unit tangent and unit polar vector as one component are known as *adapted* and *directed* curve frames, respectively. Rational representations are desirable for practical free–form design and its application to motion planning or swept surface constructions, on account of their compatibility with standard computer–aided design systems. In general, moving frames along polynomial or rational curves do not admit rational dependence on the curve parameter, and one can only achieve piecewise–rational frames approximation schemes.

The search for curves with rational adapted and directed frames is necessarily restricted to curves with rational unit tangent vector and unit polar vector, known as *Pythagorean–hodograph* (PH) and *Pythagorean* (P) curves, respectively. The first derivatives of PH curves and P curves exhibit a special Pythagorean structure in terms of their Cartesian components which can be effectively represented by use of two appropriate algebraic tools, namely the *Hopf map* and the *quaternion algebra*.

The focus of the thesis is on the identification, construction and applications of some remarkable new classes of polynomial space curves with associated rational moving frames of practical importance. Among all the different orthonormal frames that can be defined on a given space curve, the *Frenet frame* and the *rotation–minimizing frame* are of special interest in virtue of their distinctive geometric properties.

After introducing the basic theory related to moving adapted and directed frames on regular polynomial space curves, relations between the helicity condition, existence of rational Frenet frames, and a certain "double" Pythagorean structure are elucidated in terms of the quaternion and Hopf map representations. A categorization for the low–degrees of these curve types is developed, together with algorithms for their construction, and a selection of computed examples is included, to highlight their attractive features.

The existence of non–degenerate polynomial space curves with rational rotation–minimizing frames is then newly demonstrated. For spatial PH quintics and P quartics, sufficient and necessary constraints that characterize the existence of rational rotation–minimizing adapted and direct frames are derived, leading to an easily–implemented algorithm. Finally, in order to solve practical design problems using the different classes of polynomial space curves introduced, several methods for their geometric construction by the solution of interpolation problems are presented.

ACKNOWLEDGMENTS

I am deeply grateful to Dr. Alessandra Sestini for having followed and advised me with patient encouragement and continuous availability during the last three years. The time we spent working together allowed me to learn and make the most of my PhD experience.

I would like to thank Prof. Rida T. Farouki, for his kind and valuable guidance. Moreover, he gave me the opportunity to visit the Department of Mechanical and Aeronautical Engineering at the University of California, Davis, where the first structure of my thesis was planned.

I sincerely thank Prof. Carla Manni for all the precious comments and advice, that allowed me to see things from a different point of view.

Many thanks to the reviewers of the thesis, Prof. Bert Jüttler and Prof. Takis Sakkalis, for their detailed and constructive reports.

I would also like to thank the Coordinator of my PhD program, Prof. Rocco De Nicola, for his helpful suggestions, and Prof. Luigi Brugnano for all his theoretical and computational teachings over the years.

Special thanks go to all the friends I met in the Department of Systems and Computer Science at the University of Florence for the pleasant atmosphere which surrounded the working environment.

Finally, I would like to thank my family for their constant support, and Stefano, who is by my side every single day of my life.

PUBLICATIONS

The original results here presented have appeared previously in the following publications.

[P1] R. T. Farouki, C. Giannelli, C. Manni, and A. Sestini (2008), Identification of spatial PH quintic Hermite interpolants with near–optimal shape measures, *Computer Aided Geometric Design* **25**, 274–297.
[http://dx.doi.org/10.1016/j.cagd.2007.09.007]

[P2] R. T. Farouki, C. Giannelli, and A. Sestini (2009), Helical polynomial curves and double Pythagorean hodographs I. Quaternion and Hopf map representations, *Journal of Symbolic Computation* **44**, 161-179.
[http://dx.doi.org/10.1016/j.jsc.2008.07.004]

[P3] R. T. Farouki, C. Giannelli, and A. Sestini (2009), Helical polynomial curves and double Pythagorean hodographs II. Enumeration of low–degree curves, *Journal of Symbolic Computation* **44**, 307–332.
[http://dx.doi.org/10.1016/j.jsc.2008.07.003]

[P4] R. T. Farouki and C. Giannelli (2009), Spatial camera orientation control by rotation-minimizing directed frames, *Computer Animation and Virtual Worlds* **20**, 457–472.
[http://dx.doi.org/10.1002/cav.274]

[P5] R. T. Farouki, C. Giannelli, C. Manni, and A. Sestini (2009), Quintic space curves with rational rotation–minimizing frames, *Computer Aided Geometric Design* **26**, 580–592.
[http://dx.doi.org/10.1016/j.cagd.2009.01.005]

[P6] R. T. Farouki, C. Giannelli, and A. Sestini (2010), Geometric design using space curves with rational rotation–minimizing frames, (M. Daehlen et al., eds.) *Lecture Notes in Computer Science*, Vol. 5862, pp. 194–208, Springer.
[http://dx.doi.org/10.1007/978-3-642-11620-9_13]

CONTENTS

LIST OF FIGURES

LIST OF TABLES

ACRONYMS

DP Double Pythagorean

DPH Double Pythagorean–hodograph

ERF Euler–Rodrigues frame

FAF Frenet adapted frame

FDF Frenet directed frame

P Pythagorean

PH Pythagorean–hodograph

RMAF Rotation–minimizing adapted frame

RMDF Rotation–minimizing directed frame

RRMF Rational rotation–minimizing frame

INTRODUCTION

In applications such as computer animation, motion control, and swept surface constructions, it is often necessary to specify the variation of an orthonormal frame along a curved path, that describes the orientation of a rigid body as it traverses this path. In typical cases, one frame vector is prescribed *a priori* (e.g., the unit tangent vector to the path, or the unit polar vector from a fixed origin to each point of the path) and only one degree of freedom remains, associated with the orientation of the two frame vectors in the plane orthogonal to this prescribed vector at each curve point. Frames that incorporate the unit tangent and unit polar vector as one component are known as *adapted* and *directed* curve frames, respectively [28]. On account of its compatibility with standard computer–aided design system representations, a desirable property for practical free–form design and its application to motion planning or surface modeling is the *rational* dependence on the curve parameter. The focus of this thesis is on the identification, construction and applications of some remarkable new classes of polynomial space curves with associated rational moving frames of practical importance. Among all the different orthonormal frames that can be defined on a given space curve, the ones here considered are of special interest in virtue of their distinctive geometric properties.

The thesis is organized into four main parts which in turn contain several chapters. This structure can be briefly summarized as follows.

> PART I introduces the basic theory related to moving adapted and directed frames on a space curve;
>
> PART II shows how curves with rational frames can be defined through the identification of special classes of polynomial space curves satisfying the desired properties;
>
> PART III presents several methods for the geometric construction of the different classes of polynomial space curves introduced in PART II together with some examples of possible practical application;
>
> PART IV collects the appendices of the thesis which embrace a historical survey on previous and related works on curves with particular *Pythagorean* structures together with a short summary on the two commonly used models for their representation.

The following three sections briefly summarize the specific contents of the above mentioned parts.

REFERENCE FRAMES ALONG A 3D TRAJECTORY

The most commonly studied orthonormal frames on a space curve are the *adapted* ones, in which one frame vector is coincident with the curve unit tangent, and the other two vectors span the *normal plane* (orthogonal to the tangent vector) at each point. This is a natural choice in, for example, specifying the motion of an aircraft or spacecraft, in which a principal axis of the vehicle remains aligned with its trajectory, or in constructing a *swept surface* through the motion of a planar "profile curve" along a "sweep curve," such that the plane containing the profile curve always remains orthogonal to the sweep curve. The key ideas related to the theory of adapted frames on space curves are reviewed in Chapter 1.

The *Frenet adapted frame* defined by the curve intrinsic geometry is perhaps the most familiar example. However, an infinitude of adapted frames exists on any given space curve, due to the residual freedom associated with the orientation of the basis vectors that span the normal plane at each point and the Frenet frame may result a poor choice for motion planning or swept surface constructions, since it incurs "unnecessary" rotation of the basis vectors in the normal plane. The fact that the principal normal vector always points to the center of curvature often yields awkward–looking motions, or unreasonably "twisted" swept surfaces.

To address this problem, the construction of *rotation–minimizing adapted frames* (RMAFs) on space curves has recently been the subject of intensive study. The advantages of rotation–minimizing frames for construction of swept surfaces were first noted by Klok [62], who characterized them as solutions to certain differential equations. Guggenheimer [46] subsequently showed that solutions to these equations correspond to frame vectors in the normal plane with an angular orientation relative to the principal normal and binormal given (up to a constant) by the integral of the curve torsion with respect to arc length. This integral does not admit analytic reduction for the commonly–used polynomial and rational curves. Hence, several schemes have been proposed to approximate rotation–minimizing adapted frames on a given curve, or to approximate a given curve by simpler segments with known rotation–minimizing frames, see for example [36, 52, 55, 56, 104].

Instead of an adapted frame along a space curve, Chapter 2 introduces the notion of a *directed* frame along the curve. Whereas one vector of the adapted frame is determined by the curve tangent at each point, the direction from a fixed point in space (conventionally chosen as the origin) to each curve point determines one vector of the directed frame. To be more precise, a directed frame on a space curve is a varying orthonormal basis where one frame vector is coincident with the unit *polar* vector, and the other two frame vectors span the *image plane* orthogonal to this polar vector.

A special instance, the *Frenet directed frame*, is identified by analogy with the adapted–orthonormal frames on space curves. Specifically, the theory of the Frenet directed frame coincides with that of the Frenet adapted frame, applied to the *anti–hodograph* (i.e., indefinite integral) of the given curve, rather than the curve itself. This analogy motivates us to introduce the *polar curvature* and *polar torsion* of space curves.

As with the adapted frames, an infinitude of directed frames exists, and it is again desirable to identify the *rotation–minimizing directed frames* (RMDFs). In fact, the theories of RMAFs and RMDFs are intimately connected — the former theory carries over to the latter context if applied to the anti–hodograph of the given curve. RMDFs may offer a useful camera orientation control strategy as an alternative to the usual maintenance of vertical orientation and a key motivation for studying rotation–minimizing directed frames arises from the problem of specifying camera motion relative to a fixed object. The problem pertains to both a real "physical" camera used in the production of a movie or in a video inspection process as in the endoscopic surgery imaging, and a "virtual" camera in a simulated environment, as in the navigation of virtual scenarios and interactive computer games. It is presumed that a motion of the camera center along a space curve is prescribed, during which its optical axis must always point toward a stationary object located at the origin. This fixes the unit polar vector as one member of the orthonormal frame that specifies the camera orientation, but — as with adapted frames — a residual degree of freedom exists, associated with the basis vectors spanning the plane orthogonal to this polar vector. The choice of a rotation–minimizing directed frame yields a smooth, natural variation of perspective on the object fixed at the origin as the camera executes the prescribed path.

CURVES WITH DIFFERENT PYTHAGOREAN STRUCTURES

The scientific research has recently dedicated a very broad activity in the study and analysis of a particular class of polynomial curves endowed with a special structure, by virtue of which they are generally called *Pythagorean-hodograph* (PH) *curves* [24]. There is an intimate connection between PH curves — i.e., polynomial curves $\mathbf{r}(t) = (x(t), y(t), z(t))$ that satisfy

$$|\mathbf{r}'(t)|^2 \;=\; x'^2(t) + y'^2(t) + z'^2(t) \;=\; \sigma^2(t)$$

for some polynomial $\sigma(t)$ — and curves with rational adapted frames. Namely, since satisfaction of the above condition is necessary for a rational unit tangent, the search for curves with rational adapted frames may be restricted to PH curves.

The Pythagorean–hodograph structure ensures that PH space curves have the following distinguishing properties:

- a polynomial *arc–length* function;
- rational adapted frames;
- rational *offsets*, i.e., loci of points that maintain a fixed distance from the curve; to be more precise, both the offset (or parallel) curves to planar PH curves and the *pipe surfaces* based on spatial PH curves as spines admit rational parametrizations;
- *swept surfaces* whose spine curves are PH curves admit rational parametrization.

If these special algebraic properties motivated Farouki and Sakkalis to introduce the PH class of polynomial curves [42], the later research has shown that they are well–suited for applications to interpolation schemes and problems in computer–aided design and manufacturing (CAD/CAM). A brief overview of the existing literature on *planar* and *spatial* Pythagorean–hodograph curves is presented in Appendix A.

In Chapter 3 the PH condition is throughly discussed and analyzed in term of the complementary *quaternion* and *Hopf map* models of spatial PH curves, and their connections — including conversions between these two forms. A brief introduction to basic quaternion division algebra concepts is presented in Appendix B, while Appendix C discusses the Hopf fibration. Although the Hopf map model could provide a simpler perspective on the particular Pythagorean structure, the quaternion form has enjoyed more widespread use in practical algorithms for the construction and analysis of spatial PH curves, by virtue of the convenient and compact algorithmic forms it implies. A detailed analysis of the relationships between these two alternative PH curve representations, and of conversions between them, is therefore of essential importance.

The polynomial form of the parametric speed that characterize the PH class of space curve, beyond implying *exact* measurement of arc length which can be determined without numerical quadrature by a finite sequence of arithmetic operations on the curve coefficients, is necessary for a rational unit tangent and consequently for rational moving adapted frames. In general, however, both Frenet frames and RMAFs are not rational — even for PH curves. Choi and Han [10] observed that the spatial PH curves always admit a rational adapted frame, the so–called *Euler–Rodrigues frame* (ERF). Although the ERF does not have an intuitive geometric significance, and is dependent upon the chosen Cartesian coordinates, it has the advantage of being non–singular at inflection points. These facts have motivated recent interest in two special classes of PH curves — the *double Pythagorean–hodograph* (DPH) *curves* [4, 33, 32] which have rational Frenet adapted frames and the set of PH curves with rational RMAFs [10, 30, 47]. For brevity, we shall call the latter RRMF curves — bearing in mind that they are necessarily PH curves. DPH curves are intimately related to the

theory of *helical* polynomial curves [4, 37, 70]: it was shown in [4] that all helical polynomial curves must be DPH curves, although there exist non–helical DPH curves of degree 7 or more.

Chapters 4 and 5 present a comprehensive treatment of the theory of helical polynomial curves and double PH curves, with emphasis on the relationship between the quaternion and Hopf map representations, and the enumeration of all curve types (helical and non–helical) up to degree 7. The DPH curve categorization is developed using the Hopf map form and includes methods for their construction and a selection of computed examples which highlight the double PH curve attractive features. Nevertheless, although most of the theory developed on DPH curves has been couched primarily in terms of the Hopf map representation, it is easily translated into the language of the quaternion model. For helical curves, a separate constructive approach, based upon the inverse stereographic projection of rational line/circle descriptions in the complex plane, is used to classify all types up to degree 7. Criteria to distinguish between the helical and non–helical DPH curves, in the context of the general construction procedures, are also discussed.

Investigations of RRMF curves are even more recent. Choi and Han [10] studied conditions under which the ERF of a PH curve coincides with an RMAF, and showed that, for PH cubics, the ERF and Frenet adapted frame are equivalent; for PH quintics, the ERF can be rotation–minimizing only in the degenerate case of planar curves; and the simplest non–planar PH curves for which the ERF can be an RMAF are of degree 7. More recently, Han [47] presented an algebraic criterion characterizing RRMF curves of any (odd) degree, and showed that RRMF cubics are degenerate — i.e., they are either planar PH curves, or PH curves with non–primitive hodographs.

In Chapter 6, the existence of non–degenerate quintic RRMF curves is demonstrated through a simple constructive procedure, based on a detailed analysis of the algebraic condition for rationality of the RMAF on a PH curve in the Hopf map representation. This analysis furnishes a simple complex–arithmetic algorithm for the practical construction of RRMF quintics, and permits generalization to the study of higher–order RRMF curves [30]. A subsequent simpler characterization of RRMF quintics presented in [25] is also reported.

In the context of adapted frames, rational forms can be achieved only by choosing $\mathbf{r}(t)$ to be a (spatial) PH curve. A similar resolution is possible for directed frames but in terms of the coordinate components of the curve $\mathbf{r}(t) = (x(t), y(t), z(t))$ — rather than those of the hodograph, as for the PH curves. The RMDF was shown to be related to the Frenet directed frame, through an angular displacement function specified by the integral of the polar torsion. For the special family of *Pythagorean* (P) *curves* [28] — i.e., polynomial curves $\mathbf{r}(t) = (x(t), y(t), z(t))$ that satisfy

$$|\mathbf{r}(t)|^2 = x^2(t) + y^2(t) + z^2(t) = \rho^2(t)$$

for some polynomial $\rho(t)$, this integral admits a closed–form evaluation by the partial fraction expansion of a rational function. As suggested in Chapter 7, many of the ideas and methods used in the study of PH curves carry over to the investigation of P curves.

The analysis of the properties and construction of Pythagorean curves is motivated by studying the computation of rational directed frames, but much of the established theory for the PH curves can be adapted to the case of P curves. Similarly, the theory of double PH curves can be modified to define *double P curves* having rational Frenet directed frames and polar curvature and torsion functions. Also, the recent results on PH curves with rational RMAF may be reformulated in order to define the subset of P curves with associated rational RMDF.

GEOMETRIC DESIGN APPLICATIONS

In order to solve practical design problems using parametric polynomial curves, efficient methods for their geometric construction are required. Except in the simplest cases, the non–linear nature of curves which exhibit particular Pythagorean structures precludes a direct specification by Bézier/B–spline control polygons. Instead, solution of the first order Hermite interpolation problem is a standard approach to construction of planar or spatial PH curves satisfying prescribed geometrical constraints. This allows both effective control on the curve shape and computational benefits associated with the solution procedure.

The problem of Hermite interpolation by PH curves inherently admits a *multiplicity* of formal solutions, and the issue of selecting a "good" or "best" interpolant among the complete set of formal solutions must be addressed. For example, the construction of C^1 spatial PH quintic Hermite interpolants involves a *two–parameter family* of solutions [26, 99].

Some recent progress on the issue of identifying optimal choices for the two free parameters that arise in spatial PH quintic interpolants to given first–order Hermite data is reported in Chapter 8. It is shown that the arc length of the interpolants depends on only one of the parameters, and that four general helical PH quintic interpolants always exist, corresponding to extrema of the arc length. Moreover, three alternative selection criteria are proposed. As outlined by the reported examples they appear to be valid pragmatic selection schemes, in terms of their computational simplicity and near–optimal shape quality of the interpolants they yield [29].

Since spatial PH quintics must satisfy three scalar constraints in order to be RRMF curves, relaxing from C^1 to G^1 Hermite data results in a net loss of one residual degree of freedom — i.e., the quintic RRMF interpolants to spatial G^1 Hermite data comprise a *one–parameter family* of solutions. A method for computing quintic RRMF curves that interpolate spatial G^1 Hermite data is

presented in Chapter 9. The method involves one free angular parameter, that can strongly influence the curve shape [34].

Finally, the last chapter summarizes the main results of this thesis and identifies some problems worthy of further consideration.

Part I

MOVING FRAMES ON SPACE CURVES

1

ADAPTED FRAMES

An orthonormal basis for the Euclidean three–dimensional space $\mathbb{R}^3$ is *adapted* to a spatial curve if one of the three basis vector coincides with the curve tangent, while the other two vectors are perpendicular to the associated 3D trajectory. An adapted frame is then a local system of reference which moves along the curve path. In view of the freedom to choose the orientation of the two vectors that span the plane orthogonal to the curve tangent, there exists a *one–parameter family* of adapted moving frames associated to any spatial curve.

Among all adapted frames on a given space curve, two of them are of special importance in view of different geometric features:

- the *Frenet frame* [17, 65], which defines an orthonormal basis for $\mathbb{R}^3$ in terms of the local intrinsic geometry of the curve;
- the *rotation–minimizing frame* [5, 46, 62], which exhibits the least possible frame rotation along the curve.

The variation of the Frenet frame on a space curve is described by the *Frenet–Serret equations* in which the *curvature* and *torsion* functions appear. The distinctive feature of a rotation–minimizing adapted frame, instead, is that its angular velocity maintains a zero component along the curve tangent. This means that, at every point of the curve path, there is no instantaneous rotation of the normal–plane vectors and, consequently, the geometric property characterizing these frames is that the amount of frame rotation along the curve is minimized.

If explicit formulas in terms of the first two curve derivatives permit computation of the Frenet frame, the orientation of the rotation–minimizing frame vectors at any point of the trajectory must be calculated by solving an initial–value problem. Obviously, the solution of the corresponding differential equation depends on the specified *initial condition* and on the curve path between this starting value and the curve point. This means that the frame position at any arbitrary point along the curve cannot be computed explicitly and simpler methods to approximate the rotation–minimizing differential equations solution are strongly desirable.

The structure of this chapter is as follows. First, Section 1.1 and 1.2 briefly reviews some basic concepts on parametric space curves and the familiar theory of the Frenet adapted frame on a space curve, respectively. Then Section 1.3 introduces the rotation–minimizing definition and presents a constructive description to define rotation–minimizing adapted frames along a space curve as solution of a linear system of differential equations. Finally Section 1.4 shows

some examples of swept objects along a space curve whose orientation is defined by a moving adapted frame.

1.1 PARAMETRIC SPACE CURVE

1.1.1 *Preliminaries*

There exist two standard ways to represent polynomial space curves: *implicit* and *parametric* forms. Both representations are of importance for geometric modeling: the practical utility of each one depends on the specific task to execute.

Nevertheless, in the sphere of computer aided geometric design, curves and surfaces are generally represented by means of parametric equations. Their ease of use to adapt and satisfy specific needs facilitates computer modeling and visualization. The parametric representation of a polynomial space curve describes the set of points which belong to the corresponding geometric locus by means of three generating functions $x(t), y(t), z(t)$ of a parameter t. In particular, the two commonly used models are *Bézier* and *B–spline* curves, together with their rational generalization [18, 51]. Hence, indicating with I a closed non degenerate interval of the real line, polynomial space curves are typically defined as

$$\mathbf{r}(t) = (x(t), y(t), z(t)), \qquad t \in I, \tag{1.1.1}$$

where $x(t), y(t), z(t)$ are polynomials represented in the Bernstein basis in case of Bézier curves, or *spline* represented in the B–spline basis in case of B–spline curves. The values that the three generating functions assume as t changes in the specified parametric domain are simply the Cartesian coordinates of the corresponding points on the curve.

Indicating with $\mathbf{r}'(t) = (x'(t), y'(t), z'(t))$, the curve derivative — generally called *hodograph* — we say that the parametric representation $\mathbf{r}(t)$ is

- *differentiable* if $\mathbf{r}'(t)$ exists and it is continuous for all $t \in I$;
- *regular* if $\mathbf{r}'(t) \neq (0, 0, 0)$ for all $t \in I$.

The parametric representation of a curve is not unique: if $\tau(t)$ is an invertible function from the parametric domain I to another closed non degenerate real interval, we may consider $t(\tau)$ and $\mathbf{r}(t(\tau))$ is the curve rephrased in another parametric form (*reparameterization*). Moreover, if $\tau(t)$ is an increasing function over I, more precisely if $\tau(t)$ has continuous and positive derivative, the reparameterization is said to be *admissible*. Both the differentiability and regularity property characterize the parametric representation and not the curve itself. Hence, any given curve may admit several parametric representations, some of

which are regular and others not. By performing any admissible reparameterization $\mathbf{r}(t) = \mathbf{r}(t(\tau))$ the curve derivative

$$\mathbf{r}'(\tau) = \frac{d\mathbf{r}}{d\tau} = \frac{d\mathbf{r}}{dt}\frac{dt}{d\tau} = \mathbf{r}'(t)\frac{dt}{d\tau}$$

varies its modulus according to the considered parameterization, but its direction remains unchanged. The curve *tangent*

$$\mathbf{t}(t) = \frac{\mathbf{r}'(t)}{|\,\mathbf{r}'(t)\,|} \tag{1.1.2}$$

is then an intrinsic characteristic of the curve.

The *parametric speed* of the space curve (1.1.1) is the function

$$\sigma(t) = |\,\mathbf{r}'(t)\,| = \sqrt{x'^2(t) + y'^2(t) + z'^2(t)} \tag{1.1.3}$$

of the curve parameter t, which defines the rate of change ds/dt of the curve *arc length*

$$s(t) = \int_0^t \sigma(\xi)\,d\xi\,,$$

with the parameter t. In general, we are concerned with regular curves satisfying $\sigma(t) \neq 0$ for all t. Derivatives with respect to the curve arc length s and parameter t are related by

$$\frac{d}{ds} = \frac{1}{\sigma}\frac{d}{dt}\,. \tag{1.1.4}$$

Henceforth we use primes to denote derivatives with respect to the curve parameter t and dots for derivatives with respect to arc length s.

1.1.2 *The Bézier form*

When curves and surfaces must be automatically analyzed and manipulated, the ability to represent these geometric objects in appropriate form is essential. As already mentioned above, computer aided design systems commonly use parametric representations, typically in polynomial, rational or spline form in view of the accuracy and ease of calculations these forms inherently provide.

One of the polynomial bases that most facilitates both the understanding and modification of curves and surfaces geometric shape is the Bernstein basis which allows to define Bézier curves and surfaces [18, 51], a computational graphic representations standard. Besides important algebraic and geometric properties together with an optimal numerical stability [35], Bernstein basis polynomials,

$$b_k^n(t) = \binom{n}{k}(1-t)^{n-k}t^k\,, \tag{1.1.5}$$

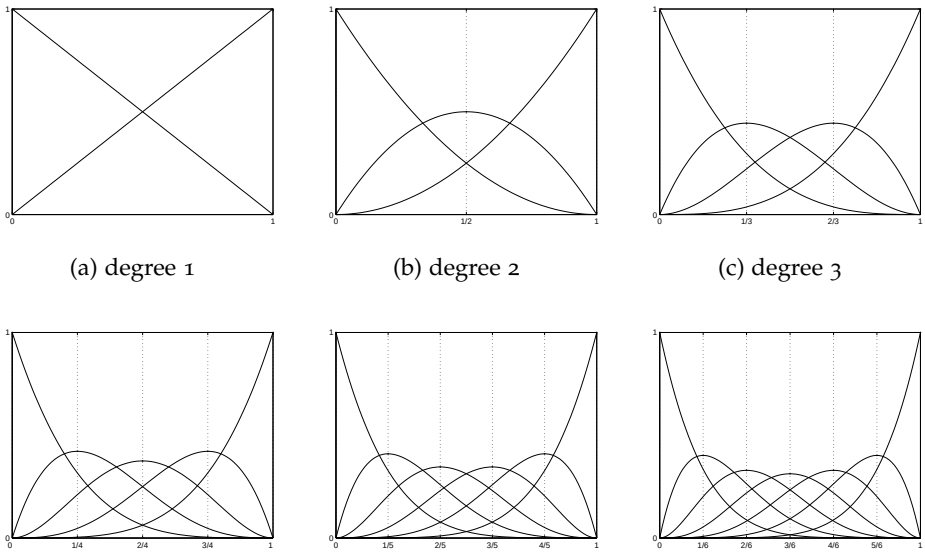

(a) degree 1 (b) degree 2 (c) degree 3

(d) degree 4 (e) degree 5 (f) degree 6

Figure 1.1: Bernstein polynomials on the interval $t \in [0, 1]$.

with $k = 0, \ldots, n$, and consequently Bézier curves,

$$\mathbf{r}(t) = \sum_{k=0}^{n} \mathbf{p}_k b_k^n(t), \tag{1.1.6}$$

with $t \in [0, 1]$, exhibit the remarkable advantage of associating a geometric meaning to the coefficients of vector polynomials expressed with respect to this basis. Figure 1.1 shows the low–degree Bernstein polynomials on the interval $[0, 1]$.

The $n + 1$ points $\mathbf{p}_0, \ldots, \mathbf{p}_n$ are the *control points* of the degree–n Bézier curve (1.1.6). In order to satisfy both functional and aesthetic requirements, by modifying the piecewise linear function which join the curve control points — called *control polygon* — we can influence the curve geometry. Figure 1.2 shows some examples of spatial Bézier curves and their control polygons. The following properties are satisfied: end–point and end–point tangent interpolation, pseudo–local control, variation diminishing, convex hull, symmetry, linear precision and invariance under affine transformations. All these particular features contribute to locate the practical soundness of the Bézier model [41].

Even if Bézier curves are an effective tool in geometric design contexts, when elaborate geometric shapes have to be modeled, curves of higher degrees are needed. In order to avoid this, we may represent the original curve using an appropriate joint of several polynomial curves of lower degree, namely we may use spline curves. A comprehensive treatment of Bézier, B–spline and related

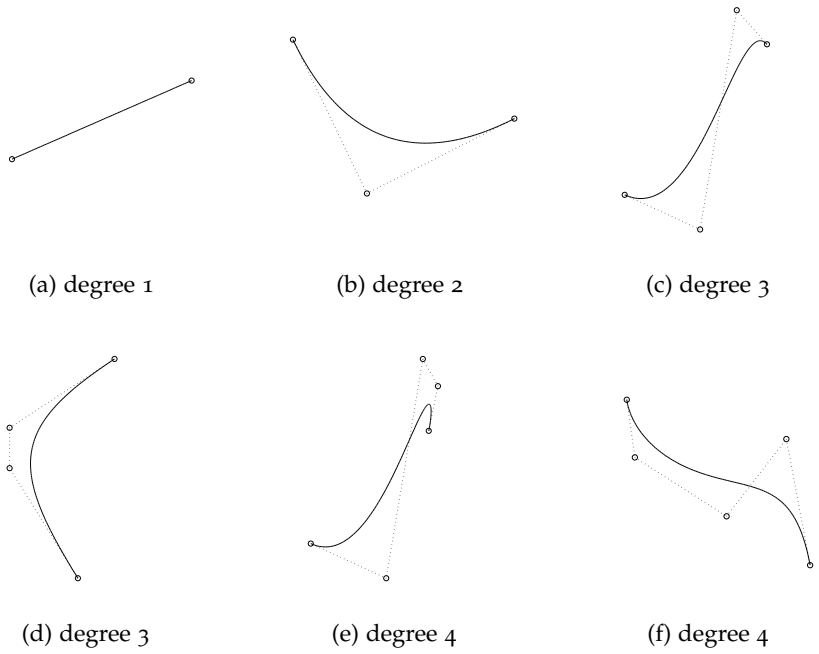

(a) degree 1 (b) degree 2 (c) degree 3

(d) degree 3 (e) degree 4 (f) degree 4

Figure 1.2: Examples of spatial Bézier curves of different degrees on the interval $t \in [0, 1]$ with their control polygon.

spline techniques may be found in [18] and [51]. Without loss of generality, the analysis presented in Part II are based on the Bézier model. Its application to spline–like approaches is addressed in Part III.

1.2 THE FRENET ADAPTED FRAME

An adapted frame on a regular parametric space curve $\mathbf{r}(t)$ is an orthonormal basis for $\mathbb{R}^3$ in which the curve tangent is chosen as one of the three frame vectors and the other two vectors span the plane orthogonal to the curve at each point. A familiar adapted frame on a space curve is the *Frenet frame*, defined [17, 65] by

$$\mathbf{t} = \frac{\mathbf{r}'}{|\mathbf{r}'|}, \qquad \mathbf{n} = \frac{\mathbf{r}' \times \mathbf{r}''}{|\mathbf{r}' \times \mathbf{r}''|} \times \mathbf{t}, \qquad \mathbf{b} = \frac{\mathbf{r}' \times \mathbf{r}''}{|\mathbf{r}' \times \mathbf{r}''|}. \tag{1.2.1}$$

Henceforth we adopt the practice of calling (1.2.1) the *Frenet adapted frame*, since in Section 2.1 we introduce an analogous type of frame called the *Frenet directed frame*.

At each point, the principal normal $\mathbf{n}$ points toward the *center of curvature*, while the binormal $\mathbf{b} = \mathbf{t} \times \mathbf{n}$ complements $\mathbf{t}$ and $\mathbf{n}$ so that $(\mathbf{t}, \mathbf{n}, \mathbf{b})$ comprise a right–handed frame. The Frenet adapted frame orientation is thus determined

FRENET–SERRET EQUATIONS	CURVATURE	TORSION
$\dot{\mathbf{t}} = \kappa\,\mathbf{n}$	$\kappa = \dot{\mathbf{t}} \cdot \mathbf{n}$	$\tau = \dot{\mathbf{n}} \cdot \mathbf{b}$
$\dot{\mathbf{n}} = -\kappa\,\mathbf{t} + \tau\,\mathbf{b}$	$\kappa = -\dot{\mathbf{n}} \cdot \mathbf{t}$	$\tau = -\dot{\mathbf{b}} \cdot \mathbf{n}$
$\dot{\mathbf{b}} = -\tau\,\mathbf{n}$	$\kappa = \lvert\, \dot{\mathbf{t}} \times \mathbf{t} \rvert$	$\tau = \det(\mathbf{t}\ \mathbf{n}\ \dot{\mathbf{n}})$
	$\kappa = \lvert\, \dot{\mathbf{n}} \times \mathbf{n} \rvert$ if $\tau = 0$	$\tau = \frac{1}{\kappa^2} \det(\mathbf{t}\ \dot{\mathbf{t}}\ \ddot{\mathbf{t}})$

Table 1.1: Frenet–Serret equations and corresponding curvature and torsion with respect to the curve arc length.

by the *intrinsic curve geometry*. The three mutually perpendicular planes spanned by the vector pairs $(\mathbf{n}, \mathbf{b})$, $(\mathbf{t}, \mathbf{n})$, and $(\mathbf{b}, \mathbf{t})$ at each point of a curve $\mathbf{r}(t)$ are known as the *normal*, *osculating*, and *rectifying* planes.

The normal plane is orthogonal to the curve tangent $\mathbf{t}$ — it "cuts the curve orthogonally" at each point $\mathbf{r}(t)$. The osculating plane exhibits *second–order contact* with the curve — it is the plane that "most nearly contains the curve" in some neighborhood of each point. Finally, the set of rectifying planes to a space curve envelope a ruled surface, known as the *rectifying developable* of that curve. A developable surface, regarded as a thin material sheet, may be "flattened" onto a plane without stretching or compressing the material — the space curve embedded in the rectifying developable is "rectified" by this process into a *straight line* of exactly the same total length.

In terms of derivatives with respect to the curve arc length s, the *Frenet–Serret equations* [17, 65],

$$\dot{\mathbf{t}} = \kappa\,\mathbf{n}\,, \qquad \dot{\mathbf{n}} = -\kappa\,\mathbf{t} + \tau\,\mathbf{b}\,, \qquad \dot{\mathbf{b}} = -\tau\,\mathbf{n}\,, \tag{1.2.2}$$

give expressions for tangent, normal and binormal derivatives — i.e., the derivatives of (1.2.1) — in terms of themselves and of *curvature* and *torsion* functions. Starting from these equations describing the variation of the Frenet adapted frame along the cure $\mathbf{r}(t)$, explicit formulas for curvature and torsion can be derived as shown in Table 1.1.

In terms of derivatives with respect to the curve parameter t, equations (1.2.2) can be expressed in matrix form as

$$\begin{bmatrix} \mathbf{t}' \\ \mathbf{n}' \\ \mathbf{b}' \end{bmatrix} = \sigma \begin{bmatrix} 0 & \kappa & 0 \\ -\kappa & 0 & \tau \\ 0 & -\tau & 0 \end{bmatrix} \begin{bmatrix} \mathbf{t} \\ \mathbf{n} \\ \mathbf{b} \end{bmatrix}, \tag{1.2.3}$$

where the parametric speed $\sigma(t)$ is defined by (1.1.3), while the curvature and torsion functions, defined now by

$$\kappa = \frac{\lvert\, \mathbf{r}' \times \mathbf{r}'' \rvert}{\lvert\, \mathbf{r}' \rvert^3} \qquad \text{and} \qquad \tau = \frac{(\mathbf{r}' \times \mathbf{r}'') \cdot \mathbf{r}'''}{\lvert\, \mathbf{r}' \times \mathbf{r}'' \rvert^2}\,, \tag{1.2.4}$$

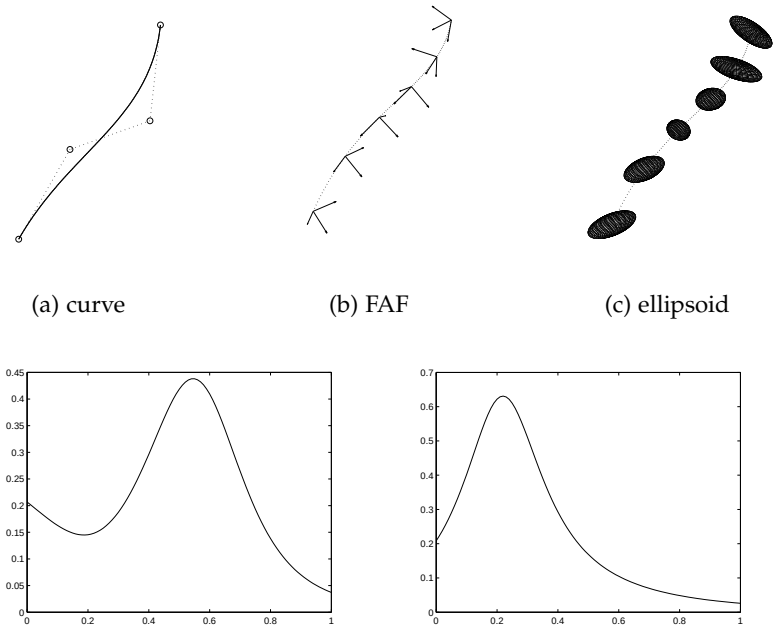

(a) curve (b) FAF (c) ellipsoid

(d) curvature (e) torsion

Figure 1.3: A cubic Bézier curve used to specify a trajectory for the spatial motion of an ellipsoid whose orientations are defined by the Frenet adapted frame (FAF). Also shown are the curvature and torsion functions.

describe the variation of the frame vectors (1.2.1) along $\mathbf{r}(t)$. More precisely, if the deviation of a curve from its tangent is evaluated by the curvature κ, the torsion τ measures the curve deviation from the osculating plane (see Figure 1.3).

In order to describe the angular velocity of the frame $(\mathbf{t}, \mathbf{n}, \mathbf{b})$ as a whole, we introduce [65] the *Darboux vector*

$$\mathbf{d} = \kappa \mathbf{b} + \tau \mathbf{t}, \tag{1.2.5}$$

in terms of which the relations (1.2.2) can be written as

$$\dot{\mathbf{t}} = \mathbf{d} \times \mathbf{t}, \qquad \dot{\mathbf{n}} = \mathbf{d} \times \mathbf{n}, \qquad \dot{\mathbf{b}} = \mathbf{d} \times \mathbf{b}. \tag{1.2.6}$$

Hence, the rate of change of the frame $(\mathbf{t}, \mathbf{n}, \mathbf{b})$ with s can be characterized as an instantaneous rotation about the vector $\mathbf{d}$, with angular velocity equal to the *total curvature* specified by

$$\omega = |\mathbf{d}| = \sqrt{\kappa^2 + \tau^2}.$$

It should be noted that, at points where $\kappa = 0$, the principal normal $\mathbf{n}$ and binormal $\mathbf{b}$ specified by (1.2.1) are indeterminate. Such points are called the

inflections of a space curve, and **n** and **b** ordinarily suffer sudden reversals upon traversing them. For a space curve with $\sigma(t) \neq 0$ for all t, the curvature can vanish only if (i) $\mathbf{r}''(t) = (0,0,0)$, or (ii) $\mathbf{r}'(t)$ and $\mathbf{r}''(t)$ are parallel.

Consider a regular and arc–length parameterized curve $\mathbf{r}(s)$, $s \in [0, L]$. From (1.1.4) we have

$$\dot{\mathbf{r}} = \frac{d\mathbf{r}}{ds} = \frac{1}{\sigma}\frac{d\mathbf{r}}{dt} = \frac{\mathbf{r}'}{|\mathbf{r}'|} = \mathbf{t},$$

so the curve first derivative is already the unit vector which defines the curve tangent, i.e. $|\dot{\mathbf{r}}(s)| = 1$ and, consequently $\dot{\mathbf{r}}(s) \cdot \dot{\mathbf{r}}(s) = 1$. By differentiating this scalar product we obtain $\dot{\mathbf{r}}(s) \cdot \ddot{\mathbf{r}}(s) = 0$, for all $s \in [0, L]$ which indicates the mutual orthogonality of the two vectors. Hence, the curvature κ defined in (1.2.4) when expressed with respect to the arc length parameter s, is simply equal to $|\ddot{\mathbf{r}}(s)|$, and the Frenet adapted frame (1.2.1) reduces to

$$\mathbf{t} = \dot{\mathbf{r}}, \qquad \mathbf{n} = \frac{\ddot{\mathbf{r}}}{\kappa}, \qquad \mathbf{b} = \frac{\dot{\mathbf{r}} \times \ddot{\mathbf{r}}}{\kappa}.$$

1.3 ROTATION–MINIMIZING ADAPTED FRAMES

The Darboux vector (1.2.5) gives the instantaneous angular velocity of the Frenet adapted frame on a space curve. From (1.2.2) we observe that **t** changes at rate κ in the direction of **n**. The change of **n** has two components: rate $-\kappa$ in the direction of **t**, and rate τ in the direction of **b**. Finally, **b** changes at rate $-\tau$ in the direction of **n**. Now changes in the direction of **t** are inevitable if we require an adapted frame, that incorporates **t** as one basis vector. However, the change of **n** in the direction of **b**, and of **b** in the direction of **n**, correspond to a rotation of these vectors within the normal plane, a consequence of the fact that **n** always points toward the center of curvature.

The variation of the frame $(\mathbf{f}_1, \mathbf{f}_2, \mathbf{f}_3)$ with $\mathbf{f}_1 = \mathbf{t}$, along the curve $\mathbf{r}(t)$ may be specified by its angular velocity $\boldsymbol{\omega}(t)$ as

$$\mathbf{f}_1' = \sigma\,\boldsymbol{\omega} \times \mathbf{f}_1, \qquad \mathbf{f}_2' = \sigma\,\boldsymbol{\omega} \times \mathbf{f}_2, \qquad \mathbf{f}_3' = \sigma\,\boldsymbol{\omega} \times \mathbf{f}_3, \tag{1.3.1}$$

or simply as

$$\dot{\mathbf{f}}_1 = \boldsymbol{\omega} \times \mathbf{f}_1, \qquad \dot{\mathbf{f}}_2 = \boldsymbol{\omega} \times \mathbf{f}_2, \qquad \dot{\mathbf{f}}_3 = \boldsymbol{\omega} \times \mathbf{f}_3, \tag{1.3.2}$$

if the curve is arc–length parameterized. The magnitude and direction of $\boldsymbol{\omega}$ specify the instantaneous angular speed $\omega = |\boldsymbol{\omega}|$ and rotation axis $\mathbf{a} = \boldsymbol{\omega}/|\boldsymbol{\omega}|$ of the frame vectors $(\mathbf{f}_1, \mathbf{f}_2, \mathbf{f}_3)$. Since $(\mathbf{f}_1, \mathbf{f}_2, \mathbf{f}_3)$ constitute a orthonormal basis for $\mathbb{R}^3$ we can write

$$\boldsymbol{\omega} = \omega_1 \mathbf{f}_1 + \omega_2 \mathbf{f}_2 + \omega_3 \mathbf{f}_3, \tag{1.3.3}$$

where the components of $\boldsymbol{\omega}$ are given by

$$\omega_1 = \mathbf{f}_3 \cdot \mathbf{f}_2' = -\mathbf{f}_2 \cdot \mathbf{f}_3', \quad \omega_2 = \mathbf{f}_1 \cdot \mathbf{f}_3' = -\mathbf{f}_3 \cdot \mathbf{f}_1', \quad \omega_3 = \mathbf{f}_2 \cdot \mathbf{f}_1' = -\mathbf{f}_1 \cdot \mathbf{f}_2'.$$

From (1.2.6) for the Frenet frame, we have $(\mathbf{f}_2, \mathbf{f}_3) = (\mathbf{n}, \mathbf{b})$ and $\boldsymbol{\omega} = \mathbf{d}$, namely

$$\omega_1 = \tau, \qquad \omega_2 = 0, \qquad \omega_3 = \kappa.$$

The necessary and sufficient condition for the frame to be rotation–minimizing is that $\boldsymbol{\omega}$ maintains a zero component ω_1 along $\mathbf{f}_1 = \mathbf{t}$, namely

$$\mathbf{f}_3 \cdot \mathbf{f}_2' = -\mathbf{f}_2 \cdot \mathbf{f}_3' = 0. \tag{1.3.4}$$

Hence, a rotation–minimizing adapted frame (RMAF) — indicated by the triple $(\mathbf{a}_1, \mathbf{a}_2, \mathbf{a}_3)$ with $\mathbf{a}_1 = \mathbf{t}$ — is characterized by the fact that its angular velocity vector $\boldsymbol{\omega}$ omits the component $\tau\,\mathbf{t}$ from the Darboux vector (1.2.5) and is thus simply $\boldsymbol{\omega} = \kappa\,\mathbf{b}$, i.e., $\omega_1 = \omega_2 = 0$ and $\omega_3 = \kappa$. Consequently, avoiding instantaneous rotation of the normal–plane vectors $\mathbf{a}_2$ and $\mathbf{a}_3$ about $\mathbf{a}_1$, it exhibits the least possible magnitude $\omega = \kappa$ of the frame angular velocity (see Figure 1.4). Analogously to the Frenet–Serret equations (1.2.2), the variation of the RMAF along the curve may be specified as

$$\dot{\mathbf{a}}_1 = \kappa\,\mathbf{n}, \qquad \dot{\mathbf{a}}_2 = \kappa\,\mathbf{b} \times \mathbf{a}_2, \qquad \dot{\mathbf{a}}_3 = \kappa\,\mathbf{b} \times \mathbf{a}_3,$$

with an instantaneous rotation axis equal to the bi–normal vector $\mathbf{b}$. Figure 1.5 shows the variation of the rotation–minimizing adapted frame along the example curve of Figure 1.3.

The basis vectors $(\mathbf{a}_2, \mathbf{a}_3)$ can be obtained from $(\mathbf{n}, \mathbf{b})$ by a rotation in the normal plane

$$\begin{bmatrix} \mathbf{a}_2 \\ \mathbf{a}_3 \end{bmatrix} = \begin{bmatrix} \cos\psi & \sin\psi \\ -\sin\psi & \cos\psi \end{bmatrix} \begin{bmatrix} \mathbf{n} \\ \mathbf{b} \end{bmatrix}, \tag{1.3.5}$$

defined by an appropriate angle function $\psi(t)$.

Klok [62] showed that the basis vectors $(\mathbf{a}_2, \mathbf{a}_3)$ of a rotation–minimizing adapted frame must satisfy the differential equations

$$\mathbf{a}_k'(t) = -\frac{\mathbf{r}''(t) \cdot \mathbf{a}_k(t)}{|\,\mathbf{r}'(t)\,|^2}\,\mathbf{r}'(t), \quad k = 2, 3, \tag{1.3.6}$$

which embrace the original definition given by Bishop [5] stating that both $\mathbf{a}_2'$ and $\mathbf{a}_3'$ have to be *parallel* to the curve tangent. Since the RMAF is of fundamental importance for the analysis of the next chapters, we briefly review how to derive (1.3.6) from the rotation–minimizing condition (1.3.4).

Consider two non–parallel planes whose common line of intersection is, without loss of generality, along $\mathbf{i}$. In particular, let π_0 and π_1 be the planes

FRENET ADAPTED FRAME	ROTATION–MINIMIZING ADAPTED FRAME
$\boldsymbol{\omega}_{FAF} = \kappa\,\mathbf{b} + \tau\,\mathbf{t}$	$\boldsymbol{\omega}_{RMAF} = \kappa\,\mathbf{b}$
$\omega_{FAF} = \sqrt{\kappa^2 + \tau^2}$	$\omega_{RMAF} = \kappa$

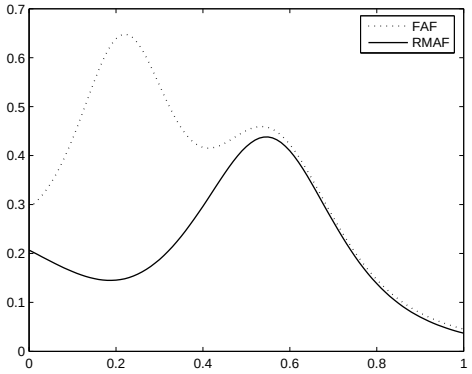

Figure 1.4: Comparison of the instantaneous angular speed $\omega = |\boldsymbol{\omega}|$ for the Frenet adapted Frame (FAF) and the rotation–minimizing adapted frame (RMAF) along the Bézier cubic shown in Figure 1.3.

spanned by the vector pairs $(\mathbf{i}, \mathbf{w})$ and $(\mathbf{i}, \mathbf{j})$, respectively, with $\mathbf{i} \cdot \mathbf{w} = 0$, $\mathbf{j} \cdot \mathbf{w} = \cos\phi$, and $|\mathbf{w}| = 1$. By indicating with S^2 the unit "2–sphere" (see Appendix C), we define the transformation $T : S^2 \cap \pi_0 \to S^2 \cap \pi_1$

$$T(\mathbf{u}) \;=\; \sqrt{1-u^2}\,\mathbf{i} + u\,\mathbf{j}\,, \tag{1.3.7}$$

which maps every normalized vector $\mathbf{u} = \sqrt{1-u^2}\,\mathbf{i} + u\,\mathbf{w}$ of π_0 into the unit vector $T(\mathbf{u})$ on π_1 so that all the vector differences $T(\mathbf{u}) - \mathbf{u}$ are mutually parallel, namely $T(\mathbf{u}) - \mathbf{u} = u(\mathbf{j} - \mathbf{w})$. Since $T(\mathbf{w}) = \mathbf{j}$, we have

$$T(\mathbf{u}) - \mathbf{u} \;=\; u\,(T(\mathbf{w}) - \mathbf{w})\;, \tag{1.3.8}$$

where $u = \mathbf{u} \cdot \mathbf{w} = \cos\theta$, being θ is the angle between $\mathbf{u}$ and $\mathbf{w}$.

Remark 1.1. For any two unit vectors $\mathbf{u} = \sqrt{1-u^2}\,\mathbf{i} + u\,\mathbf{w}$ and $\mathbf{v} = \sqrt{1-v^2}\,\mathbf{i} + v\,\mathbf{w}$ which lie on π_0, we have

$$\mathbf{u} \cdot \mathbf{v} \;=\; \sqrt{(1-u^2)(1-v^2)} + uv \;=\; T(\mathbf{u}) \cdot T(\mathbf{v})\,.$$

In view of the above observations, by explicitly differentiating the equations for $\mathbf{a}_2$ and $\mathbf{a}_3$, the following theorem proves relations (1.3.6).

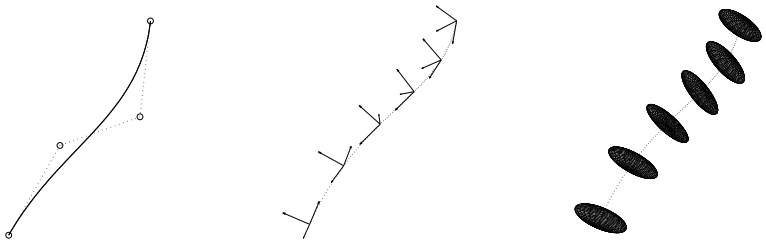

(a) curve (b) RMAF (c) ellipsoid

Figure 1.5: The cubic Bézier curve of Figure 1.3 used to specify a trajectory for the spatial motion of an ellipsoid whose orientations are defined by the rotation–minimizing adapted frame (RMAF).

Theorem 1.1. *An adapted moving frame* $(\mathbf{a}_1(t), \mathbf{a}_2(t), \mathbf{a}_3(t))$ *with* $\mathbf{a}_1 = \mathbf{t}$ *on a regular space curve* $\mathbf{r}(t)$ *is rotation–minimizing if and only if* $\mathbf{a}_2(t)$ *and* $\mathbf{a}_3(t)$ *satisfy the differential equations*

$$\mathbf{a}_2'(t) = -\frac{\mathbf{r}''(t)\cdot\mathbf{a}_2(t)}{|\,\mathbf{r}'(t)\,|^2}\,\mathbf{r}'(t)\,, \qquad \mathbf{a}_3'(t) = -\frac{\mathbf{r}''(t)\cdot\mathbf{a}_3(t)}{|\,\mathbf{r}'(t)\,|^2}\,\mathbf{r}'(t)\,, \tag{1.3.9}$$

with a unique solution for any starting values $\mathbf{a}_2(0) = \mathbf{a}_2^*$, $\mathbf{a}_3(0) = \mathbf{a}_3^*$.

Proof : Without loss of generality, let $\mathbf{r}(s)$ be an arc–length parameterized curve in the parametric domain $[0, L]$ and define an orthonormal adapted frame $(\mathbf{a}_1(s), \mathbf{a}_2(s), \mathbf{a}_3(s))$ with $\mathbf{a}_1 = \mathbf{t}$ along $\mathbf{r}(s)$ with initial orientation equal to

$$\mathbf{a}_1(0) = \mathbf{a}_1^*\,, \qquad \mathbf{a}_2(0) = \mathbf{a}_2^*\,, \qquad \mathbf{a}_3(0) = \mathbf{a}_3^*\,.$$

We seek a frame that minimizes the rotation of the two basis vectors $\mathbf{a}_2$, $\mathbf{a}_3$ that span the normal plane as s varies from 0 to L. Let $\Gamma(s)$ be the plane through $\mathbf{r}(s)$ perpendicular to $\mathbf{r}'(s)$, $\mathbf{u}(s)$ any unit vector which lies on $\Gamma(s)$, $\mathbf{n}(s)$ and $\mathbf{b}(s)$ the normal and bi–normal vectors at $\mathbf{r}(s)$. For a small parameter increment Δs, since $\dot{\mathbf{t}} = \kappa\mathbf{n}$, the first order Taylor approximation to $\mathbf{t}$ is $\mathbf{t}(s+\Delta s) \approx \mathbf{t}(s) + \Delta s\kappa(s)\mathbf{n}(s)$. Then, also $\mathbf{t}(s+\Delta s)$ is perpendicular to $\mathbf{b}(s)$, and the axis of rotation $\boldsymbol{\omega}$ to move $\Gamma(s)$ into $\Gamma(s+\Delta s)$ is parallel to $\mathbf{b}(s)$, namely

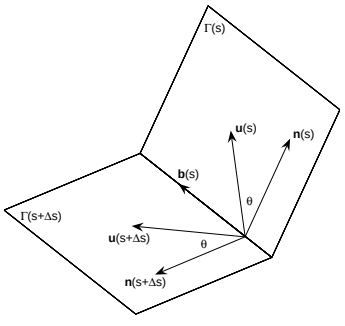

Figure 1.6: Illustration of the rotation–minimizing angle.

$\boldsymbol{\omega}(s) = \omega(s)\mathbf{b}(s)$. The unit vector $\mathbf{n}(s+\Delta s)$ on $\Gamma(s+\Delta s)$ which defines the minimum angle with $\mathbf{n}(s)$ has to be orthogonal both to $\mathbf{b}(s)$ and $\mathbf{t}(s+\Delta s)$. Being $\dot{\mathbf{n}} = \boldsymbol{\omega}\times\mathbf{n} = -\omega\mathbf{t}$, we have $\mathbf{n}(s+\Delta s) \approx \mathbf{n}(s) + \Delta s\dot{\mathbf{n}}(s) = \mathbf{n}(s) - \Delta s\omega(s)\mathbf{t}(s)$, and, consequently, unless terms of greater order, $\mathbf{b}(s)\cdot\mathbf{n}(s+\Delta s) = 0$ while the scalar product $\mathbf{t}(s+\Delta s)\cdot\mathbf{n}(s+\Delta s) \approx [-\omega(s)+\kappa(s)]\Delta s$ is zero if and only if $\omega(s) = \kappa(s)$. Thus $\boldsymbol{\omega}(s) = \kappa(s)\mathbf{b}(s)$, and

$$\dot{\mathbf{n}}(s) = \boldsymbol{\omega}(s)\times\mathbf{n}(s) = [\kappa(s)\,\mathbf{b}(s)]\times\mathbf{n}(s) = -\kappa(s)\,\mathbf{t}(s)$$

or approximately,

$$\mathbf{n}(s+\Delta s) - \mathbf{n}(s) \approx -\Delta s\,\kappa(s)\,\mathbf{t}(s)\,. \tag{1.3.10}$$

The unit vector $\mathbf{u}(s+\Delta s) \in \Gamma(s+\Delta s)$ obtained through (1.3.7) verifies (1.3.8), i.e.,

$$\mathbf{u}(s+\Delta s) - \mathbf{u}(s) = \mathbf{n}(s)\cdot\mathbf{u}(s)\,[\,\mathbf{n}(s+\Delta s) - \mathbf{n}(s)\,]$$

where $\cos(\theta) = \mathbf{n}\cdot\mathbf{u}$ (see Figure 1.6). By (1.3.10), the above equation reduces to

$$\mathbf{u}(s+\Delta s) - \mathbf{u}(s) = -\Delta s\,\kappa(s)\,[\,\mathbf{n}(s)\cdot\mathbf{u}(s)\,]\,\mathbf{t}(s)\,, \tag{1.3.11}$$

and, since $\mathbf{n}(s) = \ddot{\mathbf{r}}(s)/\kappa(s)$, we obtain $\mathbf{u}(s+\Delta s) - \mathbf{u}(s) = -\Delta s\,[\,\ddot{\mathbf{r}}(s)\cdot\mathbf{u}(s)\,]\mathbf{t}(s)$, which passing to the limit finally results in

$$\dot{\mathbf{u}}(s) = -[\,\ddot{\mathbf{r}}(s)\cdot\mathbf{u}(s)\,]\,\dot{\mathbf{r}}(s)\,.$$

The above equation is satisfied by any unit vector orthogonal to $\dot{\mathbf{r}}(s)$ exhibiting the minimal possible rotation in order to preserve the orthogonality to $\dot{\mathbf{r}}(s)$, namely by both $\mathbf{a}_2(s)$ and $\mathbf{a}_3(s)$.

If we relax the arc–length parameterization hypothesis, equation (1.3.10) becomes

$$\mathbf{n}(t+\Delta t) - \mathbf{n}(t) \approx -\Delta t\,\sigma(t)\kappa(t)\,\mathbf{t}(t) = -\Delta t\,\kappa(t)\,\mathbf{r}'(t)$$

and consequently (1.3.11) reduces to

$$\mathbf{u}(t+\Delta t) - \mathbf{u}(t) = -\Delta t\,\kappa(t)\,[\,\mathbf{n}(t)\cdot\mathbf{u}(t)\,]\mathbf{r}'(t)\,. \tag{1.3.12}$$

In this case, remembering that $\boldsymbol{\omega} = \kappa\mathbf{b}$, the derivative of $\mathbf{t} = \mathbf{r}'/\sigma$ has to be equal via (1.3.1) to $\sigma\kappa\mathbf{n}$, namely $\kappa\mathbf{n} = (\sigma\mathbf{r}'' - \sigma'\mathbf{r}')/\sigma^3$. By substituting this value into (1.3.12) we obtain

$$\mathbf{u}(t+\Delta t) - \mathbf{u}(t) = -\Delta t\,\left[\frac{\mathbf{r}''(t)\cdot\mathbf{u}(t)}{\sigma^2(t)}\right]\,\mathbf{r}'(t)\,, \tag{1.3.13}$$

which holds for any vector in the normal plane which moves by means of the least possible rotation remaining orthogonal to $\mathbf{r}'(t)$ — again, by both $\mathbf{a}_2(t)$ and

$\mathbf{a}_3(t)$. Turning to the limit (1.3.13) finally results in the two differential equations in (1.3.9). ∎

For any admissible initial condition $(\mathbf{a}_1^*, \mathbf{a}_2^*, \mathbf{a}_3^*)$, the corresponding RMAF is given by $(\mathbf{a}_1(t), \mathbf{a}_2(t), \mathbf{a}_3(t))$ with $\mathbf{a}_1 = \mathbf{t}$ and $\mathbf{a}_2$, $\mathbf{a}_3$ so that (1.3.9) are satisfied. Substituting from (1.3.5), one can verify that (1.3.6) amounts to the equation

$$\frac{d\psi}{dt} = -|\mathbf{r}'|\tau = -|\mathbf{r}'|\frac{(\mathbf{r}' \times \mathbf{r}'') \cdot \mathbf{r}'''}{|\mathbf{r}' \times \mathbf{r}''|^2} \tag{1.3.14}$$

for the rotation angle $\psi(t)$ used to obtain $(\mathbf{a}_2, \mathbf{a}_3)$ from $(\mathbf{n}, \mathbf{b})$ in (1.3.5). Hence, as observed by Guggenheimer[1] [46], this function has the form

$$\psi(t) = \psi_0 - \int_0^t \tau(u)\,\sigma(u)\,du\,. \tag{1.3.15}$$

The above integral does not admit analytic reduction for the commonly–used polynomial and rational curves. Hence, several schemes have been proposed to approximate rotation–minimizing adapted frames on a given curve, or to approximate a given curve by "simpler" segments (e.g., circular arcs) with known rotation–minimizing frames [52, 55, 56, 103]. The spatial *Pythagorean–hodograph* curves (see Chapter 3) are an exception [22] — for these curves the integrand reduces to a rational function, which may be integrated by first computing its partial fraction decomposition.

1.4 SWEEPING

A moving frame along a space curve fixes a local coordinate system at any curve point which naturally identifies the orientation of an object moving along this trajectory. Sweep representations have many applications for describing objects such as parts of motor vehicles, aircraft or spacecraft bodies, tools, and, in general, for all the different shapes which can be decomposed quite naturally into several "tubular–like" components.

A *swept surface* is generated by moving a given (planar) *profile* (or cross–section) curve $\mathbf{p}(v)$ along a prescribed (planar or spatial) *sweep* (or spine) curve $\mathbf{s}(u)$. If the profile $\mathbf{p}(v)$ is described relative to a moving *adapted* frame $(\mathbf{f}_1(u), \mathbf{f}_2(u), \mathbf{f}_3(u))$ associated with the given sweep curve $\mathbf{s}(u)$ [62], where $\mathbf{f}_1$ coincides with the unit tangent to $\mathbf{s}(u)$, then the parametric representation of the swept surface $\mathbf{S}(u, v)$, obtained by moving $\mathbf{p}(v) = (p_0(v), p_1(v))$ along the curve $\mathbf{s}(u)$, is given by

$$\mathbf{S}(u, v) = \mathbf{s}(u) + p_0(v)\,\mathbf{f}_2(u) + p_1(v)\,\mathbf{f}_3(u)\,, \tag{1.4.1}$$

for each pair $(u, v) \in [u_0, u_1] \times [v_0, v_1]$. Special cases of swept surfaces are *translational surfaces* and *surfaces of revolution*. In the first case the profile curve is simply

1 An incorrect sign before the integral is given in [46].

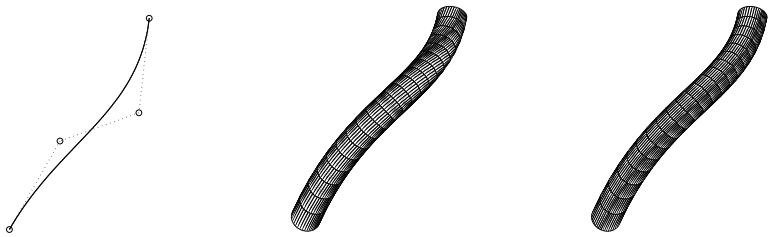

(a) curve (b) FAF (c) RMAF

Figure 1.7: A pipe surface swept by a circle whose center moves along the space curve of Figure 1.3. The isoparametric curves obtained using the FAF and the RMAF to orient the circle in the normal plane are shown.

translated along the sweep curve, while in the second one the surface is the result of rotating the planar profile curve about some axis [51]. A generalization of swept representation leads to the *generalized cylinder* modeling method where the planar profile curve may change during the motion along the spine curve [86, 59].

In classical differential geometry, an *envelope* of a family of curves (or surfaces) is a curve (surface) that is tangent to each member of the family at some point. A *canal surface* with *spine* curve $\mathbf{s}(u)$ and radius variation $r(u)$ is the envelope of the one–parameter of spheres centered at any point on $\mathbf{s}(u)$. When the radius function r is constant, the canal surface — generally called *pipe* (or *tubular*) surface — may be regarded as a swept surface generated by moving a profile circle along the spine curve following a prescribed orthonormal adapted frame $(\mathbf{f}_1(u), \mathbf{f}_2(u), \mathbf{f}_3(u))$ on it. A parametric representation for the pipe surface with spheres centered at $\mathbf{s}(u)$ and constant radius r can be expressed as

$$\mathbf{P}(u,v) \;=\; \mathbf{s}(u) + r\,\frac{1-v^2}{1+v^2}\,\mathbf{f}_2(u) + r\,\frac{2v}{1+v^2}\,\mathbf{r}(u). \tag{1.4.2}$$

This concept generalizes the classical *offsets* of plane curves (see Appendix A).

In order to specify the position and orientation of the swept profile object along the prescribed trajectory, the crucial point is to define a suitable orthornormal frame at each point of the sweep curve. A standard choice in this context is the Frenet frame, which at each point of the spine curve can be computed explicitly in terms of its first two derivatives. This implies a close relation between the frame and the geometric properties of the sweep curve that may result undesirable for swept surface constructions, since the swept surface (1.4.1) is strongly affected by the rotation of the two basis vector that spans the curve normal plane around the tangent. The Frenet frame has two serious limitations

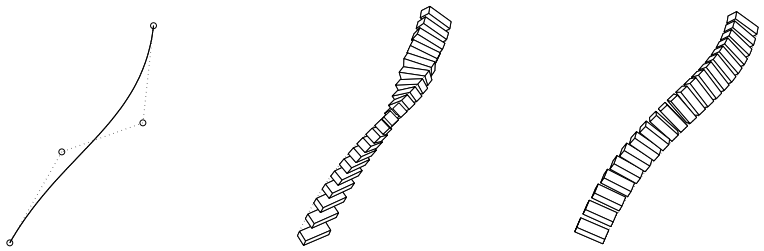

(a) curve (b) FAF (c) RMAF

Figure 1.8: The cubic Bézier curve of Figure 1.3 used to specify a trajectory for the spatial motion of a rectangular parallelepiped. The orientation of the parallelepiped defined by the FAF and the RMAF along the path are shown.

which reflect in restraints on the set of admissible trajectories. Being undefined in points with vanishing curvature, it may also reverse its orientation crossing over any inflection point. Consequently, the use of Frenet frame in practical applications is less desirable than other moving frames which do not preclude curve path with linear or planar segments as well as inflection points. In order to cope with these circumstances Klock [62], before introducing the rotation–minimizing approach, proposed a generalized Frenet frame swept. Nevertheless, a desirable property for practical free–form design and its application to motion planning or swept surface construction is the *rotation–minimizing* property. The minimization of the frame rotation along the curve that describes the desired trajectory holds strong sway over the orientation of the resulting motion or corresponding surface shape (see Figure 1.8 and 1.7, respectively). Since, in general, RMAFs are non–rational moving frames several piecewise–rational RMAF approximation schemes have been developed through the years [36, 56, 103, 104] and their consequent employment in the approximation of swept surfaces has been investigated [55, 58].

2

DIRECTED FRAMES

A varying orthonormal basis for $\mathbb{R}^3$ is *directed* on a space curve if one of the three frame vectors coincides with the unit polar vector from the origin to each curve point. As with adapted frames, there exists a whole one–parameter family of local directed system of reference which moves along the three–dimensional trajectory described by any given space curve. To facilitate computation of a moving directed frame, it is shown that the basic theory is equivalent to the established theory for adapted frames — for which one frame vector coincides with the tangent at each curve point — if one replaces the given space curve by its *anti–hodograph* (i.e., indefinite integral).

Although the focus of this chapter is on developing basic theory and algorithms for the computation of moving directed frames on space curves, we briefly mention here some possible applications to motivate this problem. The problem of camera motion planning within real or virtual environments has been considered by numerous authors — for example references [14, 76]. Such studies typically address global qualitative aspects of the camera path, and seek to formulate an automatic (or semi–automatic) means of generating a "natural" image perspective while avoiding collisions or obscurations of the camera by obstacles in the environment.

The precise specification of the image frame orientation about the camera "roll" axis, as it traverses a prescribed spatial path, does not appear to have received much attention. For a physical camera on a mount that offers three translational and two rotational (altitude and azimuth) degrees of freedom, the image frame orientation is completely determined by the requirement of maintaining a "target" object[1] centered in the field of view. Thus, a physical camera mount must offer a third rotational freedom, about the optical axis, to provide full control over the image frame orientation. Alternatively, for a digital camera with a circular field of view, this freedom can be emulated by software image rotations. For a *virtual* camera within a computer–modeled environment, complete control of image frame orientation is readily available using simple geometric transformations.

Besides cinematography, video games, and "virtual reality" applications, other possible applications include the medical practice of *endoscopic surgery*[2]

1 Conventionally, we take a target object at the origin, although a moving target is easily accommodated by considering only the *relative* motion between camera and target.

2 A number of patents describing systems to automatically orient endoscope images relative to a "preferred" direction (typically, the force of gravity) have also been issued—for example, see [69, 89].

[7, 15, 49, 93], the *field de–rotator* for a telescope on an altazimuth mount, orientational path planning for surface inspection probes with anisotropic sensors, and video inspections of aircraft engines, gas turbines, pipes, and other confined spaces. It is behind our present scope to dwell on the technical details of particular applications. Our focus is, instead, on developing the basic theory of two particular directed frames of particular geometric importance: the *Frenet directed frame* and the *rotation–minimizing directed frame* (RMDF), together with algorithms for their computation.

The structure of this chapter is as follows. The idea of a *directed* frame on a space curve, relative to a fixed point, is introduced in Section 2.1, and a special case — the Frenet directed frame — is identified by analogy with the Frenet adapted frame. The variation of the Frenet directed frame is then described in terms of the *polar curvature* and the *polar torsion*, analogs of the "ordinary" curvature and torsion governing the Frenet adapted frame. Properties of the *anti–hodograph* (indefinite integral) of a parametric space curve, a concept that elucidates relationships between the Frenet adapted and directed frame, are analyzed in Section 2.2. The computation of RMDFs, whose angular velocity maintains a vanishing component along the curve polar vector, is then addressed in Section 2.3, arguing by analogy with the theory of adapted frames.

2.1 THE FRENET DIRECTED FRAME

For a space curve $\mathbf{r}(t) = (x(t), y(t), z(t))$ the function

$$r(t) = |\mathbf{r}(t)| = \sqrt{x^2(t) + y^2(t) + z^2(t)} \tag{2.1.1}$$

specifies the radial distance of each curve point from the origin. If $r(t) \neq 0$ for all t, we can define a unit *polar vector* at each curve point by

$$\mathbf{o}(t) = \frac{\mathbf{r}(t)}{r(t)}\,. \tag{2.1.2}$$

Since the polar vector is always specified by the direction from the origin to each curve point, we call an orthonormal frame that incorporates this vector as one element a *directed* frame on the curve.

If the curve satisfies $r(t) \neq 0$ for all t, and the tangent (1.1.2) is thus defined at each point, we can employ $\mathbf{o}(t)$ and $\mathbf{t}(t)$ to define a "canonical" directed frame, in a manner analogous to that of the Frenet adapted frame (1.2.1). Upon replacing $\mathbf{r}'$, $\mathbf{r}''$, $\mathbf{r}'''$ in (1.2.1) by $\mathbf{r}$, $\mathbf{r}'$, $\mathbf{r}''$ we obtain the directed frame defined by

$$\mathbf{o} = \frac{\mathbf{r}}{|\mathbf{r}|}\,, \qquad \mathbf{u} = \frac{\mathbf{r}\times\mathbf{r}'}{|\mathbf{r}\times\mathbf{r}'|}\times\mathbf{o}\,, \qquad \mathbf{v} = \frac{\mathbf{r}\times\mathbf{r}'}{|\mathbf{r}\times\mathbf{r}'|}\,. \tag{2.1.3}$$

Because of its close relation to (1.2.1), we call this "canonical" directed frame the *Frenet directed frame*. The definition of the frame $(\mathbf{o}, \mathbf{u}, \mathbf{v})$ motivates us to introduce

the *anti–hodograph*[3] of a space curve $\mathbf{r}(t)$. Just as the hodograph is the derivative $\mathbf{r}'(t)$, regarded as a parametric curve in its own right, the anti–hodograph is the indefinite integral $\int \mathbf{r}(t)\, dt$ — also viewed as a parametric curve (there are infinitely many anti–hodographs, because of the arbitrary integration constant, but they are merely translates of each other).

Comparing (1.2.1) with (2.1.3), we see that the Frenet directed frame is simply *the Frenet frame of the anti–hodograph* of $\mathbf{r}(t)$. This means that we can write the derivative of the frame (2.1.3) in a form analogous to (1.2.3) as

$$\begin{bmatrix} \mathbf{o}' \\ \mathbf{u}' \\ \mathbf{v}' \end{bmatrix} = r \begin{bmatrix} 0 & \lambda & 0 \\ -\lambda & 0 & \upsilon \\ 0 & -\upsilon & 0 \end{bmatrix} \begin{bmatrix} \mathbf{o} \\ \mathbf{u} \\ \mathbf{v} \end{bmatrix}, \tag{2.1.4}$$

where the functions

$$r = |\mathbf{r}|, \qquad \lambda = \frac{|\mathbf{r} \times \mathbf{r}'|}{|\mathbf{r}|^3}, \qquad \upsilon = \frac{(\mathbf{r} \times \mathbf{r}') \cdot \mathbf{r}''}{|\mathbf{r} \times \mathbf{r}'|^2} \tag{2.1.5}$$

define the parametric speed, curvature, and torsion of the anti–hodograph.

As previously noted, the polar vector $\mathbf{o}(t)$ specifies the direction from the origin to each point of the curve $\mathbf{r}(t)$. In the context of a camera that moves along $\mathbf{r}(t)$ and is always aimed toward an object located at the origin, $\mathbf{o}(t)$ defines the *optical axis* of the camera lens. Thus, the plane orthogonal to the vector $\mathbf{o}$ — spanned by the vectors $(\mathbf{u}, \mathbf{v})$ — is called the *image plane*.

At each point of $\mathbf{r}(t)$, the orthogonal unit vectors $(\mathbf{u}, \mathbf{v})$ may be regarded as specifying Cartesian axes in the image plane. By analogy with the Frenet adapted frame, we call $\mathbf{u}$ the *principal axis* and $\mathbf{v}$ the *bi–axis* for the image plane. These axes vary as the camera traverses the path $\mathbf{r}(t)$ while pointing toward the origin — their variation is described by equations (2.1.4).

We have called the plane through each curve point $\mathbf{r}(t)$ that is orthogonal to $\mathbf{o}$ — i.e., spanned by $(\mathbf{u}, \mathbf{v})$ — the image plane. Consider now the plane that is orthogonal to $\mathbf{v}$ at each curve point, spanned by $(\mathbf{o}, \mathbf{u})$. We observe from (2.1.3) that $\mathbf{v}$ is perpendicular to $\mathbf{t}$, so this plane must be *tangent* to the curve at the point $\mathbf{r}(t)$. Since the instantaneous camera trajectory lies in this plane, we call it the *motion plane*. Finally, the plane that is orthogonal to $\mathbf{u}$ at each point of $\mathbf{r}(t)$ — spanned by $(\mathbf{v}, \mathbf{o})$ — is mutually perpendicular to the image and motion planes: we call it the *orthogonal* plane.

Table 2.1 enumerates the correspondence of geometrical entities associated with the Frenet adapted and directed frames. We have also introduced here the terms *polar curvature* and *polar torsion* as synonyms for the curvature λ and torsion υ of the anti–hodograph — as defined by (2.1.5).

3 We choose this term by analogy with the occasional usage of *anti–derivative* to denote the indefinite integral of a function.

FRENET ADAPTED FRAME	FRENET DIRECTED FRAME
tangent vector $\mathbf{t}$	polar vector $\mathbf{o}$
principal normal $\mathbf{n}$	principal axis $\mathbf{u}$
binormal vector $\mathbf{b}$	bi–axis vector $\mathbf{v}$
normal plane = span$(\mathbf{n}, \mathbf{b})$	image plane = span$(\mathbf{u}, \mathbf{v})$
osculating plane = span$(\mathbf{t}, \mathbf{n})$	motion plane = span$(\mathbf{o}, \mathbf{u})$
rectifying plane = span$(\mathbf{b}, \mathbf{t})$	orthogonal plane = span$(\mathbf{v}, \mathbf{o})$
parametric speed σ	polar distance r
curvature κ	polar curvature λ
torsion τ	polar torsion υ

Table 2.1: Corresponding properties of Frenet *adapted* and *directed* frames.

By analogy with the Darboux vector (1.2.5) the angular velocity of the Frenet directed frame $(\mathbf{o}, \mathbf{u}, \mathbf{v})$ with respect to the curve $\mathbf{r}(t)$ can be expressed as

$$\mathbf{e} = \frac{r}{\sigma}(\lambda\,\mathbf{v} + \upsilon\,\mathbf{o})\,. \tag{2.1.6}$$

In terms of this *polar Darboux vector* $\mathbf{e}$, we have

$$\dot{\mathbf{o}} = \mathbf{e} \times \mathbf{o}\,, \qquad \dot{\mathbf{u}} = \mathbf{e} \times \mathbf{u}\,, \qquad \dot{\mathbf{v}} = \mathbf{e} \times \mathbf{v}\,.$$

For the Frenet directed frame $(\mathbf{o}, \mathbf{u}, \mathbf{v})$ the magnitude of the angular velocity (2.1.6) is $|\mathbf{e}| = |r/\sigma|\sqrt{\lambda^2 + \upsilon^2}$.

Figure 2.1 shows the variation of the Frenet directed frame $(\mathbf{o}, \mathbf{u}, \mathbf{v})$ along a quintic Bézier curve. When this frame is used to orient a camera viewing an ellipsoid centered at the origin, the polar vector $\mathbf{o}$ specifies the optical axis, while the principal axis and bi–axis vectors $\mathbf{u}$ and $\mathbf{v}$ specify the orientation of the image frame in the image plane orthogonal to the optical axis.

2.2 PROPERTIES OF THE ANTI–HODOGRAPH

Because of its importance in the theory of directed frames, we review here some basic properties of the anti–hodograph of a space curve $\mathbf{r}(t)$. For a degree–n Bézier curve of the form (1.1.6) with control points $\mathbf{p}_0, \ldots, \mathbf{p}_n$, the hodograph (derivative) curve

$$\mathbf{d}(t) = \mathbf{r}'(t) = \sum_{k=0}^{n-1} \mathbf{d}_k \binom{n-1}{k} (1-t)^{n-1-k} t^k$$

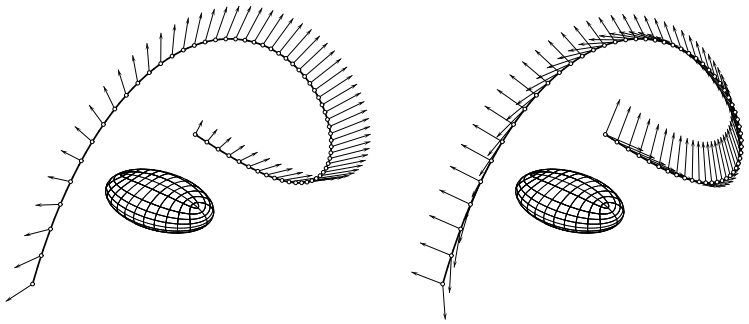

Figure 2.1: An ellipsoid is to be inspected by a camera that traverses a spatial path, keeping its optical axis passing through the center of the ellipsoid. Left: a sampling of the polar vectors **o** along the path, specifying the orientation of the camera optical axis. Right: a sampling of the principal axis and bi–axis vectors of the Frenet directed frame, **u** and **v**, that span the image plane.

is defined by the n control points $\mathbf{d}_k = n(\mathbf{p}_{k+1} - \mathbf{p}_k)$, $k = 0, \ldots, n-1$, while the anti–hodograph (indefinite integral) curve

$$\mathbf{s}(t) = \int \mathbf{r}'(t)\, dt = \sum_{k=0}^{n+1} \mathbf{s}_k \binom{n+1}{k} (1-t)^{n+1-k} t^k$$

has (modulo a vector integration constant) the $n+2$ control points

$$\mathbf{s}_0 = (0,0,0) \quad \text{and} \quad \mathbf{s}_k = \frac{1}{n+1} \sum_{j=0}^{k-1} \mathbf{p}_j\,, \qquad k = 1, \ldots, n+1\,.$$

As is well–known, if the hodograph $\mathbf{d}(t)$ passes through the origin for $t = t^*$, the point $\mathbf{r}(t^*)$ can be a *cusp* of the curve, since the tangent $\mathbf{t}$ can suffer an abrupt reversal at $t = t^*$. Likewise, if a tangent line to $\mathbf{d}(t)$ passes through the origin for $t = t^*$, the point $\mathbf{r}(t^*)$ is generally an *inflection* of the curve, since the vectors $\mathbf{r}'(t^*)$ and $\mathbf{r}''(t^*)$ are parallel.

Since any curve $\mathbf{r}(t)$ is the hodograph of its anti–hodograph $\mathbf{s}(t)$, similar relations between these curves can be deduced. Namely, when the curve $\mathbf{r}(t)$ passes through the origin for $t = t^*$, the point $\mathbf{s}(t^*)$ can be a *cusp* on the anti–hodograph. Likewise, if a tangent line to $\mathbf{r}(t)$ passes through the origin for $t = t^*$, the point $\mathbf{s}(t^*)$ is generally an *inflection* of the anti–hodograph. As previously noted, the curvature and torsion of the anti–hodograph $\mathbf{s}(t)$ are the *polar curvature* and *polar torsion* of the curve $\mathbf{r}(t)$.

Remark 2.1. *Clearly, any polynomial curve has a polynomial anti–hodograph, and conversely any polynomial anti–hodograph specifies (modulo translation) a unique polynomial curve. However, this correspondence does not extend to the anti–hodographs of rational curves, since rational functions may not have rational indefinite integrals —*

the anti–hodograph of a rational Bézier curve, for example, may incur transcendental (logarithm or arc–tangent) terms.

2.3 ROTATION–MINIMIZING DIRECTED FRAMES

It is known [36] that, if a space curve is modeled as an elastic fiber subject to bending and twisting, the least value of the elastic strain energy will be achieved when the "twist" angle is specified by a rotation–minimizing adapted frame. Analogously, the rotation–minimizing directed frames identify solutions to a similar minimum–energy problem involving orientation relative to a fixed point in space, and thus deserve to be more systematically studied.

Since $r = \sqrt{\mathbf{r}\cdot\mathbf{r}}$, the arc length derivative of the polar vector (2.1.2) is

$$\frac{d\mathbf{o}}{ds} = \frac{1}{\sigma}\frac{d}{dt}\frac{\mathbf{r}}{r} = \frac{r^2\,\mathbf{r}' - (\mathbf{r}\cdot\mathbf{r}')\,\mathbf{r}}{\sigma\, r^3} = \frac{(\mathbf{o}\times\mathbf{t})\times\mathbf{o}}{r},$$

which can be written as

$$\frac{d\mathbf{o}}{ds} = \boldsymbol{\omega}\times\mathbf{o} \qquad \text{with} \quad \boldsymbol{\omega} = \alpha\,\mathbf{o} + \frac{\mathbf{o}\times\mathbf{t}}{r}, \tag{2.3.1}$$

where α is an arbitrary scalar function. If the curve $\mathbf{r}(t)$ is traversed at unit speed, $\boldsymbol{\omega}$ defines the *angular velocity* of the unit vector $\mathbf{o}$ — arising from the requirement that it always points from the origin toward $\mathbf{r}(t)$.

As far as $\mathbf{o}$ is concerned, the component $\alpha\,\mathbf{o}$ of $\boldsymbol{\omega}$ is immaterial, since it specifies an instantaneous rotation of $\mathbf{o}$ about itself. However, if we consider $\mathbf{o}$ as a component of a *directed frame* $(\mathbf{d}_1, \mathbf{d}_2, \mathbf{d}_3)$ with $\mathbf{d}_1 = \mathbf{o}$, the component $\alpha\,\mathbf{o}$ of the instantaneous angular velocity $\boldsymbol{\omega}$ is significant — it specifies the angular velocity of the frame vectors $(\mathbf{u}, \mathbf{v})$ spanning the plane orthogonal to $\mathbf{o}$.

By analogy with the *adapted* rotation–minimizing frames $(\mathbf{a}_1, \mathbf{a}_2, \mathbf{a}_3)$ with $\mathbf{a}_1 = \mathbf{t}$ on a space curve $\mathbf{r}(t)$ — characterized by the fact that the frame vectors $(\mathbf{a}_2, \mathbf{a}_3)$ have zero angular velocity component in the direction of the tangent $\mathbf{t}$ — we characterize a *directed* rotation–minimizing frame $(\mathbf{d}_1, \mathbf{d}_2, \mathbf{d}_3)$ by the property that the frame vectors $(\mathbf{d}_2, \mathbf{d}_3)$ maintain a zero angular velocity component in the direction of the polar vector $\mathbf{d}_1 \equiv \mathbf{o}$. Hence, setting $\alpha \equiv 0$ in (2.3.1) so that

$$\boldsymbol{\omega} = \frac{\mathbf{o}\times\mathbf{t}}{r} = \frac{\mathbf{r}\times\mathbf{r}'}{\sigma r^2} = \frac{r}{\sigma}\lambda\,\mathbf{v}, \tag{2.3.2}$$

a directed rotation–minimizing frame $(\mathbf{d}_1, \mathbf{d}_2, \mathbf{d}_3)$ is specified in terms of this angular velocity function by the differential relations

$$\dot{\mathbf{d}}_1 = \boldsymbol{\omega}\times\mathbf{d}_1\,, \qquad \dot{\mathbf{d}}_2 = \boldsymbol{\omega}\times\mathbf{d}_2\,, \qquad \dot{\mathbf{d}}_3 = \boldsymbol{\omega}\times\mathbf{d}_3\,. \tag{2.3.3}$$

Hence, the RMDFs corresponds to omitting the component $(r/\sigma)\upsilon\mathbf{o}$ from the Frenet directed frame angular velocity (2.1.6) — for the rotation–minimizing

frame we have $\omega = |\boldsymbol{\omega}|$ equals to $(r/\sigma)|\lambda|$, which can also be written as $|\sin\zeta|/r$ where ζ is the angle between the polar and hodograph vectors, $\mathbf{r}(t)$ and $\mathbf{r}'(t)$. Hence, ω vanishes if $\mathbf{r}(t)$ and $\mathbf{r}'(t)$ are collinear — that is, the camera is moving directly toward or away from the origin. For a fixed relative orientation ζ of $\mathbf{r}(t)$ and $\mathbf{r}'(t)$, note that ω is inversely proportional to the camera distance $r(t) = |\mathbf{r}(t)|$ from the origin.

To integrate equations (2.3.3), an initial frame $(\mathbf{d}_1^*, \mathbf{d}_2^*, \mathbf{d}_3^*)$ for $s = t = 0$ must be specified. Now $\mathbf{d}_1^* = \mathbf{r}(0)/r(0)$ is uniquely determined, but there exists a one–parameter family of vector pairs $(\mathbf{d}_2^*, \mathbf{d}_3^*)$ consistent with the requirement that $(\mathbf{d}_1^*, \mathbf{d}_2^*, \mathbf{d}_3^*)$ must be a right–handed orthonormal frame. Hence, as with the adapted rotation–minimizing frames, there exists a one–parameter family of directed rotation–minimizing frames on a given space curve. Any two of these frames exhibit a constant angular displacement between their $(\mathbf{d}_2, \mathbf{d}_3)$ vectors along the curve. For brevity, we refer to adapted and directed rotation–minimizing frames by the acronyms RMAF and RMDF.

Now since $\mathbf{o}$ is uniquely specified by (2.1.2) and we can define $\mathbf{d}_3$ as $\mathbf{o} \times \mathbf{d}_2$, it suffices to determine $\mathbf{d}_2$. Invoking the angular velocity (2.3.2), converting back to derivatives with respect to t, and setting

$$k_x = \frac{yz' - y'z}{x^2 + y^2 + z^2}, \qquad k_y = \frac{zx' - z'x}{x^2 + y^2 + z^2}, \qquad k_z = \frac{xy' - x'y}{x^2 + y^2 + z^2},$$

we obtain from (2.3.3) the linear system of first–order differential equations

$$\mathbf{d}_2' = \begin{bmatrix} 0 & -k_z & k_y \\ k_z & 0 & -k_x \\ -k_y & k_x & 0 \end{bmatrix} \mathbf{d}_2$$

(with non–constant coefficients) for the Cartesian components of $\mathbf{d}_2$. We note that the matrix elements are *rational functions* of the curve parameter t. A single first–order differential equation with non–constant coefficients may sometimes be integrated by identifying an appropriate integrating factor, but this approach does not, in general, extend to first–order systems.

Instead of attempting to construct RMDFs by direct integration of these equations, we argue by analogy with the construction of RMAFs. Namely, we express the RMDF basis vectors $(\mathbf{d}_2, \mathbf{d}_3)$ that span the image plane in terms of the two Frenet directed frame vectors $(\mathbf{u}, \mathbf{v})$ given by (2.1.3) in the form

$$\begin{bmatrix} \mathbf{d}_2 \\ \mathbf{d}_3 \end{bmatrix} = \begin{bmatrix} \cos\psi & \sin\psi \\ -\sin\psi & \cos\psi \end{bmatrix} \begin{bmatrix} \mathbf{u} \\ \mathbf{v} \end{bmatrix}, \tag{2.3.4}$$

i.e., $(\mathbf{d}_2, \mathbf{d}_3)$ are obtained from $(\mathbf{u}, \mathbf{v})$ at each curve point by rotation through a suitable angle ψ in the plane orthogonal to $\mathbf{o}$. The advantage of this approach is that it reduces the RMDF computation to determining the scalar function $\psi(t)$ that relates $(\mathbf{d}_2, \mathbf{d}_3)$ to the known vectors $(\mathbf{u}, \mathbf{v})$.

Since, on replacing a curve by its anti–hodograph, the theory of RMDFs coincides with that of RMAFs, we deduce that the desired angle function in (2.3.4) is given by

$$\psi(t) = \psi_0 - \int_0^t \upsilon(u)\, r(u)\, du\,. \tag{2.3.5}$$

Comparing the integrals in (1.3.15) and (2.3.5) we note that, for general polynomial or rational curves, the torsion $\tau(t)$ and the polar torsion $\upsilon(t)$ of a curve are both rational in the parameter t, but since the corresponding parametric speeds $\sigma(t)$ and $r(t)$ specified by (1.1.3) and (2.1.1) are *square roots* of polynomials, we cannot, in general, obtain a closed–form reduction of these integrals.

For the PH curves, σ is a polynomial in t, so the integrand in (1.3.15) is a rational function [22], and (1.3.15) can be determined analytically by partial fraction decomposition. A similar resolution is possible for the RMDF, but the coordinate components of the *curve* rather than its *hodograph* must be elements of a Pythagorean quartuple. The computation of exact RMDFs suggest to introduce the class of *Pythagorean (P) curves* (see Chapter 7), for which r is a polynomial in t and the integrand in (2.3.5) is thus rational.

Example 2.1. Consider the path $\mathbf{r}(\theta) = (a\cos\theta, a\sin\theta, h)$ — that is, a circle of radius a at height h above the (x, y) plane. For this path, the Frenet directed frame specified by (2.1.3) is

$$\mathbf{o} = \frac{(a\cos\theta, a\sin\theta, h)}{\sqrt{a^2+h^2}}\,, \quad \mathbf{u} = (-\sin\theta, \cos\theta, 0)\,, \quad \mathbf{v} = \frac{(-h\cos\theta, -h\sin\theta, a)}{\sqrt{a^2+h^2}}\,.$$

Note that $\mathbf{u}$ coincides with the unit tangent $\mathbf{t}$ to the path. The polar distance, curvature, and torsion functions are all constant, namely

$$r = \sqrt{a^2+h^2}\,, \quad \lambda = \frac{a}{a^2+h^2}\,, \quad \upsilon = \frac{h}{a^2+h^2}\,.$$

Since the parametric speed has the constant value $\sigma = a$, the angular speed of the Frenet directed frame is $|\mathbf{e}| = r\sqrt{\lambda^2+\upsilon^2}/\sigma = 1/a$, and for the RMDF we have $|\boldsymbol{\omega}| = r\lambda/\sigma = 1/\sqrt{a^2+h^2}$. Hence, the angular speeds coincide when $h = 0$, but for $h >> r$ the angular speed of the RMDF is significantly lower. With $\psi_0 = 0$, the angle function (2.3.5) specifying the orientation of the RMDF relative to the Frenet directed frame is simply

$$\psi(\theta) = -\frac{\theta}{\sqrt{1+(a/h)^2}}\,.$$

For a complete traversal of the path, the RMDF experiences a total rotation of $-2\pi/\sqrt{1+(a/h)^2}$ (always less of a full revolution) relative to the Frenet directed frame. Since the latter is of period 2π in θ, we see that the RMDF is not, in general, continuous around a closed path. Figure 2.2 illustrates the variation of

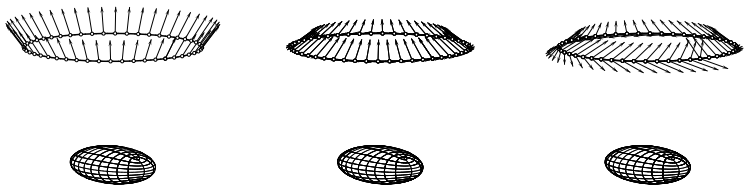

Figure 2.2: Left: variation of the polar vector **o** around the path of Example 2.1. Center: variation of the Frenet directed frame vectors **u** and **v** (the **u** vectors are difficult to discern here, since they coincide with the curve tangent **t**). Right: variation of the RMDF frame vectors $\mathbf{d}_2$ and $\mathbf{d}_3$ — note that the RMDF does not, in general, exhibit a periodic variation along a smooth closed path.

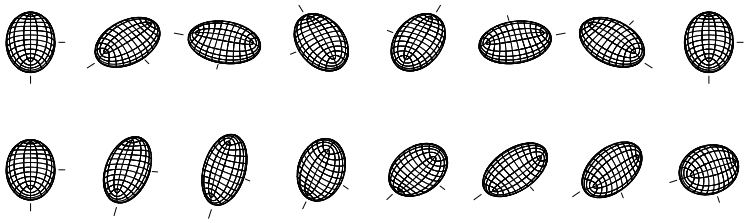

Figure 2.3: Comparison of ellipsoid views as the camera follows the path of Example 2.1, using the Frenet directed frame (upper) and rotation–minimizing directed frame (lower) to orient the camera image plane about its optical axis.

the polar vector **o** and the directed frame pairs $(\mathbf{u}, \mathbf{v})$ and $(\mathbf{d}_2, \mathbf{d}_3)$ orthogonal to it, in the case $a = 6$ and $h = 8$, while Figure 2.3 illustrates views of the ellipsoid oriented in accordance with these frames.

Example 2.2. Consider the circular helix $\mathbf{r}(\theta) = (a\cos\theta, a\sin\theta, k\theta)$. Setting $c = k/a$, the Frenet directed frame is

$$\begin{aligned}
\mathbf{o} &= \frac{(\cos\theta, \sin\theta, c\theta)}{\sqrt{1+c^2\theta^2}}\,,\\
\mathbf{u} &= \frac{(-c^2\theta(\cos\theta+\theta\sin\theta)-\sin\theta, c^2\theta(\theta\cos\theta-\sin\theta)+\cos\theta, c)}{\sqrt{1+c^2\theta^2}\sqrt{1+c^2+c^2\theta^2}}\,,\\
\mathbf{v} &= \frac{(c(\sin\theta-\theta\cos\theta), -c(\cos\theta+\theta\sin\theta), 1)}{\sqrt{1+c^2+c^2\theta^2}}\,,
\end{aligned}$$

while the polar distance and polar curvature and torsion are given by

$$r = a\sqrt{1+c^2\theta^2}\,, \quad \lambda = \frac{\sqrt{1+c^2+c^2\theta^2}}{a(1+c^2\theta^2)^{3/2}} \quad \upsilon = \frac{c\theta}{a(1+c^2+c^2\theta^2)}\,.$$

The orientation of the RMDF relative to the Frenet directed frame, given by (2.3.5) with $\psi_0 = 0$, reduces to

$$\psi = \tan^{-1}\frac{\sqrt{1+c^2\theta^2}}{c} - \tan^{-1}\frac{1}{c} - \frac{\sqrt{1+c^2\theta^2}-1}{c}\,.$$

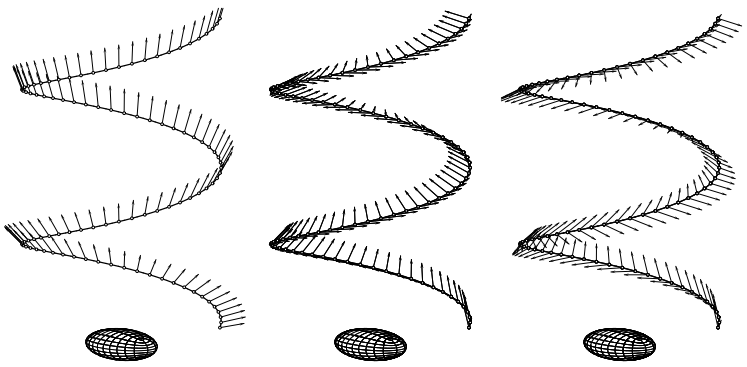

Figure 2.4: Left: the polar vector $\mathbf{o}$ around the circular helix path of Example 2.2. Center: the Frenet directed frame vectors $\mathbf{u}$ and $\mathbf{v}$ spanning the image plane along this path. Right: the corresponding RMDF frame vectors $\mathbf{d}_2$ and $\mathbf{d}_3$.

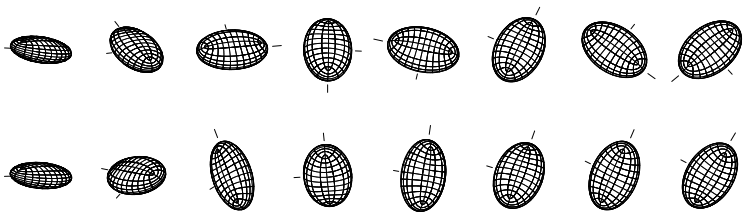

Figure 2.5: Comparison of ellipsoid views as the camera follows the path of Example 2.2, using the Frenet directed frame (upper) and rotation–minimizing directed frame (lower) to orient the camera image plane about its optical axis.

Figure 2.4 illustrates the variation of the polar vector $\mathbf{o}$ along $\mathbf{r}(\theta)$, together with the Frenet vectors $(\mathbf{u}, \mathbf{v})$ and rotation–minimizing vectors $(\mathbf{d}_2, \mathbf{d}_3)$ in the image plane, for the case $a = 8$, $k = 2$. Figure 2.5 shows a sampling of views of the ellipsoid, when the camera image plane is oriented by these vector pairs. The polar curvature and torsion for this path are shown in Figure 2.6. Note that λ and

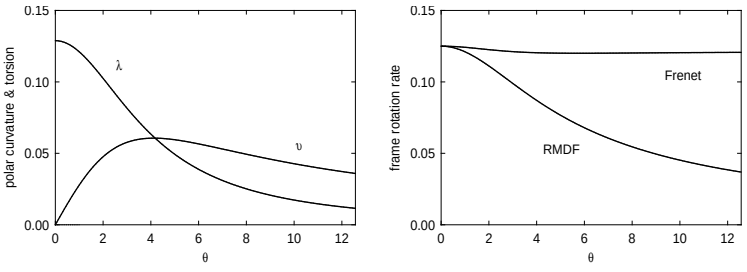

Figure 2.6: Left: variation of polar curvature λ and polar torsion υ along the path shown in Figure 2.4. Right: rotation rates $r\sqrt{\lambda^2 + \upsilon^2}/\sigma$ and $r\lambda/\sigma$ for the Frenet directed frame and rotation–minimizing directed frame on this path.

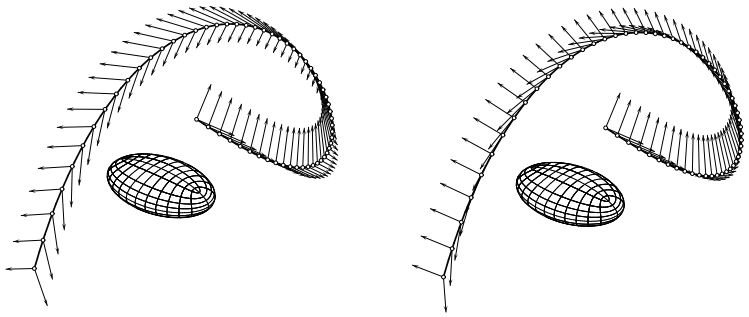

Figure 2.7: Comparison of the rotation–minimizing directed frame (left) with the Frenet directed frame (right) along the path shown in Figure 2.1. The two frames are identical at the initial curve point just above the ellipsoid target.

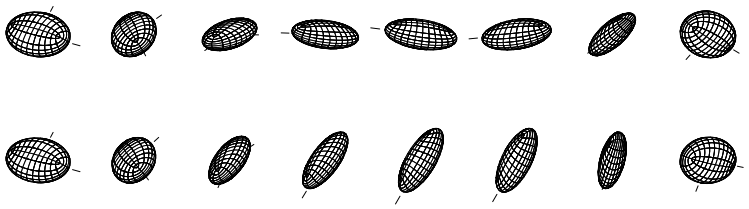

Figure 2.8: Comparison of ellipsoid views as the camera follows the path shown in Figure 2.1, using the Frenet directed frame (upper) and rotation–minimizing directed frame (lower) to orient the camera image plane about its optical axis.

υ both decrease with θ, decaying like θ^{-2} and θ^{-1} respectively for large θ. Thus, the difference between the Frenet directed frame and the rotation–minimizing frame becomes more pronounced with increasing θ.

Example 2.3. Returning to the path in Figure 2.1 (a quintic Bézier curve), Figure 2.7 gives a comparison of the Frenet vectors $(\mathbf{u}, \mathbf{v})$ and rotation–minimizing vectors $(\mathbf{d}_2, \mathbf{d}_3)$ spanning the image plane, while Figure 2.8 shows a sampling of views of the ellipsoid, oriented by these vectors. Figure 2.9 illustrates the variation of the polar curvature λ and polar torsion υ along this curve. Also shown are the angular speeds of the Frenet directed frame and the rotation–minimizing directed frame — $r\sqrt{\lambda^2 + \upsilon^2}/\sigma$ and $r\lambda/\sigma$, respectively.

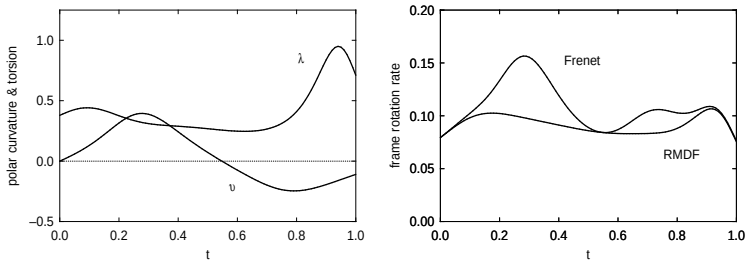

Figure 2.9: Left: variation of polar curvature λ and polar torsion υ along the path shown in Figure 2.1. Right: rotation rates $r\sqrt{\lambda^2+\upsilon^2}/\sigma$ and $r\lambda/\sigma$ for the Frenet directed frame and rotation–minimizing directed frame on this path.

Part II

CURVES WITH RATIONAL FRAMES

3

SPATIAL PYTHAGOREAN–HODOGRAPH CURVES

In computer aided geometric design, the mathematical discipline that provides both the theoretical backgrounds and the numerical tools for the automated manipulation of geometric data, curves and surfaces are generally specified in parametric rational form. In particular, the two standard Bézier/B-spline schemes offer a simple and intuitive tool to easily deal with these geometric objects [18, 51]. Nevertheless, in contrast with these traditional schemes, the search for curves with rational frames must be restricted to curves which, exhibiting particular *Pythagorean* structures, require models that are inherently non–linear in nature. However, by use of two appropriate algebraic tools, namely the *Hopf map* and the *quaternion algebra*, their construction and analysis is greatly facilitated.

Pythagorean–hodograph (PH) space curves are polynomial parametric curves $\mathbf{r}(t)$ with the distinctive property that their hodographs $\mathbf{r}'(t) = (x'(t), y'(t), z'(t))$ satisfy the Pythagorean condition (see Figure 3.1)

$$x'^2(t) + y'^2(t) + z'^2(t) = \sigma^2(t), \tag{3.0.1}$$

for some polynomial $\sigma(t)$. In order to satisfy this condition the real polynomials $x'(t)$, $y'(t)$, $z'(t)$, $\sigma(t)$ must be expressible in terms of other real polynomials $u(t)$, $v(t)$, $p(t)$, $q(t)$ in the form

$$\begin{aligned} x'(t) &= u^2(t) + v^2(t) - p^2(t) - q^2(t), \\ y'(t) &= 2\,[u(t)q(t) + v(t)p(t)]\,, \\ z'(t) &= 2\,[v(t)q(t) - u(t)p(t)]\,, \end{aligned} \tag{3.0.2}$$

with corresponding *polynomial* parametric speed

$$\sigma(t) = u^2(t) + v^2(t) + p^2(t) + q^2(t)\,.$$

If the polynomials $u(t)$, $v(t)$, $p(t)$, $q(t)$ are of degree m at most, the PH curve $\mathbf{r}(t)$ obtained by integrating the hodograph $\mathbf{r}'(t)$ is of *odd* degree, $n = 2m + 1$. The distinctive feature of PH curves offers many advantages in several applications. For a complete review of the construction and properties of planar and spatial PH curves, see [23, 24].

This chapter begins with a review of the quaternion and Hopf map representations of spatial PH curves in Sections 3.1 and 3.2, while conversions between these forms are treated in Section 3.3. Conditions that incur *linear* and *planar* degenerations of spatial PH curves are then identified in Section 3.4, in terms both of the quaternion and Hopf map representations.

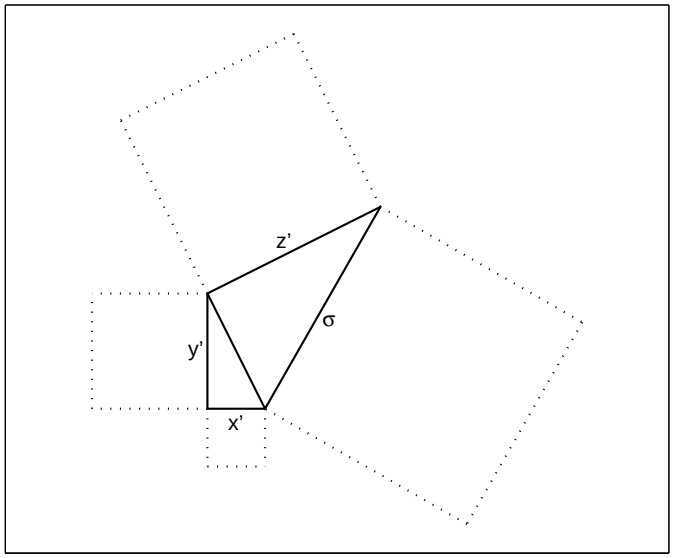

Figure 3.1: The spatial Pythagorean–hodograph structure.

3.1 QUATERNION FORM OF SPATIAL PH CURVES

Pythagorean–hodograph curves admit [13, 27] a compact description using the algebra of quaternions (see Appendix B for a review). Namely, the PH condition is equivalent to the requirement that the hodograph $\mathbf{r}'(t)$ can be expressed as a quaternion product of the form

$$\mathbf{r}'(t) = \mathcal{A}(t)\,\mathbf{u}\,\mathcal{A}^*(t)\,, \tag{3.1.1}$$

where $\mathbf{u}$ is any fixed unit vector and

$$\mathcal{A}(t) = \sum_{l=0}^{m} \mathcal{A}_l \binom{m}{l} (1-t)^{m-l} t^l \tag{3.1.2}$$

denotes the Bernstein form of a quaternion polynomial of degree $m = \frac{1}{2}(n-1)$ for a PH curve of odd degree n, and $\mathcal{A}^*(t)$ is the conjugate of $\mathcal{A}(t)$.

Integrating the hodograph (3.1.1) then gives the Bézier form

$$\mathbf{r}(t) = \sum_{i=0}^{n} \mathbf{p}_i \binom{n}{i} (1-t)^{n-i}\, t^i$$

of the degree n PH curve, with control points $\mathbf{p}_i = x_i\,\mathbf{i} + y_i\,\mathbf{j} + z_i\,\mathbf{k}$ given in terms of the quaternion coefficients $\mathcal{A}_l$ for $l = 0, \ldots, m$, with the initial control

point $\mathbf{p}_0$ taken as arbitrary integration constant. In particular, for PH curves of degree 3, 5 and 7 we have, respectively,

$$\mathcal{A}(t) = \mathcal{A}_0(1-t) + \mathcal{A}_1 t\,, \tag{3.1.3}$$
$$\mathcal{A}(t) = \mathcal{A}_0(1-t)^2 + \mathcal{A}_1 2(1-t)t + \mathcal{A}_2 t^2\,, \tag{3.1.4}$$
$$\mathcal{A}(t) = \mathcal{A}_0\,(1-t)^3 + \mathcal{A}_1\,3\,(1-t)^2\,t + \mathcal{A}_2\,3\,(1-t)\,t^2 + \mathcal{A}_3\,t^3\,. \tag{3.1.5}$$

The corresponding control points are

$$\begin{aligned}
\mathbf{p}_1 &= \mathbf{p}_0 + \tfrac{1}{3}(\mathcal{A}_0\,\mathbf{u}\,\mathcal{A}_0^*)\,,\\
\mathbf{p}_2 &= \mathbf{p}_1 + \tfrac{1}{6}(\mathcal{A}_0\,\mathbf{u}\,\mathcal{A}_1^* + \mathcal{A}_1\,\mathbf{u}\,\mathcal{A}_0^*)\,,\\
\mathbf{p}_3 &= \mathbf{p}_2 + \tfrac{1}{3}(\mathcal{A}_1\,\mathbf{u}\,\mathcal{A}_1^*)\,,
\end{aligned}$$

for spatial PH cubics,

$$\begin{aligned}
\mathbf{p}_1 &= \mathbf{p}_0 + \tfrac{1}{5}(\mathcal{A}_0\,\mathbf{u}\,\mathcal{A}_0^*)\,,\\
\mathbf{p}_2 &= \mathbf{p}_1 + \tfrac{1}{10}(\mathcal{A}_0\,\mathbf{u}\,\mathcal{A}_1^* + \mathcal{A}_1\,\mathbf{u}\,\mathcal{A}_0^*)\,,\\
\mathbf{p}_3 &= \mathbf{p}_2 + \tfrac{1}{30}(\mathcal{A}_0\,\mathbf{u}\,\mathcal{A}_2^* + 4\,\mathcal{A}_1\,\mathbf{u}\,\mathcal{A}_1^* + \mathcal{A}_2\,\mathbf{u}\,\mathcal{A}_0^*)\,,\\
\mathbf{p}_4 &= \mathbf{p}_3 + \tfrac{1}{10}(\mathcal{A}_1\,\mathbf{u}\,\mathcal{A}_2^* + \mathcal{A}_2\,\mathbf{u}\,\mathcal{A}_1^*)\,,\\
\mathbf{p}_5 &= \mathbf{p}_4 + \tfrac{1}{5}(\mathcal{A}_2\,\mathbf{u}\,\mathcal{A}_2^*)\,,
\end{aligned} \tag{3.1.6}$$

for spatial PH quintics, and

$$\begin{aligned}
\mathbf{p}_1 &= \mathbf{p}_0 + \tfrac{1}{7}(\mathcal{A}_0\,\mathbf{u}\,\mathcal{A}_0^*)\,,\\
\mathbf{p}_2 &= \mathbf{p}_1 + \tfrac{1}{14}\,(\mathcal{A}_0\,\mathbf{u}\,\mathcal{A}_1^* + \mathcal{A}_1\,\mathbf{i}\,\mathcal{A}_0^*)\,,\\
\mathbf{p}_3 &= \mathbf{p}_2 + \tfrac{1}{35}\,(\mathcal{A}_0\,\mathbf{u}\,\mathcal{A}_2^* + 3\,\mathcal{A}_1\,\mathbf{u}\,\mathcal{A}_1^* + \mathcal{A}_2\,\mathbf{u}\,\mathcal{A}_0^*)\,,\\
\mathbf{p}_4 &= \mathbf{p}_3 + \tfrac{1}{140}\,(\mathcal{A}_0\,\mathbf{u}\,\mathcal{A}_3^* + 9\,\mathcal{A}_1\,\mathbf{u}\,\mathcal{A}_2^* + 9\,\mathcal{A}_2\,\mathbf{u}\,\mathcal{A}_1^* + \mathcal{A}_3\,\mathbf{u}\,\mathcal{A}_0^*)\,,\\
\mathbf{p}_5 &= \mathbf{p}_4 + \tfrac{1}{35}\,(\mathcal{A}_1\,\mathbf{u}\,\mathcal{A}_3^* + 3\,\mathcal{A}_2\,\mathbf{u}\,\mathcal{A}_2^* + \mathcal{A}_3\,\mathbf{u}\,\mathcal{A}_1^*)\,,\\
\mathbf{p}_6 &= \mathbf{p}_5 + \tfrac{1}{14}\,(\mathcal{A}_2\,\mathbf{u}\,\mathcal{A}_3^* + \mathcal{A}_3\,\mathbf{u}\,\mathcal{A}_2^*)\,,\\
\mathbf{p}_7 &= \mathbf{p}_6 + \tfrac{1}{7}(\mathcal{A}_3\,\mathbf{u}\,\mathcal{A}_3^*)\,,
\end{aligned} \tag{3.1.7}$$

for spatial PH curve of degree 7.

In view of the arbitrary choice of $\mathbf{u}$, we henceforth assume $\mathbf{u} = \mathbf{i}$, so that

$$\mathbf{r}'(t) = \mathcal{A}(t)\,\mathbf{i}\,\mathcal{A}^*(t) \tag{3.1.8}$$

coincides with (3.0.2) when $\mathcal{A}(t) = u(t) + v(t)\,\mathbf{i} + p(t)\,\mathbf{j} + q(t)\,\mathbf{k}$. In fact, in terms of the component polynomials $u(t)$, $v(t)$, $p(t)$, $q(t)$ of $\mathcal{A}(t)$, we have

$$\begin{aligned}
\mathbf{r}'(t) &= [\,u^2(t) + v^2(t) - p^2(t) - q^2(t)\,]\,\mathbf{i}\\
&\quad + 2\,[\,u(t)q(t) + v(t)p(t)\,]\,\mathbf{j} + 2\,[\,v(t)q(t) - u(t)p(t)\,]\,\mathbf{k}\,.
\end{aligned} \tag{3.1.9}$$

Note that, any unit quaternion $\mathcal{Q}$ of the form $\mathcal{Q}(\phi) = \cos\phi + \sin\phi\,\mathbf{i}$ satisfies $\mathcal{Q}(\phi)\,\mathbf{i}\,\mathcal{Q}^*(\phi) = \mathbf{i}$ for $0 \leqslant \phi \leqslant 2\pi$, so the hodograph (3.1.8) can also be written

as $\mathbf{r}'(t) = \mathcal{C}(t)\,\mathbf{i}\,\mathcal{C}^*(t)$, where $\mathcal{C}(t) = \mathcal{A}(t)\mathcal{Q}(\phi)$ is defined by (3.1.2) with the coefficients $\mathcal{A}_i$, $i = 0,\ldots,n$ replaced with $\mathcal{C}_i = \mathcal{A}_i\mathcal{Q}$, $i = 0,\ldots,n$. This implies that one component of one of the quaternions $\mathcal{A}_i$ can be freely chosen and, accordingly, any given Pythagorean hodograph $\mathbf{r}'(t)$ is generated through (3.1.8) by a *one–parameter family* of quaternion polynomials [27]. Moreover, the angular variable may be specified as a function $\phi(t)$ of the curve parameter t without any change in the hodograph (3.1.8).

Remark 3.1. A *primitive* hodograph $\mathbf{r}'(t) = (x'(t), y'(t), z'(t))$ is characterized by the fact that $\gcd(x'(t), y'(t), z'(t)) = \text{constant}$. Primitive hodographs are preferred in practice, since a common real root of $x'(t)$, $y'(t)$, $z'(t)$ may incur a *cusp* (sudden tangent reversal) on the curve $\mathbf{r}(t)$. Moreover, as long as we are not concerned with the crossover parametric speed, a non–primitive hodograph adds essentially just a redundant information. However, choosing relatively prime polynomials $u(t)$, $v(t)$, $p(t)$, $q(t)$ as components of $\mathcal{A}(t)$ does not guarantee a primitive $\mathbf{r}'(t)$. The hodograph (3.1.9) may be rewritten in terms of complex polynomials $u \pm iv$ and $p \pm iq$ as

$$\begin{aligned} x' &= (u+iv)(u-iv) - (p+iq)(p-iq)\,, \\ y' &= i\,[(u-iv)(p-iq) - (u+iv)(p+iq)]\,, \\ z' &= -\,[(u-iv)(p-iq) + (u+iv)(p+iq)]\,, \end{aligned}$$

where $i = \sqrt{-1}$ is the standard imaginary unit. Hence,

$$\left.\begin{aligned} x' = 0 \;&\Leftrightarrow\; (u+iv)(u-iv) = (p+iq)(p-iq) \\ y' = 0 \;&\Leftrightarrow\; (u-iv)(p-iq) = (u+iv)(p+iq) \\ z' = 0 \;&\Leftrightarrow\; (u-iv)(p-iq) = -(u+iv)(p+iq) \end{aligned}\right\} \Leftrightarrow \begin{array}{c} u+iv = p-iq = 0 \\ \text{or} \\ u-iv = p+iq = 0\,. \end{array}$$

In addition, it can be proved that any multiple root of either $u+iv = p-iq = 0$ or $u-iv = p+iq = 0$ is also a multiple root of $\mathbf{r}'$ [37]. This implies that the common factor (if any) of x', y', z' is given by

$$\gcd(x', y', z') \;=\; \gcd(u+i\,v, p-i\,q)\cdot\gcd(u-i\,v, p+i\,q)\,. \tag{3.1.10}$$

Since u, v, p, q are real polynomials (3.1.10) reduces to

$$\gcd(x', y', z') \;=\; |\,\gcd(u+i\,v, p-i\,q)\,|^2\,. \tag{3.1.11}$$

This defines a *real* even–degree polynomial $f(t)$, with no real roots. A non–primitive spatial Pythagorean hodograph can thus be written in the form

$$h(t)\,\mathcal{B}(t)\,\mathbf{i}\,\mathcal{B}^*(t) \tag{3.1.12}$$

for a suitable quaternion polynomial $\mathcal{B}(t)$, of degree $m-r$ when $\deg(h) = 2r$. Of course, if $u(t)$, $v(t)$, $p(t)$, $q(t)$ are not relatively prime, $\gcd(u, v, p, q)$ will also contribute to $h(t)$ in (3.1.12).

3.2 HOPF MAP FORM OF SPATIAL PH CURVES

As an alternative to the quaternion representation, Choi et al. [13] observed that the spatial Pythagorean hodograph (3.0.2) can be generated from a pair of complex polynomials through the *Hopf map* $H : \mathbb{C} \times \mathbb{C} \to \mathbb{R}^3$ (see Appendix C for a review). This map can be regarded as associating complex number pairs $\alpha = u + i\,v$, $\beta = q + i\,p$ with points $\mathbf{p} = (x, y, z) \in \mathbb{R}^3$ according to

$$\mathbf{p} \;=\; H(\alpha, \beta) \;=\; (|\alpha|^2 - |\beta|^2, 2\,\mathrm{Re}(\alpha\overline{\beta}), 2\,\mathrm{Im}(\alpha\overline{\beta}))\,. \tag{3.2.1}$$

When we restrict (3.2.1) to complex numbers satisfying $|\alpha|^2 + |\beta|^2 = 1$, it can be interpreted as a map between the "3–sphere" $S^3 : u^2 + v^2 + p^2 + q^2 = 1$ in the space $\mathbb{R}^4$ spanned by coordinates (u, v, p, q), and the standard "2–sphere" $S^2 : x^2 + y^2 + z^2 = 1$ in $\mathbb{R}^3$ with (x, y, z) as coordinates.

One can easily verify that the hodograph $\mathbf{r}'(t)$ defined by (3.0.2) is generated from the complex polynomials $\alpha(t) = u(t) + i\,v(t)$ and $\beta(t) = q(t) + i\,p(t)$ as

$$\mathbf{r}'(t) \;=\; H(\alpha(t), \beta(t))\,. \tag{3.2.2}$$

As with the quaternion form, the relationship between $\mathbf{r}'(t)$ and $\alpha(t)$, $\beta(t)$ is not one–to–one: we generate exactly the same hodograph on replacing the latter by $\alpha(t)\,(\cos\phi + i\,\sin\phi)$ and $\beta(t)\,(\cos\phi + i\,\sin\phi)$ for $0 \leqslant \phi \leqslant 2\pi$.

Within the Hopf map context, for a PH curve of degree $n = 2m + 1$, the hodograph is constructed according to (3.2.2) from two polynomials $\alpha(t)$, $\beta(t)$ of degree m. In the following we will assume these polynomial are specified in Bernstein form as

$$\alpha(t) \;=\; \sum_{l=0}^{m} \alpha_l \binom{m}{l} (1-t)^{m-l} t^l\,, \quad \beta(t) \;=\; \sum_{l=0}^{m} \beta_l \binom{m}{l} (1-t)^{m-l} t^l\,. \tag{3.2.3}$$

Remark 3.2. The hodograph (3.2.2) is primitive if and only if $\gcd(\alpha(t), \beta(t)) =$ constant. When $\alpha(t)$, $\beta(t)$ have a non–constant common factor $\mathbf{w}(t)$, we may write $\mathbf{r}'(t) = |\mathbf{w}(t)|^2 H(\tilde{\alpha}(t), \tilde{\beta}(t))$ where $\alpha(t) = \mathbf{w}(t)\tilde{\alpha}(t)$, $\beta(t) = \mathbf{w}(t)\tilde{\beta}(t)$. The common factor $\mathbf{w}(t)$ influences only the *magnitude* of the hodograph — $\tilde{\alpha}(t)$ and $\tilde{\beta}(t)$ alone determine its direction.

The magnitude of the hodograph (3.2.2) is simply $|\mathbf{r}'(t)| = |\alpha(t)|^2 + |\beta(t)|^2$ but the orientational dependence of $\mathbf{r}'(t)$ on $\alpha(t)$ and $\beta(t)$ has a less–intuitive interpretation than the quaternion model. Writing $\mathcal{A}(t) = |\mathcal{A}(t)|\,(\cos\frac{1}{2}\theta(t) + \sin\frac{1}{2}\theta(t)\,\mathbf{n}(t))$ in the latter context, we may identify $|\mathcal{A}(t)|^2$ as the magnitude of the hodograph $\mathbf{r}'(t)$, while its orientation is obtained by rotating the vector $\mathbf{i}$ through angle $\theta(t)$ about the unit vector $\mathbf{n}(t)$ — see Appendix B.

3.3 CONVERSION BETWEEN REPRESENTATIONS

By identifying the imaginary unit i with the quaternion basis element $\mathbf{i}$, the polynomial $\mathcal{A}(t) = u(t) + v(t)\,\mathbf{i} + p(t)\,\mathbf{j} + q(t)\,\mathbf{k}$ in the quaternion form (3.1.8) can be expressed in terms of the complex polynomials $\boldsymbol{\alpha}(t) = u(t) + \mathrm{i}\,v(t)$ and $\boldsymbol{\beta}(t) = q(t) + \mathrm{i}\,p(t)$ in the Hopf map form (3.2.2) as

$$\mathcal{A}(t) \;=\; \boldsymbol{\alpha}(t) \,+\, \mathbf{k}\,\boldsymbol{\beta}(t)\,. \tag{3.3.1}$$

Conversely, we can obtain $\boldsymbol{\alpha}(t)$ and $\boldsymbol{\beta}(t)$ from $\mathcal{A}(t)$ through the expressions

$$\boldsymbol{\alpha}(t) \;=\; \tfrac{1}{2}\,[\,\mathcal{A}(t) - \mathbf{i}\,\mathcal{A}(t)\,\mathbf{i}\,]\,, \qquad \boldsymbol{\beta}(t) \;=\; -\,\tfrac{1}{2}\,\mathbf{k}\,[\,\mathcal{A}(t) + \mathbf{i}\,\mathcal{A}(t)\,\mathbf{i}\,]\,. \tag{3.3.2}$$

Of course, expressions (3.3.1) and (3.3.2) are actually specific instances among the one–parameter family of quaternion polynomials $\mathcal{A}(t)$ or complex polynomial pairs $\boldsymbol{\alpha}(t)$, $\boldsymbol{\beta}(t)$ that define a given hodograph $\mathbf{r}'(t)$ through (3.1.8) or (3.2.2).

Given a Pythagorean hodograph $\mathbf{r}'(t) = (x'(t), y'(t), z'(t))$ the quaternion pre–image $\mathcal{A}(t)$ under the map $\mathbb{H} \to \mathbb{R}^3$ defined by (3.1.8) is the solution of a quaternion equation of the form (B.2.11) in Appendix B. Hence, from (B.2.12), $\mathcal{A}(t)$ can be expressed as

$$\mathcal{A}(t) \;=\; \sqrt{\sigma(t)}\,\mathbf{v}(t)\,(\cos\phi + \sin\phi\,\mathbf{i})\,, \tag{3.3.3}$$

where $\sigma(t) = |\mathbf{r}'(t)|$, $\mathbf{v}(t) = (\sigma(t)\mathbf{i} + \mathbf{r}'(t))/(|\sigma(t)\mathbf{i} + \mathbf{r}'(t)|)$, and ϕ is a free angular parameter. For each t, the above relation identifies the pre–image of a given point $\mathbf{r}'(t)$ in $\mathbb{R}^3$ as a circle in the quaternion space $\mathbb{H}$, traced by increasing ϕ from 0 to 2π. From (3.3.2), for the Hopf map $H : \mathbb{C} \times \mathbb{C} \to \mathbb{R}^3$, the one–parameter family of pre–image complex polynomials $\boldsymbol{\alpha}(t)$, $\boldsymbol{\beta}(t)$ is given in terms of the free angular parameter ϕ by

$$\begin{aligned}
\boldsymbol{\alpha}(t) &= \tfrac{1}{2}\,\sqrt{\sigma(t)}\,[\,\mathbf{v}(t)\,(\cos\phi + \sin\phi\,\mathbf{i}) - \mathbf{i}\,\mathbf{v}(t)\,(\cos\phi + \sin\phi\,\mathbf{i})\,\mathbf{i}\,]\,,\\
\boldsymbol{\beta}(t) &= -\,\tfrac{1}{2}\,\sqrt{\sigma(t)}\,\mathbf{k}\,[\,\mathbf{v}(t)\,(\cos\phi + \sin\phi\,\mathbf{i}) + \mathbf{i}\,\mathbf{v}(t)\,(\cos\phi + \sin\phi\,\mathbf{i})\,\mathbf{i}\,]\,.
\end{aligned}$$

Expanding equation (3.3.3), we obtain

$$\begin{aligned}
\mathcal{A}(t) \;=& \frac{\sqrt{\sigma(t)}}{|\sigma(t)\,\mathbf{i} + \mathbf{r}'(t)|}\,\big[-(\sigma(t) + x'(t))\sin\phi + (\sigma(t) + x'(t))\cos\phi\,\mathbf{i}\\
&+(y'(t)\cos\phi + z'(t)\sin\phi)\,\mathbf{j} + (z'(t)\cos\phi - y'(t)\sin\phi)\,\mathbf{k}\big]
\end{aligned}$$

and consequently,

$$\begin{aligned}
\boldsymbol{\alpha}(t) =& \frac{\sqrt{\sigma(t)}}{|\sigma(t)\,\mathbf{i} + \mathbf{r}'(t)|}\,(\sigma(t) + x'(t))(-\sin\phi + \mathrm{i}\,\cos\phi)\,,\\
\boldsymbol{\beta}(t) =& \frac{\sqrt{\sigma(t)}}{|\sigma(t)\,\mathbf{i} + \mathbf{r}'(t)|}\,[\,(z'(t)\cos\phi - y'(t)\sin\phi\,) +\\
&\mathrm{i}\,(\,y'(t)\cos\phi + z'(t)\sin\phi)\,]\,.
\end{aligned}$$

3.4 DEGENERATE SPATIAL PH CURVES

Integrating the hodograph (3.0.2) may yield *linear* or *planar* PH curves as special cases. Since we are interested in generic PH curves (i.e., true space curves), we need criteria to identify such degenerate cases. For this purpose we use primarily the quaternion form (3.1.8), but also express the results in terms of the Hopf map form (3.2.2).

Linear degenerations of spatial PH curves correspond to vanishing of the curvature $\kappa = \sigma^{-3}|\,\mathbf{r}' \times \mathbf{r}''\,|$, and in [22] it was shown that all spatial PH curves satisfy

$$|\,\mathbf{r}'(t) \times \mathbf{r}''(t)\,|^2 \;=\; \sigma^2(t)\rho(t)\,, \tag{3.4.1}$$

where the polynomial ρ may be specified as

$$\rho(t) \;=\; |\mathbf{r}''(t)|^2 \;-\; \sigma'^2(t)\,,$$

that is [37],

$$\begin{aligned}\rho \;=\; 4\,[\,&(up' - u'p)^2 \,+\, (uq' - u'q)^2 \,+\, (vp' - v'p)^2 \,+\, (vq' - v'q)^2 \\ &+\, 2(uv' - u'v)(pq' - p'q)\,]\,.\end{aligned} \tag{3.4.2}$$

The condition for degeneration to a straight line is thus equivalent to $\rho(t) \equiv 0$. For a degree–n PH curve, $\rho(t)$ is of degree $2n-6$ and is therefore a constant for PH cubics, and a quartic for PH quintics [24].

Planar degenerations of spatial PH curves correspond to vanishing of the torsion and hence of the polynomial $(\mathbf{r}'(t) \times \mathbf{r}''(t)) \cdot \mathbf{r}'''(t)$. For a degree–$n$ PH curve, this polynomial is generally of degree $3n-9$. For PH cubics, it reduces to a constant, while for PH quintics $(\mathbf{r}'(t) \times \mathbf{r}''(t)) \cdot \mathbf{r}'''(t)$ is a polynomial of degree 6.

Propositions 3.1 and 3.2 below state precise conditions for linear and planar degeneration of spatial PH curves in terms of the quaternion model. For the proofs, we refer the reader to Section 22.2 of [24]. In Remarks 3.3 and 3.4, these conditions are translated into the Hopf map model.

Proposition 3.1. *Let $\mathcal{A}_1$ be expressed in terms of $\mathcal{A}_0$ $(\neq 0)$ as*

$$\mathcal{A}_1 \;=\; \mathcal{A}_0\,(\alpha + \beta\,\mathbf{i} + \gamma\,\mathbf{j} + \delta\,\mathbf{k})\,. \tag{3.4.3}$$

Then the spatial PH cubic defined by substituting (3.1.3) *into* (3.1.8) *and integrating degenerates to a straight line if and only if $\gamma = \delta = 0$, and to a planar curve other than a straight line if and only if $\beta = 0$ and $(\gamma, \delta) \neq (0, 0)$.*

Remark 3.3. In the Hopf map model, one can easily verify that the conditions of Proposition 3.1 are equivalent to requiring the Bernstein coefficients of the complex polynomials $\boldsymbol{\alpha}(t)$, $\boldsymbol{\beta}(t)$ to satisfy $\boldsymbol{\alpha}_1 : \boldsymbol{\beta}_1 = \boldsymbol{\alpha}_0 : \boldsymbol{\beta}_0$ for degeneration to a straight line, and $\boldsymbol{\alpha}_1 = \lambda\,\boldsymbol{\alpha}_0 - \mathbf{z}\,\overline{\boldsymbol{\beta}}_0$and $\boldsymbol{\beta}_1 = \lambda\,\boldsymbol{\beta}_0 + \mathbf{z}\,\overline{\boldsymbol{\alpha}}_0$ with λ real and $\mathbf{z}$ complex for degeneration to a planar curve other than a straight line.

For spatial PH quintics, the condition for degeneration to a straight line is a direct generalization of that for spatial PH cubics, but the planarity condition is somewhat more subtle.

Proposition 3.2. *Let $\mathcal{A}_1, \mathcal{A}_2$ be expressed in terms of $\mathcal{A}_0$ ($\neq 0$) as*

$$\mathcal{A}_1 = \mathcal{A}_0 (\alpha_1 + \beta_1 \mathbf{i} + \gamma_1 \mathbf{j} + \delta_1 \mathbf{k}), \quad \mathcal{A}_2 = \mathcal{A}_0 (\alpha_2 + \beta_2 \mathbf{i} + \gamma_2 \mathbf{j} + \delta_2 \mathbf{k}). \tag{3.4.4}$$

Then the spatial PH quintic specified by (3.1.8) *and* (3.1.4) *is a straight line if and only if $\gamma_1 = \gamma_2 = \delta_1 = \delta_2 = 0$, and a plane curve other than a straight line if and only if $\beta_1 = \beta_2 = \gamma_1\delta_2 - \gamma_2\delta_1 = 0$ with $\gamma_1, \gamma_2, \delta_1, \delta_2$ not all zero, provided that $\gcd(x', y', z')$ is a non–zero constant in (3.1.8).*

Remark 3.4. The conditions of Proposition 3.2 for degeneration to a straight line are equivalent to requiring the Bernstein coefficients of the polynomials $\boldsymbol{\alpha}(t)$, $\boldsymbol{\beta}(t)$ in the Hopf map model to satisfy $\boldsymbol{\alpha}_2 : \boldsymbol{\beta}_2 = \boldsymbol{\alpha}_1 : \boldsymbol{\beta}_1 = \boldsymbol{\alpha}_0 : \boldsymbol{\beta}_0$. For degeneration to a planar curve other than a straight line, the conditions stated in Proposition 3.2 translate into $\boldsymbol{\alpha}_1 = \lambda_1 \boldsymbol{\alpha}_0 - \mu_1 \mathbf{z}\, \overline{\boldsymbol{\beta}}_0$, $\boldsymbol{\alpha}_2 = \lambda_2 \boldsymbol{\alpha}_0 - \mu_2 \mathbf{z}\, \overline{\boldsymbol{\beta}}_0$ and $\boldsymbol{\beta}_1 = \lambda_1 \boldsymbol{\beta}_0 + \mu_1 \mathbf{z}\, \overline{\boldsymbol{\alpha}}_0$, $\boldsymbol{\beta}_2 = \lambda_2 \boldsymbol{\beta}_0 + \mu_2 \mathbf{z}\, \overline{\boldsymbol{\alpha}}_0$ with $\lambda_1, \lambda_2, \mu_1, \mu_2$ real and $\mathbf{z}$ complex, provided that the hodograph (3.2.2) is primitive.

A general condition for degeneration to a line — which easily explains the first part of Propositions 3.1 and 3.2 — was recently introduced in [44].

4

CURVES WITH RATIONAL FRENET FRAME

Rational forms are always preferred in computer–aided design whenever possible, since they are exactly compatible with the representation of most CAD systems and permit efficient computations. In general, however, both the Frenet adapted frame defined in (1.2.1) and the rotation–minimizing adapted frame that satisfies (1.3.6), are not rational, even for Pythagorean–hodograph curves.

As outlined in the previous chapter, the unit tangent $\mathbf{t}$ to a polynomial curve has a rational dependence on the parameter if and only if the curve hodograph is Pythagorean. However, the principal normal $\mathbf{n}$ and binormal $\mathbf{b}$ defined by (1.2.1) are not, in general, rational unit vectors since the quantity $|\mathbf{r}' \times \mathbf{r}''|$ generically incurs the square root of a polynomial. Likewise, the curvature κ given by (1.2.4) does not, in general, have a rational dependence on t (although the torsion τ does). To secure a rational dependence of $(\mathbf{t}, \mathbf{n}, \mathbf{b})$ and κ, τ on the curve parameter, we must consider the *double* PH (DPH) curves by studying the structure of $|\mathbf{r}' \times \mathbf{r}''|$ in greater detail.

The double PH condition is discussed in Section 4.1, and analyzed in the context of the quaternion and Hopf map models of spatial PH curves in Sections 4.2 and 4.3, respectively. A categorization of all DPH curve types up to degree 7 is developed in Section 4.4, by using the Hopf map form to show systems of equations and constraints needed for their constructions. A selection of computed examples of each DPH curve type is included, to highlight their attractive features.

4.1 CHARACTERIZATION OF DOUBLE PH CURVES

By substituting from (3.0.2) into

$$|\mathbf{r}' \times \mathbf{r}''|^2 = (y'z'' - y''z')^2 + (z'x'' - z''x')^2 + (x'y'' - x''y')^2 , \quad (4.1.1)$$

one may directly verify equation (3.4.1) with $\rho(t)$ given by (3.4.2). The polynomial ρ can be written in terms of the polynomials u, v, p, q and their derivatives u', v', p', q' in several different ways. For example, it can be written [24] as

$$\begin{aligned} \rho \;=\; 4\,[\,&(uv' - u'v + pq' - p'q)^2 \,+\, (up' - u'p - vq' + v'q)^2 \\ &+ (uq' - u'q + vp' - v'p)^2 \,-\, (uv' - u'v - pq' + p'q)^2\,] , \end{aligned}$$

or as a sum of just two squares,

$$\rho \;=\; 4\,[\,(up' - u'p + vq' - v'q)^2 \,+\, (uq' - u'q - vp' + v'p)^2\,] . \quad (4.1.2)$$

The importance of form (4.1.2) is that it allows to characterize the conditions under which $\rho(t)$ is a perfect square, and thus the Frenet adapted frame $(\mathbf{t}, \mathbf{n}, \mathbf{b})$ and the curvature κ and torsion τ all have a *rational* dependence on the curve parameter t.

Remark 4.1. Geometrically, degenerate spatial PH curves are characterized by collinear or coplanar Bézier control points, and they are trivially double PH curves. For the linear case, $\mathbf{r}'$ and $\mathbf{r}''$ are always parallel, so $|\,\mathbf{r}' \times \mathbf{r}''\,| \equiv 0$. In the planar case, we can choose coordinates such that $z' \equiv 0$ and $z'' \equiv 0$, so $|\,\mathbf{r}' \times \mathbf{r}''\,|^2$ becomes the perfect square $(x'y'' - x''y')^2$.

A polynomial space curve $\mathbf{r}(t)$ is said to be a "double PH curve" if $|\,\mathbf{r}'(t)\,|$ and $|\,\mathbf{r}'(t) \times \mathbf{r}''(t)\,|$ are both *polynomial* functions of t — i.e., if the conditions

$$|\,\mathbf{r}'\,|^2 \;=\; x'^2 + y'^2 + z'^2 \;\equiv\; \sigma^2\,, \tag{4.1.3}$$

$$|\,\mathbf{r}' \times \mathbf{r}''\,|^2 \;=\; (y'z'' - y''z')^2 + (z'x'' - z''x')^2 + (x'y'' - x''y')^2 \;\equiv\; (\sigma\omega)^2 \tag{4.1.4}$$

are simultaneously satisfied for some polynomials $\sigma(t)$, $\omega(t)$. In other words, in addition to the usual PH condition (4.1.3), for a double PH (or DPH) curve we require the polynomial ρ in the relation (3.4.1), satisfied by all PH curves, to be a perfect square: $\rho = \omega^2$ for some polynomial $\omega(t)$. Beltran and Monterde called such curves the "PH curves of second class" or "2–PH curves" [4], and they determined that the cubic and quintic double PH curves are exactly the *helical* PH curves [37] of equal degree — but double PH curves of degree 7 exist that are not helical, i.e., they do not satisfy (5.0.1) and (5.0.2) below.

For a double PH curve with $\rho(t) = \omega^2(t)$, the Frenet frame vectors and the curvature and torsion functions are given by the rational expressions

$$\mathbf{t} = \frac{\mathbf{r}'}{\sigma}\,, \quad \mathbf{n} = \frac{\sigma\mathbf{r}'' - \sigma'\mathbf{r}'}{\sigma\omega}\,, \quad \mathbf{b} = \frac{\mathbf{r}' \times \mathbf{r}''}{\sigma\omega}\,, \quad \kappa = \frac{\omega}{\sigma^2}\,, \quad \tau = \frac{(\mathbf{r}' \times \mathbf{r}'') \cdot \mathbf{r}'''}{\sigma^2\omega^2}\,. \tag{4.1.5}$$

Hence, the DPH curves may be regarded as the complete set of polynomial curves that have rational Frenet adapted frames [102].

Now for a PH curve of degree n, $\deg(\rho) = 2n - 6$. In the present context, the expression (4.1.2) for $\rho(t)$ as a sum of squares is the most interesting, since it implies [4] that to satisfy the second Pythagorean condition (4.1.4), the three polynomials $2(up' - u'p + vq' - v'q)$, $2(uq' - u'q - vp' + v'p)$, ω must comprise a Pythagorean triple, satisfying

$$4\,[\,(up' - u'p + vq' - v'q)^2 \;+\; (uq' - u'q - vp' + v'p)^2\,] \;\equiv\; \omega^2\,. \tag{4.1.6}$$

The solutions of this equation must be [66] of the form

$$\begin{aligned} up' - u'p + vq' - v'q \;&=\; h(a^2 - b^2)\,, \\ uq' - u'q - vp' + v'p \;&=\; 2hab\,, \\ \omega \;&=\; 2h(a^2 + b^2)\,, \end{aligned} \tag{4.1.7}$$

for polynomials $h(t)$, $a(t)$, $b(t)$ with $\gcd(a(t), b(t)) = \text{constant}$. For instances with $\gcd(up' - u'p + vq' - v'q, uq' - u'q - vp' + v'p) = \text{constant}$, we may take $h(t) = 1$, and we then have a *primitive* Pythagorean triple.

4.2 QUATERNION FORM OF DOUBLE PH CURVES

Consider a spatial PH curve with parametric speed and first two derivatives specified in terms of a quaternion polynomial $\mathcal{A}(t)$ by

$$\sigma(t) = |\mathcal{A}(t)|^2, \quad \mathbf{r}'(t) = \mathcal{A}(t)\,\mathbf{i}\,\mathcal{A}^*(t), \quad \mathbf{r}''(t) = \mathcal{A}'(t)\,\mathbf{i}\,\mathcal{A}^*(t) + \mathcal{A}(t)\,\mathbf{i}\,\mathcal{A}'^*(t).$$

Regarding $\mathbf{r}'(t)$ and $\mathbf{r}''(t)$ as pure vector quaternions, the quantity $\mathbf{r}'(t) \times \mathbf{r}''(t)$ is the vector part of their quaternion product, and it can be expressed as one half this product minus its conjugate. Thus, writing

$$2\,\mathbf{r}' \times \mathbf{r}'' \;=\; (\mathcal{A}\,\mathbf{i}\,\mathcal{A}^*)\,(\mathcal{A}'\,\mathbf{i}\,\mathcal{A}^* + \mathcal{A}\,\mathbf{i}\,\mathcal{A}'^*) \;-\; (\mathcal{A}'\,\mathbf{i}\,\mathcal{A}^* + \mathcal{A}\,\mathbf{i}\,\mathcal{A}'^*)^*\,(\mathcal{A}\,\mathbf{i}\,\mathcal{A}^*)^*$$

and simplifying, we obtain

$$2\,\mathbf{r}' \times \mathbf{r}'' \;=\; \mathcal{A}\,\mathbf{i}\,(\mathcal{A}^*\mathcal{A}' - \mathcal{A}'^*\mathcal{A})\,\mathbf{i}\,\mathcal{A}^* \;+\; \sigma\,(\mathcal{A}'\mathcal{A}^* - \mathcal{A}\mathcal{A}'^*)\,.$$

Now since $\sigma(t) = \mathcal{A}(t)\mathcal{A}^*(t) = \mathcal{A}^*(t)\mathcal{A}(t)$, we have

$$\sigma' \;=\; \mathcal{A}'\mathcal{A}^* + \mathcal{A}\,\mathcal{A}'^* \;=\; \mathcal{A}'^*\mathcal{A} + \mathcal{A}^*\mathcal{A}'\,,$$

and by invoking these relations we deduce that

$$\mathbf{r}' \times \mathbf{r}'' \;=\; \mathcal{A}\,\mathbf{i}\,\mathcal{A}^*\mathcal{A}'\,\mathbf{i}\,\mathcal{A}^* \;+\; \sigma\,\mathcal{A}'\mathcal{A}^*\,.$$

Using $\sigma(t) = \mathcal{A}(t)\mathcal{A}^*(t)$, we re–write this as

$$\mathbf{r}' \times \mathbf{r}'' \;=\; \mathcal{A}\left(\mathbf{i}\,\mathcal{A}^*\mathcal{A}'\,\mathbf{i} \;+\; \mathcal{A}^*\mathcal{A}'\right)\mathcal{A}^*\,.$$

Now for $\mathcal{A}(t) = u(t) + v(t)\,\mathbf{i} + p(t)\,\mathbf{j} + q(t)\,\mathbf{k}$, the products $\mathcal{A}^*\mathcal{A}'$ and $\mathbf{i}\,\mathcal{A}^*\mathcal{A}'\,\mathbf{i}$ are given by

$$\begin{aligned}
\mathcal{A}^*\mathcal{A}' \;&=\; (uu' + vv' + pp' + qq') \;+\; (uv' - u'v - pq' + p'q)\,\mathbf{i} \\
&\quad + (up' - u'p + vq' - v'q)\,\mathbf{j} \;+\; (uq' - u'q - vp' + v'p)\,\mathbf{k}\,, \\
\mathbf{i}\,\mathcal{A}^*\mathcal{A}'\,\mathbf{i} \;&=\; -\,(uu' + vv' + pp' + qq') \;-\; (uv' - u'v - pq' + p'q)\,\mathbf{i} \\
&\quad + (up' - u'p + vq' - v'q)\,\mathbf{j} \;+\; (uq' - u'q - vp' + v'p)\,\mathbf{k}\,,
\end{aligned}$$

so $\mathbf{i}\,\mathcal{A}^*(t)\mathcal{A}'(t)\,\mathbf{i} + \mathcal{A}^*(t)\mathcal{A}'(t)$ is just twice the $(\mathbf{j}, \mathbf{k})$ part of $\mathcal{A}^*(t)\mathcal{A}'(t)$. Thus, in terms of the polynomials

$$\begin{aligned}
f(t) &= u(t)p'(t) - u'(t)p(t) + v(t)q'(t) - v'(t)q(t)\,, \\
g(t) &= u(t)q'(t) - u'(t)q(t) - v(t)p'(t) - v'(t)p(t)\,,
\end{aligned}$$

appearing in (4.1.2), we have

$$\mathbf{r}'(t) \times \mathbf{r}''(t) \;=\; 2\,\mathcal{A}(t)\,[\,f(t)\,\mathbf{j} + g(t)\,\mathbf{k}\,]\,\mathcal{A}^*(t)\,, \tag{4.2.1}$$

and the squared modulus of this vector is

$$|\,\mathbf{r}'(t) \times \mathbf{r}''(t)\,|^2 \;=\; 4\,\sigma^2(t)\,[\,f^2(t) + g^2(t)\,]\,.$$

Hence, $|\,\mathbf{r}'(t) \times \mathbf{r}''(t)\,|$ is a polynomial in t if and only if the two polynomials $f(t)$, $g(t)$ are elements of a Pythagorean triple, and are thus [66] of the form

$$f(t) \;=\; h(t)\,[\,a^2(t) - b^2(t)\,]\,, \qquad g(t) \;=\; 2\,h(t)a(t)b(t)\,, \tag{4.2.2}$$

for polynomials $a(t)$, $b(t)$, $h(t)$ with $\gcd(a(t), b(t)) = \text{constant}$.

Note that, since the components of $\mathbf{r}'(t) \times \mathbf{r}''(t)$ satisfy the Pythagorean condition (4.1.4) if $\mathbf{r}(t)$ is a double PH curve, it must be expressible in the form[1] (3.1.12) in terms of a real polynomial $h(t)$ and a quaternion polynomial $\mathcal{B}(t)$. If $\mathbf{r}(t)$ is of degree n, we must have $\deg(\mathbf{r}' \times \mathbf{r}'') = 2n - 4 = \deg(h) + 2\deg(\mathcal{B})$.

Proposition 4.1. *For a DPH curve* $\mathbf{r}(t)$ *specified by a quaternion polynomial* (3.1.2) *satisfying the conditions* (4.1.6) *and* (4.1.7)*, the cross product* $\mathbf{r}'(t) \times \mathbf{r}''(t)$ *can be expressed in the quaternion Pythagorean form* (3.1.12) *with* $\mathcal{B}(t)$ *given by*

$$\mathcal{B}(t) \;=\; \mathcal{A}(t)\,\mathcal{C}(t)\,, \quad \text{where} \;\; \mathcal{C}(t) \;=\; -\,b(t) + a(t)\,\mathbf{i} + a(t)\,\mathbf{j} + b(t)\,\mathbf{k}\,. \tag{4.2.3}$$

Proof : Invoking the form (4.2.1), and multiplying both sides of

$$\mathcal{B}(t)\,\mathbf{i}\,\mathcal{B}^*(t) \;=\; 2\,\mathcal{A}(t)\,[\,(a^2(t) - b^2(t))\,\mathbf{j} + 2\,a(t)b(t)\,\mathbf{k}\,]\,\mathcal{A}^*(t) \tag{4.2.4}$$

on the left by $\mathcal{A}^*(t)$ and the right by $\mathcal{A}(t)$, we obtain

$$\mathcal{Q}(t)\,\mathbf{i}\,\mathcal{Q}^*(t) \;=\; 2\,\sigma^2(t)\,[\,(a^2(t) - b^2(t))\,\mathbf{j} + 2\,a(t)b(t)\,\mathbf{k}\,]\,,$$

where we set $\mathcal{Q}(t) = \mathcal{A}^*(t)\,\mathcal{B}(t)$. One may then deduce (see Appendix B) that the general solution to this equation has the form

$$\mathcal{Q} \;=\; \sigma\,\frac{((a^2 + b^2)\,\mathbf{i} + (a^2 - b^2)\,\mathbf{j} + 2ab\,\mathbf{k})}{\sqrt{a^2 + b^2}}\,(\cos\phi + \sin\phi\,\mathbf{i})\,,$$

where ϕ is a free angular parameter. Hence we obtain

$$\mathcal{B} \;=\; \mathcal{A}\,\frac{((a^2 + b^2)\,\mathbf{i} + (a^2 - b^2)\,\mathbf{j} + 2ab\,\mathbf{k})}{\sqrt{a^2 + b^2}}\,(\cos\phi + \sin\phi\,\mathbf{i})\,,$$

and in order to ensure that $\mathcal{B}(t)$ is a polynomial, we choose the dependence of ϕ on t defined by

$$\sin\phi(t) \;=\; \frac{b(t)}{\sqrt{a^2(t) + b^2(t)}}\,, \qquad \cos\phi(t) \;=\; \frac{a(t)}{\sqrt{a^2(t) + b^2(t)}}\,.$$

Substituting and simplifying, this gives the solution (4.2.3) for $\mathcal{B}(t)$. ∎

1 We assume here the generic form, appropriate to the case where the components of $\mathbf{r}'(t) \times \mathbf{r}''(t)$ are not necessarily relatively prime.

4.3 HOPF MAP FORM OF DOUBLE PH CURVES

The Hopf map form (3.2.2) constructs spatial Pythagorean hodographs from two complex polynomials $\alpha(t) = u(t) + i\,v(t)$, $\beta(t) = q(t) + i\,p(t)$. Forming the combination

$$\alpha\beta' - \alpha'\beta \;=\; (uq' - u'q - vp' + v'p) \;+\; i\,(up' - u'p + vq' - v'q) \quad (4.3.1)$$

of these polynomials, from (4.1.2) we obtain that

$$\rho(t) \;=\; 4\,|\,\alpha(t)\beta'(t) - \alpha'(t)\beta(t)\,|^2\,. \quad (4.3.2)$$

Thus, the DPH curves are spatial PH curves for which $|\alpha(t)\beta'(t) - \alpha'(t)\beta(t)|^2$ is the perfect square of a real polynomial. Due to its importance in the theory of double PH curves, we call $\alpha(t)\beta'(t) - \alpha'(t)\beta(t)$ the *proportionality polynomial* of $\alpha(t)$, $\beta(t)$. It vanishes identically if and only if $\alpha(t)$, $\beta(t)$ are (complex) constant multiples of each other (see also Lemma 3.1 in [44]). In the Hopf map representation, the curvature of spatial PH curves is given by

$$\kappa(t) \;=\; 2\,\frac{|\,\alpha(t)\beta'(t) - \alpha'(t)\beta(t)\,|}{(|\alpha(t)|^2 + |\beta(t)|^2)^2}\,,$$

so vanishing of (4.3.1) identifies degeneration to a straight line. When (4.3.1) does not vanish identically, its real roots (if any) identify *inflections* of a PH space curve, at which the normal vectors $\mathbf{n}$, $\mathbf{b}$ may suffer sudden reversals.

Now in the Hopf map representation, the conditions (4.1.7) for a spatial PH curve to be a *double* PH curve can be expressed as

$$\alpha(t)\beta'(t) - \alpha'(t)\beta(t) \;=\; h(t)\,\mathbf{w}^2(t) \quad (4.3.3)$$

for some real polynomial $h(t)$ and complex polynomial $\mathbf{w}(t) = a(t) + i\,b(t)$ with $\gcd(a(t), b(t)) = \text{constant}$, such that

$$\deg(h(t)) \;+\; 2\,\deg(\mathbf{w}(t)) \;=\; 2\,\deg(\alpha(t), \beta(t)) - 2. \quad (4.3.4)$$

Identifying $\mathbb{C}$ with $\mathbb{R}^2$, the complex polynomials $\alpha(t)$, $\beta(t)$ may be regarded as defining plane curves, and from the complex representation of planar PH curves [20] the expression on the right in (4.3.3) is seen to define a planar Pythagorean hodograph. These observations reveal the following connection between double (spatial) PH curves and planar PH curves.

Proposition 4.2. *A spatial PH curve specified through the Hopf map* (3.2.2) *by two complex polynomials* $\alpha(t)$, $\beta(t)$ *is a double PH curve if and only if their proportionality polynomial* (4.3.1) *defines a planar Pythagorean hodograph.*

One may deduce the Hopf map form of the polynomial (4.3.2) in the relation (3.4.1) directly, as follows. From (3.2.1) and (3.2.2) the components of $\mathbf{r}'(t)$ are written as

$$x'(t) = \boldsymbol{\alpha}(t)\overline{\boldsymbol{\alpha}}(t) - \boldsymbol{\beta}(t)\overline{\boldsymbol{\beta}}(t), \quad y'(t) + i z'(t) = 2\,\boldsymbol{\alpha}(t)\overline{\boldsymbol{\beta}}(t), \tag{4.3.5}$$

and differentiating then gives

$$x''(t) = \boldsymbol{\alpha}'(t)\overline{\boldsymbol{\alpha}}(t) + \boldsymbol{\alpha}(t)\overline{\boldsymbol{\alpha}}'(t) - \boldsymbol{\beta}'(t)\overline{\boldsymbol{\beta}}(t) - \boldsymbol{\beta}(t)\overline{\boldsymbol{\beta}}'(t), \tag{4.3.6}$$

$$y''(t) + i z''(t) = 2\,[\,\boldsymbol{\alpha}'(t)\overline{\boldsymbol{\beta}}(t) + \boldsymbol{\alpha}(t)\overline{\boldsymbol{\beta}}'(t)\,]. \tag{4.3.7}$$

Substituting from (4.3.5) and (4.3.6)–(4.3.7) into

$$y'z'' - y''z' = -\tfrac{1}{2}\,i\,[(y' - i z')(y'' + i z'') - (y' + i z')(y'' - i z'')\,],$$

$$(x'y'' - x''y') + i\,(z'x'' - z''x') = x'(y'' - i z'') - x''(y' - i z'),$$

and writing

$$\boldsymbol{\eta}(t) = \boldsymbol{\alpha}(t)\boldsymbol{\beta}'(t) - \boldsymbol{\alpha}'(t)\boldsymbol{\beta}(t), \tag{4.3.8}$$

after some manipulation one obtains

$$y'(t)z''(t) - y''(t)z'(t) = 2\,i\,[\,\overline{\boldsymbol{\alpha}}(t)\overline{\boldsymbol{\beta}}(t)\boldsymbol{\eta}(t) - \boldsymbol{\alpha}(t)\boldsymbol{\beta}(t)\overline{\boldsymbol{\eta}}(t)\,],$$

$$[\,x'(t)y''(t) - x''(t)y'(t)\,] + i\,[\,z'(t)x''(t) - z''(t)x'(t)\,] = 2\,[\,\overline{\boldsymbol{\alpha}}^2(t)\boldsymbol{\eta}(t) + \boldsymbol{\beta}^2(t)\overline{\boldsymbol{\eta}}(t)\,].$$

By direct substitution and simplification, one can then deduce that

$$\begin{aligned} |\,\mathbf{r}' \times \mathbf{r}''\,|^2 &= (y'z'' - y''z')^2 + (z'x'' - z''x')^2 + (x'y'' - x''y')^2 \\ &= 4\,|\overline{\boldsymbol{\alpha}}\,\overline{\boldsymbol{\beta}}\,\boldsymbol{\eta} - \boldsymbol{\alpha}\,\boldsymbol{\beta}\,\overline{\boldsymbol{\eta}}|^2 + 4\,|\overline{\boldsymbol{\alpha}}^2\boldsymbol{\eta} + \boldsymbol{\beta}^2\overline{\boldsymbol{\eta}}|^2 = 4\,(|\boldsymbol{\alpha}|^2 + |\boldsymbol{\beta}|^2)^2\,|\boldsymbol{\eta}|^2. \end{aligned}$$

Since $\sigma(t) = |\boldsymbol{\alpha}(t)|^2 + |\boldsymbol{\beta}(t)|^2$ in the Hopf map representation, we deduce that $\rho(t) = 4\,|\boldsymbol{\eta}(t)|^2$ where $\boldsymbol{\eta}(t)$ is defined by (4.3.8).

Assuming $\boldsymbol{\alpha}(t)$, $\boldsymbol{\beta}(t)$ and $h(t)$, $\mathbf{w}(t)$ are specified in Bernstein form as

$$\boldsymbol{\alpha}(t) = \sum_{l=0}^{m} \boldsymbol{\alpha}_l \binom{m}{l} (1-t)^{m-l} t^l, \quad \boldsymbol{\beta}(t) = \sum_{l=0}^{m} \boldsymbol{\beta}_l \binom{m}{l} (1-t)^{m-l} t^l,$$

$$h(t) = \sum_{l=0}^{d} h_l \binom{d}{l} (1-t)^{d-l} t^l, \quad \mathbf{w}(t) = \sum_{l=0}^{e} \mathbf{w}_l \binom{e}{l} (1-t)^{e-l} t^l,$$

where from (4.3.4) we must have $d + 2e = 2m - 2$, we now elucidate certain connections between the Hopf map and quaternion representations.

Remark 4.2. From the Hopf map form (4.3.2) of $\rho(t)$ and the condition (4.3.3) for a double PH curve we may infer that, for DPH curves, $\rho(t) = 4\,h^2(t)\,|\,\mathbf{w}(t)\,|^4$. Thus, the polynomial $\omega(t)$ defined for DPH curves by $\rho(t) = \omega^2(t)$ is simply $\omega(t) = 2\,h(t)\,|\,\mathbf{w}(t)\,|^2$. For *helical* curves, we deduce (see Remark 5.1 below) that the triple product $[\,\mathbf{r}'(t) \times \mathbf{r}''(t)\,] \cdot \mathbf{r}'''(t)$ is proportional to $(2\,h(t)\,|\,\mathbf{w}(t)\,|^2)^3$.

Remark 4.3. If $h(t)$ is a non–constant polynomial, we must have $h(t) \geqslant 0$ for all t in order to write $|\,\mathbf{r}'(t) \times \mathbf{r}''(t)\,| = 2\sigma(t)h(t)|\,\mathbf{w}(t)\,|^2$. Otherwise, if $h(t)$ is not non–negative for all t, we must replace $h(t)$ by $|h(t)|$ in the expression for $|\,\mathbf{r}'(t) \times \mathbf{r}''(t)\,|$, which is then the *absolute value* of a polynomial in t. In practice, the choice $h(t) =$ constant may be preferable—as with the case of *primitive* planar Pythagorean hodographs [42].

We conclude with two observations connecting the quaternion and Hopf map formulations of the double PH curves.

Remark 4.4. *(Quaternion form of proportionality polynomial.)* Identifying the imaginary unit i with the quaternion basis element $\mathbf{i}$, let the coefficients of $\boldsymbol{\alpha}(t)$ and $\boldsymbol{\beta}(t)$ be

$$\boldsymbol{\alpha}_l \;=\; \alpha_l \,+\, a_l\,\mathbf{i} \qquad \text{and} \qquad \boldsymbol{\beta}_l \;=\; \beta_l \,+\, b_l\,\mathbf{i}\,, \qquad l = 0, \ldots, m\,.$$

Then the Bernstein coefficients of the corresponding quaternion polynomial (3.1.2) defined by (3.3.1) are

$$\mathcal{A}_l \;=\; \boldsymbol{\alpha}_l \,+\, \mathbf{k}\,\boldsymbol{\beta}_l \;=\; (\alpha_l + a_l\,\mathbf{i}) + \mathbf{k}\,(\beta_l + b_l\,\mathbf{i}) \;=\; \alpha_l \,+\, a_l\,\mathbf{i} \,+\, b_l\,\mathbf{j} \,+\, \beta_l\,\mathbf{k}$$

for $l = 0, \ldots, m$. One can then verify that

$$\mathbf{j}\,(\boldsymbol{\alpha}_k\boldsymbol{\beta}_l - \boldsymbol{\alpha}_l\boldsymbol{\beta}_k) \;=\; \tfrac{1}{2}(\mathcal{A}_k^*\mathcal{A}_l - \mathcal{A}_l^*\mathcal{A}_k)\times\mathbf{i}\,, \tag{4.3.9}$$

and hence the proportionality polynomial $\boldsymbol{\alpha}(t)\boldsymbol{\beta}'(t) - \boldsymbol{\alpha}'(t)\boldsymbol{\beta}(t)$ in the Hopf map model is related to the quaternion polynomial $\mathcal{A}(t)$ by

$$\mathbf{j}\,[\,\boldsymbol{\alpha}(t)\boldsymbol{\beta}'(t) - \boldsymbol{\alpha}'(t)\boldsymbol{\beta}(t)\,] \;=\; \tfrac{1}{2}\,[\,\mathcal{A}^*(t)\mathcal{A}'(t) - \mathcal{A}'^*(t)\mathcal{A}(t)\,]\times\mathbf{i}\,. \tag{4.3.10}$$

Note here that $\frac{1}{2}\,[\,\mathcal{A}^*(t)\mathcal{A}'(t) - \mathcal{A}'^*(t)\mathcal{A}(t)\,] = \mathrm{vect}(\mathcal{A}^*(t)\mathcal{A}'(t))$ is a pure vector quaternion, and equation (4.3.10) amounts to identifying the real and imaginary parts of $\boldsymbol{\alpha}(t)\boldsymbol{\beta}'(t) - \boldsymbol{\alpha}'(t)\boldsymbol{\beta}(t)$ with the $\mathbf{k}$ and $\mathbf{j}$ components of $\mathcal{A}^*(t)\mathcal{A}'(t)$.

Remark 4.5. *(Quaternion form of double PH condition.)* Identifying again the imaginary unit i with the quaternion basis element $\mathbf{i}$, the complex polynomial $\mathbf{w}(t) = a(t) + b(t)\,\mathbf{i}$ and the quaternion polynomial $\mathcal{C}(t)$ introduced in (4.2.3) satisfy

$$\tfrac{1}{2}\,\mathcal{C}(t)\,\mathbf{i}\,\mathcal{C}^*(t) \;=\; (a^2(t) - b^2(t))\,\mathbf{j} \,+\, 2\,a(t)b(t)\,\mathbf{k} \;=\; \mathbf{w}^2(t)\,\mathbf{j}\,.$$

Hence, using (4.3.10), the DPH condition (4.3.3) in the Hopf map model can be written in quaternion form as

$$\begin{aligned}(\tfrac{1}{2}\,[\,\mathcal{A}^*(t)\mathcal{A}'(t)-\mathcal{A}'^*(t)\mathcal{A}(t)\,]\times\mathbf{i})\,\mathbf{j} \;&=\; \mathbf{j}\,\big(\boldsymbol{\alpha}(t)\boldsymbol{\beta}'(t)-\boldsymbol{\alpha}'(t)\boldsymbol{\beta}(t)\big)\,\mathbf{j}\\ &=\; h(t)\,\mathbf{j}\,\mathbf{w}^2(t)\,\mathbf{j} \;=\; \tfrac{1}{2}\,h(t)\,\mathbf{j}\,\mathcal{C}(t)\,\mathbf{i}\,\mathcal{C}^*(t)\,.\end{aligned}$$

This relation can be more conveniently expressed in the form

$$[\,\mathcal{A}^*(t)\mathcal{A}'(t)-\mathcal{A}'^*(t)\mathcal{A}(t)\,]\times\mathbf{i} \;=\; h(t)\,\mathcal{D}(t)\,\mathbf{i}\,\mathcal{D}^*(t)\,, \tag{4.3.11}$$

where we define

$$\mathcal{D}(t) \;=\; \mathbf{j}\,\mathcal{C}(t) \;=\; -\,a(t)+b(t)\,\mathbf{i}-b(t)\,\mathbf{j}-a(t)\,\mathbf{k}\,. \tag{4.3.12}$$

Hence, a spatial PH curve specified through (3.1.8) by a quaternion polynomial $\mathcal{A}(t)$ is a DPH curve if and only if the relation (4.3.11) holds for some quaternion polynomial $\mathcal{D}(t)$ of the special form (4.3.12).

4.4 CLASSIFICATION OF LOW-DEGREE DPH CURVES

Following [4] and [70], greater emphasis will be placed here on expression (4.3.3) of the double PH condition in the Hopf map model. The proportionality polynomial $\boldsymbol{\alpha}(t)\boldsymbol{\beta}'(t)-\boldsymbol{\alpha}'(t)\boldsymbol{\beta}(t)$, introduced in Section 4.3, plays a prominent role in the ensuing discussion. In Section 4.4.1 we review how the proportionality polynomial for all PH cubics, and all *helical* PH quintics, satisfies the DPH condition (4.3.3), and Section 4.4.2 then discusses the case of degree 7 DPH curves.

4.4.1 *Double PH cubics and quintics*

Spatial PH cubics are defined by two linear complex polynomials $\boldsymbol{\alpha}(t)$, $\boldsymbol{\beta}(t)$. In this case, since

$$\boldsymbol{\alpha}(t)\boldsymbol{\beta}'(t)-\boldsymbol{\alpha}'(t)\boldsymbol{\beta}(t) \;=\; \boldsymbol{\alpha}_0\boldsymbol{\beta}_1-\boldsymbol{\alpha}_1\boldsymbol{\beta}_0$$

is just a complex constant, we must have $\deg(h(t))=0$ and $\deg(\mathbf{w}(t))=0$ to satisfy (4.3.3). We may, without loss of generality, take $h(t)=1$ and $\mathbf{w}(t)=\mathbf{w}_0$, and the double PH condition then amounts to

$$\boldsymbol{\alpha}_0\boldsymbol{\beta}_1-\boldsymbol{\alpha}_1\boldsymbol{\beta}_0 \;=\; \mathbf{w}_0^2\,.$$

Clearly, this is satisfied for arbitrary complex values $\boldsymbol{\alpha}_0$, $\boldsymbol{\alpha}_1$, $\boldsymbol{\beta}_0$, $\boldsymbol{\beta}_1$ by taking either of the complex values $\sqrt{\boldsymbol{\alpha}_0\boldsymbol{\beta}_1-\boldsymbol{\alpha}_1\boldsymbol{\beta}_0}$ for $\mathbf{w}_0$. Hence *every* spatial PH cubic is a double PH curve — and is also a helical curve [43].

Spatial PH quintics are defined by quadratic polynomials $\boldsymbol{\alpha}(t)$, $\boldsymbol{\beta}(t)$. In this case, the proportionality polynomial (4.3.1) is the quadratic

$$2\,(\boldsymbol{\alpha}_0\boldsymbol{\beta}_1 - \boldsymbol{\alpha}_1\boldsymbol{\beta}_0)\,(1-t)^2 \;+\; (\boldsymbol{\alpha}_0\boldsymbol{\beta}_2 - \boldsymbol{\alpha}_2\boldsymbol{\beta}_0)\,2(1-t)t \;+\; 2\,(\boldsymbol{\alpha}_1\boldsymbol{\beta}_2 - \boldsymbol{\alpha}_2\boldsymbol{\beta}_1)\,t^2$$

and satisfaction of the double PH condition (4.3.3) can be achieved with either (a) $\deg(h(t)) = 0$ and $\deg(\mathbf{w}(t)) = 1$; or (b) $\deg(h(t)) = 2$ and $\deg(\mathbf{w}(t)) = 0$.

The case $\deg(h) = 0$ *and* $\deg(\mathbf{w}) = 1$

Choosing $h(t) = 1$ and a linear polynomial with Bernstein coefficients $\mathbf{w}_0, \mathbf{w}_1$ for $\mathbf{w}(t)$ in (4.3.3) for case (a), we obtain the equations

$$2\,(\boldsymbol{\alpha}_0\boldsymbol{\beta}_1 - \boldsymbol{\alpha}_1\boldsymbol{\beta}_0) = \mathbf{w}_0^2, \quad (\boldsymbol{\alpha}_0\boldsymbol{\beta}_2 - \boldsymbol{\alpha}_2\boldsymbol{\beta}_0) = \mathbf{w}_0\mathbf{w}_1, \quad 2\,(\boldsymbol{\alpha}_1\boldsymbol{\beta}_2 - \boldsymbol{\alpha}_2\boldsymbol{\beta}_1) = \mathbf{w}_1^2\,.$$

These equations can be satisfied for some $\mathbf{w}_0$, $\mathbf{w}_1$ if and only if the coefficients of $\boldsymbol{\alpha}(t)$, $\boldsymbol{\beta}(t)$ satisfy

$$4\,(\boldsymbol{\alpha}_0\boldsymbol{\beta}_1 - \boldsymbol{\alpha}_1\boldsymbol{\beta}_0)\,(\boldsymbol{\alpha}_1\boldsymbol{\beta}_2 - \boldsymbol{\alpha}_2\boldsymbol{\beta}_1) \;=\; (\boldsymbol{\alpha}_0\boldsymbol{\beta}_2 - \boldsymbol{\alpha}_2\boldsymbol{\beta}_0)^2\,.$$

The case $\deg(h) = 2$ *and* $\deg(\mathbf{w}) = 0$

Taking a quadratic with Bernstein coefficients h_0, h_1, h_2 for $h(t)$ and $\mathbf{w}(t) = \mathbf{w}_0$ in case (b), and equating coefficients of the quadratic polynomials on the left and right in (4.3.3), yields the system of equations

$$2\,(\boldsymbol{\alpha}_0\boldsymbol{\beta}_1 - \boldsymbol{\alpha}_1\boldsymbol{\beta}_0) = h_0\mathbf{w}_0^2, \;\; (\boldsymbol{\alpha}_0\boldsymbol{\beta}_2 - \boldsymbol{\alpha}_2\boldsymbol{\beta}_0) = h_1\mathbf{w}_0^2, \;\; 2\,(\boldsymbol{\alpha}_1\boldsymbol{\beta}_2 - \boldsymbol{\alpha}_2\boldsymbol{\beta}_1) = h_2\mathbf{w}_0^2$$

which can be satisfied if and only if

$$\arg(\boldsymbol{\alpha}_0\boldsymbol{\beta}_1 - \boldsymbol{\alpha}_1\boldsymbol{\beta}_0) = \arg(\boldsymbol{\alpha}_0\boldsymbol{\beta}_2 - \boldsymbol{\alpha}_2\boldsymbol{\beta}_0) = \arg(\boldsymbol{\alpha}_1\boldsymbol{\beta}_2 - \boldsymbol{\alpha}_2\boldsymbol{\beta}_1) \quad (\mathrm{mod}\ \pi)$$

— i.e., the complex numbers $\boldsymbol{\alpha}_0\boldsymbol{\beta}_1 - \boldsymbol{\alpha}_1\boldsymbol{\beta}_0$, $\boldsymbol{\alpha}_0\boldsymbol{\beta}_2 - \boldsymbol{\alpha}_2\boldsymbol{\beta}_0$, $\boldsymbol{\alpha}_1\boldsymbol{\beta}_2 - \boldsymbol{\alpha}_2\boldsymbol{\beta}_1$ must be *real multiples* of each other in this case.

4.4.2 *Double PH curves of degree 7*

Spatial PH curves of degree 7 are specified by two cubic complex polynomials $\boldsymbol{\alpha}(t)$, $\boldsymbol{\beta}(t)$. In this case, the proportionality polynomial (4.3.1) is the quartic

$$\begin{aligned}
&\quad 3\,(\boldsymbol{\alpha}_0\boldsymbol{\beta}_1 - \boldsymbol{\alpha}_1\boldsymbol{\beta}_0)\,(1-t)^4 \\
&+\; \tfrac{3}{2}\,(\boldsymbol{\alpha}_0\boldsymbol{\beta}_2 - \boldsymbol{\alpha}_2\boldsymbol{\beta}_0)\,4(1-t)^3 t \\
&+\; [\,\tfrac{1}{2}\,(\boldsymbol{\alpha}_0\boldsymbol{\beta}_3 - \boldsymbol{\alpha}_3\boldsymbol{\beta}_0) + \tfrac{3}{2}\,(\boldsymbol{\alpha}_1\boldsymbol{\beta}_2 - \boldsymbol{\alpha}_2\boldsymbol{\beta}_1)\,]\,6(1-t)^2 t^2 \\
&+\; \tfrac{3}{2}\,(\boldsymbol{\alpha}_1\boldsymbol{\beta}_3 - \boldsymbol{\alpha}_3\boldsymbol{\beta}_1)\,4(1-t)t^3 \\
&+\; 3\,(\boldsymbol{\alpha}_2\boldsymbol{\beta}_3 - \boldsymbol{\alpha}_3\boldsymbol{\beta}_2)\,t^4\,,
\end{aligned}$$

and (4.3.3) may be satisfied with either (a) $\deg(h(t)) = 0$ and $\deg(\mathbf{w}(t)) = 2$; or (b) $\deg(h(t)) = 2$ and $\deg(\mathbf{w}(t)) = 1$; or (c) $\deg(h(t)) = 4$ and $\deg(\mathbf{w}(t)) = 0$. Note that the six complex values $\alpha_i\beta_j - \alpha_j\beta_i$ for $0 \leqslant i, j \leqslant 3$ occurring in the coefficients of $\alpha(t)\beta'(t) - \alpha'(t)\beta(t)$ are not independent: they must satisfy the *compatibility condition*

$$\begin{aligned}(\alpha_0\beta_1 - \alpha_1\beta_0)(\alpha_2\beta_3 - \alpha_3\beta_2) \;=\; & \\ (\alpha_0\beta_2 - \alpha_2\beta_0)(\alpha_1\beta_3 - \alpha_3\beta_1) - (\alpha_1\beta_2 - \alpha_2\beta_1)(\alpha_0\beta_3 - \alpha_3\beta_0)\,.&\end{aligned} \tag{4.4.1}$$

For the above mentioned combinations of the degrees of $h(t)$ and $\mathbf{w}(t)$ in (4.3.3), we now illustrate methods for the construction of DPH curves with a selection of computed examples.

The case $\deg(h) = 0$ *and* $\deg(\mathbf{w}) = 2$

If we choose $h(t) = 1$ and a quadratic with Bernstein coefficients $\mathbf{w}_0$, $\mathbf{w}_1$, $\mathbf{w}_2$ for $\mathbf{w}(t)$ in case (a), we obtain from (4.3.3) the equations

$$\begin{aligned} 3\,(\alpha_0\beta_1 - \alpha_1\beta_0) &= \mathbf{w}_0^2\,,\\ 3\,(\alpha_0\beta_2 - \alpha_2\beta_0) &= 2\,\mathbf{w}_0\mathbf{w}_1\,,\\ (\alpha_0\beta_3 - \alpha_3\beta_0) + 3\,(\alpha_1\beta_2 - \alpha_2\beta_1) &= \tfrac{2}{3}\,(2\,\mathbf{w}_1^2 + \mathbf{w}_0\mathbf{w}_2)\,,\\ 3\,(\alpha_1\beta_3 - \alpha_3\beta_1) &= 2\,\mathbf{w}_1\mathbf{w}_2\,,\\ 3\,(\alpha_2\beta_3 - \alpha_3\beta_2) &= \mathbf{w}_2^2\,. \end{aligned} \tag{4.4.2}$$

Setting $\alpha_1\beta_2 - \alpha_2\beta_1 = \mathbf{z}$, $\alpha_0\beta_3 - \alpha_3\beta_0 = \frac{4}{3}\mathbf{w}_1^2 + \frac{2}{3}\mathbf{w}_0\mathbf{w}_2 - 3\mathbf{z}$, and invoking (4.4.1), we note that the values $\mathbf{w}_0$, $\mathbf{w}_1$, $\mathbf{w}_2$ and $\mathbf{z}$ must satisfy

$$\left(\tfrac{1}{3}\mathbf{w}_0^2\right)\left(\tfrac{1}{3}\mathbf{w}_2^2\right) \;=\; \left(\tfrac{2}{3}\mathbf{w}_0\mathbf{w}_1\right)\left(\tfrac{2}{3}\mathbf{w}_1\mathbf{w}_2\right) - \mathbf{z}\,\left(\tfrac{4}{3}\mathbf{w}_1^2 + \tfrac{2}{3}\mathbf{w}_0\mathbf{w}_2 - 3\mathbf{z}\right)\,,$$

which reduces to the quadratic equation

$$27\,\mathbf{z}^2 \;-\; \left(12\,\mathbf{w}_1^2 + 6\,\mathbf{w}_0\mathbf{w}_2\right)\,\mathbf{z} \;+\; \left(4\,\mathbf{w}_1^2 - \mathbf{w}_0\mathbf{w}_2\right)\mathbf{w}_0\mathbf{w}_2 \;=\; 0$$

in $\mathbf{z}$. The solutions of this equation indicate that, in this case, $\alpha_1\beta_2 - \alpha_2\beta_1$ must be given in terms of $\mathbf{w}_0$, $\mathbf{w}_1$, $\mathbf{w}_2$ by

$$\alpha_1\beta_2 - \alpha_2\beta_1 \;=\; \tfrac{1}{3}\,\mathbf{w}_0\mathbf{w}_2 \quad \text{or} \quad \tfrac{1}{9}(4\,\mathbf{w}_1^2 - \mathbf{w}_0\mathbf{w}_2)\,. \tag{4.4.3}$$

Example 4.1. In equations (4.4.2) we choose the numerical values

$$h_0 = 1\,, \quad \mathbf{w}_0 = 1\,, \quad \mathbf{w}_1 = 1 + i\,, \quad \mathbf{w}_2 = i\,.$$

Assigning values to α_0, α_1, β_0 and solving the bilinear system specified by (4.4.2) and the second expression in (4.4.3) for the other coefficients, we obtain

$$\begin{aligned} &\alpha_0 = 1\,, && \alpha_1 = 2i\,, && \alpha_2 = -4 + \tfrac{5}{3}\,i\,, && \alpha_3 = -4 - 2i\,,\\ &\beta_0 = i\,, && \beta_1 = -\tfrac{5}{3}\,, && \beta_2 = -1 - \tfrac{10}{3}i\,, && \beta_3 = 2 - 3i\,. \end{aligned}$$

The resulting hodograph

$$\begin{aligned} x'(t) &= 14\,t^6 - 28\,t^5 + 14\,t^4 + 7\,t^2\,, \\ y'(t) &= -12\,t^6 + 28\,t^5 - 20\,t^4 + 4\,t^3 - 6\,t^2 + 2\,t\,, \\ z'(t) &= -84\,t^6 + 192\,t^5 - 136\,t^4 + 32\,t^3 - 46\,t^2 + 12\,t - 2\,, \end{aligned}$$

is non–primitive, since $\gcd(x'(t), y'(t), z'(t)) = 2\,t^4 - 4\,t^3 + 2\,t^2 + 1$. We have

$$\begin{aligned} \sigma(t) &= |\,\mathbf{r}'(t)\,| = (43\,t^2 - 12\,t + 2)(2\,t^4 - 4\,t^3 + 2\,t^2 + 1)\,, \\ |\,\mathbf{r}'(t) \times \mathbf{r}''(t)\,| &= 2\,(2\,t^4 - 4\,t^3 + 2\,t^2 + 1)\,\sigma(t)\,. \end{aligned}$$

This curve has an especially simple rational Frenet adapted frame, given by

$$\begin{aligned} \mathbf{t} &= \frac{(7\,t^2, -6\,t^2 + 2\,t, -42\,t^2 + 12\,t - 2)}{43\,t^2 - 12\,t + 2}\,, \\ \mathbf{n} &= \frac{(-42\,t^2 + 14\,t, -7\,t^2 - 12\,t + 2, -6\,t^2 + 2\,t)}{43\,t^2 - 12\,t + 2}\,, \\ \mathbf{b} &= \frac{(-6\,t^2 - 12\,t + 2, 42\,t^2 - 14\,t, -7\,t^2)}{43\,t^2 - 12\,t + 2}\,, \end{aligned}$$

and the rational curvature function is just $\kappa(t) = 2/(43\,t^2 - 12\,t + 2)\,\sigma(t)$.

Example 4.2. Using the numerical values of the previous example, but the first rather than the second expression in (4.4.3), we obtain

$$\begin{aligned} &\alpha_0 = 1\,, \quad &&\alpha_1 = 2\,i\,, \quad &&\alpha_2 = -4 + 3\,i\,, \quad &&\alpha_3 = -12 - 2\,i\,, \\ &\beta_0 = i\,, \quad &&\beta_1 = -\tfrac{5}{3}\,, \quad &&\beta_2 = -\tfrac{7}{3} - \tfrac{10}{3}\,i\,, \quad &&\beta_3 = 2 - \tfrac{29}{3}\,i\,. \end{aligned}$$

The corresponding hodograph components

$$\begin{aligned} x'(t) &= \tfrac{86}{9}\,t^6 + \tfrac{44}{3}\,t^5 + 14\,t^4 + \tfrac{16}{3}\,t^3 + 7\,t^2\,, \\ y'(t) &= -\tfrac{4}{3}\,t^6 - 4\,t^5 - 4\,t^4 + 4\,t^3 - 6\,t^2 + 2\,t\,, \\ z'(t) &= -\tfrac{124}{3}\,t^6 - 80\,t^5 - 56\,t^4 - \tfrac{80}{3}\,t^3 - 46\,t^2 + 12\,t - 2\,, \end{aligned}$$

possess no common factor, and we have

$$\begin{aligned} \sigma(t) &= |\,\mathbf{r}'(t)\,| = \tfrac{382}{9}\,t^6 + \tfrac{244}{3}\,t^5 + 58\,t^4 + \tfrac{80}{3}\,t^3 + 47\,t^2 - 12\,t + 2\,, \\ |\,\mathbf{r}'(t) \times \mathbf{r}''(t)\,| &= 2(2\,t^4 - 4\,t^3 + 2\,t^2 + 1)\,\sigma(t)\,. \end{aligned}$$

The case $\deg(h) = 2$ *and* $\deg(\mathbf{w}) = 1$

In case (b) we take $h(t)$ quadratic and $\mathbf{w}(t)$ linear with Bernstein coefficients h_0, h_1, h_2 and $\mathbf{w}_0, \mathbf{w}_1$ and thus obtain from (4.3.3) the equations

$$\begin{aligned} 3\,(\alpha_0\beta_1 - \alpha_1\beta_0) &= h_0\mathbf{w}_0^2\,, \\ 3\,(\alpha_0\beta_2 - \alpha_2\beta_0) &= h_1\mathbf{w}_0^2 + h_0\mathbf{w}_0\mathbf{w}_1\,, \\ (\alpha_0\beta_3 - \alpha_3\beta_0) + 3\,(\alpha_1\beta_2 - \alpha_2\beta_1) &= \tfrac{1}{3}\,(h_2\mathbf{w}_0^2 + 4\,h_1\mathbf{w}_0\mathbf{w}_1 + h_0\mathbf{w}_1^2)\,, \\ 3\,(\alpha_1\beta_3 - \alpha_3\beta_1) &= h_2\mathbf{w}_0\mathbf{w}_1 + h_1\mathbf{w}_1^2\,, \\ 3\,(\alpha_2\beta_3 - \alpha_3\beta_2) &= h_2\mathbf{w}_1^2\,. \end{aligned} \tag{4.4.4}$$

Setting $\alpha_1\beta_2 - \alpha_2\beta_1 = \mathbf{z}$, $\alpha_0\beta_3 - \alpha_3\beta_0 = \frac{1}{3}\,(h_2\mathbf{w}_0^2 + 4\,h_1\mathbf{w}_0\mathbf{w}_1 + h_0\mathbf{w}_1^2) - 3\mathbf{z}$, we see from (4.4.1) that the values h_0, h_1, h_2, $\mathbf{w}_0, \mathbf{w}_1$, $\mathbf{z}$ must satisfy

$$\begin{aligned}\left(\tfrac{1}{3}h_0\mathbf{w}_0^2\right)\left(\tfrac{1}{3}h_2\mathbf{w}_1^2\right) \;=\; \tfrac{1}{3}\left(h_1\mathbf{w}_0^2 + h_0\mathbf{w}_0\mathbf{w}_1\right)\,\tfrac{1}{3}\left(h_2\mathbf{w}_0\mathbf{w}_1 + h_1\mathbf{w}_1^2\right)\\ -\mathbf{z}\,\left[\,\tfrac{1}{3}(h_2\mathbf{w}_0^2 + 4h_1\mathbf{w}_0\mathbf{w}_1 + h_0\mathbf{w}_1^2) - 3\,\mathbf{z}\,\right],\end{aligned}$$

yielding the quadratic equation

$$\begin{aligned}27\,\mathbf{z}^2 \;-\; 3\,(h_2\mathbf{w}_0^2 + 4\,h_1\mathbf{w}_0\mathbf{w}_1 + h_0\mathbf{w}_1^2)\,\mathbf{z}\\ + h_1\mathbf{w}_0\mathbf{w}_1(h_2\mathbf{w}_0^2 + h_1\mathbf{w}_0\mathbf{w}_1 + h_0\mathbf{w}_1^2) \;=\; 0\end{aligned}$$

whose solutions indicate that $\alpha_1\beta_2 - \alpha_2\beta_1$ must be given in terms of h_0, h_1, h_2 and $\mathbf{w}_0, \mathbf{w}_1$ by

$$\alpha_1\beta_2 - \alpha_2\beta_1 \;=\; \tfrac{1}{3}h_1\mathbf{w}_0\mathbf{w}_1 \quad\text{or}\quad \tfrac{1}{9}(h_2\mathbf{w}_0^2 + h_1\mathbf{w}_0\mathbf{w}_1 + h_0\mathbf{w}_1^2)\,. \qquad (4.4.5)$$

Example 4.3. In equations (4.4.4) we choose the numerical values

$$h_0 = 1\,,\quad h_1 = 2\,,\quad h_2 = 1\,,\quad \mathbf{w}_0 = \mathrm{i}\,,\quad \mathbf{w}_1 = 1\,.$$

Assigning values to α_0, α_1, β_0 and solving the bilinear system specified by (4.4.4) and the second expression in (4.4.5) for the other coefficients then gives

$$\begin{aligned}&\alpha_0 = 1\,, && \alpha_1 = 1\,, && \alpha_2 = 2 - \tfrac{1}{3}\,\mathrm{i}\,, && \alpha_3 = 2 - 5\,\mathrm{i}\,,\\ &\beta_0 = -1\,, && \beta_1 = -\tfrac{4}{3}\,, && \beta_2 = -\tfrac{8}{3} + \tfrac{2}{3}\mathrm{i}\,, && \beta_3 = -2 + 7\,\mathrm{i}\,.\end{aligned}$$

The corresponding hodograph components are

$$\begin{aligned}x'(t) \;&=\; -14\,t^6 - 6\,t^5 + 3\,t^4 - 4\,t^3 - t^2 - 2\,t\,,\\ y'(t) \;&=\; -52\,t^6 + 4\,t^5 - 18\,t^4 + 4\,t^3 - 12\,t^2 - 2\,t - 2\,,\\ z'(t) \;&=\; -4\,t^6 - 4\,t^5 + 2\,t^4 - 2\,t^2\,.\end{aligned}$$

This hodograph is non–primitive: it has $\gcd(x'(t), y'(t), z'(t)) = 2\,t^2 - 2\,t + 1$ as the common factor of its components. For this curve, we have

$$\begin{aligned}\sigma(t) \;&=\; |\,\mathbf{r}'(t)\,| \;=\; (2\,t^2 - 2\,t + 1)(27\,t^4 + 26\,t^3 + 21\,t^2 + 6\,t + 2)\,,\\ |\,\mathbf{r}'(t) \times \mathbf{r}''(t)\,| \;&=\; 2\,|\,2\,t^2 - 2\,t - 1\,|\,(2\,t^2 - 2\,t + 1)\,\sigma(t)\,.\end{aligned}$$

The rational Frenet adapted frame is defined by

$$\begin{aligned}\mathbf{t} &= -\frac{(t(t+1)(7t^2+3t+2), 2(13t^4+12t^3+10t^2+3t+1), 2t^2(t+1)^2)}{27t^4+26t^3+21t^2+6t+2}\,,\\ \mathbf{n} &= \frac{(2(11t^4+8t^3+8t^2+3t+1), -t(t+1)(7t^2+3t+2), 2t(t+1)(7t^2+3t+2))}{27t^4+26t^3+21t^2+6t+2}\,,\\ \mathbf{b} &= \frac{(-2t(t+1)(7t^2+3t+2), 2t^2(t+1)^2, 23t^4+18t^3+17t^2+6t+2)}{27t^4+26t^3+21t^2+6t+2}\,,\end{aligned}$$

and the rational curvature function is

$$\kappa(t) \;=\; \frac{|\,4\,t^2 - 4\,t - 2\,|}{(2\,t^2 - 2\,t + 1)\,(27\,t^4 + 26\,t^3 + 21\,t^2 + 6\,t + 2)^2}\,.$$

Example 4.4. Using the numerical values of the previous example, but the first rather than the second expression in (4.4.5), we obtain

$$\begin{aligned} &\alpha_0 = 1\,, && \alpha_1 = 1\,, && \alpha_2 = 2+\mathrm{i}\,, && \alpha_3 = 2-\mathrm{i}\,,\\ &\beta_0 = -1\,, && \beta_1 = -\tfrac{4}{3}\,, && \beta_2 = -\tfrac{8}{3}-\tfrac{2}{3}\mathrm{i}\,, && \beta_3 = -2+\tfrac{5}{3}\,\mathrm{i}\,. \end{aligned}$$

The corresponding hodograph is primitive, with components

$$\begin{aligned} x'(t) &= -\tfrac{22}{9}\,t^6 - \tfrac{10}{3}\,t^5 + 11\,t^4 - 4\,t^3 - t^2 - 2\,t\,,\\ y'(t) &= -\tfrac{124}{3}\,t^6 + 68\,t^5 - 26\,t^4 + 4\,t^3 - 12\,t^2 - 2\,t - 2\,,\\ z'(t) &= -\tfrac{28}{3}\,t^6 + 12\,t^5 + 2\,t^4 - \tfrac{16}{3}\,t^3 - 2\,t^2\,, \end{aligned}$$

and we have

$$\begin{aligned} \sigma(t) &= |\,\mathbf{r}'(t)\,| = \tfrac{382}{9}\,t^6 - \tfrac{206}{3}\,t^5 + 25\,t^4 - 4\,t^3 + 13\,t^2 + 2\,t + 2\,,\\ |\,\mathbf{r}'(t)\times\mathbf{r}''(t)\,| &= 2\,|\,2\,t^2 - 2\,t - 1\,|(2\,t^2 - 2\,t + 1)\,\sigma(t)\,. \end{aligned}$$

The case $\deg(h) = 4$ *and* $\deg(\mathbf{w}) = 0$

Finally, choosing $h(t)$ as a quartic with Bernstein coefficients $h_0, \ldots, h_4$ and $\mathbf{w}(t) = \mathbf{w}_0$ in case (c), and equating coefficients of the quartic polynomials on the left and right in (4.3.3), yields the equations

$$\begin{aligned} 3\,(\alpha_0\beta_1 - \alpha_1\beta_0) &= h_0\mathbf{w}_0^2\,,\\ 3\,(\alpha_0\beta_2 - \alpha_2\beta_0) &= 2\,h_1\mathbf{w}_0^2\,,\\ (\alpha_0\beta_3 - \alpha_3\beta_0) + 3\,(\alpha_1\beta_2 - \alpha_2\beta_1) &= 2\,h_2\mathbf{w}_0^2\,,\\ 3\,(\alpha_1\beta_3 - \alpha_3\beta_1) &= 2\,h_3\mathbf{w}_0^2\,,\\ 3\,(\alpha_2\beta_3 - \alpha_3\beta_2) &= h_4\mathbf{w}_0^2\,. \end{aligned} \tag{4.4.6}$$

Setting $\alpha_1\beta_2 - \alpha_2\beta_1 = \mathbf{z}$, $\alpha_0\beta_3 - \alpha_3\beta_0 = 2\,h_2\mathbf{w}_0^2 - 3\mathbf{z}$, and invoking (4.4.1), we see that the values $h_0, \ldots, h_4$, $\mathbf{w}_0$, and $\mathbf{z}$ must satisfy

$$\left(\tfrac{1}{3}h_0\mathbf{w}_0^2\right)\left(\tfrac{1}{3}h_4\mathbf{w}_0^2\right) = \left(\tfrac{2}{3}h_1\mathbf{w}_0^2\right)\left(\tfrac{2}{3}h_3\mathbf{w}_0^2\right) - \mathbf{z}\,(2\,h_2\mathbf{w}_0^2 - 3\mathbf{z})\,,$$

which reduces to the quadratic equation

$$27\,\mathbf{z}^2 - 18\,h_2\mathbf{w}_0^2\,\mathbf{z} + (4\,h_1h_3 - h_0h_4)\,\mathbf{w}_0^4 = 0$$

in $\mathbf{z}$. The solutions of this equation indicate that, in this case, $\alpha_1\beta_2 - \alpha_2\beta_1$ must be given in terms of $h_0, \ldots, h_4$ and $\mathbf{w}_0$ by

$$\alpha_1\beta_2 - \alpha_2\beta_1 = \frac{1}{9}\left(3\,h_2 \pm \sqrt{9\,h_2^2 + 3\,h_0h_4 - 12\,h_1h_3}\right)\mathbf{w}_0^2\,. \tag{4.4.7}$$

Example 4.5. In equations (4.4.6) we choose the numerical values

$$h_0 = -1\,, \quad h_1 = 2\,, \quad h_2 = 3\,, \quad h_3 = 4\,, \quad h_4 = -5\,, \quad \mathbf{w}_0 = 1\,.$$

Choosing complex values for α_0, α_1, β_0 and solving for the five remaining coefficients from the system of bilinear equations defined by (4.4.6) and (4.4.7) with the "+" sign, we obtain

$$\begin{aligned} &\alpha_0 = 1\,, && \alpha_1 = 1-i\,, && \alpha_2 = -1+4i\,, && \alpha_3 = -1+9i\,,\\ &\beta_0 = -1+i\,, && \beta_1 = -\tfrac{1}{3}+2i\,, && \beta_2 = -\tfrac{5}{3}-5i\,, && \beta_3 = -5-10i\,. \end{aligned}$$

The components of the hodograph defined through (3.2.2) by the cubic complex polynomials $\alpha(t)$, $\beta(t)$ are then

$$\begin{aligned} x'(t) &= -48\,t^6 + 216\,t^5 - 276\,t^4 + 48\,t^3 + 20\,t^2 - 2\,t - 1\,,\\ y'(t) &= -120\,t^6 + 600\,t^5 - 872\,t^4 + 208\,t^3 + 18\,t^2 - 2\,t - 2\,,\\ z'(t) &= -80\,t^6 + 384\,t^5 - 552\,t^4 + 128\,t^3 + 12\,t^2 - 2\,. \end{aligned}$$

This hodograph is primitive, and we have

$$\begin{aligned} \sigma(t) &= |\,\mathbf{r}'(t)\,| = 152\,t^6 - 744\,t^5 + 1068\,t^4 - 248\,t^3 - 26\,t^2 + 2\,t + 3\,,\\ |\,\mathbf{r}'(t)\times\mathbf{r}''(t)\,| &= 2\,|\,12\,t^4 - 8\,t^3 + 12\,t^2 - 12\,t + 1\,|\,\sigma(t)\,. \end{aligned}$$

Example 4.6. Using equations (4.4.6) again, we now choose the numerical values

$$h_0 = 1\,, \quad h_1 = 2\,, \quad h_2 = 2\,, \quad h_3 = 2\,, \quad h_4 = 1\,, \quad \mathbf{w}_0 = 1\,.$$

Choosing complex values for α_0, α_1, β_0 and solving for the five remaining coefficients from the system of bilinear equations defined by (4.4.6) and (4.4.7) with the "−" sign, we obtain

$$\begin{aligned} &\alpha_0 = 1\,, && \alpha_1 = 1\,, && \alpha_2 = 2+i\,, && \alpha_3 = 2+3i\,,\\ &\beta_0 = -1\,, && \beta_1 = -\tfrac{2}{3}\,, && \beta_2 = -\tfrac{2}{3}-i\,, && \beta_3 = -2i\,. \end{aligned}$$

These give the hodograph components

$$\begin{aligned} x'(t) &= 2\,t^6 - 4\,t^5 + 6\,t^4 + 3\,t^2 + 2\,t\,,\\ y'(t) &= -4\,t^6 + 16\,t^5 - 28\,t^4 + 12\,t^3 - 8\,t^2 + 2\,t - 2\,,\\ z'(t) &= 4\,t^6 - 12\,t^5 + 12\,t^4 + 4\,t^3\,. \end{aligned}$$

This hodograph is also primitive, with

$$\begin{aligned} \sigma(t) &= |\,\mathbf{r}'(t)\,| = 6\,t^6 - 20\,t^5 + 30\,t^4 - 8\,t^3 + 9\,t^2 - 2\,t + 2\,,\\ |\,\mathbf{r}'(t)\times\mathbf{r}''(t)\,| &= 2\,|\,2\,t^4 - 4\,t^3 + 6\,t^2 - 4\,t - 1\,|\,\sigma(t)\,. \end{aligned}$$

4.4.3 *Construction of degree 7 double PH curves*

The above characterizations for degree 7 double PH curves of different types furnish algorithms for constructing examples of these curves.

First, we assign numerical values for the coefficients of $h(t)$ and $\mathbf{w}(t)$ on the right–hand side of equations (4.4.2), (4.4.4), or (4.4.6). An appropriate value for $\mathbf{z} = \alpha_1\beta_2 - \alpha_2\beta_1$ is then determined through the corresponding compatibility constraint from expression (4.4.3), (4.4.5), or (4.4.7). This assignment, together with equations (4.4.2), (4.4.4), or (4.4.6), define a system comprising six bilinear equations in the eight unknowns $\alpha_0, \ldots, \alpha_3$ and $\beta_0, \ldots, \beta_3$.

Since these equations are (by construction) consistent, and the variables are inherently *complex*, one can in principle assign two of them arbitrarily, and then solve the six equations for the remaining variables. Of course, this purely algebraic process is not suited to constructing curves with prescribed geometrical properties. We expect that it can be suitably modified to furnish more geometrically intuitive constructions for double PH curves of different types, but the formulation of such algorithms is deferred to a future study.

Remark 4.6. Since equations (4.4.2)–(4.4.3), (4.4.4)–(4.4.5), or (4.4.6)–(4.4.7) depend only on the combinations $\alpha_i\beta_j - \alpha_j\beta_i$, if (α_k, β_k) for $0 \leqslant k \leqslant 3$ is any solution, then $(\alpha_k\mathbf{z}, \beta_k/\mathbf{z})$ for $0 \leqslant k \leqslant 3$ is also a solution for each $\mathbf{z} \neq 0$. Hence, one may initially assign arbitrary complex values to any *three* of the coefficients (α_k, β_k) for $0 \leqslant k \leqslant 3$, and then determine corresponding values for the other five. This yields another freedom of initial assignment, beyond the two arising from the difference between the number of unknowns and equations.

5

HELICAL POLYNOMIAL CURVES

In classical differential geometry [17, 65, 94], a (*cylindrical*) *helix* or *curve of constant slope* is a curve whose tangent $\mathbf{t}$ maintains a constant inclination with respect to a fixed line. Let $\mathbf{a}$ be the unit vector along the fixed direction (the *axis*) and let ψ be the constant angle (the *pitch angle*). Then a helix is defined by

$$\mathbf{t} \cdot \mathbf{a} = \cos\psi = \text{constant}, \tag{5.0.1}$$

which, in virtue of the Frenet–Serret equations (1.2.2), differentiated gives $\mathbf{n} \cdot \mathbf{a} = 0$. It follows that for a a helix

$$\mathbf{t} \cdot \mathbf{a} = \cos\psi\,, \qquad \mathbf{n} \cdot \mathbf{a} = 0\,, \qquad \mathbf{b} \cdot \mathbf{a} = \sin\psi\,.$$

Thus, the axis is parallel to the rectifying plane of the curve, and can be expressed as

$$\mathbf{a} = \mathbf{t}\cos\psi + \mathbf{b}\sin\psi\,, \tag{5.0.2}$$

which differentiated implies $\kappa\cos\psi - \tau\sin\psi = 0$, namely[1]

$$\frac{\kappa}{\tau} = \tan\psi = \text{constant}\,. \tag{5.0.3}$$

If a curve is of constant slope, i.e. if condition (5.0.1) holds, the ratio of curvature to torsion is constant. Conversely, if a curve satisfies condition (5.0.3) we can always find a constant vector $\mathbf{a}$ specified by (5.0.2) that satisfies (5.0.1). This characterization of a helix as the unique curve in 3D–space for which the ratio of curvature to torsion is constant is a result known as *Theorem of Lancret* [94].

Theorem 5.1 (Lancret)**.** *A necessary and sufficient condition for a curve to be a helix is that the ratio of curvature to torsion be constant.*

A helical curve $\mathbf{r}(t)$ may also be characterized by the fact that the locus traced by its unit tangent vector $\mathbf{t} = \mathbf{r}'/|\mathbf{r}'|$ — i.e., the *tangent indicatrix* of $\mathbf{r}(t)$ — is a circle[2] on the unit sphere [94]. This characteristic property has been used in [70] to give a geometrically intuitive and quite general construction of helical polynomial curves, based on the Hopf map model.

Starting from the above analysis, we can give several equivalent characterizations of helical curves [17]. Let $\mathbf{r} : I \to \mathbb{R}^3$ be a parametrized curve with $\tau(t) \neq 0$, $t \in I$. Then $\mathbf{r}$ is a helix if and only if

1 Since κ is by definition non–negative, but τ is a signed quantity, the constant in (5.0.3) may change sign at special curve points where $\kappa = \tau = 0$.

2 The center of the circle and its angular radius identify the helix axis $\mathbf{a}$ and pitch angle ψ.

Figure 5.1: The circular helix (left) and a pipe surface constructed on it (right).

- the ratio of curvature to torsion is constant,
- both its tangent and binormal vector make a constant angle with the axis,
- its normal is perpendicular to a fixed direction,
- its tangent indicatrix is a circle on the unit sphere.

In relation to the last item, a curve is said to be *monotone helical* if its tangent indicatrix is a simply–traced circle on the unit sphere [37] — i.e., it does not indicate any reversals in the sense of the tangent rotation. Figure 5.1 shows the familiar circular helix, and the pipe surface constructed on it. Note that this is a *transcendental* curve (defined by trigonometric functions). We focus here on polynomial helical curves.

When the axis of a helical space curve coincides with the z–axis, it has a parametrization of the form $\mathbf{r}(t) = (x(t), y(t), s(t)\cos\psi)$, where $s(t)$ is the arc–length function [94]. For $\mathbf{r}(t)$ to be a polynomial curve, it must be a PH curve, since only PH curves have a polynomial for $s(t)$. If $\sigma(t) = ds/dt$ is the parametric speed, the projection $\tilde{\mathbf{r}}(t) = (x(t), y(t))$ onto the (x, y)–plane defines a *planar* PH curve satisfying

$$x'^2(t) + y'^2(t) \equiv \sigma^2(t)\sin^2\psi\,.$$

Hence, in these special coordinates, helical polynomial curves can be obtained from *planar* PH curves through spatial hodographs of the form

$$\mathbf{r}'(t) = (u^2(t) - v^2(t), 2u(t)v(t), (u^2(t) + v^2(t))\cot\psi)\,,$$

for relatively prime polynomials $u(t)$, $v(t)$. The disadvantage of this approach is that, unlike the quaternion and Hopf map forms used here, the above description is not invariant under general rotations in $\mathbb{R}^3$. Moreover, it is not very useful in addressing the problem of determining whether a given polynomial curve is helical and, if so, identifying its axis.

The plan for the reminder of this chapter is as follows. First, the relation between Pythagorean–hodograph curves, double Pythagorean–hodograph curves

and helical polynomial curves is discussed in Section 5.1. The focus of Section 5.2 is on the helical DPH curves, using the approach presented in [70], based upon rational line/circle parameterizations in the complex plane to classify all types up to degree 7. Section 5.3 presents criteria to distinguish between the helical and non–helical DPH curves of each type. Finally, Section 5.4 provides a comprehensive selection of examples of both the helical and non–helical degree 7 DPH curves.

5.1 HOW PH, DPH, AND HELICES RELATE TO EACH OTHER

The unit tangent $\mathbf{t}$ to a Pythagorean–hodograph curve is defined in terms of the polynomials $u(t)$, $v(t)$, $p(t)$, $q(t)$ and $\sigma(t)$ by

$$\mathbf{t} = \frac{\mathbf{r}'}{|\,\mathbf{r}'\,|} = \frac{(u^2+v^2-p^2-q^2, 2(uq+vp), 2(vq-up))}{\sigma}\,. \tag{5.1.1}$$

Hence a *helical* polynomial curve, that satisfies (5.0.1), must be a PH curve [37]. Moreover, since

$$\frac{\kappa}{\tau} = \frac{|\,\mathbf{r}'\times\mathbf{r}''\,|^2}{|\,\mathbf{r}'\,|^3[\mathbf{r}'\times\mathbf{r}'']\cdot\mathbf{r}'''} = \tan\psi$$

from (3.4.1) it follows that, for a pitch angle ψ, all helical space curves have to satisfy the relation

$$\rho^{3/2} = \tan\psi\,[\mathbf{r}'\times\mathbf{r}'']\cdot\mathbf{r}'''\,,$$

implying that ρ is a perfect square (since the right–hand side is a polynomial). Hence, every *helical* PH curve must be a DPH curve. Beltran and Monterde [4] showed that for, cubics and quintics, there is a exact coincidence of helical curves and DPH curves, but quoted an example of a DPH curve of degree 7 that is non–helical. From (4.1.5) follows that for DPH curves, the curvature/torsion ratio becomes

$$\frac{\kappa(t)}{\tau(t)} = \frac{\omega^3(t)}{[\,\mathbf{r}'(t)\times\mathbf{r}''(t)\,]\cdot\mathbf{r}'''(t)}\,, \tag{5.1.2}$$

and hence we have the following observation.

Remark 5.1. If a polynomial space curve $\mathbf{r}(t)$ is helical, $[\,\mathbf{r}'(t)\times\mathbf{r}''(t)\,]\cdot\mathbf{r}'''(t)$ must be proportional to the cube of a polynomial $\omega(t)$.

For PH cubics, the ratio (5.1.2) is always constant since the numerator and denominator are individually constant.[3] For the DPH quintics, they are both

3 The fact that all PH cubics are helical curves is one of the first known properties [43] of the spatial PH curves.

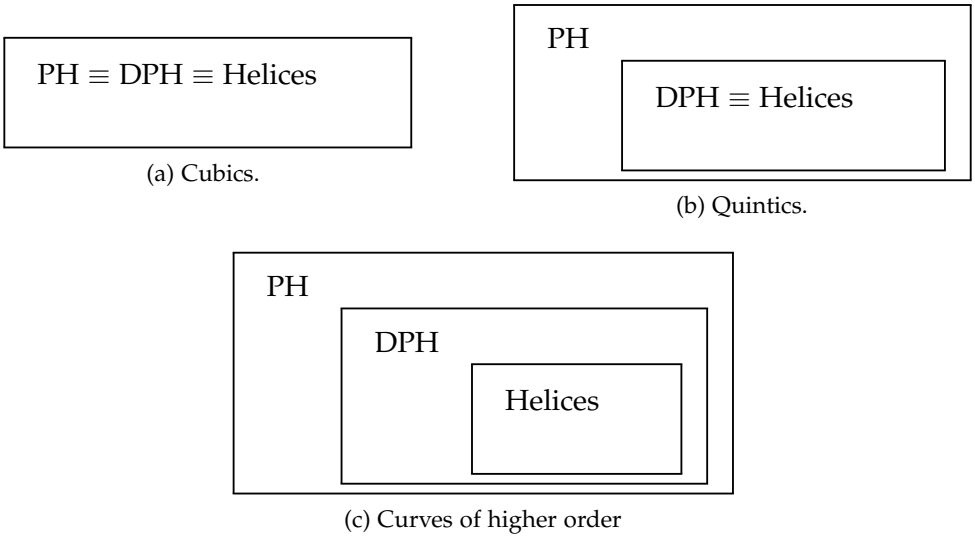

(a) Cubics.

(b) Quintics.

(c) Curves of higher order

Figure 5.2: PH, DPH, and polynomial helices.

polynomials of degree 6, and $(\mathbf{r}' \times \mathbf{r}'') \cdot \mathbf{r}'''$ must be a multiple of ω^3 since all double PH quintics are helical. For higher–order DPH curves, satisfaction of the condition $(\mathbf{r}' \times \mathbf{r}'') \cdot \mathbf{r}''' = \omega^3 \tan\psi$ for some constant $\tan\psi$ can be used to distinguish the helical DPH curves from those that are non–helical.

As observed in [37], the helical PH quintics comprise a proper subset of all spatial PH quintics. For PH quintics, $\rho(t)$ is not merely a constant, and for a double PH curve it must be the perfect square of a quadratic. The set of double PH quintics coincides precisely with the set of helical PH quintics, but this coincidence does not extend to higher degree PH curves [4].

5.2 HOPF MAP FORM OF HELICAL CURVES

Based on the Hopf map model for spatial PH curves and the property that helical curves exhibit a circular tangent indicatrix on the unit sphere, an elegant general construction for helical polynomial curves of arbitrary degree was proposed in [70]. Let's review the general schema of this procedure.

For the hodograph defined in terms of complex polynomials $\alpha(t)$, $\beta(t)$ through the Hopf map construction (3.2.2), the tangent indicatrix is given by

$$\mathbf{t} = \frac{H(\alpha,\beta)}{|\alpha|^2+|\beta|^2} = \frac{(|\alpha|^2-|\beta|^2, 2\,\mathrm{Re}(\alpha\overline{\beta}), 2\,\mathrm{Im}(\alpha\overline{\beta}))}{|\alpha|^2+|\beta|^2}\,.$$

The final expression above defines the *normalized* Hopf map, which we denote by $\hat{H}(\alpha,\beta)$. Note that $\hat{H}$ maps complex values α, β with $|\alpha|^2+|\beta|^2 = 1$ to a *unit* vector in $\mathbb{R}^3$ or, equivalently, a point on the unit sphere S^2.

As noted in [70], the normalized Hopf map satisfies

$$\hat{H}(\alpha, \beta) = \hat{H}(\alpha/\beta, 1)\,,$$

and hence, for the purpose of investigating the tangent indicatrix, it suffices to consider only the *ratio* $\alpha(t)/\beta(t)$ of the complex polynomials in (3.2.2). Thus, different spatial PH curves defined by integrating (3.2.2) with different choices for $\alpha(t)$, $\beta(t)$ may nevertheless exhibit identical tangent indicatrices, if they have the same ratio $\alpha(t)/\beta(t)$. Such curves differ in the *magnitude*, but not the *direction*, of their hodograph vectors $\mathbf{r}'(t)$ at each parameter value t.

Now the ratio $\mathbf{z}(t) = \alpha(t)/\beta(t)$ of the polynomials $\alpha(t)$, $\beta(t)$ specifies a rational curve in the complex plane, and through the normalized Hopf map an image $\mathbf{c}(t) = \hat{H}(\mathbf{z}(t), 1)$ of this curve on the unit sphere S^2 in $\mathbb{R}^3$ is defined, with $|\mathbf{c}(t)| \equiv 1$. In fact, as observed in [70], the map $\mathbf{z} \to \hat{H}(\mathbf{z}, 1)$ from $\mathbb{C}$ to S^2 is just the inverse of the familiar *stereographic projection*, used in complex analysis to visualize the "extended" complex plane [75]. Drawing rays from the north pole of S^2 through each point $\mathbf{z} \in \mathbb{C}$, we associate with each $\mathbf{z}$ the point of S^2 at which such a ray pierces the sphere — see also Appendix C. In this manner, "infinitely distant" points in $\mathbb{C}$ — regardless of direction — are all mapped to the north pole of S^2, and we regard the extended complex plane as comprising all finite complex values $\mathbf{z}$ augmented by the single value ∞.

As is well known [75], all circles on S^2 are mapped to either lines or circles in $\mathbb{C}$ by stereographic projection, depending on whether or not the circle on S^2 passes through the north pole. Monterde [70] thus observes that, if we are interested in helical polynomial curves, with circular tangent indicatrices on S^2, their construction can be reduced by the above arguments to identifying those pairs of complex polynomials $\alpha(t)$, $\beta(t)$ whose ratios $\mathbf{z}(t) = \alpha(t)/\beta(t)$ define rational parameterizations of lines or circles in $\mathbb{C}$.

5.2.1 *Complex representation of lines/circles*

Given complex numbers $\mathbf{a}_0$, $\mathbf{a}_1$, $\mathbf{b}_0$, $\mathbf{b}_1$ that satisfy $\mathbf{a}_0\mathbf{b}_1 - \mathbf{a}_1\mathbf{b}_0 \neq 0$, consider the complex–valued function

$$\mathbf{z}(t) = \frac{\mathbf{a}_0(1-t) + \mathbf{a}_1 t}{\mathbf{b}_0(1-t) + \mathbf{b}_1 t} \tag{5.2.1}$$

of a real parameter t. This may be viewed as a mapping $t \to \mathbf{z}(t)$ of the real axis to a locus in the complex plane, as specified by a *Möbius transformation*. Form (5.2.1) defines all *lines* and *circles* in the complex plane [75, 90].

If $\mathbf{b}_1\overline{\mathbf{b}}_0 - \overline{\mathbf{b}}_1\mathbf{b}_0 = 2\,i\,\mathrm{Im}(\mathbf{b}_1\overline{\mathbf{b}}_0) \neq 0$, expression (5.2.1) defines a circle — one can easily verify that

$$\mathbf{z}_c = \frac{\mathbf{a}_1\overline{\mathbf{b}}_0 - \mathbf{a}_0\overline{\mathbf{b}}_1}{\mathbf{b}_1\overline{\mathbf{b}}_0 - \overline{\mathbf{b}}_1\mathbf{b}_0} \qquad \text{and} \qquad R = \left|\frac{\mathbf{a}_0\mathbf{b}_1 - \mathbf{a}_1\mathbf{b}_0}{\mathbf{b}_1\overline{\mathbf{b}}_0 - \overline{\mathbf{b}}_1\mathbf{b}_0}\right|$$

identify the center and radius, so that

$$|\,\mathbf{z}(t)-\mathbf{z}_c|^2 \;\equiv\; R^2\,.$$

If $\mathbf{b}_1\overline{\mathbf{b}}_0-\overline{\mathbf{b}}_1\mathbf{b}_0=0$, however, $\mathbf{z}_c$ and R become infinite, and $\mathbf{z}(t)$ degenerates to a straight line. This may be seen by noting that the derivative

$$\frac{d\mathbf{z}}{dt} \;=\; \frac{\mathbf{a}_1\mathbf{b}_0-\mathbf{a}_0\mathbf{b}_1}{[\,\mathbf{b}_0(1-t)+\mathbf{b}_1 t\,]^2}$$

has direction specified by

$$\arg\left(\frac{d\mathbf{z}}{dt}\right) \;=\; \arg(\mathbf{a}_1\mathbf{b}_0-\mathbf{a}_0\mathbf{b}_1) \;-\; 2\arg(\mathbf{b}_0(1-t)+\mathbf{b}_1 t)\,.$$

Writing $\mathbf{b}_0=b_0+i\,\beta_0$ and $\mathbf{b}_1=b_1+i\,\beta_1$, we note that

$$\arg(\mathbf{b}_0(1-t)+\mathbf{b}_1 t) \;=\; \tan^{-1}\frac{\beta_0(1-t)+\beta_1 t}{b_0(1-t)+b_1 t} \pmod{\pi}\,.$$

Now $[\,\beta_0(1-t)+\beta_1 t\,]\,/\,[\,b_0(1-t)+b_1 t\,]=$ constant, so $\arg(d\mathbf{z}/dt)=$ constant $(\mathrm{mod}\ \pi)$, if and only if $b_0\beta_1-b_1\beta_0=\mathrm{Im}(\mathbf{b}_1\overline{\mathbf{b}}_0)=(\mathbf{b}_1\overline{\mathbf{b}}_0-\overline{\mathbf{b}}_1\mathbf{b}_0)/2\,i=0$.

The condition $b_0\beta_1-b_1\beta_0=0$ implies that the complex coefficients in the denominator of (5.2.1) are of the form $(\mathbf{b}_0,\mathbf{b}_1)=(k_0\mathbf{w},k_1\mathbf{w})$ for some complex value $\mathbf{w}$ and real values k_0, k_1. Writing $\mathbf{c}_0=\mathbf{a}_0/\mathbf{w}$, $\mathbf{c}_1=\mathbf{a}_1/\mathbf{w}$ we see that, for a straight line, the form (5.2.1) can be reduced to

$$\mathbf{z}(t) \;=\; \frac{\mathbf{c}_0(1-t)+\mathbf{c}_1 t}{k_0(1-t)+k_1 t}\,, \tag{5.2.2}$$

i.e., straight lines may be characterized by *real* denominators.

In order to construct different helical curve types, there are two ways to generate higher–order line/circle parameterizations from the basic form (5.2.1). We may multiply both the numerator and denominator of (5.2.1) by a complex polynomial, to obtain $\mathbf{z}(t)=\boldsymbol{\alpha}(t)/\boldsymbol{\beta}(t)$ where $\gcd(\boldsymbol{\alpha}(t),\boldsymbol{\beta}(t))\neq$ constant — this does not change the tangent indicatrix, but it does alter the *magnitude* of the hodograph $\mathbf{r}'(t)$ upon substituting $\boldsymbol{\alpha}(t)$, $\boldsymbol{\beta}(t)$ into (3.2.2). Curves defined in this manner are *monotone helical*, since they originate from faithful circle parameterizations. Alternatively, a rational transformation $t\to f(t)/g(t)$ of the curve parameter may be invoked, defined by real polynomials[4] $f(t)$, $g(t)$ of degree $\geqslant 2$. This yields, in general, a parameterization $\mathbf{z}(t)=\boldsymbol{\alpha}(t)/\boldsymbol{\beta}(t)$ with $\gcd(\boldsymbol{\alpha}(t),\boldsymbol{\beta}(t))=$ constant that is not faithful, and the resulting curves are general helices — i.e., they may reverse their sense of tangent rotation. These "multiplication" and "re–parameterization" procedures for generating helical curves may also be combined, but only for curves of degree $\geqslant 7$.

4 These polynomials are assumed to be relatively prime, i.e., $\gcd(f(t),g(t))=$ constant.

5.2.2 *Spatial PH cubics*

The rational linear form (5.2.1) is the simplest (lowest–order) parameterization of lines and circles. By substituting the linear complex polynomials

$$\boldsymbol{\alpha}(t) \;=\; \mathbf{a}_0(1-t)+\mathbf{a}_1 t\,, \qquad \boldsymbol{\beta}(t) \;=\; \mathbf{b}_0(1-t)+\mathbf{b}_1 t$$

into the Hopf map specification (3.2.2) of a spatial Pythagorean hodograph and integrating, we obtain a spatial PH cubic. In this case, we have

$$\boldsymbol{\alpha}(t)\boldsymbol{\beta}'(t)-\boldsymbol{\alpha}'(t)\boldsymbol{\beta}(t) \;=\; \mathbf{a}_0\mathbf{b}_1-\mathbf{a}_1\mathbf{b}_0\,,$$

which may be interpreted as being of the form (4.3.3) with $h(t) = 1$ and $\mathbf{w}^2(t) = \mathbf{a}_0\mathbf{b}_1 - \mathbf{a}_1\mathbf{b}_0$, i.e., $\deg(h(t)) = 0$ and $\deg(\mathbf{w}(t)) = 0$. Hence, all spatial PH cubics are helical, and are also double PH curves. Moreover, since the rational linear form (5.2.1) is a faithful parameterization of lines/circles in the complex plane, and the inverse stereographic projection from the complex plane to the unit sphere is one–to–one, all PH cubics are monotone helical.

5.2.3 *Helical PH quintics*

To define helical PH quintics by means of the normalized Hopf map, we must use rational *quadratic* parameterizations of lines and circles in the complex plane. These must be true quadratic parameterizations, not degree–elevated versions of (5.2.1). There are two essentially distinct methods of obtaining such quadratic parameterizations from the basic form (5.2.1).

Quadratic re–parameterization

The first method involves introducing a non–linear (real) transformation of the parameter t. Imposing on (5.2.1) the parameter transformation defined by the rational quadratic function

$$t \;\rightarrow\; \frac{f(t)}{g(t)} \;=\; \frac{f_0(1-t)^2+f_1 2(1-t)t+f_2 t^2}{g_0(1-t)^2+g_1 2(1-t)t+g_2 t^2}\,, \tag{5.2.3}$$

we obtain the quadratic line/circle parameterization

$$\mathbf{z}(t) \;=\; \frac{\boldsymbol{\alpha}(t)}{\boldsymbol{\beta}(t)} \;=\; \frac{\boldsymbol{\alpha}_0(1-t)^2+\boldsymbol{\alpha}_1 2(1-t)t+\boldsymbol{\alpha}_2 t^2}{\boldsymbol{\beta}_0(1-t)^2+\boldsymbol{\beta}_1 2(1-t)t+\boldsymbol{\beta}_2 t^2}\,,$$

where

$$\boldsymbol{\alpha}_i \;=\; f_i(\mathbf{a}_1-\mathbf{a}_0)+g_i\mathbf{a}_0\,, \quad \boldsymbol{\beta}_i \;=\; f_i(\mathbf{b}_1-\mathbf{b}_0)+g_i\mathbf{b}_0\,, \quad i=0,1,2\,.$$

We then find that the proportionality polynomial has the form

$$\boldsymbol{\alpha}(t)\boldsymbol{\beta}'(t)-\boldsymbol{\alpha}'(t)\boldsymbol{\beta}(t) \;=\; h(t)\,(\mathbf{a}_0\mathbf{b}_1-\mathbf{a}_1\mathbf{b}_0)\,,$$

where $h(t)$ is the real quadratic polynomial defined by

$$h(t) = f'(t)g(t) - f(t)g'(t), \tag{5.2.4}$$

with Bernstein coefficients

$$h_0 = 2(f_1 g_0 - f_0 g_1), \quad h_1 = f_2 g_0 - f_0 g_2, \quad h_2 = 2(f_2 g_1 - f_1 g_2). \tag{5.2.5}$$

This is an instance of (4.3.3) with $\deg(h(t)) = 2$, $\deg(\mathbf{w}(t)) = 0$. The spatial PH quintics defined in this manner are thus double PH curves — as observed in [4], they correspond to general helical PH quintics.

Invoking the relation (3.3.1) between the quaternion and Hopf map models, we see that these helical quintics may be specified by a quadratic quaternion polynomial $\mathcal{A}(t) = \boldsymbol{\alpha}(t) + \mathbf{k}\,\boldsymbol{\beta}(t)$ with Bernstein coefficients of the form

$$\mathcal{A}_i = f_i\,[\,\mathbf{a}_1 - \mathbf{a}_0 + \mathbf{k}\,(\mathbf{b}_1 - \mathbf{b}_0)\,] + g_i\,[\,\mathbf{a}_0 + \mathbf{k}\,\mathbf{b}_0\,], \quad i = 0, 1, 2. \tag{5.2.6}$$

Since $\mathcal{A}_0, \mathcal{A}_1, \mathcal{A}_2$ are linearly dependent upon just two quaternions, $\mathbf{a}_1 - \mathbf{a}_0 + \mathbf{k}\,(\mathbf{b}_1 - \mathbf{b}_0)$ and $\mathbf{a}_0 + \mathbf{k}\,\mathbf{b}_0$, they reside in a two–dimensional subspace of $\mathbb{H}$. Hence, as noted in [37], these helical PH curves are characterized by the fact that $\mathcal{A}_1$ is linearly dependent on $\mathcal{A}_0$ and $\mathcal{A}_2$, i.e.,

$$\mathcal{A}_1 = \mathcal{A}_0\,c_0 + \mathcal{A}_2\,c_2$$

for appropriate values $c_0, c_2 \in \mathbb{R}$. Substituting from (5.2.6) into this relation, we find that these coefficients are given in terms of the quantities (5.2.5) by

$$c_0 = \frac{h_2}{2h_1} \qquad \text{and} \qquad c_2 = \frac{h_0}{2h_1}.$$

Linear polynomial multiplication

A different way of obtaining a quadratic rational parameterization from (5.2.1) is to multiply the numerator and denominator by the same (complex) linear polynomial, $\mathbf{w}(t) = \mathbf{w}_0(1-t) + \mathbf{w}_1 t$. The parameterization $\mathbf{z}(t) = \boldsymbol{\alpha}(t)/\boldsymbol{\beta}(t)$ defined in this manner is specified by

$$\begin{aligned}
\boldsymbol{\alpha}(t) &= [\,\mathbf{a}_0(1-t) + \mathbf{a}_1 t\,]\,[\,\mathbf{w}_0(1-t) + \mathbf{w}_1 t\,], \\
&= \mathbf{a}_0\mathbf{w}_0(1-t)^2 + \tfrac{1}{2}(\mathbf{a}_0\mathbf{w}_1 + \mathbf{a}_1\mathbf{w}_0)2(1-t)t + \mathbf{a}_1\mathbf{w}_1 t^2, \\
\boldsymbol{\beta}(t) &= [\,\mathbf{b}_0(1-t) + \mathbf{b}_1 t\,]\,[\,\mathbf{w}_0(1-t) + \mathbf{w}_1 t\,], \\
&= \mathbf{b}_0\mathbf{w}_0(1-t)^2 + \tfrac{1}{2}(\mathbf{b}_0\mathbf{w}_1 + \mathbf{b}_1\mathbf{w}_0)2(1-t)t + \mathbf{b}_1\mathbf{w}_1 t^2,
\end{aligned}$$

and hence we obtain

$$\boldsymbol{\alpha}(t)\boldsymbol{\beta}'(t) - \boldsymbol{\alpha}'(t)\boldsymbol{\beta}(t) = (\mathbf{a}_0\mathbf{b}_1 - \mathbf{a}_1\mathbf{b}_0)\,[\,\mathbf{w}_0(1-t) + \mathbf{w}_1 t\,]^2.$$

Clearly, this corresponds to the case where $\deg(h(t)) = 0$ and $\deg(\mathbf{w}(t)) = 1$ in (4.3.3) — note that the factor $\sqrt{\mathbf{a}_0\mathbf{b}_1 - \mathbf{a}_1\mathbf{b}_0}$ can be absorbed into $\mathbf{w}_0$, $\mathbf{w}_1$. As

observed by Beltran and Monterde [4], this case corresponds to the monotone helical PH quintics. The reason for this is clear from the present arguments: obviously, multiplying the numerator and denominator of (5.2.1) by the *same* complex polynomial $\mathbf{w}(t)$ does not change the faithfulness of the line/circle parameterization (i.e., the monotonicity of the tangent indicatrix). The sole effect of this multiplication is to modulate the hodograph *magnitude* $|\mathbf{r}'(t)|$ by the factor $|\mathbf{w}(t)|^2$ — the direction of $\mathbf{r}'(t)$ remains unchanged.

In [37] the monotone–helical PH quintics were characterized in terms of the quaternion model by the fact that their quaternion coefficients satisfy

$$\mathcal{A}_1 \;=\; \mathcal{A}_0\,\mathbf{c}_0 \;+\; \mathcal{A}_2\,\mathbf{c}_2\,, \tag{5.2.7}$$

$\mathbf{c}_0 = c_0 + \gamma_0\,\mathbf{i}$, $\mathbf{c}_2 = c_2 + \gamma_2\,\mathbf{i}$ being complex numbers (regarded as quaternions with vanishing $\mathbf{j}$ and $\mathbf{k}$ components) that satisfy

$$4\,\mathbf{c}_0\mathbf{c}_2 \;=\; 1\,. \tag{5.2.8}$$

We can verify that this is equivalent to the above Hopf map characterization by invoking the relation (3.3.1) between the Hopf map and quaternion models.

For $\boldsymbol{\alpha}(t)$ and $\boldsymbol{\beta}(t)$ as defined above, we obtain the quadratic quaternion polynomial $\mathcal{A}(t) = \boldsymbol{\alpha}(t) + \mathbf{k}\,\boldsymbol{\beta}(t)$ with Bernstein coefficients

$$\begin{aligned}
\mathcal{A}_0 \;&=\; (\mathbf{a}_0 + \mathbf{k}\,\mathbf{b}_0)\,\mathbf{w}_0\,,\\
\mathcal{A}_1 \;&=\; \tfrac{1}{2}\,[\,(\mathbf{a}_0 + \mathbf{k}\,\mathbf{b}_0)\,\mathbf{w}_1 + (\mathbf{a}_1 + \mathbf{k}\,\mathbf{b}_1)\,\mathbf{w}_0\,]\,,\\
\mathcal{A}_2 \;&=\; (\mathbf{a}_1 + \mathbf{k}\,\mathbf{b}_1)\,\mathbf{w}_1\,.
\end{aligned}$$

Bearing in mind that complex numbers have commutative products, one can then verify that

$$\mathcal{A}_0\,\mathbf{w}_1 \;=\; (\mathbf{a}_0 + \mathbf{k}\,\mathbf{b}_0)\,\mathbf{w}_1\mathbf{w}_0 \qquad \text{and} \qquad \mathcal{A}_2\,\mathbf{w}_0 \;=\; (\mathbf{a}_1 + \mathbf{k}\,\mathbf{b}_1)\,\mathbf{w}_0\mathbf{w}_1\,,$$

and dividing (on the right) by $\mathbf{w}_0$ and $\mathbf{w}_1$, respectively, we obtain

$$\mathcal{A}_1 \;=\; \mathcal{A}_0\left(\frac{\mathbf{w}_1}{2\,\mathbf{w}_0}\right) \;+\; \mathcal{A}_2\left(\frac{\mathbf{w}_0}{2\,\mathbf{w}_1}\right)\,.$$

$\mathcal{A}_1$ is thus of the form (5.2.7) where $\mathbf{c}_0 = \mathbf{w}_1/2\mathbf{w}_0$, $\mathbf{c}_2 = \mathbf{w}_0/2\mathbf{w}_1$ satisfy (5.2.8).

Degenerate common case

The cases discussed in the two previous Sections are not entirely disjoint. There are specific circumstances for these two cases in which $\boldsymbol{\alpha}(t)\boldsymbol{\beta}'(t) - \boldsymbol{\alpha}(t)\boldsymbol{\beta}'(t)$ will degenerate to a common special form. Generically, the polynomial $h(t)$ in the quadratic re–parameterization method is a "true" quadratic — i.e., its discriminant is non–zero, and it is not the square of a linear polynomial. If its coefficients satisfy $h_0 h_2 = h_1^2$, however, $\boldsymbol{\alpha}(t)\boldsymbol{\beta}'(t) - \boldsymbol{\alpha}(t)\boldsymbol{\beta}'(t)$ will be the product of a complex constant and the square of a real linear polynomial.

Likewise, the coefficients of the polynomial $\mathbf{w}_0(1-t)+\mathbf{w}_1 t$ in the second method above are generically linearly independent — i.e., $(\mathbf{w}_0,\mathbf{w}_1)\neq(\mathbf{c}\,w_0,\mathbf{c}\,w_1)$ for some complex value $\mathbf{c}$ and real values w_0, w_1. However, if the polynomial is of the form $\mathbf{c}\,[w_0(1-t)+w_1 t]$, then $\boldsymbol{\alpha}(t)\boldsymbol{\beta}'(t)-\boldsymbol{\alpha}'(t)\boldsymbol{\beta}(t)$ in this case is also the product of a complex constant and the square of a real linear polynomial.

5.2.4 *Helical PH curves of degree 7*

Helical PH curves of degree 7 may be generated through the normalized Hopf map using *cubic* parameterizations of lines and circles in the complex plane. These may be constructed in three essentially distinct ways — of which two are direct extensions of the methods employed above for helical PH quintics, and the third is a "hybrid" of these two.

Cubic re–parameterization

By analogy with the first method used in Section 5.2.3, a rational cubic line/circle parameterization is defined by imposing the parameter transformation

$$t \;\rightarrow\; \frac{f(t)}{g(t)} \;=\; \frac{f_0(1-t)^3+f_1 3(1-t)^2 t+f_2 3(1-t)t^2+f_3 t^3}{g_0(1-t)^3+g_1 3(1-t)^2 t+g_2 3(1-t)t^2+g_3 t^3} \tag{5.2.9}$$

on (5.2.1). This yields

$$\mathbf{z}(t) \;=\; \frac{\boldsymbol{\alpha}(t)}{\boldsymbol{\beta}(t)} \;=\; \frac{\boldsymbol{\alpha}_0(1-t)^3+\boldsymbol{\alpha}_1 3(1-t)^2 t+\boldsymbol{\alpha}_2 3(1-t)t^2+\boldsymbol{\alpha}_3 t^3}{\boldsymbol{\beta}_0(1-t)^3+\boldsymbol{\beta}_1 3(1-t)^2 t+\boldsymbol{\beta}_2 3(1-t)t^2+\boldsymbol{\beta}_3 t^3}\,,$$

where

$$\boldsymbol{\alpha}_i \;=\; f_i(\mathbf{a}_1-\mathbf{a}_0)+g_i\mathbf{a}_0\,, \quad \boldsymbol{\beta}_i \;=\; f_i(\mathbf{b}_1-\mathbf{b}_0)+g_i\mathbf{b}_0\,, \quad i=0,1,2,3\,.$$

For this type of circle parameterization, we find that

$$\boldsymbol{\alpha}(t)\boldsymbol{\beta}'(t)-\boldsymbol{\alpha}'(t)\boldsymbol{\beta}(t) \;=\; h(t)\,(\mathbf{a}_0\mathbf{b}_1-\mathbf{a}_1\mathbf{b}_0)\,,$$

where the real quartic polynomial $h(t)$ has the form (5.2.4), and its Bernstein coefficients are given by

$$\begin{aligned} h_0 \;&=\; 3(f_1 g_0-f_0 g_1)\,, \quad h_1 \;=\; \tfrac{3}{2}(f_2 g_0-f_0 g_2)\,,\\ h_2 \;&=\; \tfrac{3}{2}(f_2 g_1-f_1 g_2)+\tfrac{1}{2}(f_3 g_0-f_0 g_3)\,,\\ h_3 \;&=\; \tfrac{3}{2}(f_3 g_1-f_1 g_3)\,, \quad h_4 \;=\; 3(f_3 g_2-f_2 g_3)\,. \end{aligned} \tag{5.2.10}$$

This corresponds to the case $\deg(h(t))=4$ and $\deg(\mathbf{w}(t))=0$ of (4.3.3), and it defines a general helical double PH curve of degree seven.

In the quaternion model, such curves are specified by a cubic quaternion polynomial $\mathcal{A}(t)=\boldsymbol{\alpha}(t)+\mathbf{k}\,\boldsymbol{\beta}(t)$ with Bernstein coefficients

$$\mathcal{A}_i \;=\; f_i\,[\,\mathbf{a}_1-\mathbf{a}_0+\mathbf{k}\,(\mathbf{b}_1-\mathbf{b}_0)\,]+g_i\,[\,\mathbf{a}_0+\mathbf{k}\,\mathbf{b}_0\,], \quad i=0,1,2,3\,. \tag{5.2.11}$$

Since $\mathcal{A}_0, \mathcal{A}_1, \mathcal{A}_2, \mathcal{A}_3$ are linearly dependent on the two quaternions, $\mathbf{a}_1 - \mathbf{a}_0 + \mathbf{k}\,(\mathbf{b}_1 - \mathbf{b}_0)$ and $\mathbf{a}_0 + \mathbf{k}\,\mathbf{b}_0$, they reside in a two–dimensional subspace of $\mathbb{H}$. Hence, $\mathcal{A}_1$, $\mathcal{A}_2$ must be expressible in terms of $\mathcal{A}_0$, $\mathcal{A}_3$ in the form

$$\mathcal{A}_1 \;=\; \mathcal{A}_0\, c_{10} \,+\, \mathcal{A}_3\, c_{13}\,, \qquad \mathcal{A}_2 \;=\; \mathcal{A}_0\, c_{20} \,+\, \mathcal{A}_3\, c_{23}\,, \tag{5.2.12}$$

for suitable values $c_{10}, c_{13}, c_{20}, c_{23} \in \mathbb{R}$. Substituting from (5.2.11) into the above, these coefficients can be expressed in terms of (5.2.10) and $k = f_3 g_0 - f_0 g_3$ as

$$c_{10} \;=\; \frac{2h_3}{3k}\,, \qquad c_{13} \;=\; \frac{h_0}{3k}\,, \qquad c_{20} \;=\; \frac{h_4}{3k}\,, \qquad c_{23} \;=\; \frac{2h_1}{3k}\,. \tag{5.2.13}$$

Quadratic polynomial multiplication

Instead of a cubic re–parameterization, we now consider the cubic line/circle parameterizations defined by multiplying the numerator and denominator of (5.2.1) by a complex quadratic polynomial. Writing

$$\begin{aligned} \boldsymbol{\alpha}(t) \;&=\; [\,\mathbf{a}_0(1-t) + \mathbf{a}_1 t\,]\,[\,\mathbf{w}_0(1-t)^2 + \mathbf{w}_1 2(1-t)t + \mathbf{w}_2 t^2\,]\,, \\ \boldsymbol{\beta}(t) \;&=\; [\,\mathbf{b}_0(1-t) + \mathbf{b}_1 t\,]\,[\,\mathbf{w}_0(1-t)^2 + \mathbf{w}_1 2(1-t)t + \mathbf{w}_2 t^2\,]\,, \end{aligned} \tag{5.2.14}$$

the Bernstein coefficients of the cubics $\boldsymbol{\alpha}(t)$ and $\boldsymbol{\beta}(t)$ are given by

$$\begin{aligned} \boldsymbol{\alpha}_0 &= \mathbf{a}_0\mathbf{w}_0, & \boldsymbol{\beta}_0 &= \mathbf{b}_0\mathbf{w}_0, \\ \boldsymbol{\alpha}_1 &= \tfrac{1}{3}(2\,\mathbf{a}_0\mathbf{w}_1 + \mathbf{a}_1\mathbf{w}_0), & \boldsymbol{\beta}_1 &= \tfrac{1}{3}(2\,\mathbf{b}_0\mathbf{w}_1 + \mathbf{b}_1\mathbf{w}_0), \\ \boldsymbol{\alpha}_2 &= \tfrac{1}{3}(2\,\mathbf{a}_1\mathbf{w}_1 + \mathbf{a}_0\mathbf{w}_2), & \boldsymbol{\beta}_2 &= \tfrac{1}{3}(2\,\mathbf{b}_1\mathbf{w}_1 + \mathbf{b}_0\mathbf{w}_2), \\ \boldsymbol{\alpha}_3 &= \mathbf{a}_1\mathbf{w}_2\,, & \boldsymbol{\beta}_3 &= \mathbf{b}_1\mathbf{w}_2\,. \end{aligned}$$

One can then verify that

$$\boldsymbol{\alpha}(t)\boldsymbol{\beta}'(t) - \boldsymbol{\alpha}'(t)\boldsymbol{\beta}(t) = (\mathbf{a}_0\mathbf{b}_1 - \mathbf{a}_1\mathbf{b}_0)[\,\mathbf{w}_0(1-t)^2 + \mathbf{w}_1 2(1-t)t + \mathbf{w}_2 t^2\,]^2,$$

corresponding to $\deg(h(t)) = 0$ and $\deg(\mathbf{w}(t)) = 2$ in (4.3.3) — note that the complex constant $\sqrt{\mathbf{a}_0\mathbf{b}_1 - \mathbf{a}_1\mathbf{b}_0}$ can be absorbed into $\mathbf{w}_0$, $\mathbf{w}_1$, $\mathbf{w}_2$. As in the quintic case, multiplying the numerator and denominator of (5.2.1) preserves the faithfulness of the line/circle parameterization. Hence, in this case, we have a monotone–helical double PH curve of degree 7.

Comparing with the quaternion model for this case, the cubic quaternion polynomial $\mathcal{A}(t) = \boldsymbol{\alpha}(t) + \mathbf{k}\,\boldsymbol{\beta}(t)$ has the Bernstein coefficients

$$\mathcal{A}_0 = (\mathbf{a}_0 + \mathbf{k}\,\mathbf{b}_0)\mathbf{w}_0\,, \quad \mathcal{A}_1 = \tfrac{1}{3}\,[\,2\,(\mathbf{a}_0 + \mathbf{k}\,\mathbf{b}_0)\mathbf{w}_1 + (\mathbf{a}_1 + \mathbf{k}\,\mathbf{b}_1)\mathbf{w}_0\,]\,,$$

$$\mathcal{A}_2 = \tfrac{1}{3}\,[\,2\,(\mathbf{a}_1 + \mathbf{k}\,\mathbf{b}_1)\mathbf{w}_1 + (\mathbf{a}_0 + \mathbf{k}\,\mathbf{b}_0)\mathbf{w}_2\,]\,, \quad \mathcal{A}_3 = (\mathbf{a}_1 + \mathbf{k}\,\mathbf{b}_1)\mathbf{w}_2\,.$$

By arguments similar to those of Section 5.2.3, we may infer that a degree 7 PH curve is monotone helical if and only if $\mathcal{A}_1$, $\mathcal{A}_2$ can be expressed in terms of $\mathcal{A}_0$, $\mathcal{A}_3$ in the form

$$\mathcal{A}_1 \;=\; \mathcal{A}_0\, \mathbf{c}_{10} \,+\, \mathcal{A}_3\, \mathbf{c}_{13}\,, \qquad \mathcal{A}_2 \;=\; \mathcal{A}_0\, \mathbf{c}_{20} \,+\, \mathcal{A}_3\, \mathbf{c}_{23}\,, \tag{5.2.15}$$

where the coefficients $\mathbf{c}_{10}$, $\mathbf{c}_{13}$, $\mathbf{c}_{20}$, $\mathbf{c}_{23}$ are given in terms of $\mathbf{w}_0$, $\mathbf{w}_1$, $\mathbf{w}_2$ by

$$\mathbf{c}_{10} = \frac{2\mathbf{w}_1}{3\mathbf{w}_0}, \qquad \mathbf{c}_{13} = \frac{\mathbf{w}_0}{3\mathbf{w}_2}, \qquad \mathbf{c}_{20} = \frac{\mathbf{w}_2}{3\mathbf{w}_0}, \qquad \mathbf{c}_{23} = \frac{2\mathbf{w}_1}{3\mathbf{w}_2}, \quad (5.2.16)$$

and satisfy

$$\mathbf{c}_{10} = 3\,\mathbf{c}_{20}\mathbf{c}_{23} \quad \text{and} \quad \mathbf{c}_{23} = 3\,\mathbf{c}_{10}\mathbf{c}_{13}\,. \quad (5.2.17)$$

Degenerate common case

As with the helical PH quintics, there is a common special instance between the cases in which the cubic line/circle representation is obtained purely by re–parameterization, and purely by multiplication. If the real quartic $h(t)$ in the former case is actually the square of a real quadratic, and the complex quadratic $\mathbf{w}_0(1-t)^2 + \mathbf{w}_1 2(1-t)t + \mathbf{w}_2 t^2$ in the latter case can be written as $\mathbf{c}\,[w_0(1-t)^2 + w_1 2(1-t)t + w_2 t^2\,]$, then $\boldsymbol{\alpha}(t)\boldsymbol{\beta}'(t) - \boldsymbol{\alpha}'(t)\boldsymbol{\beta}(t)$ is in both cases a complex constant times the square of a real quadratic polynomial.

Re–parameterization and multiplication

A new approach becomes possible with the degree 7 helical PH curves, since cubic line/circle parameterizations $\mathbf{z}(t) = \boldsymbol{\alpha}(t)/\boldsymbol{\beta}(t)$ can be generated from (5.2.1) in a "hybrid" manner: we can combine a quadratic re–parameterization with multiplication by a complex linear polynomial. Imposing the parameter transformation (5.2.3) on (5.2.1) and multiplying the numerator and denominator by $\mathbf{w}_0(1-t) + \mathbf{w}_1 t$, we obtain the cubics $\boldsymbol{\alpha}(t)$, $\boldsymbol{\beta}(t)$ with Bernstein coefficients

$$\begin{aligned}
\boldsymbol{\alpha}_0 &= [\,f_0(\mathbf{a}_1 - \mathbf{a}_0) + g_0\mathbf{a}_0\,]\,\mathbf{w}_0\,,\\
\boldsymbol{\alpha}_1 &= \tfrac{1}{3}\{\,[\,f_0(\mathbf{a}_1 - \mathbf{a}_0) + g_0\mathbf{a}_0\,]\,\mathbf{w}_1 + 2\,[\,f_1(\mathbf{a}_1 - \mathbf{a}_0) + g_1\mathbf{a}_0\,]\,\mathbf{w}_0\,\}\,,\\
\boldsymbol{\alpha}_2 &= \tfrac{1}{3}\{\,[\,f_2(\mathbf{a}_1 - \mathbf{a}_0) + g_2\mathbf{a}_0\,]\,\mathbf{w}_0 + 2\,[\,f_1(\mathbf{a}_1 - \mathbf{a}_0) + g_1\mathbf{a}_0\,]\,\mathbf{w}_1\,\}\,,\\
\boldsymbol{\alpha}_3 &= [\,f_2(\mathbf{a}_1 - \mathbf{a}_0) + g_2\mathbf{a}_0\,]\,\mathbf{w}_1\,,\\
\boldsymbol{\beta}_0 &= [\,f_0(\mathbf{b}_1 - \mathbf{b}_0) + g_0\mathbf{b}_0\,]\,\mathbf{w}_0\,,\\
\boldsymbol{\beta}_1 &= \tfrac{1}{3}\{\,[\,f_0(\mathbf{b}_1 - \mathbf{b}_0) + g_0\mathbf{b}_0\,]\,\mathbf{w}_1 + 2\,[\,f_1(\mathbf{b}_1 - \mathbf{b}_0) + g_1\mathbf{b}_0\,]\,\mathbf{w}_0\,\}\,,\\
\boldsymbol{\beta}_2 &= \tfrac{1}{3}\{\,[\,f_2(\mathbf{b}_1 - \mathbf{b}_0) + g_2\mathbf{b}_0\,]\,\mathbf{w}_0 + 2\,[\,f_1(\mathbf{b}_1 - \mathbf{b}_0) + g_1\mathbf{b}_0\,]\,\mathbf{w}_1\,\}\,,\\
\boldsymbol{\beta}_3 &= [\,f_2(\mathbf{b}_1 - \mathbf{b}_0) + g_2\mathbf{b}_0\,]\,\mathbf{w}_1\,,
\end{aligned} \quad (5.2.18)$$

and in this case, we find that

$$\boldsymbol{\alpha}(t)\boldsymbol{\beta}'(t) - \boldsymbol{\alpha}'(t)\boldsymbol{\beta}(t) = h(t)\,(\mathbf{a}_0\mathbf{b}_1 - \mathbf{a}_1\mathbf{b}_0)\,[\mathbf{w}_0(1-t) + \mathbf{w}_1 t]^2\,,$$

$h(t)$ being the real quadratic polynomial with the Bernstein coefficients (5.2.5). This corresponds to the case $\deg(h(t)) = 2$ and $\deg(\mathbf{w}(t)) = 1$ of (4.3.3).

It should be noted that the *order* of the operations characterizing this case (*first* re–parameterization, *then* multiplication) is important, since it is not possible to

achieve a cubic line/circle parameterization through a polynomial multiplication followed by a re–parameterization. For this case, setting

$$\mathcal{V}_0 \;=\; \mathbf{a}_1 - \mathbf{a}_0 + \mathbf{k}\,(\mathbf{b}_1 - \mathbf{b}_0) \qquad \text{and} \qquad \mathcal{V}_1 \;=\; \mathbf{a}_0 + \mathbf{k}\,\mathbf{b}_0\,,$$

we find that the quaternion representation is defined by the cubic polynomial $\mathcal{A}(t) = \boldsymbol{\alpha}(t) + \mathbf{k}\,\boldsymbol{\beta}(t)$ with Bernstein coefficients

$$\begin{aligned}
\mathcal{A}_0 &= (f_0\mathcal{V}_0 + g_0\mathcal{V}_1)\mathbf{w}_0\,,\\
\mathcal{A}_1 &= \tfrac{1}{3}(f_0\mathcal{V}_0 + g_0\mathcal{V}_1)\mathbf{w}_1 \;+\; \tfrac{2}{3}(f_1\mathcal{V}_0 + g_1\mathcal{V}_1)\mathbf{w}_0\,,\\
\mathcal{A}_2 &= \tfrac{1}{3}(f_2\mathcal{V}_0 + g_2\mathcal{V}_1)\mathbf{w}_0 \;+\; \tfrac{2}{3}(f_1\mathcal{V}_0 + g_1\mathcal{V}_1)\mathbf{w}_1\,,\\
\mathcal{A}_3 &= (f_2\mathcal{V}_0 + g_2\mathcal{V}_1)\mathbf{w}_1\,.
\end{aligned}$$

As in the preceding cases $\mathcal{A}_1, \mathcal{A}_2$ can be expressed in terms of $\mathcal{A}_0, \mathcal{A}_3$ as

$$\mathcal{A}_1 \;=\; \mathcal{A}_0\,\mathbf{c}_{10} \;+\; \mathcal{A}_3\,\mathbf{c}_{13}\,, \qquad \mathcal{A}_2 \;=\; \mathcal{A}_0\,\mathbf{c}_{20} \;+\; \mathcal{A}_3\,\mathbf{c}_{23}\,. \tag{5.2.19}$$

In this case, the complex coefficients $\mathbf{c}_{10}$, $\mathbf{c}_{13}$ and $\mathbf{c}_{20}$, $\mathbf{c}_{23}$ are given in terms of $\mathbf{w}_0$, $\mathbf{w}_1$, $\mathbf{w}_2$ and the quantities (5.2.5) defined in Section 5.2.3 by

$$\mathbf{c}_{10} = \frac{h_1\mathbf{w}_1 + h_2\mathbf{w}_0}{3\,h_1\mathbf{w}_0}, \;\; \mathbf{c}_{13} = \frac{h_0\mathbf{w}_0}{3\,h_1\mathbf{w}_1}, \;\; \mathbf{c}_{20} = \frac{h_2\mathbf{w}_1}{3\,h_1\mathbf{w}_0}, \;\; \mathbf{c}_{23} = \frac{h_1\mathbf{w}_0 + h_0\mathbf{w}_1}{3\,h_1\mathbf{w}_1}. \tag{5.2.20}$$

Note that the coefficients $\mathbf{c}_{10}$, $\mathbf{c}_{13}$ and $\mathbf{c}_{20}$, $\mathbf{c}_{23}$ depend only on the three ratios h_0/h_1, h_2/h_1, and $\mathbf{w}_1/\mathbf{w}_0$. It can be shown that they must satisfy

$$(9\,\mathbf{c}_{13}\mathbf{c}_{20} - 1)^2 \;=\; 9\,(3\,\mathbf{c}_{13}\mathbf{c}_{10} - \mathbf{c}_{23})\,(3\,\mathbf{c}_{23}\mathbf{c}_{20} - \mathbf{c}_{10})\,. \tag{5.2.21}$$

5.2.5 *Higher–order helical PH curves*

To construct higher–order generalizations of the helical PH curves of degree 5 and 7 described in Sections 5.2.3 and 5.2.4, one may use re–parameterizations $t \to f(t)/g(t)$ of the line/circle (5.2.1) defined by polynomials $f(t)$ and $g(t)$ with $m = \deg(f, g) \geqslant 4$. Curves defined in this manner have the common feature that the coefficients of $\boldsymbol{\alpha}(t)$, $\boldsymbol{\beta}(t)$ are of the form

$$\boldsymbol{\alpha}_i \;=\; f_i(\mathbf{a}_1 - \mathbf{a}_0) + g_i\mathbf{a}_0\,, \quad \boldsymbol{\beta}_i \;=\; f_i(\mathbf{b}_1 - \mathbf{b}_0) + g_i\mathbf{b}_0\,, \quad i = 0, \ldots, m\,.$$

Invoking the relation (3.3.1) between the quaternion and Hopf map models, we see that such curves are characterized by quaternion coefficients of the form

$$\mathcal{A}_i \;=\; f_i\,[\,\mathbf{a}_1 - \mathbf{a}_0 + \mathbf{k}\,(\mathbf{b}_1 - \mathbf{b}_0)\,] \;+\; g_i\,[\,\mathbf{a}_0 + \mathbf{k}\,\mathbf{b}_0\,], \quad i = 0, \ldots, m$$

for real values $f_0, \ldots, f_m$ and $g_0, \ldots, g_m$. The $m+1$ quaternions $\mathcal{A}_0, \ldots, \mathcal{A}_m$ are thus linearly dependent on just two quaternions — $\mathbf{a}_1 - \mathbf{a}_0 + \mathbf{k}\,(\mathbf{b}_1 - \mathbf{b}_0)$ and

$\mathbf{a}_0 + \mathbf{k}\,\mathbf{b}_0$ — and reside within a two–dimensional subspace of $\mathbb{H}$. Hence, as observed in [37] for the PH quintics ($m = 2$) and in [70] for general m, such helical PH curves are characterized by the fact that the interior coefficients $\mathcal{A}_1, \ldots, \mathcal{A}_{m-1}$ are linearly dependent on the outer coefficients $\mathcal{A}_0$ and $\mathcal{A}_m$.

As generalizations of the degree 5 and 7 monotone helical curves discussed in Sections 5.2.3 and 5.2.4, a line/circle parameterization $\mathbf{z}(t) = \boldsymbol{\alpha}(t)/\boldsymbol{\beta}(t)$ of degree m may be specified by multiplying $\mathbf{a}_0(1-t) + \mathbf{a}_1 t$ and $\mathbf{b}_0(1-t) + \mathbf{b}_1 t$ by a polynomial $\mathbf{w}(t)$ of degree $m-1$ with Bernstein coefficients $\mathbf{w}_0, \ldots, \mathbf{w}_{m-1}$. The coefficients of $\boldsymbol{\alpha}(t)$ and $\boldsymbol{\beta}(t)$ are then given by $\boldsymbol{\alpha}_0 = \mathbf{a}_0\mathbf{w}_0$, $\boldsymbol{\alpha}_m = \mathbf{a}_1\mathbf{w}_{m-1}$ and $\boldsymbol{\beta}_0 = \mathbf{b}_0\mathbf{w}_0$, $\boldsymbol{\beta}_m = \mathbf{b}_1\mathbf{w}_{m-1}$ while for $k = 1, \ldots, m-1$ we have

$$\boldsymbol{\alpha}_k = \frac{(m-k)\mathbf{a}_0\mathbf{w}_k + k\,\mathbf{a}_1\mathbf{w}_{k-1}}{m}\,, \quad \boldsymbol{\beta}_k = \frac{(m-k)\mathbf{b}_0\mathbf{w}_k + k\,\mathbf{b}_1\mathbf{w}_{k-1}}{m}\,,$$

and such curves satisfy $\boldsymbol{\alpha}(t)\boldsymbol{\beta}'(t) - \boldsymbol{\alpha}'(t)\boldsymbol{\beta}(t) = (\mathbf{a}_0\mathbf{b}_1 - \mathbf{a}_1\mathbf{b}_0)\,\mathbf{w}^2(t)$. As in Sections 5.2.3 and 5.2.4, the quaternion form of these curves is characterized by the fact that $\mathcal{A}_1, \ldots, \mathcal{A}_m$ can be written as linear combinations of $\mathcal{A}_0, \mathcal{A}_m$ with suitable complex coefficients $\mathbf{c}_{k0}$, $\mathbf{c}_{km}$ for $k = 1, \ldots, m-1$.

Finally, as generalizations of the degree 7 helical curves identified by combining re–parameterization and multiplication, one may invoke any combination of (real) rational re–parameterizations and complex polynomial multiplications, specified in a particular order.

5.3 NON–HELICAL DOUBLE PH CURVES

A helical PH curve must be a double PH curve, but not all double PH curves are helical. As already observed, the lowest–order double PH curves that are non–helical have degree 7. We now seek criteria that serve to distinguish the non–helical double PH curves of degree 7 from the helical curves, for each of the three types enumerated in Section 4.4.2.

Assuming $\boldsymbol{\alpha}(t) \not\equiv 0$ and $\boldsymbol{\beta}(t) \not\equiv 0$ in (3.2.2), we begin with some observations concerning the possible common factors of these polynomials.

Lemma 5.1. *For cubic polynomials* $\boldsymbol{\alpha}(t)$, $\boldsymbol{\beta}(t)$ *let* $\boldsymbol{\gamma}(t) = \gcd(\boldsymbol{\alpha}(t), \boldsymbol{\beta}(t))$ *where* $r = \deg(\boldsymbol{\gamma}(t))$ *satisfies* $0 \leqslant r \leqslant 3$, *so that* $\boldsymbol{\alpha}(t) = \boldsymbol{\gamma}(t)\,\tilde{\boldsymbol{\alpha}}(t)$, $\boldsymbol{\beta}(t) = \boldsymbol{\gamma}(t)\,\tilde{\boldsymbol{\beta}}(t)$ *with* $\gcd(\tilde{\boldsymbol{\alpha}}(t), \tilde{\boldsymbol{\beta}}(t)) = \text{constant}$ *and* $\deg(\tilde{\boldsymbol{\alpha}}(t), \tilde{\boldsymbol{\beta}}(t)) = 3 - r$. *The condition* (4.3.3) *for a DPH curve then becomes*

$$\boldsymbol{\gamma}^2(t)\,[\,\tilde{\boldsymbol{\alpha}}(t)\tilde{\boldsymbol{\beta}}'(t) - \tilde{\boldsymbol{\alpha}}'(t)\tilde{\boldsymbol{\beta}}(t)\,] \;=\; h(t)\,\mathbf{w}^2(t)\,, \tag{5.3.1}$$

and we must have $r \leqslant 1$ *for a curve satisfying this condition to be non–helical.*

Proof : If $r = 3$, the cubics $\boldsymbol{\alpha}(t)$, $\boldsymbol{\beta}(t)$ are proportional, and hence the curve degenerates (see Section 3.4) to a straight line — which is trivially helical. If $r = 2$, we have $\boldsymbol{\alpha}(t) = \boldsymbol{\gamma}(t)\,\tilde{\boldsymbol{\alpha}}(t)$, $\boldsymbol{\beta}(t) = \boldsymbol{\gamma}(t)\,\tilde{\boldsymbol{\beta}}(t)$ with $\tilde{\boldsymbol{\alpha}}(t)$, $\tilde{\boldsymbol{\beta}}(t)$ linear and $\boldsymbol{\gamma}(t)$

quadratic, so that $\mathbf{z}(t) = \boldsymbol{\alpha}(t)/\boldsymbol{\beta}(t) = \tilde{\boldsymbol{\alpha}}(t)/\tilde{\boldsymbol{\beta}}(t)$ defines a line/circle of the form (5.2.1) in the complex plane, and the double PH curve is helical (see Section 5.2). Thus, we must have $r \leqslant 1$ for a non–helical DPH curve of degree 7. ∎

Lemma 5.2. *For cubics $\boldsymbol{\alpha}(t)$, $\boldsymbol{\beta}(t)$ let r be the degree of $\boldsymbol{\gamma}(t) = \gcd(\boldsymbol{\alpha}(t), \boldsymbol{\beta}(t))$ and let $\boldsymbol{\alpha}(t) = \boldsymbol{\gamma}(t)\,\tilde{\boldsymbol{\alpha}}(t)$, $\boldsymbol{\beta}(t) = \boldsymbol{\gamma}(t)\,\tilde{\boldsymbol{\beta}}(t)$ as in Lemma 5.1. Then* (4.3.3) *cannot be satisfied with $r = 1$ if $h(t)$ is a constant or a perfect square.*

Proof : If $r = 1$, $\boldsymbol{\alpha}(t) = \boldsymbol{\gamma}(t)\,\tilde{\boldsymbol{\alpha}}(t)$ and $\boldsymbol{\beta}(t) = \boldsymbol{\gamma}(t)\,\tilde{\boldsymbol{\beta}}(t)$ with $\boldsymbol{\gamma}(t)$ linear and $\tilde{\boldsymbol{\alpha}}(t)$, $\tilde{\boldsymbol{\beta}}(t)$ quadratic and relatively prime. In this case, $\tilde{\boldsymbol{\alpha}}(t)\tilde{\boldsymbol{\beta}}'(t) - \tilde{\boldsymbol{\alpha}}'(t)\tilde{\boldsymbol{\beta}}(t)$ is quadratic, and it must be a perfect square if $h(t)$ in (5.3.1) is a constant or a perfect square, i.e., we must have

$$\tilde{\boldsymbol{\alpha}}(t)\tilde{\boldsymbol{\beta}}'(t) - \tilde{\boldsymbol{\alpha}}'(t)\tilde{\boldsymbol{\beta}}(t) \;=\; \delta^2(t) \tag{5.3.2}$$

for some linear polynomial $\delta(t)$. Then, if τ is the root of $\delta(t)$, we have

$$\tilde{\boldsymbol{\alpha}}(\tau)\tilde{\boldsymbol{\beta}}'(\tau) - \tilde{\boldsymbol{\alpha}}'(\tau)\tilde{\boldsymbol{\beta}}(\tau) \;=\; \tilde{\boldsymbol{\alpha}}(\tau)\tilde{\boldsymbol{\beta}}''(\tau) - \tilde{\boldsymbol{\alpha}}''(\tau)\tilde{\boldsymbol{\beta}}(\tau) \;=\; 0\,. \tag{5.3.3}$$

Now since $\gcd(\tilde{\boldsymbol{\alpha}}(t), \tilde{\boldsymbol{\beta}}(t)) = \text{constant}$, $\tilde{\boldsymbol{\alpha}}(\tau)$ and $\tilde{\boldsymbol{\beta}}(\tau)$ cannot be both zero. If we assume both are non–zero, equations (5.3.3) imply that

$$\tilde{\boldsymbol{\alpha}}(\tau) \,:\, \tilde{\boldsymbol{\alpha}}'(\tau) \,:\, \tilde{\boldsymbol{\alpha}}''(\tau) \;=\; \tilde{\boldsymbol{\beta}}(\tau) \,:\, \tilde{\boldsymbol{\beta}}'(\tau) \,:\, \tilde{\boldsymbol{\beta}}''(\tau)\,.$$

But since $\tilde{\boldsymbol{\alpha}}(t)$ and $\tilde{\boldsymbol{\beta}}(t)$ are quadratic, this implies that they are proportional — contradicting $\gcd(\tilde{\boldsymbol{\alpha}}(t), \tilde{\boldsymbol{\beta}}(t)) = \text{constant}$. If we assume $\tilde{\boldsymbol{\alpha}}(\tau) = 0 \neq \tilde{\boldsymbol{\beta}}(\tau)$, equations (5.3.3) imply that $\tilde{\boldsymbol{\alpha}}'(\tau) = \tilde{\boldsymbol{\alpha}}''(\tau) = 0$, so $\tilde{\boldsymbol{\alpha}}(t) = \boldsymbol{\alpha}_0(t-\tau)^2$ for some constant $\boldsymbol{\alpha}_0 \neq 0$. Substituting in (5.3.2) and writing $\delta(t) = \delta_0(t-\tau)^2$ gives

$$2\,\boldsymbol{\alpha}_0\,\tilde{\boldsymbol{\beta}}(t) \;=\; [\,\boldsymbol{\alpha}_0\,\tilde{\boldsymbol{\beta}}'(t) - \delta_0^2(t-\tau)^2\,]\,(t-\tau)\,,$$

contradicting the assumption that $\tilde{\boldsymbol{\beta}}(\tau) \neq 0$. A similar contradiction arises if we assume $\tilde{\boldsymbol{\alpha}}(\tau) \neq 0 = \tilde{\boldsymbol{\beta}}(\tau)$. Hence, we infer that (4.3.3) cannot be satisfied by cubics $\boldsymbol{\alpha}(t)$, $\boldsymbol{\beta}(t)$ with $\boldsymbol{\gamma}(t) = \gcd(\boldsymbol{\alpha}(t), \boldsymbol{\beta}(t))$ of degree 1 if $h(t)$ is a constant or a perfect square. ∎

The following lemmas give useful alternatives to the (rational) line/circle representations discussed in Section 5.2.1, that will be invoked subsequently.

Lemma 5.3. *Let $\mathbf{a}_1$, $\mathbf{a}_2$, $\mathbf{b}_1$, $\mathbf{b}_2$ be complex constants such that $\mathbf{a}_1\mathbf{b}_2 - \mathbf{a}_2\mathbf{b}_1 \neq 0$, and let ϕ be a real variable. Then if $|\mathbf{b}_1| \neq |\mathbf{b}_2|$ the function*

$$\mathbf{z}(\phi) \;=\; \frac{\mathbf{a}_1 e^{i\phi} + \mathbf{a}_2}{\mathbf{b}_1 e^{i\phi} + \mathbf{b}_2} \tag{5.3.4}$$

defines a circle with center and radius given by

$$\mathbf{z}_c \;=\; \frac{\mathbf{a}_1\overline{\mathbf{b}}_1 - \mathbf{a}_2\overline{\mathbf{b}}_2}{|\mathbf{b}_1|^2 - |\mathbf{b}_2|^2} \qquad \text{and} \qquad R \;=\; \left| \frac{\mathbf{a}_2\mathbf{b}_1 - \mathbf{a}_1\mathbf{b}_2}{|\mathbf{b}_1|^2 - |\mathbf{b}_2|^2} \right|,$$

while if $|\mathbf{b}_1| = |\mathbf{b}_2|$ the function (5.3.4) *defines a straight line.*

Proof : The condition $\mathbf{a}_1\mathbf{b}_2 - \mathbf{a}_2\mathbf{b}_1 \neq 0$ guarantees that the numerator and denominator of (5.3.4) are not proportional, so $\mathbf{z}(\phi)$ does not degenerate to a constant. By subtracting $\mathbf{z}_c$ from $\mathbf{z}(\phi)$ and simplifying, one obtains

$$\mathbf{z}(\phi) - \mathbf{z}_c \;=\; \frac{\mathbf{a}_2\mathbf{b}_1 - \mathbf{a}_1\mathbf{b}_2}{|\mathbf{b}_1|^2 - |\mathbf{b}_2|^2}\;\frac{\overline{\mathbf{b}}_1 e^{-i\phi} + \overline{\mathbf{b}}_2}{\mathbf{b}_1 e^{i\phi} + \mathbf{b}_2}\; e^{i\phi}\,,$$

and since the two factors dependent on ϕ have unit magnitude, we see that $|\mathbf{z}(\phi) - \mathbf{z}_c| = R$. For the case $|\mathbf{b}_1| = |\mathbf{b}_2|$, in which $\mathbf{z}_c$ and R become infinite, we have a circle of infinite radius — i.e., a straight line. ∎

Lemma 5.4. *If τ_1, τ_2 are both real or complex conjugates,*[5] *the function*

$$\mathbf{z}(t) \;=\; \frac{\mathbf{a}_1(t-\tau_1)^m + \mathbf{a}_2(t-\tau_2)^m}{\mathbf{b}_1(t-\tau_1)^m + \mathbf{b}_2(t-\tau_2)^m}$$

of the real variable t defines, for integer m, a line/circle in the complex plane.

Proof : Writing $\mathbf{f}(t) = (t-\tau_1)^m/(t-\tau_2)^m$ we have

$$\mathbf{z}(t) \;=\; \frac{\mathbf{a}_1\mathbf{f}(t) + \mathbf{a}_2}{\mathbf{b}_1\mathbf{f}(t) + \mathbf{b}_2}\,.$$

If τ_1, τ_2 are real, $\mathbf{f}(t)$ becomes a *real* function $f(t)$, and we may regard $\mathbf{z}(t)$ as arising from a real re–parameterization $t \to f(t)$ applied to the rational linear form (5.2.1) of a line/circle. On the other hand, if τ_1, τ_2 are complex conjugates, we have $\mathbf{f}(t) = \exp(i\,2m\arg(t-\tau_1))$, and writing $\phi = 2m\arg(t-\tau_1)$ we see that $\mathbf{z}(t)$ has the alternative line/circle form (5.3.4). ∎

These lemmas simplify the identification of criteria to distinguish helical and non–helical degree 7 DPH curves, as described in the following sections.

5.3.1 *First case:* $\deg(h) = 0$, $\deg(\mathbf{w}) = 2$

In this case $h(t)$ is a constant, h_0. To identify the non–helical DPH curves of this type, we set $\boldsymbol{\gamma}(t) = \gcd(\boldsymbol{\alpha}(t), \boldsymbol{\beta}(t))$ and $r = \deg(\boldsymbol{\gamma}(t))$ as in Lemma 5.1.

Proposition 5.1. *A degree 7 DPH curve satisfying* (4.3.3) *with $h(t)$ constant and $\mathbf{w}(t)$ quadratic is non–helical if the roots τ_1, τ_2 of $\mathbf{w}(t)$ are neither both real nor complex conjugates, and $\boldsymbol{\alpha}(t)$, $\boldsymbol{\beta}(t)$ can be expressed in terms of them as*

$$\boldsymbol{\alpha}(t) \;=\; \mathbf{a}_1(t-\tau_1)^3 + \mathbf{a}_2(t-\tau_2)^3, \quad \boldsymbol{\beta}(t) \;=\; \mathbf{b}_1(t-\tau_1)^3 + \mathbf{b}_2(t-\tau_2)^3, \qquad (5.3.5)$$

where $\mathbf{a}_1\mathbf{b}_2 - \mathbf{a}_2\mathbf{b}_1 \neq 0$.

5 Here, the case of complex conjugates subsumes the case of a (real) double root, $\tau_1 = \tau_2$.

Proof : By Lemmas 5.1 and 5.2, we need only consider $\gamma(t) = \gcd(\alpha(t), \beta(t))$ of degree $r = 0$. For relatively prime cubics $\alpha(t)$, $\beta(t)$ satisfying

$$\alpha(t)\beta'(t) - \alpha'(t)\beta(t) \;=\; h_0\, w^2(t)\,, \tag{5.3.6}$$

let τ_1, τ_2 be the roots of the quadratic $w(t)$. Then τ_1, τ_2 must be double roots of (4.3.1), and we have

$$\alpha(\tau_i)\beta'(\tau_i) - \alpha'(\tau_i)\beta(\tau_i) \;=\; \alpha(\tau_i)\beta''(\tau_i) - \alpha''(\tau_i)\beta(\tau_i) \;=\; 0 \tag{5.3.7}$$

for $i = 1, 2$. To study when these conditions can be satisfied, we note that if $\tau_1 \neq \tau_2$ we may write $\alpha(t)$, $\beta(t)$ in the Bernstein–like form

$$\alpha(t) = \sum_{k=0}^{3} p_k \binom{3}{k} (\tau_2 - t)^{3-k} (t - \tau_1)^k\,, \quad \beta(t) = \sum_{k=0}^{3} q_k \binom{3}{k} (\tau_2 - t)^{3-k} (t - \tau_1)^k$$

for suitable complex coefficients p_k, q_k. We note that $(\alpha(\tau_i), \beta(\tau_i)) \neq (0, 0)$ for $i = 1, 2$ since $\gcd(\alpha(t), \beta(t)) =$ constant, and consider two possible cases:

case (a): $\alpha(\tau_i) \neq 0$ and $\beta(\tau_i) \neq 0$ for $i = 1, 2$. In this case the relations (5.3.7) can be written as

$$\frac{\alpha'(\tau_i)}{\alpha(\tau_i)} = \frac{\beta'(\tau_i)}{\beta(\tau_i)}\,, \qquad \frac{\alpha''(\tau_i)}{\alpha(\tau_i)} = \frac{\beta''(\tau_i)}{\beta(\tau_i)}$$

for $i = 1, 2$. In terms of the coefficients p_k, q_k these imply that

$$\frac{p_1}{p_0} = \frac{q_1}{q_0}\,, \qquad \frac{p_2}{p_0} = \frac{q_2}{q_0}\,, \qquad \frac{p_2}{p_3} = \frac{q_2}{q_3}\,, \qquad \frac{p_1}{p_3} = \frac{q_1}{q_3}\,.$$

Now satisfying these conditions with p_1, p_2 and q_1, q_2 not all zero implies that $\alpha(t)$, $\beta(t)$ are proportional — contradicting $\gcd(\alpha(t), \beta(t)) =$ constant. We may satisfy them without contradiction, however, by taking $p_1 = p_2 = 0$ and $q_1 = q_2 = 0$, so that

$$\alpha(t) \;=\; p_0(\tau_2 - t)^3 + p_3(t - \tau_1)^3\,, \quad \beta(t) \;=\; q_0(\tau_2 - t)^3 + q_3(t - \tau_1)^3\,,$$

where $p_0 q_3 - p_3 q_0 \neq 0$ is stipulated to ensure non–proportionality. Hence, setting $a_1 = p_3$, $a_2 = -p_0$ and $b_1 = q_3$, $b_2 = -q_0$, the polynomials (5.3.5) define a non–helical DPH curve provided that τ_1, τ_2 are not both real and not complex conjugates since, by Lemma 5.4, $z(t) = \alpha(t)/\beta(t)$ does not define a line/circle in the complex plane.

case (b): At least one of $\alpha(\tau_i)$ and $\beta(\tau_i)$ for $i = 1, 2$ is zero. Assuming that $\alpha(\tau_1) = 0$, we have $\beta(\tau_1) \neq 0$, i.e., $q_0 \neq 0$, since $\gcd(\alpha(t), \beta(t)) =$ constant. Equations (5.3.7) then imply that $\alpha'(\tau_1) = \alpha''(\tau_1) = 0$, so $p_0 = p_1 = p_2 = 0$ and $\alpha(t) = p_3(t - \tau_1)^3$. From (5.3.7) with $i = 2$ we then infer that $q_1 = q_2 = 0$,

and hence $\boldsymbol{\beta}(t) = \mathbf{q}_0(\tau_2 - t)^3 + \mathbf{q}_3(t-\tau_1)^3$. Thus, $\boldsymbol{\alpha}(t)$ and $\boldsymbol{\beta}(t)$ in this case are also of the form (5.3.5), but with $\mathbf{a}_1 = \mathbf{p}_3$, $\mathbf{a}_2 = 0$ and $\mathbf{b}_1 = \mathbf{q}_3$, $\mathbf{b}_2 = -\mathbf{q}_0$. Analogous results are obtained when $\boldsymbol{\alpha}(\tau_2) = 0 \neq \boldsymbol{\beta}(\tau_2)$ or $\boldsymbol{\alpha}(\tau_1) \neq 0 = \boldsymbol{\beta}(\tau_1)$ or $\boldsymbol{\alpha}(\tau_2) \neq 0 = \boldsymbol{\beta}(\tau_2)$ — namely, one of the coefficients $\mathbf{a}_1$, $\mathbf{a}_2$ and $\mathbf{b}_1$, $\mathbf{b}_2$ in (5.3.5) vanishes. Again, the curve is non–helical, since $\mathbf{z}(t) = \boldsymbol{\alpha}(t)/\boldsymbol{\beta}(t)$ does not describe a line/circle under the stated constraints on τ_1, τ_2.

We assumed above that $\mathbf{w}(t)$ has distinct roots τ_1, τ_2. If $\tau_1 = \tau_2$, so $\mathbf{w}(t)$ has a double root and $\mathbf{w}^2(t)$ is the fourth power of a linear polynomial, one may verify that (5.3.6) can only be satisfied with $h_0 = 0$ and $\boldsymbol{\alpha}(t)$, $\boldsymbol{\beta}(t)$ proportional, contradicting $\gcd(\boldsymbol{\alpha}(t), \boldsymbol{\beta}(t)) = \text{constant}$. ∎

5.3.2 *Second case:* $\deg(h) = 2$, $\deg(\mathbf{w}) = 1$

By Lemma 5.1 we need only consider cases in which $\boldsymbol{\gamma}(t) = \gcd(\boldsymbol{\alpha}(t), \boldsymbol{\beta}(t))$ is of degree $r = 1$ or $r = 0$. In the following propositions, we shall see that non–helical DPH curves can exist only in the latter case.

Proposition 5.2. *There are no non–helical degree 7 DPH curves satisfying* (4.3.3) *with* $h(t)$ *quadratic,* $\mathbf{w}(t)$ *linear, and* $\boldsymbol{\gamma}(t) = \gcd(\boldsymbol{\alpha}(t), \boldsymbol{\beta}(t))$ *of degree* $r = 1$.

Proof : By Lemma 5.2, we need only consider quadratics $h(t)$ with two *distinct* roots τ_1, τ_2 in this case, and from (5.3.1) it is apparent that $\tilde{\boldsymbol{\alpha}}(t)\tilde{\boldsymbol{\beta}}'(t) - \tilde{\boldsymbol{\alpha}}'(t)\tilde{\boldsymbol{\beta}}(t)$ and $\boldsymbol{\gamma}(t)$ must be proportional to $h(t)$ and $\mathbf{w}(t)$, respectively. For suitable coefficients $\mathbf{p}_0, \mathbf{p}_1, \mathbf{p}_2$ and $\mathbf{q}_0, \mathbf{q}_1, \mathbf{q}_2$ we may write

$$\begin{aligned}\tilde{\boldsymbol{\alpha}}(t) &= \mathbf{p}_0(\tau_2 - t)^2 + \mathbf{p}_1 2(\tau_2 - t)(t - \tau_1) + \mathbf{p}_2(t-\tau_1)^2\,,\\ \tilde{\boldsymbol{\beta}}(t) &= \mathbf{q}_0(\tau_2 - t)^2 + \mathbf{q}_1 2(\tau_2 - t)(t - \tau_1) + \mathbf{q}_2(t-\tau_1)^2\,,\end{aligned}$$

and the fact that $\tilde{\boldsymbol{\alpha}}(t)\tilde{\boldsymbol{\beta}}'(t) - \tilde{\boldsymbol{\alpha}}'(t)\tilde{\boldsymbol{\beta}}(t)$ must vanish at τ_1 and τ_2 implies that

$$\mathbf{p}_0\mathbf{q}_1 - \mathbf{p}_1\mathbf{q}_0 = 0 \qquad \text{and} \qquad \mathbf{p}_1\mathbf{q}_2 - \mathbf{p}_2\mathbf{q}_1 = 0\,.$$

Now if $\mathbf{p}_1$, $\mathbf{q}_1$ are not both zero, these equations imply that $\tilde{\boldsymbol{\alpha}}(t)$, $\tilde{\boldsymbol{\beta}}(t)$ must be proportional,[6] which contradicts $\gcd(\tilde{\boldsymbol{\alpha}}(t), \tilde{\boldsymbol{\beta}}(t)) = \text{constant}$. But they are satisfied without contradiction if $\mathbf{p}_1 = \mathbf{q}_1 = 0$. Taking $\mathbf{a}_1 = \mathbf{p}_0$, $\mathbf{a}_2 = \mathbf{p}_2$ and $\mathbf{b}_1 = \mathbf{q}_0$, $\mathbf{b}_2 = \mathbf{q}_2$ and a suitable choice of constants, we then have

$$\begin{aligned}\boldsymbol{\alpha}(t) &= \mathbf{w}(t)\,[\,\mathbf{a}_1(t-\tau_1)^2 + \mathbf{a}_2(t-\tau_2)^2\,]\,,\\ \boldsymbol{\beta}(t) &= \mathbf{w}(t)\,[\,\mathbf{b}_1(t-\tau_1)^2 + \mathbf{b}_2(t-\tau_2)^2\,]\,,\end{aligned}$$

where the roots τ_1, τ_2 must be both real or complex conjugates, since $h(t)$ is a real polynomial. Hence, Lemma 5.4 indicates that $\mathbf{z}(t) = \boldsymbol{\alpha}(t)/\boldsymbol{\beta}(t)$ describes a line/circle in the complex plane, so the DPH curve must be helical. ∎

6 They are trivially proportional when one of them vanishes identically.

If $\deg(h) = 2$, $\deg(\mathbf{w}) = 1$ and $\alpha(t)$, $\beta(t)$ are relatively prime, it is not so easy to derive a characterization for these polynomials in terms of the roots of $h(t)$ and $\mathbf{w}(t)$, analogous to (5.3.5), that yields non–helical curves. However, we may appeal to the analysis of helical DPH curves in Section 5.2.4 to obtain a simple resolution of this question.

Proposition 5.3. *All double PH curves of degree 7 that satisfy (4.3.3) with* $h(t)$ *quadratic,* $\mathbf{w}(t)$ *linear, and* $\gcd(\alpha(t), \beta(t))$ *of degree* $r = 0$ *are non–helical.*

Proof : Section 5.2.4 enumerates all possible construction modes for degree 7 helical curves, starting from a line/circle parameterization of the form (5.2.1) in the complex plane. These include a cubic re–parameterization, multiplication with a quadratic polynomial, and a quadratic re–parameterization followed by multiplication with a linear polynomial. Of these, only the latter mode yields helical curves with $\deg(h) = 2$ and $\deg(\mathbf{w}) = 1$ in (4.3.3), and for such curves $\alpha(t)$ and $\beta(t)$ must have the linear polynomial $\mathbf{w}(t)$ as a common factor. Hence, degree 7 DPH curve with $h(t)$ quadratic, $\mathbf{w}(t)$ linear, and $\gcd(\alpha(t), \beta(t)) =$ constant are necessarily non–helical. ∎

5.3.3 *Third case:* $\deg(h) = 4$, $\deg(\mathbf{w}) = 0$

In this case, we find that a simple quadratic expression in the Bernstein coefficients of the real quartic polynomial $h(t)$ serves to distinguish between helical and non–helical double PH curves.

Proposition 5.4. *A degree 7 double PH curve with* $\deg(h) = 4$ *and* $\deg(\mathbf{w}) = 0$ *in* (4.3.3) *is helical or non–helical according to whether or not the quantity*

$$\Delta = 9\,h_2^2 + 3\,h_0 h_4 - 12\,h_1 h_3\,, \tag{5.3.8}$$

defined in terms of the Bernstein coefficients of $h(t)$*, is non–negative.*

Proof : As already noted, a degree 7 double PH curve with $\deg(h) = 4$ and $\deg(\mathbf{w}) = 0$ in (4.3.3) is helical if and only if the real quartic polynomial $h(t)$ can be written in terms of real cubics $f(t)$, $g(t)$ in the form (5.2.4). This is equivalent to the requirement that the Bernstein coefficients of $h(t)$ should be such as to admit real solutions of equations (5.2.10) for the Bernstein coefficients of $f(t)$, $g(t)$. Now the system (5.2.10) may be interpreted as *five* linear equations in the *six* quantities $f_i g_j - f_j g_i$ with $i \neq j$ for $0 \leqslant i, j \leqslant 3$. So we can choose one of these quantities arbitrarily. Setting $f_2 g_1 - f_1 g_2 = c$, we obtain

$$f_1 g_0 - f_0 g_1 = \tfrac{1}{3} h_0\,, \quad f_2 g_0 - f_0 g_2 = \tfrac{2}{3} h_1\,, \quad f_3 g_0 - f_0 g_3 = 2h_2 - 3c\,,$$

$$f_2 g_1 - f_1 g_2 = c\,, \quad f_3 g_1 - f_1 g_3 = \tfrac{2}{3} h_3\,, \quad f_3 g_2 - f_2 g_3 = \tfrac{1}{3} h_4\,.$$

However, these equations in f_i, g_i for $0 \leqslant i \leqslant 3$ may not be consistent. Since

$$(f_2 g_0 - f_0 g_2)(f_3 g_1 - f_1 g_3) - (f_2 g_1 - f_1 g_2)(f_3 g_0 - f_0 g_3) \\ = (f_1 g_0 - f_0 g_1)(f_3 g_2 - f_2 g_3)\,,$$

the values $h_0, \ldots, h_4$ and c must satisfy the consistency condition

$$\left(\tfrac{2}{3} h_1\right)\left(\tfrac{2}{3} h_3\right) - c(2h_2 - 3c) = \left(\tfrac{1}{3} h_0\right)\left(\tfrac{1}{3} h_4\right)\,,$$

which can be reduced to a quadratic equation in c, namely

$$27\,c^2 - 18\,h_2 c + 4\,h_1 h_3 - h_0 h_4 = 0\,.$$

Clearly, the solutions

$$c = f_2 g_1 - f_1 g_2 = \tfrac{1}{9}\,(\,3h_2 \pm \sqrt{9h_2^2 + 3h_0 h_4 - 12 h_1 h_3}\,)$$

can be real if and only if the discriminant Δ defined by (5.3.8) is non–negative. In such cases, $h(t)$ can be expressed in the form (5.2.4) for real cubics $f(t)$, $g(t)$ and the degree 7 double PH is helical, since $\boldsymbol{\alpha}(t)/\boldsymbol{\beta}(t)$ corresponds to the real cubic re–parameterization (5.2.9) of the line/circle (5.2.1).

In all other cases, no real cubics $f(t)$, $g(t)$ exist, such that $h(t)$ is given by (5.2.4). Since these cases do not correspond to real cubic re–parameterizations of the line/circle (5.2.1), they define *non–helical* degree 7 double PH curves. ∎

5.4 COMPUTED EXAMPLES

5.4.1 *Degree 7 helical DPH curves*

We begin with examples that illustrate the direct construction of helical DPH curves of degree 7 from complex–plane line/circle parameterizations, through the Hopf map method described in Section 5.2.

Example 5.1. Cubic re-parameterization.

Using the complex line/circle (5.2.1) defined by $(\mathbf{a}_0, \mathbf{a}_1) = (1, 1+i)$ and $(\mathbf{b}_0, \mathbf{b}_1) = (1-i, i)$ and re–parameterization function (5.2.9) specified by $(f_0, f_1, f_2, f_3) = (1, 2, 2, 1)$ and $(g_0, g_1, g_2, g_3) = (1, 2, 3, 3)$ we obtain the form $\mathbf{z}(t) = \boldsymbol{\alpha}(t)/\boldsymbol{\beta}(t)$ with $(\boldsymbol{\alpha}_0, \boldsymbol{\alpha}_1, \boldsymbol{\alpha}_2, \boldsymbol{\alpha}_3) = (1+i, 2+2i, 3+2i, 3+i)$ and $(\boldsymbol{\beta}_0, \boldsymbol{\beta}_1, \boldsymbol{\beta}_2, \boldsymbol{\beta}_3) = (i, 2i, 1+i, 2-i)$. The corresponding coefficients $\mathcal{A}_l = \boldsymbol{\alpha}_l + \mathbf{k}\,\boldsymbol{\beta}_l$ of the cubic quaternion polynomial $\mathcal{A}(t)$ are then

$$(\mathcal{A}_0, \mathcal{A}_1, \mathcal{A}_2, \mathcal{A}_3) = (1 + \mathbf{i} + \mathbf{j}, 2 + 2\,\mathbf{i} + 2\,\mathbf{j}, 3 + 2\,\mathbf{i} + \mathbf{j} + \mathbf{k}, 3 + \mathbf{i} - \mathbf{j} + 2\,\mathbf{k})$$

and from (3.1.7) with $\mathbf{u} = \mathbf{i}$ we obtain the control points

$$\begin{aligned}
\mathbf{p}_0 &= (0.0000, 0.0000, 0.0000)\,, & \mathbf{p}_1 &= (0.1429, 0.2857, -0.2857)\,,\\
\mathbf{p}_2 &= (0.4286, 0.8571, -0.8571)\,, & \mathbf{p}_3 &= (1.0000, 1.7714, -1.7143)\,,\\
\mathbf{p}_4 &= (2.1000, 2.8286, -2.4857)\,, & \mathbf{p}_5 &= (3.6143, 3.9143, -2.6571)\,,\\
\mathbf{p}_6 &= (5.0429, 5.0571, -1.9429)\,, & \mathbf{p}_7 &= (5.7571, 6.4857, -0.5143)\,.
\end{aligned}$$

This helical curve has the curvature/torsion ratio $|\kappa(t)/\tau(t)| = \sqrt{5}/2$.

Example 5.2. Quadratic polynomial multiplication.

Using $(\mathbf{a}_0, \mathbf{a}_1) = (5\,\mathbf{i}, 1 + \mathbf{i})$ and $(\mathbf{b}_0, \mathbf{b}_1) = (1 - \mathbf{i}, 2 + 5\,\mathbf{i})$ in (5.2.1), and the complex quadratic specified by $(\mathbf{w}_0, \mathbf{w}_1, \mathbf{w}_2) = (1, 1 + \mathbf{i}, 1)$ in (5.2.14), yields the rational cubic $\mathbf{z}(t) = \boldsymbol{\alpha}(t)/\boldsymbol{\beta}(t)$ with $(\boldsymbol{\alpha}_0, \boldsymbol{\alpha}_1, \boldsymbol{\alpha}_2, \boldsymbol{\alpha}_3) = (5\,\mathbf{i}, -3 + \frac{11}{3}\,\mathbf{i}, 3\,\mathbf{i}, 1 + \mathbf{i})$ and $(\boldsymbol{\beta}_0, \boldsymbol{\beta}_1, \boldsymbol{\beta}_2, \boldsymbol{\beta}_3) = (1 - \mathbf{i}, 2 + \frac{5}{3}\,\mathbf{i}, -\frac{5}{3} + \frac{13}{3}\,\mathbf{i}, 2 + 5\,\mathbf{i})$. For the coefficients $\mathcal{A}_\iota = \boldsymbol{\alpha}_\iota + \mathbf{k}\,\boldsymbol{\beta}_\iota$ of the cubic quaternion polynomial $\mathcal{A}(t)$, we then have

$$(\mathcal{A}_0, \mathcal{A}_1, \mathcal{A}_2, \mathcal{A}_3) = (5\,\mathbf{i} - \mathbf{j} + \mathbf{k}, -3 + \tfrac{11}{3}\,\mathbf{i} + \tfrac{5}{3}\,\mathbf{j} + 2\,\mathbf{k}, 3\,\mathbf{i} + \tfrac{13}{3}\,\mathbf{j} - \tfrac{5}{3}\,\mathbf{k}, 1 + \mathbf{i} + 5\,\mathbf{j} + 2\,\mathbf{k})$$

and from (3.1.7) with $\mathbf{u} = \mathbf{i}$ we obtain the control points

$$\begin{aligned}
\mathbf{p}_0 &= (0.0000, 0.0000, 0.0000)\,, & \mathbf{p}_1 &= (3.2857, -1.4286, 1.4286)\,,\\
\mathbf{p}_2 &= (5.8571, -1.1905, 2.9524)\,, & \mathbf{p}_3 &= (8.4000, -0.1048, 4.7619)\,,\\
\mathbf{p}_4 &= (9.4286, 3.5810, 6.5905)\,, & \mathbf{p}_5 &= (7.6857, 6.7238, 7.0286)\,,\\
\mathbf{p}_6 &= (5.4952, 9.2476, 7.0286)\,, & \mathbf{p}_7 &= (1.6381, 11.2476, 6.1714)\,.
\end{aligned}$$

These control points define a monotone–helical curve, with curvature/torsion ratio $|\kappa(t)/\tau(t)| = \sqrt{829}/2$.

Example 5.3. Re-parameterization and multiplication.

The values $(\mathbf{a}_0, \mathbf{a}_1) = (1 + \mathbf{i}, 1)$ and $(\mathbf{b}_0, \mathbf{b}_1) = (1 - \mathbf{i}, 2)$ in (5.2.1), together with $(f_0, f_1, f_2) = (1, 2, 1)$, $(g_0, g_1, g_2) = (1, 2, 2)$, and $(\mathbf{w}_0, \mathbf{w}_1) = (1, 1 + \mathbf{i})$ in (5.2.18) yield $\mathbf{z}(t) = \boldsymbol{\alpha}(t)/\boldsymbol{\beta}(t)$ with $(\boldsymbol{\alpha}_0, \boldsymbol{\alpha}_1, \boldsymbol{\alpha}_2, \boldsymbol{\alpha}_3) = (1, \frac{5}{3} + \frac{1}{3}\,\mathbf{i}, 2 + \frac{5}{3}\,\mathbf{i}, 1 + 3\,\mathbf{i})$ and $(\boldsymbol{\beta}_0, \boldsymbol{\beta}_1, \boldsymbol{\beta}_2, \boldsymbol{\beta}_3) = (2, \frac{10}{3} + \frac{2}{3}\,\mathbf{i}, \frac{11}{3} + \frac{7}{3}\,\mathbf{i}, 4 + 2\,\mathbf{i})$. The coefficients $\mathcal{A}_\iota = \boldsymbol{\alpha}_\iota + \mathbf{k}\,\boldsymbol{\beta}_\iota$ of the cubic quaternion polynomial $\mathcal{A}(t)$ are then

$$(\mathcal{A}_0, \mathcal{A}_1, \mathcal{A}_2, \mathcal{A}_3) = (1 + 2\,\mathbf{k}, \tfrac{5}{3} + \tfrac{1}{3}\,\mathbf{i} + \tfrac{2}{3}\,\mathbf{j} + \tfrac{10}{3}\,\mathbf{k}, 2 + \tfrac{5}{3}\,\mathbf{i} + \tfrac{7}{3}\,\mathbf{j} + \tfrac{11}{3}\,\mathbf{k}, 1 + 3\,\mathbf{i} + 2\,\mathbf{j} + 4\,\mathbf{k})$$

and from (3.1.7) with $\mathbf{u} = \mathbf{i}$ we obtain the control points

$$\begin{aligned}
\mathbf{p}_0 &= (0.0000, 0.0000, 0.0000)\,, & \mathbf{p}_1 &= (-0.4286, 0.5714, 0.0000)\,,\\
\mathbf{p}_2 &= (-1.1429, 1.5238, 0.0000)\,, & \mathbf{p}_3 &= (-2.1905, 2.9524, 0.0571)\,,\\
\mathbf{p}_4 &= (-3.5619, 4.9238, 0.3143)\,, & \mathbf{p}_5 &= (-5.2857, 7.5714, 0.9810)\,,\\
\mathbf{p}_6 &= (-7.0476, 10.7143, 2.6000)\,, & \mathbf{p}_7 &= (-8.4762, 13.5714, 5.4571)\,.
\end{aligned}$$

For this curve, the curvature/torsion ratio is $|\kappa(t)/\tau(t)| = \sqrt{10}$.

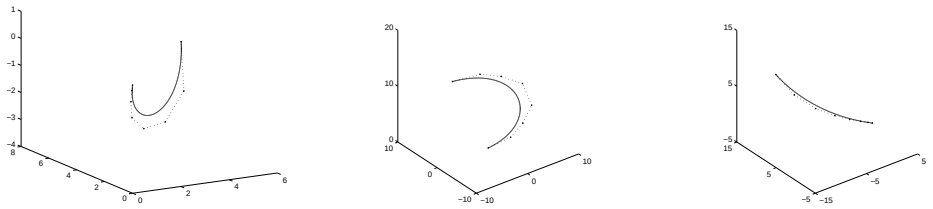

Figure 5.3: The three types of degree 7 helical DPH curves (Examples 5.1, 5.2, 5.3).

Figure 5.3 illustrates the three degree 7 helical DPH curves constructed in the preceding examples, together with their control polygons. The following examples recast the curves considered in Section 4.4.2 to illustrate the use of the criteria in Section 5.3 to distinguish between helical and non–helical DPH curves.

5.4.2 *DPH curves with* $\deg(h) = 0$, $\deg(\mathbf{w}) = 2$

Example 5.4. $\deg(h) = 0$**,** $\deg(\mathbf{w}) = 2$**, helical**.

The DPH curve of Example 4.1 has a constant curvature/torsion ratio, $|\kappa(t)/\tau(t)| = 1/7$. For this curve, we have the quaternion coefficients

$$\mathcal{A}_0 = 1 + \mathbf{j}, \qquad \mathcal{A}_1 = 2\,\mathbf{i} - \tfrac{5}{3}\,\mathbf{k},$$
$$\mathcal{A}_2 = -4 + \tfrac{5}{3}\,\mathbf{i} - \tfrac{10}{3}\,\mathbf{j} - \mathbf{k}, \qquad \mathcal{A}_3 = -4 - 2\,\mathbf{i} - 3\,\mathbf{j} + 2\,\mathbf{k}.$$

Here $\mathcal{A}_1, \mathcal{A}_2$ can be specified in terms of $\mathcal{A}_0, \mathcal{A}_3$ using (5.2.15), with the values

$$\mathbf{c}_{10} = \tfrac{1}{3}(2 + 2\,\mathrm{i}), \quad \mathbf{c}_{13} = -\tfrac{1}{3}\,\mathrm{i}, \quad \mathbf{c}_{20} = \tfrac{1}{3}\,\mathrm{i}, \quad \mathbf{c}_{23} = \tfrac{1}{3}\,(2 - 2\,\mathrm{i})$$

for the coefficients (5.2.16), which evidently satisfy the relations (5.2.17).

Example 5.5. $\deg(h) = 0$**,** $\deg(\mathbf{w}) = 2$**, non-helical**.

In the case considered in Example 4.2, the curvature and torsion have a non–constant ratio $\kappa(t)/\tau(t)$, namely

$$\frac{9\,(2\,t^4 - 4\,t^3 + 2\,t^2 + 1)^2}{460\,t^8 - 1840\,t^7 - 296\,t^6 - 2688\,t^5 + 1272\,t^4 + 624\,t^3 - 180\,t^2 + 144\,t + 63}\,.$$

In the present example, the polynomial $\mathbf{w}(t) = \mathbf{w}_0(1-t)^2 + \mathbf{w}_1 2(1-t)t + \mathbf{w}_2 t^2$ has roots $\tau_1, \tau_2 = \frac{1}{2}(1 \pm \sqrt{2} + \mathrm{i})$ that are not both real nor complex conjugates, and one can verify that $\boldsymbol{\alpha}(t)$, $\boldsymbol{\beta}(t)$ can be expressed in terms of them in the form (5.3.5), with coefficients

$$\mathbf{a}_1 = \tfrac{1}{2}\,[\,\sqrt{2} - 1 + (4\sqrt{2} - 5)\,\mathrm{i}\,], \qquad \mathbf{a}_2 = -\tfrac{1}{2}\,[\,\sqrt{2} + 1 + (4\sqrt{2} + 5)\,\mathrm{i}\,],$$
$$\mathbf{b}_1 = \tfrac{1}{3}\,[\,6 - 5\sqrt{2} + (\sqrt{2} - 1)\,\mathrm{i}\,], \qquad \mathbf{b}_2 = \tfrac{1}{3}\,[\,6 + 5\sqrt{2} - (\sqrt{2} + 1)\,\mathrm{i}\,].$$

Since $\mathbf{a}_1\mathbf{b}_2 - \mathbf{a}_2\mathbf{b}_1 = -\sqrt{2}\,i/3 \neq 0$ for these coefficients, the non–helical nature of the curve is consistent with Proposition 5.1.

5.4.3 *DPH curves with* $\deg(h) = 2$, $\deg(\mathbf{w}) = 1$

Example 5.6. $\deg(h) = 2$**,** $\deg(\mathbf{w}) = 1$**, helical**.

The curvature/torsion ratio of the DPH curve of Example 4.3 has the constant value $|\kappa(t)/\tau(t)| = 1/2$. In this case $\boldsymbol{\alpha}(t)$, $\boldsymbol{\beta}(t)$ have the common factor $\mathbf{w}(t) = t - \frac{1}{2}(1-i)$, so the helical nature of the curve is consistent with Proposition 5.2. The Bernstein coefficients of (3.1.5) for this curve are

$$\begin{aligned} \mathcal{A}_0 &= 1 - \mathbf{k}\,, & \mathcal{A}_1 &= 1 - \tfrac{4}{3}\,\mathbf{k}\,, \\ \mathcal{A}_2 &= 2 - \tfrac{1}{3}\,\mathbf{i} + \tfrac{2}{3}\,\mathbf{j} - \tfrac{8}{3}\,\mathbf{k}\,, & \mathcal{A}_3 &= 2 - 5\,\mathbf{i} + 7\,\mathbf{j} - 2\,\mathbf{k}\,. \end{aligned}$$

and in this case $\mathcal{A}_1$, $\mathcal{A}_2$ can be expressed in terms of $\mathcal{A}_0$, $\mathcal{A}_3$ in the form (5.2.19), with the values

$$\mathbf{c}_{10} = \tfrac{1}{6}(1-2i)\,, \quad \mathbf{c}_{13} = \tfrac{1}{6}\,i\,, \quad \mathbf{c}_{20} = -\tfrac{1}{6}\,i\,, \quad \mathbf{c}_{23} = \tfrac{1}{6}(1+2i)$$

of the coefficients (5.2.20). These coefficients satisfy (5.2.21), the expressions on the left and right having the common value $\frac{9}{16}$.

Example 5.7. $\deg(h) = 2$**,** $\deg(\mathbf{w}) = 1$**, non-helical**.

In Example 4.4, the curvature/torsion ratio is non–constant – namely,

$$\frac{\kappa(t)}{\tau(t)} = \frac{9\,|2\,t^2 - 2\,t - 1|\,(2\,t^2 - 2\,t + 1)^2}{2\,(92\,t^6 - 276\,t^5 - 60\,t^4 + 228\,t^3 - 126\,t^2 + 54\,t + 9)}\,.$$

In this case we find that $\gcd(\boldsymbol{\alpha}(t), \boldsymbol{\beta}(t)) = \text{constant}$, so the non–helical nature of the curve is consistent with Proposition 5.3.

5.4.4 *DPH curves with* $\deg(h) = 4$, $\deg(\mathbf{w}) = 0$

Example 5.8. $\deg(h) = 4$**,** $\deg(\mathbf{w}) = 0$**, helical**.

In Example 4.5, the curvature/torsion ratio has the constant value $|\kappa(t)/\tau(t)| = 1/8$. Note that, with the chosen values for the coefficients of $h(t)$, the quantity (5.3.8) is 0, so the fact that the curve is helical is consistent with Proposition 5.4. One can verify that for this curve, $\boldsymbol{\alpha}(t)/\boldsymbol{\beta}(t)$ may be regarded as arising from the re–parameterization defined by (5.2.9) with $(f_0, f_1, f_2, f_3) = (1, 2, -5, -10)$ and $(g_0, g_1, g_2, g_3) = (-1, -\frac{5}{3}, \frac{11}{3}, 7)$ applied to the line/circle form (5.2.1) with $(\mathbf{a}_0, \mathbf{a}_1) = (-3-3\,i, -5-6\,i)$ and $(\mathbf{b}_0, \mathbf{b}_1) = (5, 9+i)$.

For the Bernstein coefficients $\mathcal{A}_\iota = \boldsymbol{\alpha}_\iota + \mathbf{k}\,\beta_\iota$ of the quaternion polynomial (3.1.5) we obtain

$$\mathcal{A}_0 = 1 + \mathbf{j} - \mathbf{k}, \qquad \mathcal{A}_1 = 1 - \mathbf{i} + 2\,\mathbf{j} - \tfrac{1}{3}\,\mathbf{k},$$
$$\mathcal{A}_2 = -1 + 4\,\mathbf{i} - 5\,\mathbf{j} - \tfrac{5}{3}\,\mathbf{k}, \qquad \mathcal{A}_3 = -1 + 9\,\mathbf{i} - 10\,\mathbf{j} - 5\,\mathbf{k}.$$

and we note that $\mathcal{A}_1, \mathcal{A}_2$ can be written in terms of $\mathcal{A}_0, \mathcal{A}_3$ in the form (5.2.12) where, with $k = 3$, the values of the coefficients (5.2.13) are

$$c_{10} = \tfrac{8}{9}, \quad c_{13} = -\tfrac{1}{9}, \quad c_{20} = -\tfrac{5}{9}, \quad c_{23} = \tfrac{4}{9}.$$

Example 5.9. $\deg(h) = 4$**,** $\deg(\mathbf{w}) = 0$**, non-helical**.

In the case of Example 4.6, the curvature/torsion ratio is non–constant, namely

$$\frac{\kappa(t)}{\tau(t)} = \frac{|\,2\,t^4 - 4\,t^3 + 6\,t^2 - 4\,t - 1\,|}{2\,t(4\,t^3 + t^2 - 3\,t + 6)}.$$

For the specified coefficients of $h(t)$, the quantity (5.3.8) has the value $\Delta = -9$, so the non–helical nature of this curve is consistent with Proposition 5.4. This degree 7 non–helical DPH curve is illustrated in Figure 5.4.

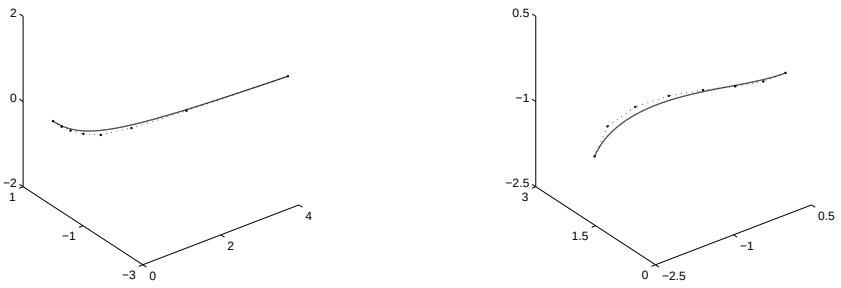

Figure 5.4: The degree 7 non–helical DPH curves of Examples 5.9 and 5.10

5.4.5 *Example of Beltran and Monterde*

Example 5.10. (Beltran and Monterde).

Beltran and Monterde [4] identify a degree 7 double PH curve $\mathbf{r}(t)$, given by

$$x(t) = \tfrac{1}{21}\,t^7 + \tfrac{1}{5}\,t^5 + t^3 - 3\,t, \quad y(t) = -\tfrac{1}{2}\,t^4 + 3\,t^2, \quad z(t) = -2\,t^3.$$

This curve has a primitive hodograph, and satisfies

$$\sigma(t) = \frac{t^6 + 3\,t^4 + 9\,t^2 + 9}{3}, \quad |\,\mathbf{r}'(t) \times \mathbf{r}''(t)\,| = 2\left(t^2+1\right)\left(t^6 + 3\,t^4 + 9\,t^2 + 9\right).$$

The curvature/torsion ratio for this curve is non–constant, namely

$$\frac{\kappa(t)}{\tau(t)} = -\frac{9\,(t^2+1)^2}{2\,t^6 + 9\,t^4 - 9}.$$

The cubic polynomials $\boldsymbol{\alpha}(t)$, $\boldsymbol{\beta}(t)$ have the Bernstein coefficients

$$\boldsymbol{\alpha}_0 = 0\,, \quad \boldsymbol{\alpha}_1 = \tfrac{1}{\sqrt{3}}\,\mathrm{i}\,, \quad \boldsymbol{\alpha}_2 = \tfrac{1}{\sqrt{3}}\,(1+2\,\mathrm{i})\,, \quad \boldsymbol{\alpha}_3 = \tfrac{1}{\sqrt{3}}\,(3+2\,\mathrm{i})\,,$$

$$\boldsymbol{\beta}_0 = \boldsymbol{\beta}_1 = \boldsymbol{\beta}_2 = \boldsymbol{\beta}_3 = \sqrt{3}\,\mathrm{i}\,,$$

and are thus given by

$$\boldsymbol{\alpha}(t) \;=\; \sqrt{3}\,\left[\,t^2 + \left(t - \tfrac{1}{3}t^3\right)\,\mathrm{i}\,\right], \qquad \boldsymbol{\beta}(t) \;=\; \sqrt{3}\,\mathrm{i}\,.$$

In this case, the proportionality polynomial is

$$\boldsymbol{\alpha}(t)\boldsymbol{\beta}'(t) - \boldsymbol{\alpha}'(t)\boldsymbol{\beta}(t) \;=\; -3\,(t+\mathrm{i})^2\,.$$

Hence, this curve satisfies the double PH condition (4.3.3) with $\deg(h) = 0$ and $\deg(\mathbf{w}) = 1$. This is a special (degenerate) DPH curve of degree 7 — for which $\boldsymbol{\alpha}(t)\boldsymbol{\beta}'(t) - \boldsymbol{\alpha}'(t)\boldsymbol{\beta}(t)$ is just quadratic, and is thus deficient in degree compared to the generic case of a quartic. It may be interpreted as a special coincidence of the cases $\deg(h) = 2$, $\deg(\mathbf{w}) = 1$ and $\deg(h) = 0$, $\deg(\mathbf{w}) = 2$ discussed in Sections 4.4.2 — in the former case, $h(t)$ is considered to exhibit a degree reduction from 2 to 0; in the latter case, $\mathbf{w}(t)$ is considered to exhibit a degree reduction from 2 to 1.

For this curve, the quaternion polynomial (3.1.5) has Bernstein coefficients

$$\mathcal{A}_0 = \sqrt{3}\,\mathbf{j}, \;\; \mathcal{A}_1 = \sqrt{3}\,(\tfrac{1}{3}\,\mathbf{i} + \mathbf{j}), \;\; \mathcal{A}_2 = \sqrt{3}\,(\tfrac{1}{3} + \tfrac{2}{3}\,\mathbf{i} + \mathbf{j}), \;\; \mathcal{A}_3 = \sqrt{3}\,(1 + \tfrac{2}{3}\,\mathbf{i} + \mathbf{j}).$$

Substituting into (3.1.7) with $\mathbf{u} = \mathbf{i}$, the Bézier control points of this curve are found to be

$$\begin{aligned}
\mathbf{p}_0 &= (0.0000, 0.0000, 0.0000)\,, & \mathbf{p}_1 &= (-0.4286, 0.0000, 0.0000)\,,\\
\mathbf{p}_2 &= (-0.8571, 0.1429, 0.0000)\,, & \mathbf{p}_3 &= (-1.2571, 0.4286, -0.0571)\,,\\
\mathbf{p}_4 &= (-1.6000, 0.8429, -0.2286)\,, & \mathbf{p}_5 &= (-1.8476, 1.3571, -0.5714)\,,\\
\mathbf{p}_6 &= (-1.9429, 1.9286, -1.1429)\,, & \mathbf{p}_7 &= (-1.7524, 2.5000, -2.0000)\,.
\end{aligned}$$

This curve is illustrated, together with its control polygon, in Figure 5.4.

6

CURVES WITH RATIONAL ROTATION–MINIMIZING FRAME

Consider an adapted frame $(\mathbf{f}_1, \mathbf{f}_2, \mathbf{f}_3)$ on a regular curve $\mathbf{r}(t)$ with $\mathbf{f}_1 \equiv \mathbf{t}$. Many adapted frames exist, since a rotation of the normal–plane vectors by an angle $\phi(t)$ defines a new adapted frame upon replacing $(\mathbf{f}_2, \mathbf{f}_3)$ by

$$\cos\phi(t)\,\mathbf{f}_2(t) - \sin\phi(t)\,\mathbf{f}_3(t)\,, \qquad \sin\phi(t)\,\mathbf{f}_2(t) + \cos\phi(t)\,\mathbf{f}_3(t)\,.$$

As we have seen in Section 1.3, the adapted moving frame $(\mathbf{f}_1, \mathbf{f}_2, \mathbf{f}_3)$ is rotation–minimizing if and only if its angular velocity maintains a zero component in the direction of the curve tangent. Polynomial curves do not ordinarily admit an *exact* closed form of a rotation–minimizing frame. This motivates the investigations on curves with rational rotation–minimizing adapted frames (for brevity, RRMF curves), since rational forms are always preferred in computer aided design systems whenever possible.

The plan for this chapter is as follows. After some preliminaries concerning rational adapted frames in Section 6.1, the condition for existence of rational RMAFs is formulated and analyzed in terms of the Hopf map form of spatial PH curves in Section 6.2. This condition is then analyzed in detail, in the context of PH cubics and quintics, in Section 6.3 and 6.4, while Section 6.5 briefly discusses the generalization of these results to higher–order RRMF curves. Finally, Section 6.6 presents a subsequent simpler characterization of RRMF curves in terms of the quaternion algebra introduced by Farouki in [25].

6.1 RATIONAL ADAPTED FRAMES ON SPATIAL PH CURVES

If we desire rational adapted frames, as already observed in the previous chapters, we may consider only PH curves — since condition (3.0.1) is necessary for $\mathbf{f}_1$ to be rational. As first noted in [52], a rational adapted frame $(\mathbf{e}_1, \mathbf{e}_2, \mathbf{e}_3)$ known [10] as the *Euler–Rodrigues frame* (ERF) can be defined on any spatial PH curve in terms of the quaternion representation as

$$\mathbf{e}_1 = \frac{\mathcal{A}\,\mathbf{i}\,\mathcal{A}^*}{|\mathcal{A}|^2}\,, \quad \mathbf{e}_2 = \frac{\mathcal{A}\,\mathbf{j}\,\mathcal{A}^*}{|\mathcal{A}|^2}\,, \quad \mathbf{e}_3 = \frac{\mathcal{A}\,\mathbf{k}\,\mathcal{A}^*}{|\mathcal{A}|^2}\,,$$

or, equivalently, in terms of the Hopf map form as

$$\begin{aligned}
\mathbf{e}_1 &= \frac{\left(|\alpha|^2 - |\beta|^2,\, 2\,\mathrm{Re}\,(\alpha\overline{\beta}),\, 2\,\mathrm{Im}\,(\alpha\overline{\beta})\right)}{|\alpha|^2 + |\beta|^2}\,, \\
\mathbf{e}_2 &= \frac{\left(-2\,\mathrm{Re}\,(\alpha\beta),\, \mathrm{Re}\,(\alpha^2 - \beta^2),\, \mathrm{Im}\,(\alpha^2 + \beta^2)\right)}{|\alpha|^2 + |\beta|^2}\,, \\
\mathbf{e}_3 &= \frac{\left(2\,\mathrm{Im}\,(\alpha\beta),\, -\mathrm{Im}\,(\alpha^2 - \beta^2),\, \mathrm{Re}\,(\alpha^2 + \beta^2)\right)}{|\alpha|^2 + |\beta|^2}\,.
\end{aligned} \tag{6.1.1}$$

Although the ERF does not have an intuitive geometric significance, and is dependent upon the chosen Cartesian coordinates, it has the advantage over the Frenet frame of being well–defined even at inflection points (when the curvature vanishes).

Any other adapted frame on a spatial PH curve, defined by a rotation $\phi(t)$ of $\mathbf{e}_2$, $\mathbf{e}_3$ in the curve normal plane, is rational if and only if

$$\cos\phi(t) = \frac{P_1(t)}{P_3(t)}\,, \qquad \sin\phi(t) = \frac{P_2(t)}{P_3(t)}\,,$$

for real polynomials $P_1(t), P_2(t), P_3(t)$ satisfying

$$\gcd(P_1(t), P_2(t), P_3(t)) = \text{constant} \quad \text{and} \quad P_1^2(t) + P_2^2(t) = P_3^2(t)\,.$$

Hence, relatively prime polynomials $a(t)$, $b(t)$ must exist [66] such that

$$P_1^2(t) = a^2(t) - b^2(t)\,, \quad P_2(t) = 2\,a(t)b(t)\,, \quad P_3(t) = a^2(t) + b^2(t)\,.$$

Thus, any other rational adapted frame $(\mathbf{f}_1, \mathbf{f}_2, \mathbf{f}_3)$ on a PH curve can be expressed in terms of the ERF as

$$\begin{aligned}
\mathbf{f}_1(t) &= \mathbf{e}_1(t)\,, \\
\mathbf{f}_2(t) &= \frac{a^2(t) - b^2(t)}{a^2(t) + b^2(t)}\,\mathbf{e}_2(t) - \frac{2\,a(t)b(t)}{a^2(t) + b^2(t)}\mathbf{e}_3(t)\,, \\
\mathbf{f}_3(t) &= \frac{2\,a(t)b(t)}{a^2(t) + b^2(t)}\,\mathbf{e}_2(t) + \frac{a^2(t) - b^2(t)}{a^2(t) + b^2(t)}\mathbf{e}_3(t)\,,
\end{aligned} \tag{6.1.2}$$

where $a(t)$, $b(t)$ are polynomials with $\gcd(a(t), b(t)) = \text{constant}$.

6.2 SPATIAL PH CURVES WITH RATIONAL RMAFS

A sufficient and necessary condition for the existence of a rational rotation–minimizing adapted frame (RMAF) on a spatial PH curve has been derived by Han, in terms of the quaternion representation [47]. In order to define an RRMF

curve, the components of the quaternion polynomial $\mathcal{A}(t) = u(t) + v(t)\,\mathbf{i} + p(t)\,\mathbf{j} + q(t)\,\mathbf{k}$ in (3.1.8) must satisfy the condition

$$\frac{uv' - u'v - pq' + p'q}{u^2 + v^2 + p^2 + q^2} = \frac{ab' - a'b}{a^2 + b^2}, \tag{6.2.1}$$

for some relatively prime polynomials $a(t), b(t)$. Note that the above condition can be concisely expressed as

$$\frac{\mathrm{scal}\,(\mathcal{A}(t)\,\mathbf{i}\,\mathcal{A}'^{*}(t))}{|\mathcal{A}(t)|^2} = \frac{\mathrm{scal}\,(\mathcal{W}(t)\,\mathbf{i}\,\mathcal{W}'^{*}(t))}{|\mathcal{W}(t)|^2},$$

where $\mathcal{W}(t) = a(t) + \mathbf{i}\,b(t)$ is a quaternion polynomial with $\gcd(a(t), b(t)) =$ constant.

By using relations (3.3.1), in terms of the Hopf map representation, this condition can be phrased as follows. In order to define an RRMF curve, the complex polynomials $\boldsymbol{\alpha}(t)$, $\boldsymbol{\beta}(t)$ in (3.2.2) must satisfy [30] the condition

$$\frac{\overline{\boldsymbol{\alpha}}\boldsymbol{\alpha}' - \overline{\boldsymbol{\alpha}}'\boldsymbol{\alpha} + \overline{\boldsymbol{\beta}}\boldsymbol{\beta}' - \overline{\boldsymbol{\beta}}'\boldsymbol{\beta}}{\overline{\boldsymbol{\alpha}}\boldsymbol{\alpha} + \overline{\boldsymbol{\beta}}\boldsymbol{\beta}} = \frac{\overline{\mathbf{w}}\mathbf{w}' - \overline{\mathbf{w}}'\mathbf{w}}{\overline{\mathbf{w}}\mathbf{w}}, \tag{6.2.2}$$

where $\mathbf{w}(t) = a(t) + \mathrm{i}\,b(t)$ is a complex polynomial with $\gcd(a(t), b(t)) =$ constant. Note that, since the numerators in (6.2.2) amount to $2\,\mathrm{i}\,\mathrm{Im}\,(\overline{\boldsymbol{\alpha}}\boldsymbol{\alpha}' + \overline{\boldsymbol{\beta}}\boldsymbol{\beta}')$ and $2\,\mathrm{i}\,\mathrm{Im}\,(\overline{\mathbf{w}}\mathbf{w}')$ and the denominators to $|\boldsymbol{\alpha}|^2 + |\boldsymbol{\beta}|^2$ and $|\mathbf{w}|^2$, respectively, this is essentially a relation between two *real* rational functions.

Remark 6.1. Henceforth, the polynomial $\mathbf{w}(t)$ in (6.2.2), written in Bernstein form as

$$\mathbf{w}(t) = \sum_{j=0}^{m} \mathbf{w}_j \binom{m}{j} (1-t)^{m-j} t^j,$$

is assumed to be nominally of the same degree m as $\boldsymbol{\alpha}(t)$, $\boldsymbol{\beta}(t)$ in (3.2.3). However, according to Remark 5.1 of [44], if (6.2.1) — or (6.2.2) — is satisfied, then $\deg(a^2 + b^2) \leqslant 2m$, and consequently $\deg(\mathbf{w}) \leqslant m$.

Remark 6.2. When $\mathbf{w}(t)$ is either a *real* polynomial or a constant, condition (6.2.2) implies that

$$\overline{\boldsymbol{\alpha}}(t)\boldsymbol{\alpha}'(t) - \overline{\boldsymbol{\alpha}}'(t)\boldsymbol{\alpha}(t) + \overline{\boldsymbol{\beta}}(t)\boldsymbol{\beta}'(t) - \overline{\boldsymbol{\beta}}'(t)\boldsymbol{\beta}(t) = 0. \tag{6.2.3}$$

If this condition holds, the angle $\phi(t)$ between the ERF and RMAF is constant. Since computation of the RMAF incurs an integration constant, we may regard (6.2.3) as the condition identifying coincidence of the RMAF and ERF: a detailed analysis of this condition was presented by Choi and Han in [10].

Henceforth, we assume that the polynomials (3.2.3) satisfy $|\boldsymbol{\alpha}_0|^2 + |\boldsymbol{\beta}_0|^2 \neq 0$ and $|\boldsymbol{\alpha}_m|^2 + |\boldsymbol{\beta}_m|^2| \neq 0$, since otherwise $\mathbf{r}'(t) = 0$ at $t = 0$ or 1. The following result helps to simplify analysis of the RRMF condition (6.2.2).

Lemma 6.1. *If (6.2.2) is satisfied for given complex polynomials* $\boldsymbol{\alpha}(t)$, $\boldsymbol{\beta}(t)$ *by a complex polynomial* $\mathbf{w}(t)$, *it is also satisfied by* $\mathbf{c}\mathbf{w}(t)$ *for any constant* $\mathbf{c} \neq 0$. *Thus, without loss of generality, one may set* $\mathbf{w}_0 = 1$ *as the leading Bernstein coefficient of* $\mathbf{w}(t)$.

Proof : The rational function on the right in (6.2.2) is unchanged if we replace $\mathbf{w}(t)$ by $\mathbf{c}\mathbf{w}(t)$, for any $\mathbf{c} \neq 0$. Since we must have $|\mathbf{w}_0| \neq 0$ if $|\boldsymbol{\alpha}_0|^2 + |\boldsymbol{\beta}_0|^2 \neq 0$, we may substitute $\mathbf{c}\mathbf{w}(t)$ with $\mathbf{c} = 1/\mathbf{w}_0$ for $\mathbf{w}(t)$. ∎

Interpreting the complex polynomials $\boldsymbol{\alpha}(t)$, $\boldsymbol{\beta}(t)$, $\mathbf{w}(t)$ as curves in the complex plane, the expressions $\overline{\boldsymbol{\alpha}}(t)\boldsymbol{\alpha}'(t) - \overline{\boldsymbol{\alpha}}'(t)\boldsymbol{\alpha}$, $\overline{\boldsymbol{\beta}}(t)\boldsymbol{\beta}'(t) - \overline{\boldsymbol{\beta}}'(t)\boldsymbol{\beta}(t)$, $\overline{\mathbf{w}}(t)\mathbf{w}'(t) - \overline{\mathbf{w}}'(t)\mathbf{w}(t)$ in (6.2.2) have an intuitive geometrical meaning: they are proportional to the *areal speed* of these curves — i.e., the rate at which the polar vector from the origin to the points of each curve sweeps out area. This interpretation deserves further consideration, but at present we find a direct algebraic analysis of condition (6.2.2) more profitable.

6.3 CHARACTERIZATION OF RRMF CUBICS

Using the quaternion representation of spatial PH curves, Han [47] has shown that only degenerate (linear or planar) cubics have rational RMAFs. Prior to analysing quintic RRMF curves, it is instructive to deduce this result from the Hopf map condition (6.2.2), using the form of $\mathbf{w}(t)$ defined in Lemma 6.1. PH cubics are generated by choosing linear polynomials

$$\boldsymbol{\alpha}(t) = \boldsymbol{\alpha}_0(1-t) + \boldsymbol{\alpha}_1 t\,, \qquad \boldsymbol{\beta}(t) = \boldsymbol{\beta}_0(1-t) + \boldsymbol{\beta}_1 t\,,$$

in (3.2.2). We assume they are relatively prime, otherwise the PH cubic degenerates to a straight line (see Remark 3.3). This implies that $\boldsymbol{\alpha}_0 : \boldsymbol{\alpha}_1 \neq \boldsymbol{\beta}_0 : \boldsymbol{\beta}_1$, and in particular $(\boldsymbol{\alpha}_0, \boldsymbol{\beta}_0) \neq (0,0)$ and $(\boldsymbol{\alpha}_1, \boldsymbol{\beta}_1) \neq (0,0)$.

Proposition 6.1. *A PH cubic defined by the Hopf map form (3.2.2) has a rational rotation– minimizing adapted frame if and only if the Bernstein coefficients* $\boldsymbol{\alpha}_0$, $\boldsymbol{\alpha}_1$ *and* $\boldsymbol{\beta}_0$, $\boldsymbol{\beta}_1$ *of the linear complex polynomials* $\boldsymbol{\alpha}(t)$ *and* $\boldsymbol{\beta}(t)$ *satisfy the constraint*

$$|\overline{\boldsymbol{\alpha}}_0\boldsymbol{\alpha}_1 + \overline{\boldsymbol{\beta}}_0\boldsymbol{\beta}_1|^2 = \left(|\boldsymbol{\alpha}_0|^2 + |\boldsymbol{\beta}_0|^2\right)\left(|\boldsymbol{\alpha}_1|^2 + |\boldsymbol{\beta}_1|^2\right)\,. \tag{6.3.1}$$

Proof : As originally shown by Han [47] and according to Remark 5.1 of [44], in this case condition (6.2.2) cannot be satisfied with $\deg(\mathbf{w}(t)) > 1$, so we may set $\mathbf{w}(t) = \mathbf{w}_0(1-t) + \mathbf{w}_1 t$. Comparing the numerators and denominators on the left and right of (6.2.2), we must have

$$\begin{aligned}
&\overline{\boldsymbol{\alpha}}_0\boldsymbol{\alpha}_1 - \overline{\boldsymbol{\alpha}}_1\boldsymbol{\alpha}_0 + \overline{\boldsymbol{\beta}}_0\boldsymbol{\beta}_1 - \overline{\boldsymbol{\beta}}_1\boldsymbol{\beta}_0 = \gamma(\overline{\mathbf{w}}_0\mathbf{w}_1 - \overline{\mathbf{w}}_1\mathbf{w}_0)\,,\\
&\overline{\boldsymbol{\alpha}}_0\boldsymbol{\alpha}_0 + \overline{\boldsymbol{\beta}}_0\boldsymbol{\beta}_0 = \gamma\,\overline{\mathbf{w}}_0\mathbf{w}_0\,,\\
&\overline{\boldsymbol{\alpha}}_0\boldsymbol{\alpha}_1 + \overline{\boldsymbol{\alpha}}_1\boldsymbol{\alpha}_0 + \overline{\boldsymbol{\beta}}_0\boldsymbol{\beta}_1 + \overline{\boldsymbol{\beta}}_1\boldsymbol{\beta}_0 = \gamma(\overline{\mathbf{w}}_0\mathbf{w}_1 + \overline{\mathbf{w}}_1\mathbf{w}_0)\,,\\
&\overline{\boldsymbol{\alpha}}_1\boldsymbol{\alpha}_1 + \overline{\boldsymbol{\beta}}_1\boldsymbol{\beta}_1 = \gamma\,\overline{\mathbf{w}}_1\mathbf{w}_1\,,
\end{aligned}$$

for some non–zero real number γ. These four equations are equivalent to

$$\begin{aligned}
\overline{\alpha}_0\alpha_0 + \overline{\beta}_0\beta_0 &= \gamma\,\overline{w}_0 w_0\,,\\
\overline{\alpha}_0\alpha_1 + \overline{\beta}_0\beta_1 &= \gamma\,\overline{w}_0 w_1\,,\\
\overline{\alpha}_1\alpha_1 + \overline{\beta}_1\beta_1 &= \gamma\,\overline{w}_1 w_1\,.
\end{aligned} \tag{6.3.2}$$

By Lemma 6.1, we may take $w_0 = 1$. The first two equations of (6.3.2) then give

$$\gamma = |\alpha_0|^2 + |\beta_0|^2\,, \qquad w_1 = \frac{\overline{\alpha}_0\alpha_1 + \overline{\beta}_0\beta_1}{|\alpha_0|^2 + |\beta_0|^2}\,. \tag{6.3.3}$$

To define a solution of equations (6.3.2), these expressions for γ, w_0, w_1 must be compatible with the third equation. Substituting for γ, w_0, w_1 into this equation, and clearing denominators, yields the constraint (6.3.1). ∎

One can easily see that, when condition (6.3.1) is satisfied, the PH cubic $r(t)$ degenerates to a straight line (whose RMAF is trivially rational)—condition (6.3.1) is equivalent to $|\alpha_0\beta_1 - \alpha_1\beta_0|^2 = 0$, so the linear polynomials $\alpha(t)$, $\beta(t)$ are proportional. By Remark 3.3, this situation identifies a straight line as a degenerate PH cubic. Now Proposition 6.1 treats the generic case, in which the left– and right–hand sides of (6.2.2) are not both identically zero. We address separately the special case (see Remark 6.2) in which both sides of (6.2.2) vanish.

Corollary 6.1. *When* $\mathrm{Im}\,(\overline{\alpha}_0\alpha_1 + \overline{\beta}_0\beta_1) = 0$, *the polynomial* $w(t)$ *is real, and* $r(t)$ *degenerates to a planar PH cubic whose RMAF is trivially rational.*

Proof : If $\overline{\alpha}_0\alpha_1 + \overline{\beta}_0\beta_1$ is real, $w(t) = w_0(1-t) + w_1 t$ is a real polynomial. Since $|\alpha_0|^2 + |\beta_0|^2 \neq 0$, we can write α_1, β_1 in terms of complex numbers c, z as $\alpha_1 = c\alpha_0 - z\overline{\beta}_0$, $\beta_1 = c\beta_0 + z\overline{\alpha}_0$. Then $\overline{\alpha}_0\alpha_1 + \overline{\beta}_0\beta_1 = c(|\alpha_0|^2 + |\beta_0|^2)$ has no imaginary part if and only if $c = \lambda \in \mathbb{R}$. By Remark 3.3, this identifies a planar PH cubic (not a straight line), whose RMAF is trivially rational. ∎

6.4 CHARACTERIZATION OF RRMF QUINTICS

Since no true spatial cubics possess rational RMAFs, we now focus on quintics. Although the analysis is more involved, invoking Lemma 6.1 allows us to reduce the RRMF condition (6.2.2) to two simple algebraic constraints on the Bernstein coefficients of the quadratic polynomials

$$\begin{aligned}
\alpha(t) &= \alpha_0\,(1-t)^2 + \alpha_1\,2(1-t)t + \alpha_2\,t^2\,,\\
\beta(t) &= \beta_0\,(1-t)^2 + \beta_1\,2(1-t)t + \beta_2\,t^2\,,
\end{aligned} \tag{6.4.1}$$

in (3.2.2), that are sufficient and necessary for a rational RMAF. Moreover, we show that the constraint admit solutions for the coefficients α_1, β_1 (with one scalar degree of freedom), for arbitrary choices of the coefficients α_0, β_0, α_2,

β_2. An algorithm to construct RRMF quintics is formulated, that is adaptable to meet geometric design requirements, and illustrative computed examples are included.

Since $\alpha(t)$ and $\beta(t)$ are quadratic for PH quintics, $\overline{\alpha}(t)\alpha'(t) - \overline{\alpha}'(t)\alpha(t) + \overline{\beta}'(t)\beta(t)$ is the quadratic polynomial

$$\begin{aligned}
&2(\overline{\alpha}_0\alpha_1 - \overline{\alpha}_1\alpha_0 + \overline{\beta}_0\beta_1 - \overline{\beta}_1\beta_0)(1-t)^2 \\
&\quad + (\overline{\alpha}_0\alpha_2 - \overline{\alpha}_2\alpha_0 + \overline{\beta}_0\beta_2 - \overline{\beta}_2\beta_0)2(1-t)t \\
&\quad + 2(\overline{\alpha}_1\alpha_2 - \overline{\alpha}_2\alpha_1 + \overline{\beta}_1\beta_2 - \overline{\beta}_2\beta_1)t^2 ,
\end{aligned}$$

and $\overline{\alpha}(t)\alpha(t) + \overline{\beta}(t)\beta(t)$ is the quartic polynomial

$$\begin{aligned}
&(\overline{\alpha}_0\alpha_0 + \overline{\beta}_0\beta_0)(1-t)^4 \\
&\quad + \tfrac{1}{2}(\overline{\alpha}_0\alpha_1 + \overline{\alpha}_1\alpha_0 + \overline{\beta}_0\beta_1 + \overline{\beta}_1\beta_0)4(1-t)^3t \\
&\quad + \left[\tfrac{1}{6}(\overline{\alpha}_0\alpha_2 + \overline{\alpha}_2\alpha_0 + \overline{\beta}_0\beta_2 + \overline{\beta}_2\beta_0) + \tfrac{2}{3}(\overline{\alpha}_1\alpha_1 + \overline{\beta}_1\beta_1)\right] 6(1-t)^2t^2 \\
&\quad + \tfrac{1}{2}(\overline{\alpha}_1\alpha_2 + \overline{\alpha}_2\alpha_1 + \overline{\beta}_1\beta_2 + \overline{\beta}_2\beta_1)4(1-t)t^3 \\
&\quad + (\overline{\alpha}_2\alpha_2 + \overline{\beta}_2\beta_2)t^4 .
\end{aligned}$$

These forms are used to derive constraints on the coefficients of $\alpha(t)$, $\beta(t)$ that are sufficient and necessary for the satisfaction of (6.2.2) by some complex polynomials $\mathbf{w}(t)$, and hence the existence of a rational RMAF.

Proposition 6.2. *A PH quintic specified by the Hopf map form (3.2.2) satisfies the rational rotation–minimizing adapted frame condition (6.2.2) for some quadratic complex polynomial* $\mathbf{w}(t)$ *if and only of the coefficients* α_0, α_1, α_2 *and* β_0, β_1, β_2 *of the quadratic complex polynomials* $\alpha(t)$ *and* $\beta(t)$ *satisfy the constraint*

$$(|\alpha_0|^2 + |\beta_0|^2)\,|\overline{\alpha}_1\alpha_2 + \overline{\beta}_1\beta_2|^2 \;=\; (|\alpha_2|^2 + |\beta_2|^2)\,|\alpha_0\overline{\alpha}_1 + \beta_0\overline{\beta}_1|^2 , \qquad (6.4.2)$$

and either of the two constraints

$$\alpha_0\beta_1 - \alpha_1\beta_0 = 0 , \qquad (6.4.3)$$

$$(|\alpha_0|^2 + |\beta_0|^2)\,(\alpha_0\beta_2 - \alpha_2\beta_0) \;=\; 2\,(\alpha_0\overline{\alpha}_1 + \beta_0\overline{\beta}_1)(\alpha_0\beta_1 - \alpha_1\beta_0) . \qquad (6.4.4)$$

Proof : If $\mathbf{w}_0$, $\mathbf{w}_1$, $\mathbf{w}_2$ are the Bernstein coefficients of $\mathbf{w}(t)$, satisfaction of (6.2.2) implies that, for some non–zero real number γ, we have

$$\begin{aligned}
\overline{\alpha}_0\alpha_1 - \overline{\alpha}_1\alpha_0 + \overline{\beta}_0\beta_1 - \overline{\beta}_1\beta_0 &= \gamma(\overline{\mathbf{w}}_0\mathbf{w}_1 - \overline{\mathbf{w}}_1\mathbf{w}_0) , \\
\overline{\alpha}_0\alpha_2 - \overline{\alpha}_2\alpha_0 + \overline{\beta}_0\beta_2 - \overline{\beta}_2\beta_0 &= \gamma(\overline{\mathbf{w}}_0\mathbf{w}_2 - \overline{\mathbf{w}}_2\mathbf{w}_0) , \\
\overline{\alpha}_1\alpha_2 - \overline{\alpha}_2\alpha_1 + \overline{\beta}_1\beta_2 - \overline{\beta}_2\beta_1 &= \gamma(\overline{\mathbf{w}}_1\mathbf{w}_2 - \overline{\mathbf{w}}_2\mathbf{w}_1) ,
\end{aligned}$$

from the equality of numerators, and

$$\begin{aligned}
&\overline{\alpha}_0\alpha_0 + \overline{\beta}_0\beta_0 \;=\; \gamma\overline{w}_0 w_0\,,\\
&\overline{\alpha}_0\alpha_1 + \overline{\alpha}_1\alpha_0 + \overline{\beta}_0\beta_1 + \overline{\beta}_1\beta_0 \;=\; \gamma(\overline{w}_0 w_1 + \overline{w}_1 w_0)\,,\\
&\overline{\alpha}_0\alpha_2 + \overline{\alpha}_2\alpha_0 + \overline{\beta}_0\beta_2 + \overline{\beta}_2\beta_0 + 4(\overline{\alpha}_1\alpha_1 + \overline{\beta}_1\beta_1)\\
&\quad = \gamma(\overline{w}_0 w_2 + \overline{w}_2 w_0 + 4\,\overline{w}_1 w_1)\,,\\
&\overline{\alpha}_1\alpha_2 + \overline{\alpha}_2\alpha_1 + \overline{\beta}_1\beta_2 + \overline{\beta}_2\beta_1 \;=\; \gamma(\overline{w}_1 w_2 + \overline{w}_2 w_1)\,,\\
&\overline{\alpha}_2\alpha_2 + \overline{\beta}_2\beta_2 \;=\; \gamma\overline{w}_2 w_2\,,
\end{aligned}$$

from the equality of denominators. These eight equations can be reduced to

$$\begin{aligned}
&\overline{\alpha}_0\alpha_0 + \overline{\beta}_0\beta_0 \;=\; \gamma\,\overline{w}_0 w_0\,,\\
&\overline{\alpha}_0\alpha_1 + \overline{\beta}_0\beta_1 \;=\; \gamma\,\overline{w}_0 w_1\,,\\
&\overline{\alpha}_0\alpha_2 + \overline{\beta}_0\beta_2 + 2(\overline{\alpha}_1\alpha_1 + \overline{\beta}_1\beta_1) \;=\; \gamma\,(\overline{w}_0 w_2 + \overline{w}_1 w_2 + 2\,\overline{w}_1 w_1)\,,\\
&\overline{\alpha}_1\alpha_2 + \overline{\beta}_1\beta_2 \;=\; \gamma\,\overline{w}_1 w_2\,,\\
&\overline{\alpha}_2\alpha_2 + \overline{\beta}_2\beta_2 \;=\; \gamma\,\overline{w}_2 w_2\,.
\end{aligned}\tag{6.4.5}$$

Now by Lemma 6.1, we may assume $w_0 = 1$. The first of equations (6.4.5) gives the proportionality constant

$$\gamma \;=\; |\alpha_0|^2 + |\beta_0|^2\,,$$

and from the second equation we obtain

$$w_1 \;=\; \frac{\overline{\alpha}_0\alpha_1 + \overline{\beta}_0\beta_1}{|\alpha_0|^2 + |\beta_0|^2}\,. \tag{6.4.6}$$

Substituting γ, w_0, w_1 into the fourth equation then yields

$$w_2 \;=\; \frac{\overline{\alpha}_1\alpha_2 + \overline{\beta}_1\beta_2}{\alpha_0\overline{\alpha}_1 + \beta_0\overline{\beta}_1}\,. \tag{6.4.7}$$

To constitute a solution of the system (6.4.5), these expressions for γ, w_0, w_1, w_2 must also satisfy the third and the fifth of these equations. Substituting γ and w_2 into the fifth equation and clearing denominators leads directly to condition (6.4.2). Similarly, upon substituting γ, w_0, w_1, w_2 into the third equation and simplifying, we obtain

$$\begin{aligned}
&(|\alpha_0|^2 + |\beta_0|^2)^2(\overline{\alpha}_1\alpha_2 + \overline{\beta}_1\beta_2) + 2\,|\overline{\alpha}_0\alpha_1 + \overline{\beta}_0\beta_1|^2\\
&\quad = (|\alpha_0|^2 + |\beta_0|^2)(\alpha_0\overline{\alpha}_1 + \beta_0\overline{\beta}_1)[\overline{\alpha}_0\alpha_2 + \overline{\beta}_0\beta_2 + 2\,(|\alpha_1|^2 + |\beta_1|^2)]\,.
\end{aligned}$$

By straightforward but laborious manipulations, this can be reduced to

$$\begin{aligned}
(\overline{\alpha}_0\overline{\beta}_1 - \overline{\alpha}_1\overline{\beta}_0)\,\big[&(|\alpha_0|^2 + |\beta_0|^2)(\alpha_0\beta_2 - \alpha_2\beta_0)\\
&-2\,(\alpha_0\overline{\alpha}_1 + \beta_0\overline{\beta}_1)(\alpha_0\beta_1 - \alpha_1\beta_0)\big] \;=\; 0\,.
\end{aligned}$$

To satisfy this condition, one of the factors on the left must vanish: constraint (6.4.3) corresponds to (the conjugate of) the first factor, and constraint (6.4.4) to the second factor. ∎

To obtain (6.4.7) we tacitly assumed that $\mathbf{w}_1 \neq 0$, i.e., $\overline{\alpha}_0\alpha_1 + \overline{\beta}_0\beta_1 \neq 0$. If $\overline{\alpha}_0\alpha_1 + \overline{\beta}_0\beta_1 = 0$, then $\mathbf{w}_1 = 0$ from the second of equations (6.4.5), and hence $\overline{\alpha}_1\alpha_2 + \overline{\beta}_1\beta_2 = 0$ from the fourth. We now address this singular case.

Remark 6.3. Consider equations (6.4.5) when $\overline{\alpha}_0\alpha_1 + \overline{\beta}_0\beta_1 = \overline{\alpha}_1\alpha_2 + \overline{\beta}_1\beta_2 = 0$, and hence $\mathbf{w}_1 = 0$. Then the constraint (6.4.2) is evidently satisfied. Regarding $\overline{\alpha}_0\alpha_1 + \overline{\beta}_0\beta_1 = \overline{\alpha}_1\alpha_2 + \overline{\beta}_1\beta_2 = 0$ as simultaneous equations for α_1 and β_1, we must have either $\alpha_0\beta_2 - \alpha_2\beta_0 = 0$ or $\alpha_1 = \beta_1 = 0$. So either (6.4.3) or (6.4.4) is also satisfied. Equations (6.4.5) reduce in this case to

$$\begin{aligned}
\overline{\alpha}_0\alpha_0 + \overline{\beta}_0\beta_0 &= \gamma\,\overline{\mathbf{w}}_0\mathbf{w}_0\,,\\
\overline{\alpha}_0\alpha_2 + \overline{\beta}_0\beta_2 + 2\,(\overline{\alpha}_1\alpha_1 + \overline{\beta}_1\beta_1) &= \gamma\,\overline{\mathbf{w}}_0\mathbf{w}_2\,,\\
\overline{\alpha}_2\alpha_2 + \overline{\beta}_2\beta_2 &= \gamma\,\overline{\mathbf{w}}_2\mathbf{w}_2\,.
\end{aligned}$$

With $\mathbf{w}_0 = 1$, we have $\gamma = |\alpha_0|^2 + |\beta_0|^2$ from the first equation, and

$$\mathbf{w}_2 = \frac{\overline{\alpha}_0\alpha_2 + \overline{\beta}_0\beta_2 + 2\,(|\alpha_1|^2 + |\beta_1|^2)}{|\alpha_0|^2 + |\beta_0|^2}$$

from the second equation. Substituting γ, $\mathbf{w}_0$, $\mathbf{w}_2$ into the third equation and simplifying then yields the single constraint

$$(|\alpha_0|^2 + |\beta_0|^2)(|\alpha_2|^2 + |\beta_2|^2) = |\overline{\alpha}_0\alpha_2 + \overline{\beta}_0\beta_2 + 2\,(|\alpha_1|^2 + |\beta_1|^2)|^2$$

in lieu of (6.4.2) and (6.4.3) or (6.4.4), when $\overline{\alpha}_0\alpha_1 + \overline{\beta}_0\beta_1 = \overline{\alpha}_1\alpha_2 + \overline{\beta}_1\beta_2 = 0$.

Corollary 6.2. *When condition (6.4.2) is satisfied in conjunction with (6.4.3), the PH quintic* $\mathbf{r}(t)$ *degenerates to a straight line, whose RMAF is trivially rational.*

Proof : From condition (6.4.3) we must have $\beta_0 = z\alpha_0$ and $\beta_1 = z\alpha_1$ for some complex number z. Substituting into (6.4.2), a laborious but straightforward calculation yields $|z\alpha_2 - \beta_2|^2 = 0$, and hence $\beta_2 = z\alpha_2$. Therefore, (6.4.2) and (6.4.3) imply that $\alpha_2 : \beta_2 = \alpha_1 : \beta_1 = \alpha_0 : \beta_0$, and we infer from Remark 3.4 that the curve must be a straight line. ∎

As in the cubic case, we address separately the special case in which (6.2.2) is satisfied with both sides vanishing identically (see Remark 6.2).

Corollary 6.3. *If* $\mathrm{Im}\,(\overline{\alpha}_0\alpha_1 + \overline{\beta}_0\beta_1) = \mathrm{Im}\,(\overline{\alpha}_1\alpha_2 + \overline{\beta}_1\beta_2) = 0$, *the polynomial* $\mathbf{w}(t)$ *is real, and* $\mathbf{r}(t)$ *is a planar PH quintic whose RMAF is trivially rational.*

Proof : When $\overline{\alpha}_0\alpha_1 + \overline{\beta}_0\beta_1$ and $\overline{\alpha}_1\alpha_2 + \overline{\beta}_1\beta_2$ are both real, the coefficients (6.4.6) and (6.4.7) are real, so $\mathbf{w}(t) = \mathbf{w}_0(1-t)^2 + \mathbf{w}_1 2(1-t)t + \mathbf{w}_2 t^2$ is a real

polynomial. In this case, the third of equations (6.4.5) implies that $\overline{\alpha}_0\alpha_2 + \overline{\beta}_0\beta_2$ is also real. Since $|\alpha_0|^2 + |\beta_0|^2 \neq 0$ and $|\alpha_2|^2 + |\beta_2|^2 \neq 0$, we can invoke the argument used in Corollary 6.1 to write

$$\alpha_1 = \lambda_1\alpha_0 - z_1\overline{\beta}_0\,, \qquad \beta_1 = \lambda_1\beta_0 + z_1\overline{\alpha}_0\,, \tag{6.4.8}$$

$$\alpha_2 = \lambda_2\alpha_0 - z_2\overline{\beta}_0\,, \qquad \beta_2 = \lambda_2\beta_0 + z_2\overline{\alpha}_0\,, \tag{6.4.9}$$

$$\alpha_1 = \lambda_3\alpha_2 - z_3\overline{\beta}_2\,, \qquad \beta_1 = \lambda_3\beta_2 + z_3\overline{\alpha}_2\,, \tag{6.4.10}$$

for $\lambda_1, \lambda_2, \lambda_3 \in \mathbb{R}$ and $z_1, z_2, z_3 \in \mathbb{C}$. Substituting from (6.4.9) for α_2, β_2 into (6.4.10) and equating with (6.4.8) then gives

$$\lambda_3\lambda_2 - z_3\overline{z}_2 = \lambda_1, \qquad \lambda_3 z_2 + \lambda_2 z_3 = z_1\,.$$

From the first equation, $z_3\overline{z}_2$ must be real. By writing $z_2 = |z_2|\exp(i\phi_2)$ and $z_3 = |z_3|\exp(i\phi_3)$, we have $z_3\overline{z}_2 = |z_3||z_2|\exp(i(\phi_3 - \phi_2))$, so $z_3\overline{z}_2$ is real if and only if $\phi_2 = \phi_3 + k\pi$ for integer k, i.e., $z_2 = cz_3$ with $c \in \mathbb{R}$. Thus, writing $z_3 = \mu_3 z$ with $z \in \mathbb{C}$ and $\mu_3 \in \mathbb{R}$, we have $z_2 = \mu_2 z$ with $\mu_2 = c\mu_3 \in \mathbb{R}$, and the second equation then gives $z = \mu_1 z$ where $\mu_1 = \lambda_3\mu_2 + \lambda_2\mu_3 \in \mathbb{R}$. Hence, we can replace z_1, z_2, z_3 in (6.4.8)–(6.4.10) by $\mu_1 z$, $\mu_2 z$, $\mu_3 z$, and the coefficients of $\alpha(t)$, $\beta(t)$ have the form identified in Remark 3.4 as specifying a planar PH quintic (other than a straight line), whose RMAF is trivially rational. ∎

Note that the analysis of RRMF cubics and quintics yields the same γ, w_1 values, since the first two equations in (6.3.2) and (6.4.5) are identical.

We now show how conditions (6.4.2) and (6.4.4) provide a simple algorithm for the construction of RRMF quintics. Note first that (6.4.2) is a scalar condition, while (6.4.4) is a condition on complex values. Hence, these conditions impose three scalar constraints on the twelve parameters in α_0, α_1, α_2, β_0, β_1, β_2. Consequently, if we freely assign four of these complex coefficients *a priori*, we expect the algorithm to exhibit one residual scalar freedom.

Proposition 6.3. *For any choice of the coefficients α_0, β_0, α_2, β_2 that satisfy $|\alpha_0|^2 + |\beta_0|^2 \neq 0$, $|\alpha_2|^2 + |\beta_2|^2 \neq 0$ the constraints (6.4.2) and (6.4.4) identifying non–degenerate RRMF quintics admit solutions, with one free parameter, for the remining coefficients α_1, β_1.*

Proof : From (6.4.2) we can write

$$\overline{\alpha}_0\alpha_1 + \overline{\beta}_0\beta_1 = k\sqrt{|\alpha_0|^2 + |\beta_0|^2}\exp i\theta_0\,, \tag{6.4.11}$$

$$\overline{\alpha}_2\alpha_1 + \overline{\beta}_2\beta_1 = k\sqrt{|\alpha_2|^2 + |\beta_2|^2}\exp i\theta_2\,, \tag{6.4.12}$$

for real k, θ_0, θ_2. Solving these as simultaneous equations for α_1, β_1 gives[1]

$$\alpha_1 = k\frac{\sqrt{|\alpha_0|^2+|\beta_0|^2}\,\overline{\beta}_2 \exp i\theta_0 - \sqrt{|\alpha_2|^2+|\beta_2|^2}\,\overline{\beta}_0 \exp i\theta_2}{\overline{\alpha}_0\overline{\beta}_2 - \overline{\alpha}_2\overline{\beta}_0}, \qquad (6.4.13)$$

$$\beta_1 = k\frac{\sqrt{|\alpha_2|^2+|\beta_2|^2}\,\overline{\alpha}_0 \exp i\theta_2 - \sqrt{|\alpha_0|^2+|\beta_0|^2}\,\overline{\alpha}_2 \exp i\theta_0}{\overline{\alpha}_0\overline{\beta}_2 - \overline{\alpha}_2\overline{\beta}_0}. \qquad (6.4.14)$$

Substituting from (6.4.11) for $\alpha_0\overline{\alpha}_1 + \beta_0\overline{\beta}_1$ into (6.4.4), and the above expressions for α_1, β_1 into the term $\alpha_0\beta_1 - \alpha_1\beta_0$, and simplifying, we obtain

$$|\alpha_0\beta_2 - \alpha_2\beta_0|^2 = 2k^2\left[\sqrt{(|\alpha_0|^2+|\beta_0|^2)(|\alpha_2|^2+|\beta_2|^2)}\exp i\theta - (\alpha_0\overline{\alpha}_2 + \beta_0\overline{\beta}_2)\right] \qquad (6.4.15)$$

where we define $\theta = \theta_2 - \theta_0$. Since the term on the left is real, the imaginary part of the term on the right must vanish — i.e., θ must be defined by

$$\sin\theta = \frac{\mathrm{Im}\,(\alpha_0\overline{\alpha}_2 + \beta_0\overline{\beta}_2)}{\sqrt{(|\alpha_0|^2+|\beta_0|^2)(|\alpha_2|^2+|\beta_2|^2)}}. \qquad (6.4.16)$$

The expression on the right always defines a permissible $\sin\theta$ value, since

$$(|\alpha_0|^2+|\beta_0|^2)(|\alpha_2|^2+|\beta_2|^2) = |\alpha_0\overline{\alpha}_2 + \beta_0\overline{\beta}_2|^2 + |\alpha_0\beta_2 - \alpha_2\beta_0|^2 \qquad (6.4.17)$$

and the expression on the right is certainly not less than $\mathrm{Im}^2(\alpha_0\overline{\alpha}_2 + \beta_0\overline{\beta}_2)$. Once θ has been computed in this manner, the corresponding value of k^2 can be found from (6.4.15) as

$$k^2 = \frac{\frac{1}{2}|\alpha_0\beta_2 - \alpha_2\beta_0|^2}{\sqrt{(|\alpha_0|^2+|\beta_0|^2)(|\alpha_2|^2+|\beta_2|^2)}\cos\theta - \mathrm{Re}\,(\alpha_0\overline{\alpha}_2 + \beta_0\overline{\beta}_2)}. \qquad (6.4.18)$$

Using (6.4.16) and (6.4.17), and choosing $\cos\theta$ positive, this can be re–written as

$$k^2 = \frac{\frac{1}{2}|\alpha_0\beta_2 - \alpha_2\beta_0|^2}{\sqrt{|\alpha_0\beta_2 - \alpha_2\beta_0|^2 + \mathrm{Re}^2(\alpha_0\overline{\alpha}_2 + \beta_0\overline{\beta}_2)} - \mathrm{Re}\,(\alpha_0\overline{\alpha}_2 + \beta_0\overline{\beta}_2)}, \qquad (6.4.19)$$

where the right–hand side is clearly non–negative. Choosing θ_0 freely, setting $\theta_2 = \theta + \theta_0$ with θ obtained from (6.4.16), and computing k from (6.4.19), we can determine α_1 and β_1 from (6.4.13) and (6.4.14). ∎

The method for constructing RRMF quintics may be summarized as follows.

1 We assume that $\alpha_0\beta_2 - \alpha_2\beta_0 \neq 0$. Otherwise, we must have either $\alpha_0\beta_1 - \alpha_1\beta_0 = 0$ or $\alpha_0\overline{\alpha}_1 + \beta_0\overline{\beta}_1 = 0$ from (6.4.4). The former identifies degeneration to a straight line (see Corollary 6.2). For the latter, we also have $\overline{\alpha}_1\alpha_2 + \overline{\beta}_1\beta_2 = 0$ by (6.4.2) — this corresponds to the singular case treated in Remark 6.3.

Algorithm

1. Choose complex values $\boldsymbol{\alpha}_0$, $\boldsymbol{\beta}_0$, $\boldsymbol{\alpha}_2$, $\boldsymbol{\beta}_2$ with $|\boldsymbol{\alpha}_0|^2 + |\boldsymbol{\beta}_0|^2 \neq 0$, $|\boldsymbol{\alpha}_2|^2 + |\boldsymbol{\beta}_2|^2 \neq 0$;
2. determine θ from expression (6.4.16);
3. determine k from expression (6.4.19);
4. determine θ_0 freely, and set $\theta_2 = \theta_0 + \theta$;
5. compute $\boldsymbol{\alpha}_1$ and $\boldsymbol{\beta}_1$ from (6.4.13) and (6.4.14);
6. construct the hodograph (3.2.2) from $\boldsymbol{\alpha}(t)$, $\boldsymbol{\beta}(t)$.

It is possible to impose desired geometrical constraints on the RRMF quintic $\mathbf{r}(t)$ under construction when selecting input values $\boldsymbol{\alpha}_0$, $\boldsymbol{\beta}_0$, $\boldsymbol{\alpha}_2$, $\boldsymbol{\beta}_2$, for this algorithm (and choosing the parameter θ_0). In the Hermite interpolation algorithm [26] for spatial PH quintics, based on the quaternion form (3.1.8), the coefficients $\mathcal{A}_0 = \boldsymbol{\alpha}_0 + \mathbf{k}\boldsymbol{\beta}_0$ and $\mathcal{A}_2 = \boldsymbol{\alpha}_2 + \mathbf{k}\boldsymbol{\beta}_2$ of the quadratic quaternion polynomial $\mathcal{A}(t)$ are fixed (modulo one scalar freedom each) by interpolating the end–derivatives $\mathbf{r}'(0)$ and $\mathbf{r}'(1)$, while interpolation of the displacement $\mathbf{r}(1) - \mathbf{r}(0)$ determines $\mathcal{A}_1 = \boldsymbol{\alpha}_1 + \mathbf{k}\boldsymbol{\beta}_1$. It can be shown (see Chapter 8) that, among the two–parameter family of interpolants, one parameter essentially controls the arc length while the other controls the curve shape at fixed arc length. Since the conditions (6.4.2) and (6.4.4) for an RRMF quintic amount to three scalar constraints, it will necessary to relax from C^1 to G^1 Hermite data — i.e., interpolation of the end–tangents $\mathbf{t}_0 = \mathbf{r}'(0)/|\mathbf{r}'(0)|$ and $\mathbf{t}_1 = \mathbf{r}'(1)/|\mathbf{r}'(1)|$. A detailed treatment of this problem is addressed in Chapter 9.

Example 6.1. Consider the choices

$$\boldsymbol{\alpha}_0 = 1 + 2i\,, \quad \boldsymbol{\beta}_0 = -2 + i\,, \quad \boldsymbol{\alpha}_2 = 2 - i\,, \quad \boldsymbol{\beta}_2 = -1 + 2i\,,$$

for which $\boldsymbol{\alpha}_0\overline{\boldsymbol{\alpha}}_2 + \boldsymbol{\beta}_0\overline{\boldsymbol{\beta}}_2 = 4 + 8i$, $\boldsymbol{\alpha}_0\boldsymbol{\beta}_2 - \boldsymbol{\alpha}_2\boldsymbol{\beta}_0 = -2 - 4i$, and $|\boldsymbol{\alpha}_0|^2 + |\boldsymbol{\beta}_0|^2 = |\boldsymbol{\alpha}_2|^2 + |\boldsymbol{\beta}_2|^2 = 10$. Then (6.4.16) and (6.4.19) give $\sin\theta = 4/5$ and $k = \sqrt{5}$. Taking $\theta_0 = 0$ and $\theta_2 = \theta$, we have $\exp i\theta_0 = 1$ and $\exp i\theta_2 = (3 + 4i)/5$, and from (6.4.13) and (6.4.14) we obtain

$$\boldsymbol{\alpha}_1 = \frac{1+i}{\sqrt{2}} \quad \text{and} \quad \boldsymbol{\beta}_1 = \frac{-3+i}{\sqrt{2}}\,.$$

From (6.4.6) and (6.4.7), the coefficients of $\mathbf{w}(t)$ are determined to be

$$\mathbf{w}_0 = 1\,, \quad \mathbf{w}_1 = \frac{1}{\sqrt{2}}\,, \quad \mathbf{w}_2 = \frac{3-4i}{5}\,,$$

and one can easily verify the complex quadratic polynomials $\boldsymbol{\alpha}(t)$, $\boldsymbol{\beta}(t)$, $\mathbf{w}(t)$ defined by these coefficients satisfy (6.2.2). For this example, the polynomials

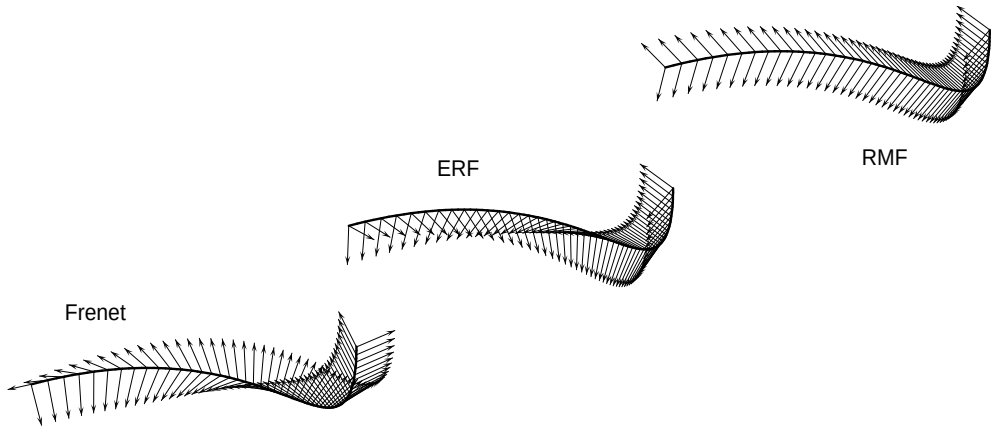

Figure 6.1: The RRMF quintic of Example 6.1, showing the Frenet adapted frame (left), Euler–Rodrigues frame (center), and the rotation–minimizing adapted frame (right). For clarity, the unit tangent vector (common to all three adapted frames) is not shown — only the two normal–plane vectors are illustrated.

$a(t) = \mathrm{Re}(\mathbf{w}(t))$, $b(t) = \mathrm{Im}(\mathbf{w}(t))$ that define the rational rotation (6.1.2) of the ERF onto the RMAF are given by

$$a(t) \;=\; (1-t)^2 + \frac{1}{\sqrt{2}}2(1-t)t + \frac{3}{5}t^2\,, \quad b(t) \;=\; -\frac{4}{5}t^2\,.$$

Once the Bernstein coefficients $\boldsymbol{\alpha}_0$, $\boldsymbol{\alpha}_1$, $\boldsymbol{\alpha}_2$ and $\boldsymbol{\beta}_0$, $\boldsymbol{\beta}_1$, $\boldsymbol{\beta}_2$ of the two quadratic polynomials $\boldsymbol{\alpha}(t)$, $\boldsymbol{\beta}(t)$ are known, the ERF can be constructed from (6.1.1).

The ERF vectors $\mathbf{e}_1(t)$, $\mathbf{e}_2(t)$, $\mathbf{e}_3(t)$ have a rational quartic dependence on the curve parameter t. Since the polynomials $a(t)$, $b(t)$ in (6.1.2) are quadratic, the RMAF vectors $\mathbf{a}_2(t)$, $\mathbf{a}_3(t)$ are nominally rational functions of degree 8 in t. Since the expressions for the ERF and RMAF vectors are rather cumbersome, we refrain from quoting them here. The MAPLE computer algebra system was used to compute them, and to verify that the ω_1 component of the angular velocity vector $\boldsymbol{\omega}$ define in (1.3.3) vanishes.

To construct the Bézier form of the RRMF quintic defined by integrating (3.2.2), it is convenient to convert to the quaternion form (3.1.8). The quaternion coefficients $\mathcal{A}_r = \boldsymbol{\alpha}_r + \mathbf{k}\boldsymbol{\beta}_r$ for $r = 0, 1, 2$ of $\mathcal{A}(t)$ are

$$\mathcal{A}_0 \;=\; 1 + 2\,\mathbf{i} + \mathbf{j} - 2\,\mathbf{k}\,, \mathcal{A}_1 \;=\; \frac{1 + \mathbf{i} + \mathbf{j} - 3\,\mathbf{k}}{\sqrt{2}}\,, \mathcal{A}_2 \;=\; 2 - \mathbf{i} + 2\,\mathbf{j} - \mathbf{k}\,,$$

and in terms of them we have the control points (3.1.6) with $\mathbf{u} = \mathbf{i}$, the initial control point $\mathbf{p}_0$ being an arbitrary integration constant. Figure 6.1 illustrates the RRMF quintic, together with its Frenet adapted frame, ERF and RMAF.

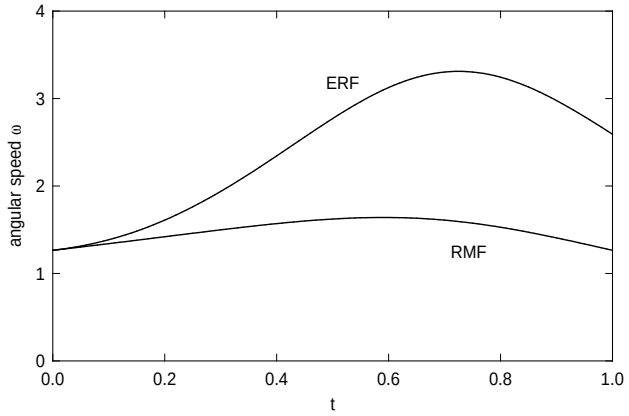

Figure 6.2: Variation of angular velocity magnitude for the Euler–Rodrigues frame and rotation–minimizing adapted frame, along the RRMF quintic of Example 6.1.

Although the RMF vectors $\mathbf{a}_2$, $\mathbf{a}_3$ and angular velocity components ω_2, ω_3 are rather complicated, the RMAF angular velocity magnitude $|\boldsymbol{\omega}|$ has a fairly manageable expression, namely

$$\frac{\sqrt{8(13+8\sqrt{2})}}{\sqrt{82t^4+(52\sqrt{2}-100)t^3+(118-22\sqrt{2})t^2-(100+30\sqrt{2})t+65+40\sqrt{2}}}.$$

For comparison, the angular velocity magnitude $|\boldsymbol{\omega}|$ for the ERF is

$$\frac{c\sqrt{(62t^2-(14-6\sqrt{2})t+8+\sqrt{2})(14t^2-(30+10\sqrt{2})t+40+25\sqrt{2})}}{82t^4+(52\sqrt{2}-100)t^3+(118-22\sqrt{2})t^2-(100+30\sqrt{2})t+65+40\sqrt{2}},$$

where $c=2\sqrt{(1005+568\sqrt{2})/217}$. Figure 6.2 compares these angular speeds.

6.5 HIGHER–ORDER RRMF CURVES

The approach used in Proposition 6.1 and 6.2 to determine conditions on the coefficients of the polynomials $\boldsymbol{\alpha}(t)$, $\boldsymbol{\beta}(t)$ that are sufficient and necessary for rational RMAFs on PH cubics and quintics can be extended to higher–order curves. To obtain RRMF curves of degree 7, for example, we must use cubic

complex polynomials $\boldsymbol{\alpha}(t)$, $\boldsymbol{\beta}(t)$ and the system of equations analogous to (6.3.2) and (6.4.5) in the case of RRMF cubics and quintics becomes

$$
\begin{aligned}
&\overline{\boldsymbol{\alpha}}_0\boldsymbol{\alpha}_0 + \overline{\boldsymbol{\beta}}_0\boldsymbol{\beta}_0 \;=\; \gamma\,\overline{\mathbf{w}}_0\mathbf{w}_0\,,\\
&\overline{\boldsymbol{\alpha}}_0\boldsymbol{\alpha}_1 + \overline{\boldsymbol{\beta}}_0\boldsymbol{\beta}_1 \;=\; \gamma\,\overline{\mathbf{w}}_0\mathbf{w}_1\,,\\
&2\,(\overline{\boldsymbol{\alpha}}_0\boldsymbol{\alpha}_2 + \overline{\boldsymbol{\beta}}_0\boldsymbol{\beta}_2) + 3\,(\overline{\boldsymbol{\alpha}}_1\boldsymbol{\alpha}_1 + \overline{\boldsymbol{\beta}}_1\boldsymbol{\beta}_1) \;=\; \gamma\,(2\,\overline{\mathbf{w}}_0\mathbf{w}_2 + 3\,\overline{\mathbf{w}}_1\mathbf{w}_1)\,,\\
&\overline{\boldsymbol{\alpha}}_0\boldsymbol{\alpha}_3 + \overline{\boldsymbol{\beta}}_0\boldsymbol{\beta}_3 + 6\,(\overline{\boldsymbol{\alpha}}_1\boldsymbol{\alpha}_2 + \overline{\boldsymbol{\beta}}_1\boldsymbol{\beta}_2) + 3\,(\overline{\boldsymbol{\alpha}}_2\boldsymbol{\alpha}_1 + \overline{\boldsymbol{\beta}}_2\boldsymbol{\beta}_1)\\
&\qquad = \gamma\,(\overline{\mathbf{w}}_0\mathbf{w}_3 + 6\,\overline{\mathbf{w}}_1\mathbf{w}_2 + 3\,\overline{\mathbf{w}}_2\mathbf{w}_1)\,,\\
&2\,(\overline{\boldsymbol{\alpha}}_1\boldsymbol{\alpha}_3 + \overline{\boldsymbol{\beta}}_1\boldsymbol{\beta}_3) + 3\,(\overline{\boldsymbol{\alpha}}_2\boldsymbol{\alpha}_2 + \overline{\boldsymbol{\beta}}_2\boldsymbol{\beta}_2) \;=\; \gamma\,(2\overline{\mathbf{w}}_1\mathbf{w}_3 + 3\overline{\mathbf{w}}_2\mathbf{w}_2)\,,\\
&\overline{\boldsymbol{\alpha}}_2\boldsymbol{\alpha}_3 + \overline{\boldsymbol{\beta}}_2\boldsymbol{\beta}_3 \;=\; \gamma\,\overline{\mathbf{w}}_2\mathbf{w}_3\,,\\
&\overline{\boldsymbol{\alpha}}_3\boldsymbol{\alpha}_3 + \overline{\boldsymbol{\beta}}_3\boldsymbol{\beta}_3 \;=\; \gamma\,\overline{\mathbf{w}}_3\mathbf{w}_3\,,
\end{aligned}
$$

Taking $\mathbf{w}_0 = 1$ again, we have $\gamma = |\boldsymbol{\alpha}_0|^2 + |\boldsymbol{\beta}_0|^2$ from the first equation, and from the second we see that $\mathbf{w}_1$ is given by the same expression (6.3.3) and (6.4.6) as in the cubic and quintic case. Then $\mathbf{w}_2$ and $\mathbf{w}_3$ can be directly obtained in terms of the coefficients of the cubics $\boldsymbol{\alpha}(t)$, $\boldsymbol{\beta}(t)$ from the third and fourth equations. Substituting these expressions for γ, $\mathbf{w}_0$, $\mathbf{w}_1$, $\mathbf{w}_2$, $\mathbf{w}_3$ into the fifth, sixth, and seventh equations yields a set of constraints on the $\boldsymbol{\alpha}(t)$, $\boldsymbol{\beta}(t)$ coefficients that are sufficient and necessary for the degree 7 spatial PH curve specified by (3.2.2) to possess a rational RMAF.

6.6 A SIMPLER CHARACTERIZATION OF RRMF QUINTICS

As first appeared visible with the analysis of double PH curves, the investigation of the existence of rational RMAFs on polynomial space curve has again highlighted the importance of the combined use of the quaternion and the Hopf map forms of spatial PH curves.

Han [47] identified the algebraic criterion (6.2.1) for the rationality of rotation–minimizing frames, in terms of the quaternion representation for spatial PH curves, and showed that non–degenerate spatial PH cubics can not be RRMF curves. The existence of non–degenerate quintic RRMF curves was first demonstrated in [30], using the Hopf map representation of spatial PH curves through the constructive process reported in Section 6.4. Specifically, Proposition 6.2 shows how to define RRMF quintics by one real and one complex constraint, of degree 6 and 4, on the six complex coefficients of the two quadratic complex polynomials $\boldsymbol{\alpha}(t)$, $\boldsymbol{\beta}(t)$ that specify the Hopf map form (3.2.2) of spatial PH quintics. Subsequently, much simpler characterizations of the RRMF quintics have been identified [25], that are just quadratic in the curve coefficients and with compact expressions in both the quaternion and the Hopf map forms. These characterizations are quoted from [25] in the following propositions.

Proposition 6.4. *A PH quintic specified by the quaternion form (3.1.8) has a rational rotation–minimizing adapted frame if and only if the coefficients $\mathcal{A}_0$, $\mathcal{A}_1$, $\mathcal{A}_2$ of the quadratic quaternion polynomial (3.1.4) satisfy the constraint*

$$\mathrm{vect}(\mathcal{A}_2\,\mathbf{i}\,\mathcal{A}_0^*) \;=\; \mathcal{A}_1\,\mathbf{i}\,\mathcal{A}_1^*\,. \tag{6.6.1}$$

Proposition 6.5. *A PH quintic specified by the Hopf map form (3.2.2) has a rational rotation–minimizing adapted frame if and only if the coefficients $\boldsymbol{\alpha}_0$, $\boldsymbol{\alpha}_1$, $\boldsymbol{\alpha}_2$ and $\boldsymbol{\beta}_0$, $\boldsymbol{\beta}_1$, $\boldsymbol{\beta}_2$ of the quadratic complex polynomials (6.4.1) satisfy the constraints*

$$\mathrm{Re}\,(\boldsymbol{\alpha}_0\overline{\boldsymbol{\alpha}}_2 - \boldsymbol{\beta}_0\overline{\boldsymbol{\beta}}_2) \;=\; |\boldsymbol{\alpha}_1|^2 - |\boldsymbol{\beta}_1|^2\,, \qquad \boldsymbol{\alpha}_0\overline{\boldsymbol{\beta}}_2 + \boldsymbol{\alpha}_2\overline{\boldsymbol{\beta}}_0 \;=\; 2\boldsymbol{\alpha}_1\overline{\boldsymbol{\beta}}_1\,. \tag{6.6.2}$$

7

PYTHAGOREAN CURVES

For an adapted moving frames along a 3D trajectory described by the parametric curve $\mathbf{r}(t)$, a rational dependence on the curve parameter is possible by choosing $\mathbf{r}(t)$ to be a spatial PH curve. A similar resolution is possible for a directed frame, but the coordinate components of the *curve* $\mathbf{r}(t) = (x(t), y(t), z(t))$ — rather than its *hodograph* $\mathbf{r}'(t) = (x'(t), y'(t), z'(t))$ — must be elements of a Pythagorean quartuple, that is, we must have

$$x^2(t) + y^2(t) + z^2(t) = r^2(t),$$

for some polynomial $r(t)$. This condition characterizes a *Pythagorean curve* — or P curve — rather than a PH curve. The computation of rational directed frames on space curves thus motivates a study of the properties and construction of P curves.

Many of the ideas and methods used in the study of PH curves carry over to the investigation of P curves. In particular, the quaternion and Hopf map formulation of spatial PH curves may offer convenient models for the representation of P curves, while, to solve practical design problems using P curves, intuitive methods for their construction are required. These are typically based on interpolation of discrete points and tangent data.

After the characterization of P curves in Section 7.1, we briefly describe two interpolation methods in Section 7.2 and 7.3. The first, based on classical Hermite interpolation of end–points and derivatives, employs P curves of degree six and requires selection of three residual (scalar) parameters. In the second method, interpolation of end–derivatives is relaxed, and instead a middle interpolation point is introduced. In this case, P curves of degree 4 can be defined, with two residual (scalar) degrees of freedom. Finally, Section 7.4 discusses double P curve and P curves with rational rotation–minimizing directed frames.

7.1 CHARACTERIZATION OF P CURVES

A spatial Pythagorean curve $\mathbf{r}(t)$ is characterized by the property that its polar distance r is a polynomial in the curve parameter t. Since this is equivalent to the requirement that its anti–hodograph is a PH curve, the P curve $\mathbf{r}(t)$ can be expressed as a quaternion product [13] of the form

$$\mathbf{r}(t) = \mathcal{A}(t)\,\mathbf{i}\,\mathcal{A}^*(t)\,, \tag{7.1.1}$$

where $\mathcal{A}(t) = u(t) + v(t)\,\mathbf{i} + p(t)\,\mathbf{j} + q(t)\,\mathbf{k}$ is a quaternion polynomial of degree m for a degree–n Pythagorean curve, $n = 2m$. We observe that, whereas regular

PH curves defined by integrating (3.1.8) are of *odd* degree, P curves defined by (7.1.1) are of *even* degree.

We present just basic outlines of two interpolation problems using P curves below — in particular, we do not address the problem of optimal choices for free parameters, since it is non–trivial and beyond our present scope.

7.2 HERMITE INTERPOLATION BY P CURVES OF DEGREE 6

Substituting the cubic quaternion polynomial (3.1.5) into expression (7.1.1) gives the Bézier form

$$\mathbf{r}(t) \;=\; \sum_{i=0}^{6} \mathbf{p}_i \binom{6}{i} (1-t)^{6-i}\, t^i$$

of a spatial P curve of degree 6 with control points $\mathbf{p}_i = x_i\,\mathbf{i} + y_i\,\mathbf{j} + z_i\,\mathbf{k}$ defined by

$$\begin{aligned}
\mathbf{p}_0 &= \mathcal{A}_0\,\mathbf{i}\,\mathcal{A}_0^*\,,\\
\mathbf{p}_1 &= \tfrac{1}{2}\,(\mathcal{A}_0\,\mathbf{i}\,\mathcal{A}_1^* + \mathcal{A}_1\,\mathbf{i}\,\mathcal{A}_0^*)\,,\\
\mathbf{p}_2 &= \tfrac{1}{5}\,(\mathcal{A}_0\,\mathbf{i}\,\mathcal{A}_2^* + 3\,\mathcal{A}_1\,\mathbf{i}\,\mathcal{A}_1^* + \mathcal{A}_2\,\mathbf{i}\,\mathcal{A}_0^*)\,,\\
\mathbf{p}_3 &= \tfrac{1}{20}\,(\mathcal{A}_0\,\mathbf{i}\,\mathcal{A}_3^* + 9\,\mathcal{A}_1\,\mathbf{i}\,\mathcal{A}_2^* + 9\,\mathcal{A}_2\,\mathbf{i}\,\mathcal{A}_1^* + \mathcal{A}_3\,\mathbf{i}\,\mathcal{A}_0^*)\,,\\
\mathbf{p}_4 &= \tfrac{1}{5}\,(\mathcal{A}_1\,\mathbf{i}\,\mathcal{A}_3^* + 3\,\mathcal{A}_2\,\mathbf{i}\,\mathcal{A}_2^* + \mathcal{A}_3\,\mathbf{i}\,\mathcal{A}_1^*)\,,\\
\mathbf{p}_5 &= \tfrac{1}{2}\,(\mathcal{A}_2\,\mathbf{i}\,\mathcal{A}_3^* + \mathcal{A}_3\,\mathbf{i}\,\mathcal{A}_2^*)\,,\\
\mathbf{p}_6 &= \mathcal{A}_3\,\mathbf{i}\,\mathcal{A}_3^*\,.
\end{aligned}$$

Interpolation of end points yields the equations

$$\mathcal{A}_0\,\mathbf{i}\,\mathcal{A}_0^* \;=\; \mathbf{p}_i \qquad \text{and} \qquad \mathcal{A}_3\,\mathbf{i}\,\mathcal{A}_3^* \;=\; \mathbf{p}_f \tag{7.2.1}$$

for $\mathcal{A}_0$ and $\mathcal{A}_3$, while interpolation of the end-derivatives gives the equations

$$\tfrac{1}{2}\left(\mathcal{A}_0\,\mathbf{i}\,\mathcal{A}_1^* + \mathcal{A}_1\,\mathbf{i}\,\mathcal{A}_0^*\right) \;=\; \mathbf{g}_i \quad \text{and} \quad \tfrac{1}{2}\left(\mathcal{A}_2\,\mathbf{i}\,\mathcal{A}_3^* + \mathcal{A}_3\,\mathbf{i}\,\mathcal{A}_2^*\right) \;=\; \mathbf{g}_f\,, \tag{7.2.2}$$

for $\mathcal{A}_1$ and $\mathcal{A}_2$, where we set

$$\mathbf{g}_i \;=\; \mathbf{p}_i \;+\; \tfrac{1}{6}\,\mathbf{d}_i\,, \quad \text{and} \quad \mathbf{g}_f \;=\; \mathbf{p}_f \;-\; \tfrac{1}{6}\,\mathbf{d}_f\,.$$

The two equations in (7.2.1) are of the well–known form $\mathcal{A}\,\mathbf{i}\,\mathcal{A}^* \;=\; \mathbf{d}$, where $\mathbf{d}$ is any non–zero vector not aligned with $-\mathbf{i}$, and can be solved directly [26] to obtain

$$\mathcal{A}_0 \;=\; \sqrt{|\mathbf{p}_i|}\,\mathbf{n}_i\,\exp(\phi_i\,\mathbf{i}) \quad \text{and} \quad \mathcal{A}_3 \;=\; \sqrt{|\mathbf{p}_f|}\,\mathbf{n}_f\,\exp(\phi_f\,\mathbf{i})\,,$$

where ϕ_i and ϕ_f are free angular variables, and we define

$$\mathbf{n}_i \;=\; \frac{\boldsymbol{\delta}_i + \mathbf{i}}{|\,\boldsymbol{\delta}_i + \mathbf{i}\,|}\,, \qquad \mathbf{n}_f \;=\; \frac{\boldsymbol{\delta}_f + \mathbf{i}}{|\,\boldsymbol{\delta}_f + \mathbf{i}\,|}\,, \tag{7.2.3}$$

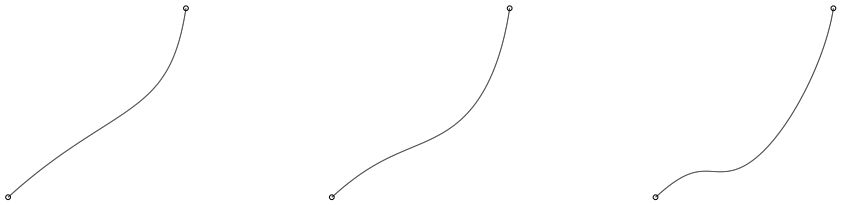

(a) $\Delta\phi = 0$ (b) $\Delta\phi = \frac{\pi}{8}$ (c) $\Delta\phi = \frac{\pi}{4}$

Figure 7.1: Three P curves of degree 6 interpolating the Hermite data of Example 7.1.

and

$$\delta_i = \frac{\mathbf{p}_i}{|\mathbf{p}_i|}, \qquad \delta_f = \frac{\mathbf{p}_f}{|\mathbf{p}_f|}. \tag{7.2.4}$$

On the other hand, equations (7.2.2) are of the form cited in Lemma 2.5 of [100], and can be solved directly to obtain

$$\mathcal{A}_1 = -\frac{(\mu_i + \mathbf{g}_i)\,\mathcal{A}_0\,\mathbf{i}}{|\mathcal{A}_0|^2} \quad \text{and} \quad \mathcal{A}_2 = -\frac{(\mu_f + \mathbf{g}_f)\,\mathcal{A}_3\,\mathbf{i}}{|\mathcal{A}_3|^2},$$

where μ_i and μ_f are free real parameters. As was shown in the PH curve context [26], the P curve (7.1.1) depends only on the difference $\Delta\phi = \phi_f - \phi_i$. Hence, solutions to the Hermite interpolation problem by P curves of degree 6, depends on the three real parameter — $\Delta\phi$, μ_i and μ_f.

Example 7.1. Figure 7.1 shows three interpolants to the data

$$\mathbf{p}_i = (0.50, 0.25, 0.50), \quad \mathbf{p}_f = (1,1,1), \quad \mathbf{d}_i = (1,0,1), \quad \mathbf{d}_f = (0,1,1).$$

In all cases we choose $\mu_i = \mu_f = 0$, while $\Delta\phi$ is gradually equal to 0, $\frac{\pi}{8}$, and $\frac{\pi}{4}$.

7.3 THREE-POINTS INTERPOLATION BY P CURVES OF DEGREE 4

Given points $\mathbf{p}_i$, $\mathbf{p}_m$, $\mathbf{p}_f$, we seek a P curve interpolant $\mathbf{r}(t)$ satisfying $\mathbf{r}(0) = \mathbf{p}_i$, $\mathbf{r}\left(\frac{1}{2}\right) = \mathbf{p}_m$, $\mathbf{r}(1) = \mathbf{p}_f$. Substituting the quadratic quaternion polynomial (3.1.4) into equation (7.1.1) gives the Bézier form (1.1.6) of a quartic P curve with control points $\mathbf{p}_i = x_i\,\mathbf{i} + y_i\,\mathbf{j} + z_i\,\mathbf{k}$ defined by

$$\begin{aligned}
\mathbf{p}_0 &= \mathcal{A}_0\,\mathbf{i}\,\mathcal{A}_0^*,\\
\mathbf{p}_1 &= \tfrac{1}{2}\left(\mathcal{A}_0\,\mathbf{i}\,\mathcal{A}_1^* + \mathcal{A}_1\,\mathbf{i}\,\mathcal{A}_0^*\right),\\
\mathbf{p}_2 &= \tfrac{1}{6}\left(\mathcal{A}_0\,\mathbf{i}\,\mathcal{A}_2^* + 4\,\mathcal{A}_1\,\mathbf{i}\,\mathcal{A}_1^* + \mathcal{A}_2\,\mathbf{i}\,\mathcal{A}_0^*\right),\\
\mathbf{p}_3 &= \tfrac{1}{2}\left(\mathcal{A}_1\,\mathbf{i}\,\mathcal{A}_2^* + \mathcal{A}_2\,\mathbf{i}\,\mathcal{A}_1^*\right),\\
\mathbf{p}_4 &= \mathcal{A}_2\,\mathbf{i}\,\mathcal{A}_2^*.
\end{aligned}$$

As in the previous case, interpolation of end points yields the equations

$$\mathcal{A}_0\,\mathbf{i}\,\mathcal{A}_0^* = \mathbf{p}_i \quad \text{and} \quad \mathcal{A}_2\,\mathbf{i}\,\mathcal{A}_2^* = \mathbf{p}_f\,, \tag{7.3.1}$$

with solutions

$$\mathcal{A}_0 = \sqrt{|\mathbf{p}_i|}\,\mathbf{n}_i\,\exp(\phi_i\,\mathbf{i}) \quad \text{and} \quad \mathcal{A}_2 = \sqrt{|\mathbf{p}_f|}\,\mathbf{n}_f\,\exp(\phi_f\,\mathbf{i})\,,$$

where ϕ_i and ϕ_f are free angular variables, and $\mathbf{n}_i$, $\mathbf{n}_f$, δ_i, δ_f are specified in (7.2.3) and (7.2.4). Now, since

$$\mathbf{r}\left(\tfrac{1}{2}\right) = \tfrac{1}{16}\left(\mathcal{A}_0 + 2\mathcal{A}_1 + \mathcal{A}_2\right)\mathbf{i}\left(\mathcal{A}_0^* + 2\mathcal{A}_1^* + \mathcal{A}_2^*\right)$$

the interpolation condition in $\mathbf{r}(\frac{1}{2}) = \mathbf{p}_m$ yields

$$\mathcal{B}\,\mathbf{i}\,\mathcal{B}^* = \mathbf{d} \tag{7.3.2}$$

where $\mathcal{B} = \mathcal{A}_0 + 2\mathcal{A}_1 + \mathcal{A}_2$ and $\mathbf{d} = 16\,\mathbf{p}_m$. From the general solution of (7.3.2), we have

$$\mathcal{B} = \sqrt{|\mathbf{d}|}\,\mathbf{n}_m\,\exp(\phi_m\,\mathbf{i})\,,$$

where ϕ_m is another free angular variable, and we define

$$\mathbf{n}_m = \frac{\delta_m + \mathbf{i}}{|\,\delta_m + \mathbf{i}\,|}\,, \qquad \delta_m = \frac{\mathbf{d}}{|\mathbf{d}|}\,.$$

Since the quartic P curve (7.1.1) depends only on the difference of ϕ_i, ϕ_m, ϕ_f, the three-point interpolant depends on just two free parameters.

Example 7.2. Figure 7.2 show different interpolants to the data

$$\mathbf{p}_i = (0.1, 0.1, 0.1)\,, \quad \mathbf{p}_m = (0.3, 0.7, 0.6)\,, \quad \mathbf{p}_f = (1.0, 1.0, 1.0)\,,$$

obtained by sampling the two free angular parameters $\Delta\phi = \phi_f - \phi_i$ and ϕ_m at the three equidistant values 0, $\frac{\pi}{8}$, $\frac{\pi}{4}$.

7.4 DOUBLE P CURVES AND P CURVES WITH RATIONAL RMDF

As already noted, the theory of directed frames coincide with that of adapted frames, applied to the anti–hodograph of the given curve. This means that much of the established results obtained in the Pythagorean–hodograph context can be adapted to the construction and analysis of Pythagorean curves. Similarly, the characterizations of Chapters 4 and 6 can be used to define "double" Pythagorean (DP) curves and Pythagorean curves with rational rotation–minimizing directed frames, respectively.

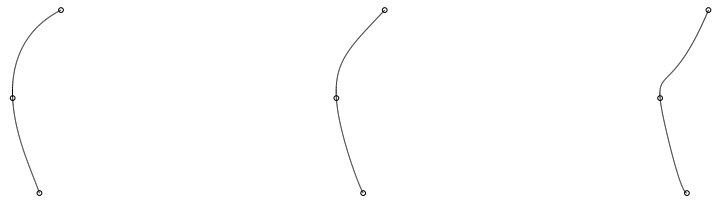

(a) $\Delta\phi = 0, \phi_m = 0$ (b) $\Delta\phi = 0, \phi_m = \frac{\pi}{8}$ (c) $\Delta\phi = 0, \phi_m = \frac{\pi}{4}$

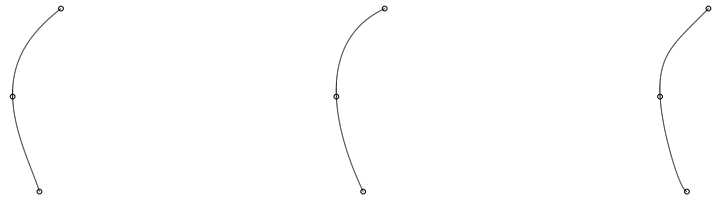

(d) $\Delta\phi = \frac{\pi}{8}, \phi_m = 0$ (e) $\Delta\phi = \frac{\pi}{8}, \phi_m = \frac{\pi}{8}$ (f) $\Delta\phi = \frac{\pi}{8}, \phi_m = \frac{\pi}{4}$

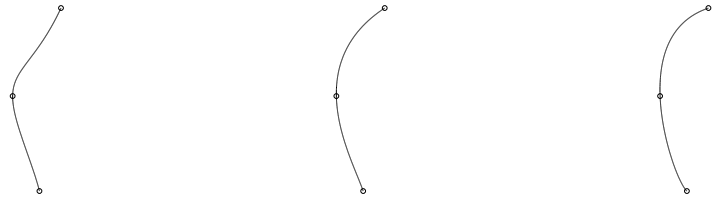

(g) $\Delta\phi = \frac{\pi}{4}, \phi_m = 0$ (h) $\Delta\phi = \frac{\pi}{4}, \phi_m = \frac{\pi}{8}$ (i) $\Delta\phi = \frac{\pi}{4}, \phi_m = \frac{\pi}{4}$

Figure 7.2: P curves of degree 4 interpolating the data of Example 7.2 for different values of the free parameters.

According to (4.1.3) and (4.1.4), a polynomial space curve $\mathbf{r}(t)$ is said to be a double P curve if $|\mathbf{r}(t)|$ and $|\mathbf{r}(t) \times \mathbf{r}'(t)|$ are both polynomial functions of t — i.e., if the conditions

$$|\mathbf{r}|^2 = x^2 + y^2 + z^2 \equiv r^2,$$
$$|\mathbf{r} \times \mathbf{r}'|^2 = (yz' - y'z)^2 + (zx' - z'x)^2 + (xy' - x'y)^2 \equiv (rw)^2$$

are simultaneously satisfied for some polynomials $r(t), w(t)$. The analysis of Chapter 4 on DPH curves of degree 3, 5, and 7 could be reformulated in terms of DP curves of degree 2, 4, and 6.

Analogously, in order to define a Pythagorean curve with a rational RMDF, the components u, v, p, q of the quaternion polynomial $\mathcal{A}(t)$ in (7.1.1) must satisfy condition (6.2.1). Translated into the Hopf map representation, this

means that the complex polynomials $\alpha(t), \beta(t)$ in $\mathbf{r}(t) = H(\alpha(t), \beta(t))$ must satisfy condition (6.2.2). The sufficient and necessary constraints (6.4.2)–(6.4.4), or the equivalent simplified version (6.6.2) — or (6.6.1) in quaternion form — introduced in Chapter 6 for the characterization of RRMF quintics, can be used to construct Pythagorean quartics with rational rotation–minimizing directed frames.

Part III

APPLICATION ALGORITHMS

8

SPATIAL PH QUINTIC HERMITE INTERPOLANTS

In order to solve practical design problems using parametric polynomial curves, efficient methods for their geometric construction are required. If the non–linear nature of Pythagorean–hodograph curves precludes a direct specification by Bézier/B–spline control polygons, the solution of the first order Hermite interpolation problem is a standard approach to construction of spatial PH curves satisfying prescribed geometrical constraints. The standard Bézier cubic, commonly used to interpolate discrete points and tangent data, has to be replaced by a PH quintic space curve in order to allow the satisfaction of the Pythagorean–hodograph condition. The problem of specifying the two free angular parameters that arise in the spatial PH quintic Hermite interpolation problem is addressed in this chapter.

Conditions on the given data that identify when the "ordinary" cubic Hermite interpolant is actually a PH curve are formulated, since it is desired that the selection criteria should reproduce such curves whenever possible. The properties of helical PH quintics are analyzed and their use in selecting Hermite interpolants is considered. It is shown that the arc lengths of the PH quintic Hermite interpolants depend on only one of the free angular parameters and that general helical PH quintic interpolants exist for arbitrary Hermite data, corresponding to solutions of minimum or maximum arc length. Motivated by the desire to improve the fairness of the interpolants to general data at reasonable computational cost, these results are then used to formulate three practical selection criteria, that all generate the cubic interpolant when possible.

The chapter is organized as follows. Section 8.1 establishes conditions on the Hermite data for the existence of a PH cubic interpolant. An analysis of helical PH quintic curves, and the determination of their axes and pitch angles, is presented in Section 8.2, while Section 8.3 introduces the PH quintic Hermite interpolation problem. Section 8.4 analyzes the arc length of spatial PH quintics, and demonstrates that general helical PH quintics interpolants exist for arbitrary Hermite data, and exhibit extremal arc lengths. The criteria for selecting the two free parameters of PH quintic Hermite interpolants are then described in Section 8.5, and Section 8.6 presents some computed examples using these criteria.

8.1 EXISTENCE OF PH CUBIC INTERPOLANTS

We determine the conditions under which initial and final points $\mathbf{p}_i$, $\mathbf{p}_f$ and derivatives $\mathbf{d}_i$, $\mathbf{d}_f$ can be interpolated by a spatial PH cubic — i.e., we identify data sets for which the "ordinary" cubic interpolant is a PH curve. Setting

$$\mathbf{w} \;=\; 3(\mathbf{p}_f - \mathbf{p}_i) - (\mathbf{d}_i + \mathbf{d}_f) \tag{8.1.1}$$

and introducing the vectors

$$\delta_i \;=\; \frac{\mathbf{d}_i}{|\mathbf{d}_i|}\,, \qquad \delta_f \;=\; \frac{\mathbf{d}_f}{|\mathbf{d}_f|}\,, \qquad \mathbf{z} \;=\; \frac{\delta_i \times \delta_f}{|\,\delta_i + \delta_f\,|}\,, \tag{8.1.2}$$

we have:

Proposition 8.1. *The cubic Hermite interpolant to the data points $\mathbf{p}_i$, $\mathbf{p}_f$ and derivatives $\mathbf{d}_i$, $\mathbf{d}_f$ is a PH curve if and only if*

$$\mathbf{w} \cdot (\delta_i - \delta_f) \;=\; 0 \tag{8.1.3}$$

and

$$\left(\mathbf{w} \cdot \frac{\delta_i + \delta_f}{|\,\delta_i + \delta_f\,|}\right)^2 \;+\; \frac{(\mathbf{w}\cdot\mathbf{z})^2}{|\mathbf{z}|^4} \;=\; |\mathbf{d}_i|\,|\mathbf{d}_f|\,. \tag{8.1.4}$$

Proof : The ordinary cubic Hermite interpolant may be written in Bézier form as

$$\mathbf{r}(t) \;=\; \mathbf{p}_i\, b_0^3(t) \;+\; (\mathbf{p}_i + \tfrac{1}{3}\mathbf{d}_i)\, b_1^3(t) \;+\; (\mathbf{p}_f - \tfrac{1}{3}\mathbf{d}_f)\, b_2^3(t) \;+\; \mathbf{p}_f\, b_3^3(t)\,, \tag{8.1.5}$$

and, from (8.1.1), its hodograph is

$$\mathbf{r}'(t) \;=\; \mathbf{d}_i\, b_0^2(t) \;+\; \mathbf{w}\, b_1^2(t) \;+\; \mathbf{d}_f\, b_2^2(t)\,. \tag{8.1.6}$$

From (3.1.1) and (3.1.3), we note that (8.1.5) is a PH cubic curve if two quaternions $\mathcal{A}_0$, $\mathcal{A}_1$ exist such that

$$\mathbf{r}'(t) \;=\; (\mathcal{A}_0\,\mathbf{u}\,\mathcal{A}_0^*)\; b_0^2(t) \;+\; \tfrac{1}{2}\,(\mathcal{A}_0\,\mathbf{u}\,\mathcal{A}_1^* + \mathcal{A}_1\,\mathbf{u}\,\mathcal{A}_0^*)\, b_1^2(t) \;+\; (\mathcal{A}_1\,\mathbf{u}\,\mathcal{A}_1^*)\; b_2^2(t)\,.$$

Assuming (without loss of generality) that $\mathbf{u} = \delta_i$, the above hodograph agrees with (8.1.6) if

$$\mathcal{A}_0\,\delta_i\,\mathcal{A}_0^* \;=\; \mathbf{d}_i\,, \quad \mathcal{A}_1\,\delta_i\,\mathcal{A}_1^* \;=\; \mathbf{d}_f\,, \quad \mathcal{A}_0\,\delta_i\,\mathcal{A}_1^* + \mathcal{A}_1\,\delta_i\,\mathcal{A}_0^* \;=\; 2\mathbf{w}\,. \tag{8.1.7}$$

Again, without loss of generality, we can assume that

$$\mathcal{A}_0 \;=\; \sqrt{|\mathbf{d}_i|}\,\delta_i\,, \tag{8.1.8}$$

and we then obtain

$$\mathcal{A}_0\,\boldsymbol{\delta}_i\,\mathcal{A}_1^* + \mathcal{A}_1\,\boldsymbol{\delta}_i\,\mathcal{A}_0^* \;=\; \sqrt{|\mathbf{d}_i|}\,(\mathcal{A}_1 - \mathcal{A}_1^*) \;=\; 2\sqrt{|\mathbf{d}_i|}\,\mathrm{vect}(\mathcal{A}_1)\,. \tag{8.1.9}$$

On the other hand, from Section B.2 we know that $\mathcal{A}_1$ has the general form

$$\mathcal{A}_1 \;=\; \sqrt{|\mathbf{d}_f|}\,\frac{\boldsymbol{\delta}_i + \boldsymbol{\delta}_f}{|\,\boldsymbol{\delta}_i + \boldsymbol{\delta}_f\,|}\,(\cos\phi + \sin\phi\,\boldsymbol{\delta}_i)\,. \tag{8.1.10}$$

From the quaternion product rules, we can write

$$\mathrm{vect}(\mathcal{A}_1) \;=\; \sqrt{|\mathbf{d}_f|}\,\left(\cos\phi\,\frac{\boldsymbol{\delta}_i + \boldsymbol{\delta}_f}{|\,\boldsymbol{\delta}_i + \boldsymbol{\delta}_f\,|} \;-\; \sin\phi\,\mathbf{z}\right)\,, \tag{8.1.11}$$

where $\mathbf{z}$ is defined by (8.1.2).

Now since the three vectors $\boldsymbol{\delta}_i + \boldsymbol{\delta}_f$, $\mathbf{z}$, $\boldsymbol{\delta}_i - \boldsymbol{\delta}_f$ satisfy

$$(\boldsymbol{\delta}_i + \boldsymbol{\delta}_f)\cdot\mathbf{z} = 0\,, \qquad \mathbf{z}\cdot(\boldsymbol{\delta}_i - \boldsymbol{\delta}_f) = 0\,, \qquad (\boldsymbol{\delta}_i - \boldsymbol{\delta}_f)\cdot(\boldsymbol{\delta}_i + \boldsymbol{\delta}_f) = 0\,,$$

they are mutually orthogonal, and from (8.1.9) and (8.1.11) we immediately infer that the third condition in (8.1.7) can be satisfied if (8.1.3) holds. This means that $\mathbf{w}$ must be a linear combination of $\boldsymbol{\delta}_i + \boldsymbol{\delta}_f$ and $\mathbf{z}$. Writing

$$\mathbf{w} \;=\; \mu\,(\boldsymbol{\delta}_i + \boldsymbol{\delta}_f) \;+\; \nu\,\mathbf{z} \tag{8.1.12}$$

and taking the dot product of both sides with $\boldsymbol{\delta}_i + \boldsymbol{\delta}_f$ and $\mathbf{z}$ gives

$$\mu \;=\; \mathbf{w}\cdot\frac{\boldsymbol{\delta}_i + \boldsymbol{\delta}_f}{|\boldsymbol{\delta}_i + \boldsymbol{\delta}_f|^2} \qquad \text{and} \qquad \nu \;=\; \frac{\mathbf{w}\cdot\mathbf{z}}{|\mathbf{z}|^2}\,. \tag{8.1.13}$$

Then if (8.1.3) holds, by comparing (8.1.7), (8.1.9), and (8.1.11) with (8.1.12) and (8.1.13), we can conclude that if the "ordinary" cubic Hermite interpolant is a PH curve, the value of the angular parameter ϕ in (8.1.10) must be such that

$$\cos\phi \;=\; \frac{1}{\sqrt{|\mathbf{d}_i|\,|\mathbf{d}_f|}}\;\mathbf{w}\cdot\frac{\boldsymbol{\delta}_i + \boldsymbol{\delta}_f}{|\,\boldsymbol{\delta}_i + \boldsymbol{\delta}_f\,|}\,, \qquad \sin\phi \;=\; \frac{-1}{\sqrt{|\mathbf{d}_i|\,|\mathbf{d}_f|}}\;\frac{\mathbf{w}\cdot\mathbf{z}}{|\mathbf{z}|^2}\,. \tag{8.1.14}$$

The identity $\cos^2\phi + \sin^2\phi = 1$ implies that the vector $\mathbf{w}$ must satisfy the constraint (8.1.4).

The same arguments show that conditions (8.1.3) and (8.1.4) are also sufficient to ensure that the cubic Hermite interpolant to the data is a PH curve. ∎

8.2 HELICAL QUINTICS

As discussed in Chapter 5, a helix is a curve whose unit tangent $\mathbf{t}$ maintains a constant angle ψ with a fixed unit vector $\mathbf{a}$ so that condition (5.0.1) holds. We

recall that, whereas all spatial PH cubics are helical [43], the helical PH quintics form a proper subset [37] of all spatial PH quintics.

Concerning PH quintics, defined in quaternion form through (3.1.1) and (3.1.4), it was shown in Appendix B of [37] that, when the four quaternions

$$\mathcal{A}_0,\ \mathcal{A}_2,\ \mathcal{A}_0\mathbf{u},\ \mathcal{A}_2\mathbf{u} \tag{8.2.1}$$

are linearly independent, the PH quintic is helical if and only if

$$\gamma_0 = \gamma_2 = 0 \qquad \text{or} \qquad 4(c_0+\gamma_0\mathbf{u})(c_2+\gamma_2\mathbf{u}) \;=\; 1\,, \tag{8.2.2}$$

where we set

$$\mathcal{A}_1 \;=\; c_0\mathcal{A}_0 \,+\, \gamma_0\mathcal{A}_0\mathbf{u} \,+\, c_2\mathcal{A}_2 \,+\, \gamma_2\mathcal{A}_2\mathbf{u}\,. \tag{8.2.3}$$

Hence, as we have reviewed with the approach of Chapter 5, we can divide helical quintics into two classes.[1] The first corresponds to helices with $\gamma_0 = \gamma_2 = 0$, so that $\mathcal{A}_1$ is a linear combination of $\mathcal{A}_0$ and $\mathcal{A}_2$. This type is called the *general* helical PH quintics: the hodograph components have no common factor, and the tangent $\mathbf{t}$ is capable of reversing its sense of rotation about $\mathbf{a}$ [37]. The second class is called the *monotone* helical PH quintics (see again Chapter 5) — the hodograph components have a common quadratic factor, and, consequently, the tangent indicatrix become a rational quadratic on the unit sphere, i.e., a single traced circle. Now for a PH quintic satisfying

$$\mathbf{r}'(0)\times\mathbf{r}'(1) \;\neq\; (0,0,0)\,,$$

the four quaternions (8.2.1) are linearly independent by Proposition B.1 in Appendix B, and we can conclude that the curve is helical if and only if (8.2.2) holds — i.e., if and only if it is a general helix or a monotone helix.

We now determine the axis $\mathbf{a}$ and pitch angle ψ for both general and monotone helical PH quintics. Consider the hodograph of a PH quintic,

$$\mathbf{r}'(t) \;=\; \sum_{i=0}^{4} \mathbf{d}_i\, b_i^4(t)\,, \tag{8.2.4}$$

where

$$\begin{aligned}
\mathbf{d}_0 \;&=\; \mathcal{A}_0\,\mathbf{u}\,\mathcal{A}_0^*\,,\\
\mathbf{d}_1 \;&=\; \tfrac{1}{2}\,(\mathcal{A}_0\,\mathbf{u}\,\mathcal{A}_1^* + \mathcal{A}_1\,\mathbf{u}\,\mathcal{A}_0^*)\,,\\
\mathbf{d}_2 \;&=\; \tfrac{1}{6}\,(\mathcal{A}_0\,\mathbf{u}\,\mathcal{A}_2^* + 4\,\mathcal{A}_1\,\mathbf{u}\,\mathcal{A}_1^* + \mathcal{A}_2\,\mathbf{u}\,\mathcal{A}_0^*)\,,\\
\mathbf{d}_3 \;&=\; \tfrac{1}{2}\,(\mathcal{A}_1\,\mathbf{u}\,\mathcal{A}_2^* + \mathcal{A}_2\,\mathbf{u}\,\mathcal{A}_1^*)\,,\\
\mathbf{d}_4 \;&=\; \mathcal{A}_2\,\mathbf{u}\,\mathcal{A}_2^*\,.
\end{aligned} \tag{8.2.5}$$

1 Al already noted, these two classes are not disjoint — it can be shown, for example, that degree–elevated PH cubics belong to both of them.

The corresponding parametric speed (1.1.3) is a quartic polynomial,

$$\sigma(t) \;=\; \mathcal{A}(t)\mathcal{A}^*(t) \;=\; \sum_{i=0}^{4} \sigma_i \, b_i^4(t)\,, \tag{8.2.6}$$

with Bernstein coefficients defined by

$$\begin{aligned}
\sigma_0 &= \mathcal{A}_0\mathcal{A}_0^*\,,\\
\sigma_1 &= \tfrac{1}{2}\,(\mathcal{A}_0\mathcal{A}_1^* + \mathcal{A}_1\mathcal{A}_0^*)\,,\\
\sigma_2 &= \tfrac{1}{6}\,(\mathcal{A}_0\mathcal{A}_2^* + 4\mathcal{A}_1\mathcal{A}_1^* + \mathcal{A}_2\mathcal{A}_0^*)\,,\\
\sigma_3 &= \tfrac{1}{2}\,(\mathcal{A}_1\mathcal{A}_2^* + \mathcal{A}_2\mathcal{A}_1^*)\,,\\
\sigma_4 &= \mathcal{A}_2\mathcal{A}_2^*\,.
\end{aligned} \tag{8.2.7}$$

Setting $\mathcal{A} = \mathcal{A}_0$ and $\mathcal{B} = \mathcal{A}_2$ in (B.2.13), we obtain

$$\begin{aligned}
(q_0, \mathbf{q}_0) &= (\mathcal{A}_0\mathcal{A}_0^*\,,\, \mathcal{A}_0\,\mathbf{u}\,\mathcal{A}_0^*)\,,\\
(q_2, \mathbf{q}_2) &= (\mathcal{A}_2\mathcal{A}_2^*\,,\, \mathcal{A}_2\,\mathbf{u}\,\mathcal{A}_2^*)\,,\\
(\nu, \mathbf{v}) &= (\mathcal{A}_0\mathcal{A}_2^* + \mathcal{A}_2\mathcal{A}_0^*\,,\, \mathcal{A}_0\,\mathbf{u}\,\mathcal{A}_2^* + \mathcal{A}_2\,\mathbf{u}\,\mathcal{A}_0^*)\,,\\
(s, \mathbf{s}) &= (-\mathcal{A}_0\,\mathbf{u}\,\mathcal{A}_2^* + \mathcal{A}_2\,\mathbf{u}\,\mathcal{A}_0^*\,,\, \mathcal{A}_0\mathcal{A}_2^* - \mathcal{A}_2\mathcal{A}_0^*)\,.
\end{aligned} \tag{8.2.8}$$

Thus, using (8.2.3), we can write

$$\begin{aligned}
\mathbf{d}_0 &= \mathbf{q}_0\,, \qquad \mathbf{d}_1 = c_0\mathbf{q}_0 + \tfrac{1}{2}(c_2\mathbf{v} + \gamma_2\mathbf{s})\,,\\
\mathbf{d}_2 &= \tfrac{1}{6}\,[4(c_0^2+\gamma_0^2)\mathbf{q}_0 + 4(c_2^2+\gamma_2^2)\mathbf{q}_2\\
&\qquad + (1 + 4c_0c_2 + 4\gamma_0\gamma_2)\mathbf{v} + 4(c_0\gamma_2 - c_2\gamma_0)\mathbf{s}\,]\,,\\
\mathbf{d}_3 &= c_2\mathbf{q}_2 + \tfrac{1}{2}(c_0\mathbf{v} - \gamma_0\mathbf{s})\,, \qquad \mathbf{d}_4 = \mathbf{q}_2\,.
\end{aligned}$$

Analogously, from (8.2.7) we obtain

$$\begin{aligned}
\sigma_0 &= q_0\,, \qquad \sigma_1 = c_0 q_0 + \tfrac{1}{2}(c_2\nu + \gamma_2 s)\,,\\
\sigma_2 &= \tfrac{1}{6}\,[4(c_0^2+\gamma_0^2)q_0 + 4(c_2^2+\gamma_2^2)q_2\\
&\quad + (1 + 4c_0c_2 + 4\gamma_0\gamma_2)\nu + 4(c_0\gamma_2 - c_2\gamma_0)s\,]\,,\\
\sigma_3 &= c_2 q_2 + \tfrac{1}{2}(c_0\nu - \gamma_0 s)\,, \qquad \sigma_4 = q_2\,.
\end{aligned}$$

In particular, for a general helical PH quintic, we have

$$\begin{aligned}
\mathbf{d}_0 &= \mathbf{q}_0\,, \qquad \mathbf{d}_1 = c_0\mathbf{q}_0 + \tfrac{1}{2}c_2\mathbf{v}\,,\\
\mathbf{d}_2 &= \tfrac{1}{6}[4c_0^2\mathbf{q}_0 + 4c_2^2\mathbf{q}_2 + (1 + 4c_0c_2)\mathbf{v}]\,,\\
\mathbf{d}_3 &= c_2\mathbf{q}_2 + \tfrac{1}{2}c_0\mathbf{v}\,, \qquad \mathbf{d}_4 = \mathbf{q}_2\,,\\
\sigma_0 &= q_0\,, \qquad \sigma_1 = c_0 q_0 + \tfrac{1}{2}c_2\nu\,,\\
\sigma_2 &= \tfrac{1}{6}[4c_0^2 q_0 + 4c_2^2 q_2 + (1 + 4c_0c_2)\nu]\,,\\
\sigma_3 &= c_2 q_2 + \tfrac{1}{2}c_0\nu\,, \qquad \sigma_4 = q_2\,.
\end{aligned} \tag{8.2.9}$$

On the other hand, for a monotone helical PH quintic, we have

$$\begin{aligned}
\mathbf{d}_0 &= \mathbf{q}_0\,, \qquad \mathbf{d}_1 = c_0\mathbf{q}_0 + \frac{c_0\mathbf{v}-\gamma_0\mathbf{s}}{8(c_0^2+\gamma_0^2)}\,,\\
\mathbf{d}_2 &= \tfrac{1}{6}\left[4(c_0^2+\gamma_0^2)\mathbf{q}_0 + \frac{\mathbf{q}_2}{4(c_0^2+\gamma_0^2)} + \frac{2c_0}{c_0^2+\gamma_0^2}(c_0\mathbf{v}-\gamma_0\mathbf{s})\right],\\
\mathbf{d}_3 &= \frac{c_0\mathbf{q}_2}{4(c_0^2+\gamma_0^2)} + \tfrac{1}{2}(c_0\mathbf{v}-\gamma_0\mathbf{s})\,, \qquad \mathbf{d}_4 = \mathbf{q}_2\,,\\
\sigma_0 &= q_0\,, \qquad \sigma_1 = c_0 q_0 + \frac{c_0\nu-\gamma_0 s}{8(c_0^2+\gamma_0^2)}\,,\\
\sigma_2 &= \tfrac{1}{6}\left[4(c_0^2+\gamma_0^2)q_0 + \frac{q_2}{4(c_0^2+\gamma_0^2)} + \frac{2c_0}{c_0^2+\gamma_0^2}(c_0\nu-\gamma_0 s)\right],\\
\sigma_3 &= \frac{c_0 q_2}{4(c_0^2+\gamma_0^2)} + \tfrac{1}{2}(c_0\nu-\gamma_0 s)\,, \qquad \sigma_4 = q_2\,.
\end{aligned} \tag{8.2.10}$$

We are now ready to prove the following results characterizing the axes and pitch angles of helical PH quintics (see also [37] for the case of general helices).

Proposition 8.2. *For a general helical PH quintic*

$$\mathbf{a} = \frac{\mathbf{s}}{|\mathbf{s}|} \qquad \text{and} \qquad \cos\psi = \frac{s}{|\mathbf{s}|}\,, \tag{8.2.11}$$

while for a monotone helical PH quintic

$$\mathbf{a} = \frac{c_0\mathbf{s}+\gamma_0\mathbf{v}}{|c_0\mathbf{s}+\gamma_0\mathbf{v}|} \qquad \text{and} \qquad \cos\psi = \frac{c_0 s+\gamma_0\nu}{|c_0\mathbf{s}+\gamma_0\mathbf{v}|}\,, \tag{8.2.12}$$

where $(\nu,\mathbf{v})$ *and* $(s,\mathbf{s})$ *are as defined in* (8.2.8).

Proof : From (5.0.1) and (8.2.4)–(8.2.7), the following relations must be satisfied

$$\mathbf{d}_i\cdot\mathbf{a} = \sigma_i\cos\psi\,, \quad i=0,\ldots,4\,. \tag{8.2.13}$$

Now in view of (8.2.9), for a general helix this is equivalent to proving that

$$\mathbf{q}_0\cdot\mathbf{a} = q_0\cos\psi\,, \quad \mathbf{q}_2\cdot\mathbf{a} = q_2\cos\psi\,, \quad \mathbf{v}\cdot\mathbf{a} = \nu\cos\psi\,.$$

Choosing $\mathbf{a}$ and $\cos\psi$ as in (8.2.11), the result is a consequence of Proposition B.2 in Appendix B. Considering (8.2.10), proving (8.2.13) in the case of a monotone helix is equivalent to showing that

$$\mathbf{q}_0\cdot\mathbf{a} = q_0\cos\psi\,, \quad \mathbf{q}_2\cdot\mathbf{a} = q_2\cos\psi\,, \quad (c_0\mathbf{v}-\gamma_0\mathbf{s})\cdot\mathbf{a} = (c_0\nu-\gamma_0 s)\cos\psi\,.$$

Choosing $\mathbf{a}$ and $\cos\psi$ as in (8.2.12), the above relations are a consequence of Proposition B.2 and the fact that

$$\begin{aligned}
(c_0\mathbf{v}-\gamma_0\mathbf{s})\cdot(c_0\mathbf{s}+\gamma_0\mathbf{v}) &= (c_0^2-\gamma_0^2)\mathbf{v}\cdot\mathbf{s} + c_0\gamma_0(|\mathbf{v}|^2-|\mathbf{s}|^2)\,,\\
(c_0\nu-\gamma_0 s)(c_0 s+\gamma_0\nu) &= (c_0^2-\gamma_0^2)\nu s + c_0\gamma_0(\nu^2-s^2)\,.
\end{aligned}$$

∎

Concerning the interpolation of arbitrary Hermite data, an example was presented in [37] to show that this is not always possible using monotone helical PH quintics. Although no proof for the existence of general helical PH quintic interpolants to arbitrary Hermite data was given in [37], no counter–example was found. We now prove, in Section 8.4 below, that four general helical PH quintic interpolants always exist for arbitrary Hermite data. Moreover, we show that such interpolants correspond to extrema of the arc length L among all PH quintic interpolants to the given Hermite data.

8.3 PH QUINTIC HERMITE INTERPOLANTS

The hodograph of a spatial PH quintic is defined by substituting the quadratic quaternion polynomial (3.1.4) into expression (3.1.1), where $\mathbf{u}$ is an arbitrary unit vector. Integrating this hodograph then gives the Bézier form

$$\mathbf{r}(t) \;=\; \sum_{i=0}^{5} \mathbf{p}_i \, b_i^5(t) \tag{8.3.1}$$

of the PH quintic, with control points $\mathbf{p}_i = x_i\,\mathbf{i} + y_i\,\mathbf{j} + z_i\,\mathbf{k}$ defined by (3.1.6). Interpolation of the end–derivatives yields the equations

$$\mathcal{A}_0\,\mathbf{u}\,\mathcal{A}_0^* \;=\; \mathbf{d}_i \qquad \text{and} \qquad \mathcal{A}_2\,\mathbf{u}\,\mathcal{A}_2^* \;=\; \mathbf{d}_f \tag{8.3.2}$$

for $\mathcal{A}_0$ and $\mathcal{A}_2$. Moreover, with $\mathbf{p}_0 = \mathbf{p}_i$ as integration constant, interpolation of the end points gives the condition

$$\begin{aligned}\int_0^1 \mathcal{A}(t)\,\mathbf{u}\,\mathcal{A}^*(t)\,dt \;&=\; \mathbf{p}_f - \mathbf{p}_i \\ &=\; \tfrac{1}{5}\,\mathcal{A}_0\,\mathbf{u}\,\mathcal{A}_0^* + \tfrac{1}{10}(\mathcal{A}_0\,\mathbf{u}\,\mathcal{A}_1^* + \mathcal{A}_1\,\mathbf{u}\,\mathcal{A}_0^*) \\ &+\; \tfrac{1}{30}(\mathcal{A}_0\,\mathbf{u}\,\mathcal{A}_2^* + 4\,\mathcal{A}_1\,\mathbf{u}\,\mathcal{A}_1^* + \mathcal{A}_2\,\mathbf{u}\,\mathcal{A}_0^*) \\ &+\; \tfrac{1}{10}(\mathcal{A}_1\,\mathbf{u}\,\mathcal{A}_2^* + \mathcal{A}_2\,\mathbf{u}\,\mathcal{A}_1^*) + \tfrac{1}{5}\,\mathcal{A}_2\,\mathbf{u}\,\mathcal{A}_2^*\,.\end{aligned} \tag{8.3.3}$$

Since equations (8.3.2) are of the form (B.2.11), they can be solved directly to obtain

$$\mathcal{A}_0 \;=\; \sqrt{|\mathbf{d}_i|}\,\mathbf{n}_i\,\exp(\phi_0\,\mathbf{u})\,, \qquad \mathcal{A}_2 \;=\; \sqrt{|\mathbf{d}_f|}\,\mathbf{n}_f\,\exp(\phi_2\,\mathbf{u})\,, \tag{8.3.4}$$

where ϕ_0 and ϕ_2 are free angular variables, and using (8.1.2) we define

$$\mathbf{n}_i \;=\; \frac{\boldsymbol{\delta}_i + \mathbf{u}}{|\,\boldsymbol{\delta}_i + \mathbf{u}\,|}\,, \qquad \mathbf{n}_f \;=\; \frac{\boldsymbol{\delta}_f + \mathbf{u}}{|\,\boldsymbol{\delta}_f + \mathbf{u}\,|}\,.$$

Knowing $\mathcal{A}_0$ and $\mathcal{A}_2$, and using (8.3.2), equation (8.3.3) can be reduced to

$$\mathcal{B}\,\mathbf{u}\,\mathcal{B}^* \;=\; \mathbf{d}$$

where $\mathcal{B} = 3\mathcal{A}_0 + 4\mathcal{A}_1 + 3\mathcal{A}_2$, and we define

$$\mathbf{d} = \mathbf{c} + 5(\mathcal{A}_0\,\mathbf{u}\,\mathcal{A}_2^* + \mathcal{A}_2\,\mathbf{u}\,\mathcal{A}_0^*)\,, \tag{8.3.5}$$

$$\mathbf{c} = 120(\mathbf{p}_f - \mathbf{p}_i) - 15(\mathbf{d}_i + \mathbf{d}_f)\,. \tag{8.3.6}$$

This equation is again of the form (B.2.11), and its general solution is

$$\mathcal{B} = \sqrt{|\mathbf{d}|}\,\mathbf{n}\,\exp(\phi_1\mathbf{u}) \tag{8.3.7}$$

where ϕ_1 is another free angular variable, and we set

$$\delta_d = \frac{\mathbf{d}}{|\mathbf{d}|} \qquad \text{and} \qquad \mathbf{n} = \frac{\delta_d + \mathbf{u}}{|\,\delta_d + \mathbf{u}\,|}\,. \tag{8.3.8}$$

Note that $\mathcal{B}$, and thus $\mathcal{A}_1 = \frac{1}{4}\,\mathcal{B} - \frac{3}{4}\,(\mathcal{A}_0 + \mathcal{A}_2)$, depends on ϕ_0, ϕ_2 as well as ϕ_1, due to the dependence of $\mathbf{d}$ on those variables. However, one can show [26] that the hodograph (3.1.1) depends only on the *differences* of ϕ_0, ϕ_1, ϕ_2. Thus, we can take $\phi_1 = 0$ without loss of generality, and regard the PH quintic interpolant as dependent on just the two angular parameters defined by

$$\alpha = \tfrac{1}{2}(\phi_0 + \phi_2) \qquad \text{and} \qquad \beta = \phi_2 - \phi_0\,. \tag{8.3.9}$$

The three quaternions $\mathcal{A}_0, \mathcal{A}_1, \mathcal{A}_2$ defining a PH quintic Hermite interpolant can then be expressed in terms of (8.3.9) as

$$\begin{aligned}
\mathcal{A}_0 &= \sqrt{|\mathbf{d}_i|}\,\mathbf{n}_i\,\exp((\alpha - \tfrac{1}{2}\beta)\mathbf{u})\,,\\
\mathcal{A}_2 &= \sqrt{|\mathbf{d}_f|}\,\mathbf{n}_f\,\exp((\alpha + \tfrac{1}{2}\beta)\mathbf{u})\,,\\
\mathcal{A}_1 &= \tfrac{1}{4}\,\sqrt{|\mathbf{d}|}\,\mathbf{n} - \tfrac{3}{4}\,(\mathcal{A}_0 + \mathcal{A}_2)\,.
\end{aligned} \tag{8.3.10}$$

8.3.1 *Reduction of quaternion expressions*

We now analyze certain quaternion expressions that will subsequently prove useful. With some algebra, one can verify that the following relations hold for any spatial PH quintic interpolant:

$$\begin{aligned}
\mathbf{v} &= \mathcal{A}_0\,\mathbf{u}\,\mathcal{A}_2^* + \mathcal{A}_2\,\mathbf{u}\,\mathcal{A}_0^* = \mathbf{e}\cos\beta + \mathbf{f}\sin\beta\,,\\
v &= \mathcal{A}_0\,\mathcal{A}_2^* + \mathcal{A}_2\,\mathcal{A}_0^* = e\cos\beta + f\sin\beta,\\
\mathbf{s} &= \mathcal{A}_0\,\mathcal{A}_2^* - \mathcal{A}_2\,\mathcal{A}_0^* = \mathbf{f}\cos\beta - \mathbf{e}\sin\beta\,,\\
s &= \mathcal{A}_2\,\mathbf{u}\,\mathcal{A}_0^* - \mathcal{A}_0\,\mathbf{u}\,\mathcal{A}_2^* = f\cos\beta - e\sin\beta\,,
\end{aligned} \tag{8.3.11}$$

where the vectors $\mathbf{e}$, $\mathbf{f}$ and the scalars e, f are given by

$$\begin{aligned}
\mathbf{e} &= 2\sqrt{|\mathbf{d}_i|\,|\mathbf{d}_f|}\,[\,(\mathbf{u}\cdot\mathbf{n}_f)\mathbf{n}_i + (\mathbf{u}\cdot\mathbf{n}_i)\mathbf{n}_f - (\mathbf{n}_i\cdot\mathbf{n}_f)\mathbf{u}\,]\\
&= 2\sqrt{|\mathbf{d}_i|\,|\mathbf{d}_f|}\,\frac{(1 - \delta_i\cdot\delta_f)\mathbf{u} + (1 + \mathbf{u}\cdot\delta_i)\delta_f + (1 + \mathbf{u}\cdot\delta_f)\delta_i}{|\mathbf{u} + \delta_i|\,|\mathbf{u} + \delta_f|},\\
e &= 2\sqrt{|\mathbf{d}_i|\,|\mathbf{d}_f|}\;\mathbf{n}_i\cdot\mathbf{n}_f,\\
\mathbf{f} &= 2\sqrt{|\mathbf{d}_i|\,|\mathbf{d}_f|}\,\mathbf{n}_f\times\mathbf{n}_i = 2\sqrt{|\mathbf{d}_i||\mathbf{d}_f|}\,\frac{\mathbf{u}\times\delta_i - \mathbf{u}\times\delta_f - \delta_i\times\delta_f}{|\mathbf{u} + \delta_i|\,|\mathbf{u} + \delta_f|}\,,\\
f &= 2\sqrt{|\mathbf{d}_i|\,|\mathbf{d}_f|}\;\mathbf{u}\cdot(\mathbf{n}_i\times\mathbf{n}_f)\,.
\end{aligned} \tag{8.3.12}$$

Thus, the vector (8.3.5) depends only on β, and has the analytic expression

$$\mathbf{d}(\beta) \;=\; \mathbf{c} \;+\; 5\,(\cos\beta\,\mathbf{e} + \sin\beta\,\mathbf{f})\,. \tag{8.3.13}$$

As β varies from 0 to 2π, $\mathbf{d}(\beta)$ traces an ellipse in $\mathbb{R}^3$ with center $\mathbf{c}$, residing in the plane with normal in the direction of

$$\mathbf{e}\times\mathbf{f} \;=\; 4\,|\mathbf{d}_i|\,|\mathbf{d}_f|\,[\,(\mathbf{u}\cdot\mathbf{n}_f)\mathbf{n}_f \;-\; (\mathbf{u}\cdot\mathbf{n}_i)\mathbf{n}_i\,]\,.$$

Correspondingly, the unit vector $\mathbf{n}$ defined by (8.3.8) also depends on β only.

Now from Proposition B.2, we can deduce that

$$\mathbf{e}\cdot\mathbf{f} \;=\; -\,ef \qquad \text{and} \qquad |\mathbf{e}|^2 - e^2 \;=\; |\mathbf{f}|^2 - f^2\,. \tag{8.3.14}$$

Assuming that $\mathbf{u} = \boldsymbol{\delta}_i$ gives the simplifications

$$\mathbf{n}_i \;=\; \boldsymbol{\delta}_i \qquad \text{and} \qquad \mathbf{n}_f \;=\; \frac{\boldsymbol{\delta}_i + \boldsymbol{\delta}_f}{|\boldsymbol{\delta}_i + \boldsymbol{\delta}_f|}\,,$$

and consequently

$$\mathbf{e} \;=\; 2\sqrt{|\mathbf{d}_i||\mathbf{d}_f|}\,\frac{\boldsymbol{\delta}_i + \boldsymbol{\delta}_f}{|\boldsymbol{\delta}_i + \boldsymbol{\delta}_f|}\,, \qquad e \;=\; 2\sqrt{|\mathbf{d}_i|\,|\mathbf{d}_f|}\;\boldsymbol{\delta}_i\cdot\frac{\boldsymbol{\delta}_i + \boldsymbol{\delta}_f}{|\boldsymbol{\delta}_i + \boldsymbol{\delta}_f|}\,,$$

$$\mathbf{f} \;=\; -\,2\sqrt{|\mathbf{d}_i||\mathbf{d}_f|}\,\frac{\boldsymbol{\delta}_i\times\boldsymbol{\delta}_f}{|\boldsymbol{\delta}_i + \boldsymbol{\delta}_f|}\,, \qquad f \;=\; 0\,. \tag{8.3.15}$$

Hence, in this case, we have

$$\mathbf{e}\cdot\mathbf{f} \;=\; 0\,, \qquad |\mathbf{e}|^2 \;=\; |\mathbf{f}|^2 \;+\; e^2\,, \qquad e \;=\; \mathbf{e}\cdot\boldsymbol{\delta}_i\,. \tag{8.3.16}$$

8.4 ARC LENGTH OF PH QUINTICS

The arc length of a spatial PH quintic is $L = \frac{1}{5}(\sigma_0 + \sigma_1 + \sigma_2 + \sigma_3 + \sigma_4)$, where the coefficients of the parametric speed $\sigma(t)$ are specified by (8.2.7). Using (8.3.10), this can be reduced to

$$L \;=\; \frac{1}{120}\,[\,15(|\mathbf{d}_i| + |\mathbf{d}_f|) + |\mathbf{d}| - 5(\mathcal{A}_0\mathcal{A}_2^* + \mathcal{A}_2\mathcal{A}_0^*)\,]\,. \tag{8.4.1}$$

Since the vector $\mathbf{d}$ defined by (8.3.5) depends only on the angle β, as expressed in (8.3.13), and $\mathcal{A}_0\,\mathcal{A}_2^* + \mathcal{A}_2\,\mathcal{A}_0^* = e\,\cos\beta + f\sin\beta$, with e and f defined in (8.3.12), L is a function of β alone. Taking $\mathbf{u} = \boldsymbol{\delta}_i$ and making use of (8.3.16), we obtain

$$|\mathbf{d}(\beta)| \;=\; \sqrt{|\mathbf{c}|^2 \;+\; 25|\mathbf{f}|^2 \;+\; 10\,\mathbf{c}\cdot(\mathbf{e}\cos\beta \;+\; \mathbf{f}\sin\beta) + 25e^2\cos^2\beta}\,. \tag{8.4.2}$$

Then we deduce that (8.4.1) is defined by the univariate function

$$L(\beta) \;=\; \frac{1}{120}\,[\,15(|\mathbf{d}_i| + |\mathbf{d}_f|) \;+\; |\mathbf{d}(\beta)| \;-\; 5\,e\cos\beta\,]\,. \tag{8.4.3}$$

Now since $L(\beta)$ is a continuous function, it assumes minimum and maximum values in the compact interval $[-\pi, +\pi]$. Moreover, since $L(\beta)$ is a periodic C^1 function if $\mathbf{d} \cdot \mathbf{d} > 0$, the extremal values are stationary points.

The stationary points of $L(\beta)$ are the roots of the equation

$$\mathbf{c} \cdot (-\mathbf{e} \sin\beta + \mathbf{f} \cos\beta) - 5e^2 \sin\beta \cos\beta = -e \sin\beta \, |\mathbf{d}(\beta)| \,. \tag{8.4.4}$$

To determine these roots, we make the substitutions

$$\cos\beta = \frac{1-\tau^2}{1+\tau^2}, \qquad \sin\beta = \frac{2\tau}{1+\tau^2}, \qquad \text{where } \tau = \tan\tfrac{1}{2}\beta \,. \tag{8.4.5}$$

Squaring both sides in (8.4.4), we obtain

$$\begin{aligned} &[-5e^2(1-\tau^2)2\tau - \mathbf{c}\cdot\mathbf{e}\,2\tau(1+\tau^2) + \mathbf{c}\cdot\mathbf{f}\,(1-\tau^2)(1+\tau^2)]^2 \\ -\;& e^2 4\tau^2 [\,\mathbf{c}\cdot\mathbf{c}\,(1+\tau^2)^2 + 25\,\mathbf{e}\cdot\mathbf{e}\,(1-\tau^2)^2 + 25\,\mathbf{f}\cdot\mathbf{f}\,4\tau^2 \\ &\qquad + 10\,\mathbf{c}\cdot\mathbf{e}\,(1-\tau^2)(1+\tau^2) + 10\,\mathbf{c}\cdot\mathbf{f}\,2\tau(1+\tau^2)\,] = 0 \end{aligned} \tag{8.4.6}$$

on substituting from (8.4.5) and using $\mathbf{f}\cdot\mathbf{f} - \mathbf{e}\cdot\mathbf{e} = -e^2$ from (8.3.14) and (8.3.16). Collecting powers of $(1+\tau^2)$ and using (8.3.16), we can rewrite this equation as

$$\begin{aligned} &100e^2\tau^2[\,e^2(1-\tau^2)^2 - (e^2 + \mathbf{f}\cdot\mathbf{f})(1-\tau^2)^2 - \mathbf{f}\cdot\mathbf{f}\,4\tau^2\,] \\ &-10e^2\mathbf{c}\cdot\mathbf{f}\,[\,(1-\tau^2)^2 + 4\tau^2\,]\,2\tau(1+\tau^2) + (1+\tau^2)^2\,[\,(\mathbf{c}\cdot\mathbf{e})^2 4\tau^2 \\ &\qquad + (\mathbf{c}\cdot\mathbf{f})^2(1-\tau^2)^2 - 2(\mathbf{c}\cdot\mathbf{e})(\mathbf{c}\cdot\mathbf{f})2\tau(1-\tau^2) - e^2\mathbf{c}\cdot\mathbf{c}\,4\tau^2\,] = 0\,, \end{aligned}$$

and hence we obtain

$$(1+\tau^2)^2(\tilde{d}_0 + \tilde{d}_1\tau + \tilde{d}_2\tau^2 + \tilde{d}_3\tau^3 + \tilde{d}_4\tau^4) =: (1+\tau^2)^2\tilde{P}(\tau) = 0\,, \tag{8.4.7}$$

where

$$\begin{aligned} \tilde{d}_0 &:= (\mathbf{c}\cdot\mathbf{f})^2\,, \\ \tilde{d}_1 &:= -20e^2\mathbf{c}\cdot\mathbf{f} - 4(\mathbf{c}\cdot\mathbf{e})(\mathbf{c}\cdot\mathbf{f})\,, \\ \tilde{d}_2 &:= -100e^2\mathbf{f}\cdot\mathbf{f} + 4(\mathbf{c}\cdot\mathbf{e})^2 - 2(\mathbf{c}\cdot\mathbf{f})^2 - 4e^2\mathbf{c}\cdot\mathbf{c}\,, \\ \tilde{d}_3 &:= -20e^2\mathbf{c}\cdot\mathbf{f} + 4(\mathbf{c}\cdot\mathbf{e})(\mathbf{c}\cdot\mathbf{f})\,, \\ \tilde{d}_4 &:= (\mathbf{c}\cdot\mathbf{f})^2\,. \end{aligned} \tag{8.4.8}$$

Summarizing, the stationary points of $L(\beta)$ are identified via (8.4.5) by the real roots (at least two) of the quartic equation

$$\tilde{P}(\tau) = 0\,. \tag{8.4.9}$$

Proposition 8.3. *When* $|\mathbf{d}(\beta)| > 0$ *and* $\delta_f \neq -\mathbf{u}$, *the arc length function* $L(\beta)$ *given by* (8.4.3) *has only one minimum and one maximum.*

Proof : Consider the auxiliary function

$$\ell(\beta) \;=\; \frac{1}{120}\,[\,|\mathbf{d}(\beta)| \;+\; 5\,e\cos\beta\,]\,. \tag{8.4.10}$$

whose stationary points are the roots of the equation

$$\mathbf{c}\cdot(-\,\mathbf{e}\sin\beta+\mathbf{f}\cos\beta)\;-\;5e^2\sin\beta\cos\beta\;=\;e\sin\beta\,|\mathbf{d}(\beta)|\,. \tag{8.4.11}$$

Comparing (8.4.4) and (8.4.11), it is clear that the stationary points of $\ell(\beta)$ are given via (8.4.5) by (at least two) real roots of the equation (8.4.9) but no solutions of (8.4.4) can be solutions[2] of (8.4.11). On the other hand, by continuity arguments both (8.4.4) and (8.4.11) have at least two solutions. Thus, we conclude that $\tilde{P}(\tau)$ has exactly four real roots: two of them correspond to solutions of (8.4.11), and the remaining two correspond to the only two solutions of (8.4.4). ∎

The next Proposition shows that any solution of (8.4.4) identifies an $L(\beta)$ corresponding to the arc length of a general helical PH quintic interpolant. Hence, the general helical PH quintic interpolants always have minimal or maximal arc length.

Proposition 8.4. *If the PH quintic Hermite interpolant defined by* (8.3.1), (3.1.6), *and* (8.3.10) *is a general helix, the corresponding angle* β *is a stationary point of the arc length function* $L(\beta)$.

Proof : The unit axis vector $\mathbf{a}$ of the helix and the constant $\cos\psi$ are as defined in (8.2.11). Using (8.3.11), we can write

$$\mathbf{a} \;=\; \frac{\mathbf{f}\cos\beta-\mathbf{e}\sin\beta}{|\,\mathbf{f}\cos\beta-\mathbf{e}\sin\beta\,|}\,. \tag{8.4.12}$$

In addition, assuming without loss of generality that $\mathbf{u}=\boldsymbol{\delta}_i$, and using (8.2.8), (8.3.11), and (8.3.15), we obtain

$$\cos\psi \;=\; -\,\frac{e\,\sin\beta}{|\,\mathbf{f}\cos\beta-\mathbf{e}\sin\beta\,|}\,. \tag{8.4.13}$$

Now (5.0.1) implies that

$$\int_0^1 |\mathbf{r}'(t)|\cos\psi\;dt \;=\; \int_0^1 \mathbf{r}'(t)\cdot\mathbf{a}\;dt \;=\; (\mathbf{p}_f-\mathbf{p}_i)\cdot\mathbf{a}\,,$$

so the arc length $L(\beta)$ must be equal to $[(\mathbf{p}_f-\mathbf{p}_i)\cdot\mathbf{a}\,]/\cos\psi$. Hence, using (8.4.3), (8.4.12), and (8.4.13), we obtain

$$15(|\mathbf{d}_i|+|\mathbf{d}_f|)\;+\;|\mathbf{d}(\beta)|\;-\;5e\cos\beta\;=\;\frac{120}{e\sin\beta}(\mathbf{p}_f-\mathbf{p}_i)\cdot(\mathbf{e}\sin\beta-\mathbf{f}\cos\beta)\,. \tag{8.4.14}$$

2 Assuming $\mathbf{d}\cdot\mathbf{d}>0$ and $\delta_f\neq-\mathbf{u}$ the only common solution of the two equations is β such that $\sin\beta=0$, and this implies $\mathbf{c}\cdot\mathbf{f}=0$, which is the case of planar data that does not concern us here.

Using the vector $\mathbf{c}$ defined by (8.3.6), this can be re–written as

$$15(|\mathbf{d}_i| + |\mathbf{d}_f|)e\sin\beta \;+\; |\mathbf{d}(\beta)|\, e\sin\beta \;-\; 5e^2\sin\beta\cos\beta \\ = \;(\mathbf{c} + 15(\mathbf{d}_i + \mathbf{d}_f)) \cdot (\mathbf{e}\sin\beta - \mathbf{f}\cos\beta)\,. \qquad (8.4.15)$$

Now the simplified expressions (8.3.15) for $\mathbf{e}$ and $\mathbf{f}$ imply that $\mathbf{f}\cdot\mathbf{d}_i = \mathbf{f}\cdot\mathbf{d}_f = 0$ and $\mathbf{e}\cdot(\mathbf{d}_i + \mathbf{d}_f) = e(|\mathbf{d}_i| + |\mathbf{d}_f|)$. Thus (8.4.15) simplifies to (8.4.4). ∎

We now show that four distinct general helical PH quintic interpolants exist for arbitrary spatial Hermite data. The construction of general helical PH quintic Hermite interpolants can be reduced [37] to determining values of the angle β that satisfy

$$\frac{(\mathbf{c}, \mathbf{d}_f, \mathbf{e}\cos\beta + \mathbf{f}\sin\beta)}{(\mathbf{d}_i, \mathbf{d}_f, \mathbf{e}\cos\beta + \mathbf{f}\sin\beta)} \frac{(\mathbf{d}_i, \mathbf{c}, \mathbf{e}\cos\beta + \mathbf{f}\sin\beta)}{(\mathbf{d}_i, \mathbf{d}_f, \mathbf{e}\cos\beta + \mathbf{f}\sin\beta)} \\ = \left[\frac{(\mathbf{d}_i, \mathbf{d}_f, \mathbf{c})}{(\mathbf{d}_i, \mathbf{d}_f, \mathbf{e}\cos\beta + \mathbf{f}\sin\beta)} + 5\right]^2 \qquad (8.4.16)$$

where $(\mathbf{x}, \mathbf{y}, \mathbf{z})$ denotes the triple product $(\mathbf{x}\times\mathbf{y})\cdot\mathbf{z}$, and $\mathbf{d}_i$, $\mathbf{d}_f$, $\mathbf{c}$, $\mathbf{e}$, $\mathbf{f}$ are as defined above. Substituting from (8.4.5), this corresponds to computing the real roots of the quartic equation

$$d_4\tau^4 + d_3\tau^3 + d_2\tau^2 + d_1\tau + d_0 \;=\; 0 \qquad (8.4.17)$$

in τ, with coefficients

$$\begin{aligned}
d_4 &= (\mathbf{c}, \mathbf{d}_f, \mathbf{e})\,(\mathbf{d}_i, \mathbf{c}, \mathbf{e}) - (\mathbf{d}_i, \mathbf{d}_f, \mathbf{c} - 5\mathbf{e})^2\,,\\
d_3 &= -2\,(\mathbf{c}, \mathbf{d}_f, \mathbf{e})\,(\mathbf{d}_i, \mathbf{c}, \mathbf{f}) - 2\,(\mathbf{d}_i, \mathbf{c}, \mathbf{e})\,(\mathbf{c}, \mathbf{d}_f, \mathbf{f})\\
&\quad -20\,(\mathbf{d}_i, \mathbf{d}_f, \mathbf{f})\,(\mathbf{d}_i, \mathbf{d}_f, \mathbf{c} - 5\mathbf{e})\,,\\
d_2 &= -2\,(\mathbf{c}, \mathbf{d}_f, \mathbf{e})\,(\mathbf{d}_i, \mathbf{c}, \mathbf{e}) + 4\,(\mathbf{c}, \mathbf{d}_f, \mathbf{f})\,(\mathbf{d}_i, \mathbf{c}, \mathbf{f})\\
&\quad -100\,(\mathbf{d}_i, \mathbf{d}_f, \mathbf{f})^2 - 2\,(\mathbf{d}_i, \mathbf{d}_f, \mathbf{c} - 5\mathbf{e})\,(\mathbf{d}_i, \mathbf{d}_f, \mathbf{c} + 5\mathbf{e})\,,\\
d_1 &= 2\,(\mathbf{c}, \mathbf{d}_f, \mathbf{f})\,(\mathbf{d}_i, \mathbf{c}, \mathbf{e}) + 2\,(\mathbf{d}_i, \mathbf{c}, \mathbf{f})\,(\mathbf{c}, \mathbf{d}_f, \mathbf{e})\\
&\quad -20\,(\mathbf{d}_i, \mathbf{d}_f, \mathbf{f})\,(\mathbf{d}_i, \mathbf{d}_f, \mathbf{c} + 5\mathbf{e})\,,\\
d_0 &= (\mathbf{c}, \mathbf{d}_f, \mathbf{e})\,(\mathbf{d}_i, \mathbf{c}, \mathbf{e}) - (\mathbf{d}_i, \mathbf{d}_f, \mathbf{c} + 5\mathbf{e})^2\,. \qquad (8.4.18)
\end{aligned}$$

On the other hand it was also shown in [37] that, to conform to the definition of a general helical PH quintic interpolant, the value of the angular variable β associated with a real root of (8.4.17) must be such that

$$\frac{(\mathbf{c}, \mathbf{d}_f, \mathbf{e}\cos\beta + \mathbf{f}\sin\beta)}{(\mathbf{d}_i, \mathbf{d}_f, \mathbf{e}\cos\beta + \mathbf{f}\sin\beta)} \;\geqslant\; 0\,, \quad \frac{(\mathbf{d}_i, \mathbf{c}, \mathbf{e}\cos\beta + \mathbf{f}\sin\beta)}{(\mathbf{d}_i, \mathbf{d}_f, \mathbf{e}\cos\beta + \mathbf{f}\sin\beta)} \;\geqslant\; 0\,. \qquad (8.4.19)$$

Two distinct general helical PH quintic interpolants are associated with each root of (8.4.17) for which these inequalities hold — see [37] — and they share the same axis and arc length, since they have the same β value.

Using MAPLE, we find that the coefficients (8.4.8) and (8.4.18) are related by

$$d_i \;=\; K\,\tilde{d}_i\,, \qquad i = 0,\ldots,4 \tag{8.4.20}$$

for some non–zero constant K (assuming that $\mathbf{u} = \boldsymbol{\delta}_i$). Since (8.4.9) and (8.4.17) have the same roots, we conclude that (8.4.17) has exactly four real roots by the proof of Proposition 8.3. On the other hand, we have already shown that there are at most two admissible roots, because the corresponding β value must be a solution of (8.4.4) — see Proposition 8.4. In the following proposition, we show that there are always exactly *two* admissible roots, and hence four general helical PH quintic interpolants.

Proposition 8.5. *For arbitrary Hermite data, each of the two values for the angular variable β that identify extrema of the arc length function $L(\beta)$ allows us to define two general helical PH quintic interpolants.*

Proof : We have already verified that each of the two β values that identify extrema of $L(\beta)$ is associated with a (real) root of (8.4.17) — see Proposition 8.3. Thus, assuming (without loss of generality) that $\mathbf{u} = \boldsymbol{\delta}_i$, we must show that satisfaction of (8.4.4) implies both the inequalities in (8.4.19). Concerning this, we observe that the two quantities in (8.4.19) have the same sign when β corresponds to any (real) solution of (8.4.17), i.e., to any solution of (8.4.16). Thus, it is more convenient to prove that the inequality

$$|\mathbf{d}_i|\,\frac{(\mathbf{c},\mathbf{d}_f,\mathbf{e}\cos\beta+\mathbf{f}\sin\beta)}{(\mathbf{d}_i,\mathbf{d}_f,\mathbf{e}\cos\beta+\mathbf{f}\sin\beta)} \;+\; |\mathbf{d}_f|\,\frac{(\mathbf{d}_i,\mathbf{c},\mathbf{e}\cos\beta+\mathbf{f}\sin\beta)}{(\mathbf{d}_i,\mathbf{d}_f,\mathbf{e}\cos\beta+\mathbf{f}\sin\beta)} \;\geqslant\; 0 \tag{8.4.21}$$

holds. From the simplified expressions for $\mathbf{e}$ and $\mathbf{f}$ in (8.3.15) we have $(\mathbf{d}_i,\mathbf{d}_f,\mathbf{e}) = 0$ and $(\mathbf{d}_i,\mathbf{d}_f,\mathbf{f}) \leqslant 0$. Then the previous inequality can be re–written as

$$\frac{(\mathbf{c},\boldsymbol{\delta}_f-\boldsymbol{\delta}_i,\mathbf{e}\cos\beta+\mathbf{f}\sin\beta)}{\sin\beta} \;\leqslant\; 0\,,$$

i.e.,

$$\mathbf{c}\cdot[\,(\boldsymbol{\delta}_f-\boldsymbol{\delta}_i)\times\mathbf{e}\,]\,\cot\beta \;+\; \mathbf{c}\cdot[\,(\boldsymbol{\delta}_f-\boldsymbol{\delta}_i)\times\mathbf{f}\,] \;\leqslant\; 0\,.$$

Now using (8.3.15), with some algebra we obtain

$$(\boldsymbol{\delta}_f-\boldsymbol{\delta}_i)\times\mathbf{e} \;=\; 2\,\mathbf{f}\,, \qquad (\boldsymbol{\delta}_f-\boldsymbol{\delta}_i)\times\mathbf{f} \;=\; -\,(1-\lambda)\,\mathbf{e}\,,$$

where $\lambda = \boldsymbol{\delta}_i\cdot\boldsymbol{\delta}_f$. Then, we may re–write (8.4.21) as

$$2\,\mathbf{c}\cdot\mathbf{f}\,\cot\beta \;-\; (1-\lambda)\mathbf{c}\cdot\mathbf{e} \;\leqslant\; 0\,. \tag{8.4.22}$$

Now from (8.4.4), we have

$$(\mathbf{c}\cdot\mathbf{f})\,\cot\beta \;-\; \mathbf{c}\cdot\mathbf{e} \;=\; 5e^2\cos\beta \;-\; e\,|\mathbf{d}(\beta)|\,.$$

Then, since $e \geqslant 0$ from (8.3.16), we can write (8.4.22) as

$$|\mathbf{d}(\beta)| \geqslant 5e\cos\beta + \frac{1+\lambda}{2e}\,\mathbf{c}\cdot\mathbf{e}\,. \tag{8.4.23}$$

Now, using the simplified expressions in (8.3.15), we have

$$e = |\mathbf{e}|\sqrt{\frac{1+\lambda}{2}}\,,$$

and (8.4.23) becomes

$$|\mathbf{d}(\beta)| \geqslant \frac{e}{|\mathbf{e}|}\left[5|\mathbf{e}|\cos\beta + \frac{\mathbf{c}\cdot\mathbf{e}}{|\mathbf{e}|}\right].$$

On the other hand, considering that $\mathbf{e}\cdot\mathbf{f} = 0$, from the expression for $\mathbf{d}(\beta)$ in (8.3.13), we obtain

$$5|\mathbf{e}|\cos\beta + \frac{\mathbf{c}\cdot\mathbf{e}}{|\mathbf{e}|} = \mathbf{d}(\beta)\cdot\frac{\mathbf{e}}{|\mathbf{e}|}\,.$$

Thus, since $|\mathbf{v}| \geqslant |\mathbf{v}\cdot\mathbf{u}|$ for any vector $\mathbf{v}$ and unit vector $\mathbf{u}$, we have $e < |\mathbf{e}|$ and the proposition is proved. ∎

Remark 8.1. The two general helical PH quintic interpolants associated with each of the two extrema of the arc length $L(\beta)$ on $[0, 2\pi]$ have not only the same arc length, but also the same axis, since they share the same β value.

Remark 8.2. It can be verified by a numerical example that, in general, the arc length of a monotone–helical PH quintic interpolant (when it exists) is not a critical value of $L(\beta)$ — see Figure 8.1.

8.5 SELECTION OF ANGULAR PARAMETERS

As observed in Section 8.3, the solution to the PH quintic Hermite interpolation problem, specified by (8.3.10), depends on the free angular parameters α, β. We wish to compute "optimal" choices for these parameters.

8.5.1 *Bivariate criterion*

As one criterion of optimality, we consider minimization of the quantity

$$F(\alpha,\beta) = \left|\mathcal{A}_1 - \tfrac{1}{2}(\mathcal{A}_0 + \mathcal{A}_2)\right|^2, \tag{8.5.1}$$

since $F(\alpha,\beta) = 0$ identifies the unique condition under which the quadratic polynomial (3.1.4) is actually a *degree–elevated linear polynomial*, so the curve becomes a degree–elevated PH cubic.

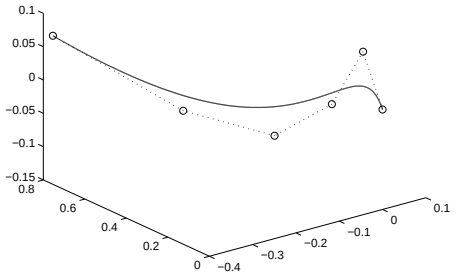

(a) General helix, with maximum arc length.

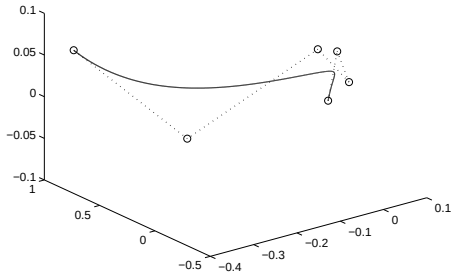

(b) General helix, with minimum arc length.

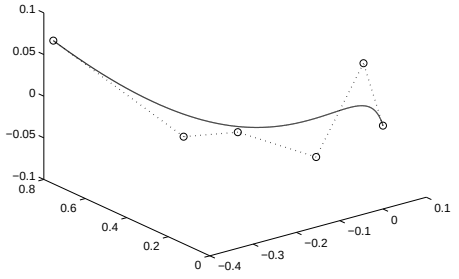

(c) A monotone helix.

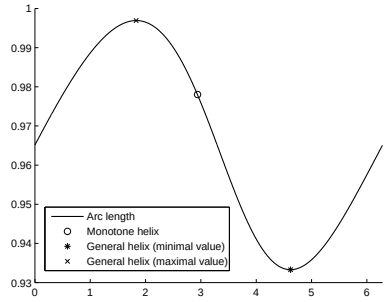

(d) The arc length plotted as a function of β.

Figure 8.1: Helical PH quintic interpolants to the Hermite data $\mathbf{p}_i = (0,\ 0,\ 0)$, $\mathbf{d}_i = (0.48147,\ 1.47196,\ 0.13832)$ and $\mathbf{p}_f = (-0.38943,\ 0.77619,\ 0.06792)$, $\mathbf{d}_f = (-1.09182,\ 0.86153,\ 0.63159)$.

In general, it is not possible to achieve $F = 0$ under the given interpolation constraints (see Section 8.1), but we regard the goal of placing $\mathcal{A}_1$ as close as possible to $\frac{1}{2}(\mathcal{A}_0 + \mathcal{A}_2)$ as being motivated by the desire for a "reasonable" quadratic pre–image curve $\mathcal{A}(t)$ in $\mathbb{H}$ for the hodograph (3.1.1). An additional motivation for the chosen F is that its dependence on α, β can be explicitly derived, and its derivatives with respect to these parameters admit closed–form expressions. Substituting from (8.3.10) and simplifying, we obtain

$$\begin{aligned} 16\,F \;=\;& |\mathbf{d}(\beta)| \\ &- \;10\,\sqrt{|\mathbf{d}(\beta)|\,|\mathbf{d}_i|}\,\left[\,\cos(\alpha - \tfrac{1}{2}\beta)\,\mathbf{n}_i - \sin(\alpha - \tfrac{1}{2}\beta)\,\mathbf{u}\times\mathbf{n}_i\,\right]\cdot\mathbf{n}(\beta) \\ &- \;10\,\sqrt{|\mathbf{d}(\beta)|\,|\mathbf{d}_f|}\,\left[\,\cos(\alpha + \tfrac{1}{2}\beta)\,\mathbf{n}_f - \sin(\alpha + \tfrac{1}{2}\beta)\,\mathbf{u}\times\mathbf{n}_f\,\right]\cdot\mathbf{n}(\beta) \\ &+ \;25\,\left[\,|\mathbf{d}_i| + |\mathbf{d}_f| + 2\sqrt{|\mathbf{d}_i|\,|\mathbf{d}_f|}\,(\mathbf{n}_i\cdot\mathbf{n}_f\cos\beta + \mathbf{u}\cdot(\mathbf{n}_i\times\mathbf{n}_f)\sin\beta)\,\right]. \end{aligned}$$

To determine the extrema of F, we require its partial derivatives F_α, F_β. The derivative of the vector (8.3.13) is given by

$$\mathbf{d}'(\beta) \;=\; 5\,(\cos\beta\,\mathbf{f} - \sin\beta\,\mathbf{e})\,.$$

Its magnitude and the square root of its magnitude have the derivatives

$$|\mathbf{d}(\beta)|' \;=\; \frac{\mathbf{d}(\beta)\cdot\mathbf{d}'(\beta)}{|\mathbf{d}(\beta)|}\,, \qquad \sqrt{|\mathbf{d}(\beta)|}\,' \;=\; \frac{|\mathbf{d}(\beta)|'}{2\sqrt{|\mathbf{d}(\beta)|}}\,.$$

For the unit vector $\boldsymbol{\delta}$ and the bisector $\mathbf{n}$, the derivatives may be written as

$$\begin{aligned}
\boldsymbol{\delta}'(\beta) &= \frac{|\mathbf{d}(\beta)|^2\,\mathbf{d}'(\beta) - [\,\mathbf{d}(\beta)\cdot\mathbf{d}'(\beta)\,]\,\mathbf{d}(\beta)}{|\mathbf{d}(\beta)|^3}\,,\\
\mathbf{n}'(\beta) &= \frac{|\mathbf{u}+\boldsymbol{\delta}(\beta)|^2\,\boldsymbol{\delta}'(\beta) - [\,(\mathbf{u}+\boldsymbol{\delta}(\beta))\cdot\boldsymbol{\delta}'(\beta)\,]\,\boldsymbol{\delta}(\beta)}{|\mathbf{u}+\boldsymbol{\delta}(\beta)|^3}\,.
\end{aligned}$$

We can then formulate the partial derivatives of F explicitly as

$$\begin{aligned}
16\,F_\alpha \;&=\; 10\,\sqrt{|\mathbf{d}(\beta)|\,|\mathbf{d}_i|}\,[\,\sin(\alpha-\tfrac{1}{2}\beta)\,\mathbf{n}_i + \cos(\alpha-\tfrac{1}{2}\beta)\,\mathbf{u}\times\mathbf{n}_i\,]\cdot\mathbf{n}(\beta)\\
&+\; 10\,\sqrt{|\mathbf{d}(\beta)|\,|\mathbf{d}_f|}\,[\,\sin(\alpha+\tfrac{1}{2}\beta)\,\mathbf{n}_f + \cos(\alpha+\tfrac{1}{2}\beta)\,\mathbf{u}\times\mathbf{n}_f\,]\cdot\mathbf{n}(\beta)\,,
\end{aligned}$$

$$\begin{aligned}
16\,F_\beta \;&=\; |\mathbf{d}(\beta)|'\\
&-\; 10\,\sqrt{|\mathbf{d}(\beta)|}\,'\sqrt{|\mathbf{d}_i|}\,[\,\cos(\alpha-\tfrac{1}{2}\beta)\,\mathbf{n}_i - \sin(\alpha-\tfrac{1}{2}\beta)\,\mathbf{u}\times\mathbf{n}_i\,]\cdot\mathbf{n}(\beta)\\
&-\; 10\,\sqrt{|\mathbf{d}(\beta)|}\,'\sqrt{|\mathbf{d}_f|}\,[\,\cos(\alpha+\tfrac{1}{2}\beta)\,\mathbf{n}_f - \sin(\alpha+\tfrac{1}{2}\beta)\,\mathbf{u}\times\mathbf{n}_f\,]\cdot\mathbf{n}(\beta)\\
&-\; 5\,\sqrt{|\mathbf{d}(\beta)|\,|\mathbf{d}_i|}\,[\,\sin(\alpha-\tfrac{1}{2}\beta)\,\mathbf{n}_i + \cos(\alpha-\tfrac{1}{2}\beta)\,\mathbf{u}\times\mathbf{n}_i\,]\cdot\mathbf{n}(\beta)\\
&+\; 5\,\sqrt{|\mathbf{d}(\beta)|\,|\mathbf{d}_f|}\,[\,\sin(\alpha+\tfrac{1}{2}\beta)\,\mathbf{n}_f + \cos(\alpha+\tfrac{1}{2}\beta)\,\mathbf{u}\times\mathbf{n}_f\,]\cdot\mathbf{n}(\beta)\\
&-\; 10\,\sqrt{|\mathbf{d}(\beta)|\,|\mathbf{d}_i|}\,[\,\cos(\alpha-\tfrac{1}{2}\beta)\,\mathbf{n}_i - \sin(\alpha-\tfrac{1}{2}\beta)\,\mathbf{u}\times\mathbf{n}_i\,]\cdot\mathbf{n}'(\beta)\\
&-\; 10\,\sqrt{|\mathbf{d}(\beta)|\,|\mathbf{d}_f|}\,[\,\cos(\alpha+\tfrac{1}{2}\beta)\,\mathbf{n}_f - \sin(\alpha+\tfrac{1}{2}\beta)\,\mathbf{u}\times\mathbf{n}_f\,]\cdot\mathbf{n}'(\beta)\\
&+\; 50\sqrt{|\mathbf{d}_i|\,|\mathbf{d}_f|}\,(\mathbf{u}\cdot(\mathbf{n}_i\times\mathbf{n}_f)\cos\beta - \mathbf{n}_i\cdot\mathbf{n}_f\sin\beta)\,.
\end{aligned}$$

An approximation of the values (α,β) that identify the global minimum of F over the domain $[0,2\pi]^2$ can be determined by means of an appropriate numerical scheme. We refer to this procedure for selecting the free angular parameters as the BV (bivariate) criterion.

8.5.2 *Helical–cubic criterion*

A simplification of the above method is embodied in the following two–step scheme. First, the value of β is computed by finding the solution of (8.4.4) that identifies curves of extremal arc length, and selecting the maximal one (since interpolants of maximal arc length are usually found to have smoother shapes). An α value is then selected by minimizing (8.5.1) considered as a function of

α alone. The desired α value can be explicitly obtained as root of F_α, i.e., by solving a homogeneous trigonometric equation. In this case, we have

$$\tan\alpha = \frac{[\sqrt{|\mathbf{d}_i|}(\tan\frac{1}{2}\beta\,\mathbf{n}_i - \mathbf{u}\times\mathbf{n}_i) - \sqrt{|\mathbf{d}_f|}(\tan\frac{1}{2}\beta\,\mathbf{n}_f + \mathbf{u}\times\mathbf{n}_f)\,]\cdot\mathbf{n}(\beta)}{[\sqrt{|\mathbf{d}_i|}(\mathbf{n}_i + \tan\frac{1}{2}\beta\,\mathbf{u}\times\mathbf{n}_i) + \sqrt{|\mathbf{d}_f|}(\mathbf{n}_f - \tan\frac{1}{2}\beta\,\mathbf{u}\times\mathbf{n}_f)\,]\cdot\mathbf{n}(\beta)}\,. \tag{8.5.2}$$

We call this method of selecting α, β the HC (helical–cubic) criterion.

8.5.3 *Cubic–cubic criterion*

Finally, we suggest a heuristic criterion based on the results of Section 8.1 for selecting the two free parameters α and β. In this approach, we select the angle β by requiring that

$$\mathcal{A}_0\,\mathbf{u}\,\mathcal{A}_2^* + \mathcal{A}_2\,\mathbf{u}\,\mathcal{A}_0^* = \mathbf{w}_h\,, \tag{8.5.3}$$

where $\mathbf{w}_h$ is a vector orthogonal to $\boldsymbol{\delta}_f - \boldsymbol{\delta}_i$ of suitable length, to make the imposition of condition (8.5.3) possible. More precisely, if $\mathbf{w}$ and $\mathbf{z}$ are defined as in Section 8.1, we set

$$\mathbf{w}_0 = \mathbf{w} - \left(\mathbf{w}\cdot\frac{\boldsymbol{\delta}_f - \boldsymbol{\delta}_i}{|\boldsymbol{\delta}_f - \boldsymbol{\delta}_i|}\right)\frac{\boldsymbol{\delta}_f - \boldsymbol{\delta}_i}{|\boldsymbol{\delta}_f - \boldsymbol{\delta}_i|}\,,$$

and define $\mathbf{w}_h$ from (8.1.4) by

$$\mathbf{w}_h = \mathbf{w}_0\sqrt{|\mathbf{d}_i|\,|\mathbf{d}_f|}\left[\left(\mathbf{w}_0\cdot\frac{\boldsymbol{\delta}_i + \boldsymbol{\delta}_f}{|\boldsymbol{\delta}_i + \boldsymbol{\delta}_f|}\right)^2 + \left(\frac{\mathbf{w}_0\cdot\mathbf{z}}{|\mathbf{z}|^2}\right)^2\right]^{-\frac{1}{2}}. \tag{8.5.4}$$

The angle α is then determined as in HC, i.e., using (8.5.2). We call this method of selecting the free angular parameters the CC (cubic–cubic) criterion.

Remark 8.3. The BV, HC, and CC criteria all produce a PH cubic interpolant when the given Hermite data are compatible with its existence. Furthermore, in such cases the interpolant will be a helix, since all PH cubics are helical.

8.6 NUMERICAL RESULTS

To illustrate the performance of the above selection criteria, we now present examples of the first–order PH quintic Hermite interpolants they generate, and compare these curves to the general helical PH quintic interpolants — referred to here as HL. For the five data sets listed in Table 1, we evaluate the integral shape measures

$$L = \int_0^1 \sigma\,dt\,, \qquad E_{RMF} = \int_0^1 \kappa^2\,\sigma\,dt\,, \qquad E = \int_0^1 \omega^2\,\sigma\,dt\,, \tag{8.6.1}$$

	$\mathbf{d}_i$	$\mathbf{d}_f$
case #1	$(1.0, 0.0, 1.0)$	$(0.0, 1.0, 1.0)$
case #2	$(-0.8, 0.3, 1.2)$	$(0.5, -1.3, -1.0)$
case #3	$(0.4, -1.5, -1.2)$	$(-1.2, -0.6, -1.2)$
case #4	$(-0.8, 0.3, 1.2)$	$(0.5, -1.3, -1.0)$
case #5	$(10.0, 0.0, 10.0)$	$(0.0, 1.0, 1.0)$

Table 8.1: Derivative data for the five test curves. In each case, the end points are $\mathbf{p}_i = (0, 0, 0)$ and $\mathbf{p}_f = (1, 1, 1)$ — except for case #4, in which the end point $\mathbf{p}_f = (0.15396, -0.60997, 0.40867)$ is chosen such that the "ordinary" cubic Hermite interpolant is actually a PH curve.

where σ is the parametric speed, κ is the usual curvature, and $\omega = \sqrt{\kappa^2 + \tau^2}$ is the *total curvature*, which depends also on the torsion τ [65]. L is the arc length, while E_{RMF} and E are energy measures corresponding to different adapted orthonormal frames along the curves — the basis vectors in the curve normal plane indicate the "twist" of the curve.

The energy measure E, employed in [26], corresponds to using the Frenet frame to specify the twist of the curve, since the total curvature ω represents the rotation rate of the Frenet frame (see Chapter 1). However, as noted in [36], E_{RMF} is preferable as an intrinsic shape measure for space curves, since it gives the least possible energy value among all adapted frames — namely, the value corresponding to a rotation–minimizing frame with rotation rate κ (see again Chapter 1).

The computed values of the integrals (8.6.1) are summarized in Table 8.2. To impart an idea of how these values relate to the overall range for each shape measure, we also present in Table 8.3 the "percent values" defined by

$$\%X \;=\; 100 \times \frac{X - X_{min}}{X_{max} - X_{min}}\,, \tag{8.6.2}$$

where X is any one of the quantities (8.6.1), with extremum values X_{min}, X_{max}. The arc length L can be obtained analytically, but numerical quadrature is required for E and E_{RMF}. Extremal values of these quantities are estimated by evaluating them on a uniform 126×126 grid over $(\alpha, \beta) \in [0, 2\pi]^2$ and augmenting these grid values with those obtained using the selection criteria HL, HC, BV, CC. The spatial PH quintics corresponding to the (α, β) values obtained from each of the selection criteria are illustrated in Figures 8.2–8.6.

In general, L is not a very reliable shape quality indicator, and its range of variation is rather small. Therefore, we focus on E and E_{RMF} — in particular, the latter, since it is the least energy among all possible adapted frames on space curves. From Tables 8.2 and 8.3, we observe that all four of the methods HL, HC,

	HL	HC	BV	CC
	case #1			
L	1.8254	1.8254	1.8164	1.8233
E	4.9737	4.9737	3.4003	4.0583
E_{RMF}	1.2736	1.2736	1.2782	1.2622
	case #2			
L	2.3597	2.3597	2.3551	2.3569
E	8.7789	8.7037	8.5180	8.5315
E_{RMF}	8.4383	8.3502	8.3022	8.2987
	case #3			
L	2.8780	2.8780	2.8754	2.8723
E	16.2503	16.2491	16.1802	16.1989
E_{RMF}	16.1767	16.1753	16.1459	16.1663
	case #4 (PH cubic)			
L	1.1469	1.1469	1.1469	1.1469
E	7.7459	7.7459	7.7459	7.7459
E_{RMF}	7.1044	7.1044	7.1044	7.1044
	case #5			
L	3.3489	3.3489	3.2865	3.3433
E	21.9795	23.0214	20.7990	21.7361
E_{RMF}	19.1460	16.1940	15.6567	15.6787

Table 8.2: Values of the integrals (8.6.1) for the five set of Hermite data in Table 8.1.

BV, CC are in reasonable agreement in selecting a "good" spatial PH quintic interpolant among the two–parameter family of formal solutions. The largest discrepancy occurs in case #5 (where $\mathbf{d}_i$ and $\mathbf{d}_f$ are of disparate magnitudes) — in this case, HL gives an appreciably poorer choice than HC, BV, CC. In the four cases other than #4 (for which the curves are identical), CC gives the least E_{RMF} value in two of them, and BV in the other two.

However, the percent differences listed in Table 3 are rather insignificant, typically $\ll 0.1\%$. This indicates that, while all four selection criteria do an excellent job of identifying PH quintic interpolants with near–optimal shape (i.e., least E_{RMF}), there exist curves among the two–parameter family of formal

	HL	HC	BV	CC
	case #1			
%L	100.0	100.0	81.42	95.63
%E	0.017063	0.017063	0.001682	0.008115
$\%E_{RMF}$	0.000119	0.000119	0.000168	0.000000
	case #2			
%L	100.0	100.0	98.42	99.04
%E	0.001426	0.001015	0.000000	0.000074
$\%E_{RMF}$	0.010571	0.005230	0.002322	0.002108
	case #3			
%L	100.0	100.0	99.56	99.01
%E	0.000635	0.000626	0.000064	0.000216
$\%E_{RMF}$	0.053331	0.051964	0.022791	0.043083
	case #4 (PH cubic)			
%L	100.0	100.0	100.0	100.0
%E	0.000134	0.000134	0.000134	0.000134
$\%E_{RMF}$	0.002277	0.002277	0.002277	0.002277
	case #5			
%L	100.0	100.0	91.28	99.22
%E	0.000341	0.000429	0.000241	0.000320
$\%E_{RMF}$	0.000624	0.000361	0.000313	0.000315

Table 8.3: Percent values of the shape integrals (8.6.1), as defined by (8.6.2).

solutions with *much worse* shape quality. A random or *ad hoc* choice for (α, β) might easily result in one of these poorly–shaped interpolants. The selection criteria proposed herein are thus of great practical importance.

Since the CC criterion is computationally much less expensive than BV, it appears to be the best "pragmatic" selection scheme. Note that HL does not produce a least E_{RMF} value in any of the test cases (except #4), so the helicity property is not necessarily *per se* a "good shape" indicator.

We conclude this section by briefly comparing our results with those of a recent study [99] that also deals with the problem of first–order Hermite interpolation by spatial PH quintics. In [99] Šír and Jüttler prove that setting the

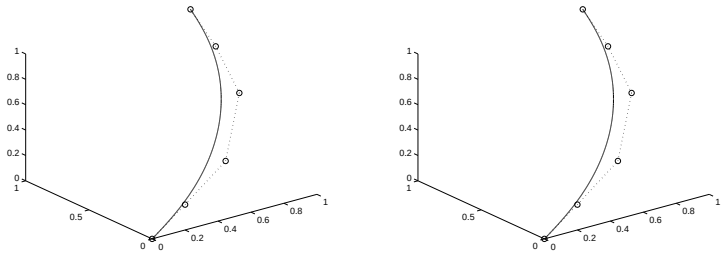

(a) HL (b) HC

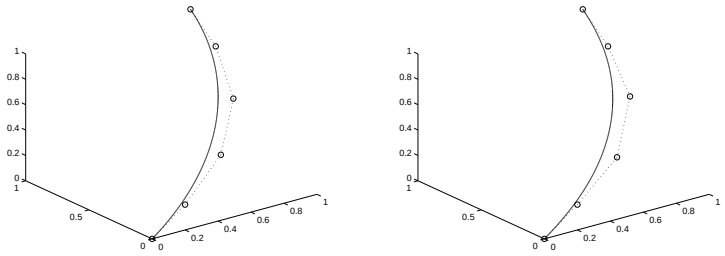

(c) BV (d) CC

Figure 8.2: The four PH quintic interpolants to the Hermite data of case #1.

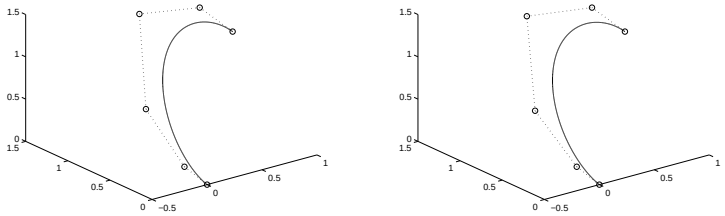

(a) HL (b) HC

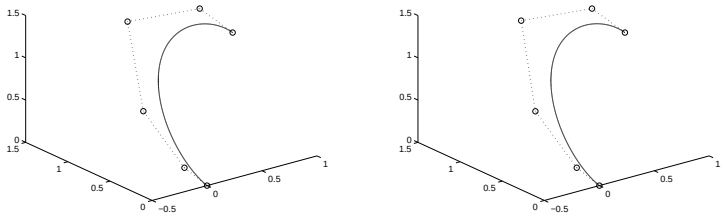

(c) BV (d) CC

Figure 8.3: The four PH quintic interpolants to the Hermite data of case #2.

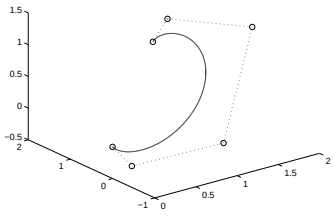

(a) HL

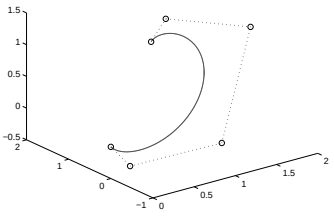

(b) HC

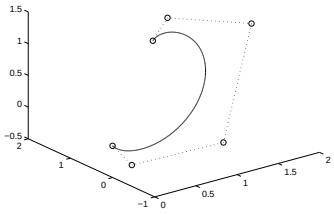

(c) BV

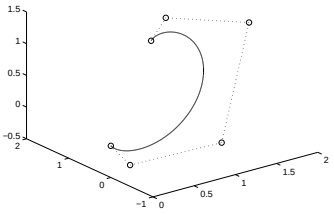

(d) CC

Figure 8.4: The four PH quintic interpolants to the Hermite data of case #3.

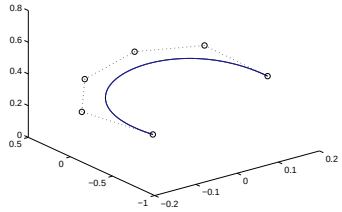

(a) HL

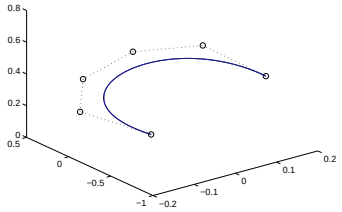

(b) HC

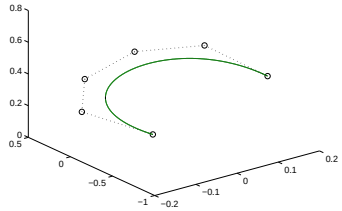

(c) BV

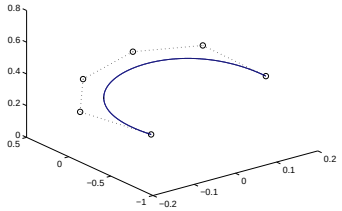

(d) CC

Figure 8.5: The four PH quintic interpolants to the Hermite data of case #4.

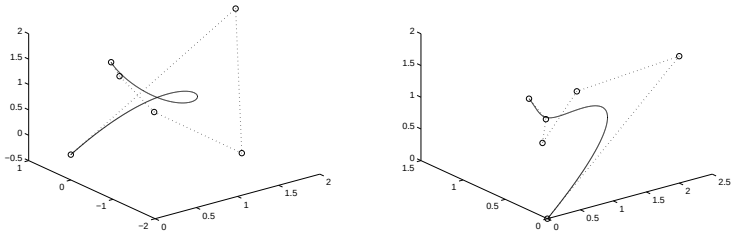

(a) HL (b) HC

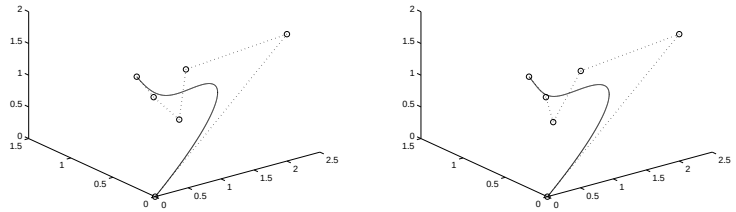

(c) BV (d) CC

Figure 8.6: The four PH quintic interpolants to the Hermite data of case #5.

two free angular parameters equal to 0 results in a solution that, among other properties, yields fourth–order convergence to an analytic curve, from which the data is presumed to be sampled.

However, we would like to emphasize here that, whenever we are interested in a *fixed* (finite) length of the sampling interval — rather than the solution behavior as this interval diminishes to zero — only data–dependent selection criteria for the free angular parameters yield "good" C^1 PH curve Hermite interpolants. To illustrate this, Figure 8.7 depicts (on the left) the PH quintic Hermite interpolant to the data of test case #3, taking $\alpha = \beta = 0$. The corresponding percent values for the quantities (8.6.1) are $\%L = 2.6$, $\%E = 0.38836$, and $\%E_{RMF} = 34.072$. Thus, using $\alpha = \beta = 0$ gives an L close to the minimum value, but E and E_{RMF} are *much larger* than obtained with any of the selection criteria HL, HC, BV, CC.

Figure 8.7 also shows (on the right) the C^1 PH quintic spline interpolating Hermite data obtained by evaluating at $t = 0, \frac{1}{2}, 1$ the "ordinary" cubic interpolant to the Hermite data of case #3, always taking $\alpha = \beta = 0$. On the other hand, Figure 8.8 confirms that this choice is appropriate when asymptotic convergence of the result is of primary concern, by illustrating the behavior of approximations to the cubic using 4 and 8 PH quintic interpolants, defined by the choices $\alpha = \beta = 0$ in each case.

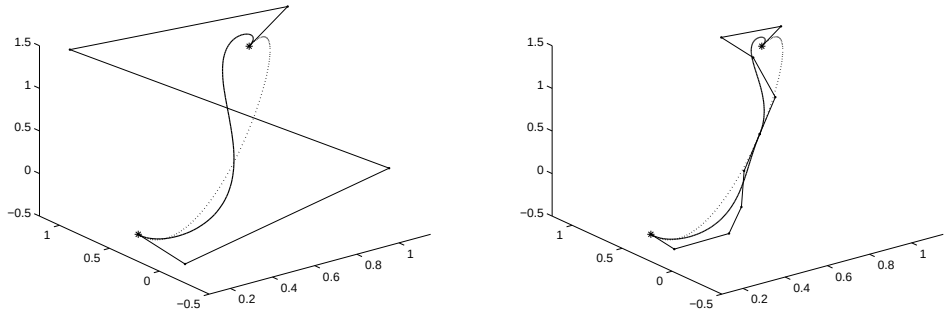

Figure 8.7: C^1 PH quintic spline curves (solid lines) interpolating the cubic curve (dotted lines) defined by the Hermite data of test case #3, and their control polygons. Here, the choices $\alpha = \beta = 0$ are always used. The number of approximating PH quintic segments is 1 on the left, and 2 on the right.

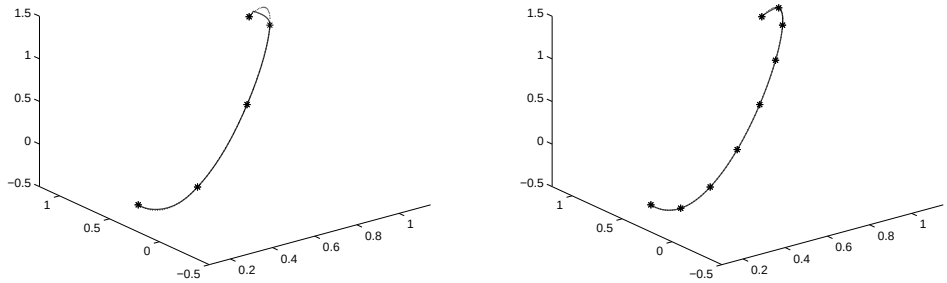

Figure 8.8: C^1 PH quintic spline curves (solid lines) interpolating the cubic (dotted lines) defined by the Hermite data of test case #3, with $\alpha = \beta = 0$. The number of PH quintic segments is 4 on the left, and 8 on the right.

9 RRMF QUINTIC HERMITE INTERPOLANTS

Space curves with rational rotation–minimizing frames are useful in animation, motion planning, swept surface constructions, and related problems in which it is necessary to describe the variation of orientation along a spatial path in a manner compatible with the rational curve and surface representations employed by modern CAD systems. To take advantage of RRMF curves in such contexts, it is necessary to characterize them as a subset of the spatial PH curves, and to formulate algorithms that facilitate their construction in a geometrically intuitive manner.

Based on the original characterization of RRMF curves given in Chapter 6, preliminary results on the geometrical construction of quintic RRMF curves by the interpolation of G^1 spatial Hermite data are presented in this chapter. This problem involves solving a non–linear system of equations in six complex unknowns. The solution is obtained by a semi–numerical scheme, in which the problem is reduced to computing positive real roots of a certain univariate polynomial. The quintic RRMF G^1 Hermite interpolants possess one residual angular degree of freedom, which can strongly influence the curve shape. Computed examples are included to illustrate the method and the resulting quintic RRMF curves.

The plan for this chapter is as follows. The problem of G^1 Hermite interpolation using RRMF quintics is formulated in Section 9.1. A procedure for solving this problem is then described in Section 9.2, and a selection of computed examples is presented in Section 9.3. Finally, Section 9.4 gives a possible geometrical significance of the free parameter involved.

9.1 INTERPOLATION OF GEOMETRICAL HERMITE DATA

As described in Section 6.4, to define an RRMF quintic we substitute two complex quadratic polynomials $\boldsymbol{\alpha}(t)$, $\boldsymbol{\beta}(t)$ expressed by the Bernstein form (6.4.1) into the Hopf map representation (3.2.2) of Pythagorean–hodograph curves. The constraints on the six coefficients $\boldsymbol{\alpha}_k$, $\boldsymbol{\beta}_k \in \mathbb{C}$ for $k = 0, 1, 2$ of these polynomilas that identify *non–degenerate* RRMF quintics are given by (6.4.2) and (6.4.4). It has been shown in Section 6.4 that these constraints are necessary and sufficient for the existence of a quadratic complex polynomial $\mathbf{w}(t) = a(t) + ib(t)$ such that the RRMF condition (6.2.2) is satisfied. Since (6.4.2) and (6.4.4) are constraints on *real* and *complex* values, respectively, they amount to *three* scalar constraints on the coefficients of the polynomials $\boldsymbol{\alpha}(t)$ and $\boldsymbol{\beta}(t)$.

Once the coefficients of the two quadratics polynomials $\alpha(t)$, $\beta(t)$ satisfying (6.4.2) and (6.4.4) are known, the three coefficients of

$$\mathbf{w}(t) = \mathbf{w}_0(1-t)^2 + \mathbf{w}_1 2(1-t)t + \mathbf{w}_2 t^2 \tag{9.1.1}$$

in (6.2.2) are given from Lemma 6.1 and equations (6.4.6)–(6.4.7) of Proposition 6.2 in terms of them by

$$\mathbf{w}_0 = 1\,, \qquad \mathbf{w}_1 = \frac{\overline{\alpha}_0\alpha_1 + \overline{\beta}_0\beta_1}{|\alpha_0|^2 + |\beta_0|^2}\,, \qquad \mathbf{w}_2 = \frac{\overline{\alpha}_1\alpha_2 + \overline{\beta}_1\beta_2}{\alpha_0\overline{\alpha}_1 + \beta_0\overline{\beta}_1}\,. \tag{9.1.2}$$

The rational RMF of degree 8 in the curve parameter t can then be expressed in terms of the ERF (6.1.1) and the polynomials $a(t) = \mathrm{Re}\,(\mathbf{w}(t))$ and $b(t) = \mathrm{Im}\,(\mathbf{w}(t))$ as in (6.1.2). Figure 9.1 compares the orientations obtained using the ERF and the RMAF to guide a rectangular parallelepiped along an RRMF quintic.

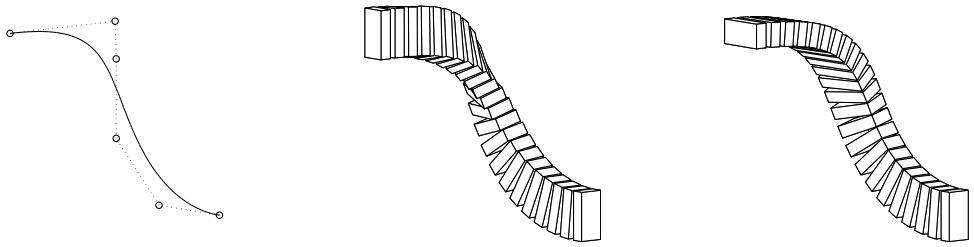

Figure 9.1: A quintic RRMF curve (left), used to specify the trajectory for the spatial motion of a rectangular parallelepiped. The orientations of the parallelepiped defined by the ERF (center) and the RMF (right) along the path are shown (coincident at the bottom right point).

In order to solve the G^1 spatial Hermite interpolation problem, we are concerned with constructing quintic RRMF curves $\mathbf{r}(t)$ for $t \in [0,1]$ that interpolate given initial/final points $\mathbf{p}_i$, $\mathbf{p}_f$ and unit tangents $\mathbf{t}_i$, $\mathbf{t}_f$. Thus, the curve defined by (3.2.1)–(3.2.2) must satisfy (6.4.2) and (6.4.4), together with

$$\mathbf{r}(0) = \mathbf{p}_i\,, \qquad \frac{\mathbf{r}'(0)}{|\mathbf{r}'(0)|} = \mathbf{t}_i\,, \qquad \mathbf{r}(1) = \mathbf{p}_f\,, \qquad \frac{\mathbf{r}'(1)}{|\mathbf{r}'(1)|} = \mathbf{t}_f\,. \tag{9.1.3}$$

The unit tangents $\mathbf{t}_i$, $\mathbf{t}_f$ can be specified in terms of polar angles θ_i, θ_f measured from the x–axis, and azimuthal angles ϕ_i, ϕ_f measured about the x–axis, as

$$\mathbf{t}_i = (\cos\theta_i, \sin\theta_i\cos\phi_i, \sin\theta_i\sin\phi_i)\,, \tag{9.1.4}$$

$$\mathbf{t}_f = (\cos\theta_f, \sin\theta_f\cos\phi_f, \sin\theta_f\sin\phi_f)\,. \tag{9.1.5}$$

Since the first condition in (9.1.3) is trivially satisfied by taking $\mathbf{p}_i$ as integration constant on integrating (3.2.2), we need only consider the displacement

$$\Delta\mathbf{p} \;=\; \int_0^1 \mathbf{r}'(t)\,dt \;=\; \mathbf{p}_f - \mathbf{p}_i$$

rather than $\mathbf{p}_i$, $\mathbf{p}_f$ individually. Now it is always possible to choose a coordinate system in which the initial tangent $\mathbf{t}_i$ is in the (x,y)–plane, the initial point $\mathbf{p}_i$ is at the origin, and the displacement $\Delta\mathbf{p} = \mathbf{p}_f - \mathbf{p}_i$ lies on the x–axis. We say that such coordinates define *canonical Hermite data*, with $\phi_i = 0$ and $\Delta\mathbf{p} = (X,0,0)$. We henceforth assume data of this form, and for brevity we write $\phi_f = \phi$ and

$$(c_i, s_i) \;=\; (\cos\tfrac{1}{2}\theta_i, \sin\tfrac{1}{2}\theta_i)\,, \qquad (c_f, s_f) \;=\; (\cos\tfrac{1}{2}\theta_f, \sin\tfrac{1}{2}\theta_f)\,. \tag{9.1.6}$$

Note that, for non–planar data, θ_i, θ_f and ϕ must not be integer multiples of π.

Interpolation of the displacement $\Delta\mathbf{p} = (X,0,0)$ by a PH quintic yields the two conditions

$$\begin{aligned} 5X \;&=\; |\boldsymbol{\alpha}_0|^2 - |\boldsymbol{\beta}_0|^2 \\ &+\; \mathrm{Re}(\boldsymbol{\alpha}_0\overline{\boldsymbol{\alpha}}_1 - \boldsymbol{\beta}_0\overline{\boldsymbol{\beta}}_1) \\ &+\; \tfrac{1}{3}\,\mathrm{Re}(\boldsymbol{\alpha}_0\overline{\boldsymbol{\alpha}}_2 - \boldsymbol{\beta}_0\overline{\boldsymbol{\beta}}_2) \;+\; \tfrac{2}{3}\,(|\boldsymbol{\alpha}_1|^2 - |\boldsymbol{\beta}_1|^2) \\ &+\; \mathrm{Re}(\boldsymbol{\alpha}_1\overline{\boldsymbol{\alpha}}_2 - \boldsymbol{\beta}_1\overline{\boldsymbol{\beta}}_2) \\ &+\; |\boldsymbol{\alpha}_2|^2 - |\boldsymbol{\beta}_2|^2\,, \end{aligned} \tag{9.1.7}$$

$$\begin{aligned} 0 \;&=\; 2\,\boldsymbol{\alpha}_0\overline{\boldsymbol{\beta}}_0 \\ &+\; \boldsymbol{\alpha}_0\overline{\boldsymbol{\beta}}_1 + \boldsymbol{\alpha}_1\overline{\boldsymbol{\beta}}_0 \\ &+\; \tfrac{1}{3}\,(\boldsymbol{\alpha}_0\overline{\boldsymbol{\beta}}_2 + \boldsymbol{\alpha}_2\overline{\boldsymbol{\beta}}_0) \;+\; \tfrac{4}{3}\,\boldsymbol{\alpha}_1\overline{\boldsymbol{\beta}}_1 \\ &+\; \boldsymbol{\alpha}_1\overline{\boldsymbol{\beta}}_2 + \boldsymbol{\alpha}_2\overline{\boldsymbol{\beta}}_1 \\ &+\; 2\,\boldsymbol{\alpha}_2\overline{\boldsymbol{\beta}}_2\,. \end{aligned} \tag{9.1.8}$$

Since (9.1.7) is a scalar equation, while (9.1.8) is a relation among complex values, interpolating $\Delta\mathbf{p}$ incurs *three* scalar constraints on the coefficients of $\boldsymbol{\alpha}(t)$, $\boldsymbol{\beta}(t)$.

From (3.2.2) and (6.4.1), we can write the interpolation of end tangents as

$$\frac{\mathbf{r}'(0)}{|\mathbf{r}'(0)|} \;=\; \frac{(|\boldsymbol{\alpha}_0|^2 - |\boldsymbol{\beta}_0|^2,\, 2\,\mathrm{Re}(\boldsymbol{\alpha}_0\overline{\boldsymbol{\beta}}_0),\, 2\,\mathrm{Im}(\boldsymbol{\alpha}_0\overline{\boldsymbol{\beta}}_0))}{|\boldsymbol{\alpha}_0|^2 + |\boldsymbol{\beta}_0|^2} \;=\; \mathbf{t}_i\,, \tag{9.1.9}$$

$$\frac{\mathbf{r}'(1)}{|\mathbf{r}'(1)|} \;=\; \frac{(|\boldsymbol{\alpha}_2|^2 - |\boldsymbol{\beta}_2|^2,\, 2\,\mathrm{Re}(\boldsymbol{\alpha}_2\overline{\boldsymbol{\beta}}_2),\, 2\,\mathrm{Im}(\boldsymbol{\alpha}_2\overline{\boldsymbol{\beta}}_2))}{|\boldsymbol{\alpha}_2|^2 + |\boldsymbol{\beta}_2|^2} \;=\; \mathbf{t}_f\,. \tag{9.1.10}$$

Since $\mathbf{t}_i$ and $\mathbf{t}_f$ are *unit* vectors, (9.1.9) and (9.1.10) each yield two scalar constraints on the coefficients of $\boldsymbol{\alpha}(t)$, $\boldsymbol{\beta}(t)$. Hence, the G^1 Hermite interpolation conditions impose *seven* scalar constraints on the *six* complex coefficients of the

polynomials $\boldsymbol{\alpha}(t)$ and $\boldsymbol{\beta}(t)$. Thus, in conjunction with the RRMF constraints (6.4.2) and (6.4.4), we have altogether *ten* scalar constraints and *twelve* scalar unknowns.

Another scalar constraint may be imposed by noting [33] that the polynomials (6.4.1) embody one non–essential freedom. As already observe in Chapter 3, if $\boldsymbol{\alpha}(t)$, $\boldsymbol{\beta}(t)$ generate a specific hodograph $\mathbf{r}'(t)$ through (3.2.2), the same hodograph is obtained on replacing them by $\exp(i\xi)\,\boldsymbol{\alpha}(t)$, $\exp(i\xi)\,\boldsymbol{\beta}(t)$ for any $\xi \in \mathbb{R}$. Hence we may assume, without loss of generality, that one of the coefficients in (6.4.1) is *real*. Thus, we expect the RRMF quintic interpolants to given spatial G^1 Hermite data to form a one–parameter family of space curves.

9.2 SOLUTION OF RRMF HERMITE SYSTEM

As noted in Section 9.1, the interpolation of G^1 Hermite data by RRMF quintic curves involves a system of eleven scalar constraints on the six complex coefficients $\boldsymbol{\alpha}_0, \boldsymbol{\alpha}_1, \boldsymbol{\alpha}_2, \boldsymbol{\beta}_0, \boldsymbol{\beta}_1, \boldsymbol{\beta}_2$, leaving one scalar degree of freedom. Consider first interpolation of the end tangents.

Proposition 9.1. *For canonical–form Hermite data, interpolation of the two end tangents* (9.1.4)–(9.1.5) *may be achieved by expressing* $\boldsymbol{\alpha}_0$, $\boldsymbol{\beta}_0$ *and* $\boldsymbol{\alpha}_2$, $\boldsymbol{\beta}_2$ *in terms of complex values* $\boldsymbol{\gamma}_0$ *and* $\boldsymbol{\gamma}_2$ *as*

$$\boldsymbol{\alpha}_0 = \boldsymbol{\gamma}_0 c_i\,, \qquad \boldsymbol{\alpha}_2 = \boldsymbol{\gamma}_2 c_f \exp(i\tfrac{1}{2}\phi)\,, \tag{9.2.1}$$

$$\boldsymbol{\beta}_0 = \boldsymbol{\gamma}_0 s_i\,, \qquad \boldsymbol{\beta}_2 = \boldsymbol{\gamma}_2 s_f \exp(-i\tfrac{1}{2}\phi)\,. \tag{9.2.2}$$

Proof : Substituting (9.2.1)–(9.2.2) in (9.1.9)–(9.1.10) and simplifying yields (9.1.4)–(9.1.5). ∎

From (9.2.1) and (9.2.2) we see that

$$|\boldsymbol{\alpha}_0|^2 + |\boldsymbol{\beta}_0|^2 = |\boldsymbol{\gamma}_0|^2 \qquad \text{and} \qquad |\boldsymbol{\alpha}_2|^2 + |\boldsymbol{\beta}_2|^2 = |\boldsymbol{\gamma}_2|^2\,.$$

Thus, denoting by ρ^2 the ratio of the end–derivative magnitudes,

$$\rho^2 = \frac{|\mathbf{r}'(1)|}{|\mathbf{r}'(0)|} = \frac{|\boldsymbol{\alpha}_2|^2 + |\boldsymbol{\beta}_2|^2}{|\boldsymbol{\alpha}_0|^2 + |\boldsymbol{\beta}_0|^2}\,, \tag{9.2.3}$$

we have

$$|\boldsymbol{\gamma}_2| = \rho\,|\boldsymbol{\gamma}_0|\,.$$

Therefore, we can write $\boldsymbol{\gamma}_0 = \gamma \exp(i\lambda_0)$ and $\boldsymbol{\gamma}_2 = \rho\,\gamma \exp(i\lambda_2)$ where $\gamma, \rho \in \mathbb{R}^+$ and $\lambda_0, \lambda_2 \in [0, 2\pi]$. The redundancy of the representation (3.2.2) can be used to

fix either λ_0 or λ_2. We choose $\lambda_0 = 0$ and, for simplicity, set $\lambda_2 = \lambda$. Invoking the notations (9.1.6), we obtain the expressions

$$\alpha_0 = \gamma\, c_i\,, \qquad \alpha_2 \;=\; \rho\,\gamma\, c_f \exp(i(\lambda + \tfrac{1}{2}\phi))\,, \tag{9.2.4}$$

$$\beta_0 = \gamma\, s_i\,, \qquad \beta_2 \;=\; \rho\,\gamma\, s_f \exp(i(\lambda - \tfrac{1}{2}\phi))\,, \tag{9.2.5}$$

where $c_i, s_i, c_f, s_f \neq 0$ and ϕ is not an integer multiple of π for non–planar data.

Consider now the RRMF conditions (6.4.2) and (6.4.4). Substituting the expressions for $\alpha_0, \beta_0, \alpha_2, \beta_2$ and simplifying yields

$$|\, c_f \exp(i\tfrac{1}{2}\phi)\, \overline{\alpha}_1 + s_f \exp(-i\tfrac{1}{2}\phi)\, \overline{\beta}_1 \,| \;=\; |\, c_i\, \overline{\alpha}_1 + s_i\, \overline{\beta}_1 \,|\,, \tag{9.2.6}$$

$$\begin{aligned} \rho\,\gamma^2 \exp(i\lambda)\,[\, c_i s_f \exp(-i\tfrac{1}{2}\phi) - c_f s_i \exp(i\tfrac{1}{2}\phi)\,] \\ = 2(c_i\overline{\alpha}_1 + s_i\overline{\beta}_1)(c_i\beta_1 - s_i\alpha_1)\,. \end{aligned} \tag{9.2.7}$$

Condition (9.2.6) implies that, for some angular parameter η, we must have

$$\exp(i\eta)\,[\, c_f \exp(i\tfrac{1}{2}\phi)\, \overline{\alpha}_1 + s_f \exp(-i\tfrac{1}{2}\phi)\, \overline{\beta}_1 \,] \;=\; c_i\, \overline{\alpha}_1 + s_i\, \overline{\beta}_1\,,$$

and hence

$$[\, s_f \exp(i\tfrac{1}{2}\phi) - s_i \exp(i\eta)\,]\, \beta_1 \;=\; [\, c_i \exp(i\eta) - c_f \exp(-i\tfrac{1}{2}\phi)\,]\, \alpha_1\,. \tag{9.2.8}$$

Now if η is such that $s_f \exp(i\frac{1}{2}\phi) = s_i \exp(i\eta)$, condition (9.2.8) implies that $\alpha_1 = 0$. This is possible only if $s_f = s_i$ and $\eta = \frac{1}{2}\phi$, or $s_f = -s_i$ and $\eta = \frac{1}{2}\phi + \pi$. In the former case (9.2.7) is satisfied by taking $\lambda = \frac{1}{2}\pi$ or $\frac{3}{2}\pi$ and $|\beta_1|^2 = \rho\,\gamma^2 |\sin\frac{1}{2}\phi|$. In the latter case (9.2.7) is satisfied with $\lambda = 0$ or π and $|\beta_1|^2 = \rho\,\gamma^2 |\cos\frac{1}{2}\phi|$. In all other cases (9.2.8) implies that

$$\beta_1 \;=\; \frac{c_i \exp(i\eta) - c_f \exp(-i\tfrac{1}{2}\phi)}{s_f \exp(i\tfrac{1}{2}\phi) - s_i \exp(i\eta)}\; \alpha_1\,. \tag{9.2.9}$$

Substituting (9.2.9) into (9.2.7), cancelling the factor[1] $c_i s_f \exp(-i\frac{1}{2}\phi) - c_f s_i \exp(i\frac{1}{2}\phi)$ from both sides, and setting $\epsilon = c_i c_f \exp(-i\frac{1}{2}\phi) + s_i s_f \exp(i\frac{1}{2}\phi)$, we obtain

$$|\alpha_1|^2 \;=\; \tfrac{1}{2}\,\rho\,\gamma^2\; \frac{|\, s_f \exp(i\tfrac{1}{2}\phi) - s_i \exp(i\eta)\,|^2}{\exp(-i\lambda)\,[\exp(i\eta) - \epsilon\,]}\,. \tag{9.2.10}$$

For a valid solution, the expression on the right must have a non–negative real value. This is equivalent to satisfaction of the relations

$$\mathrm{Im}(\, \exp(-i\lambda)\,[\exp(i\eta) - \epsilon\,]\,) \;=\; 0\,, \qquad \mathrm{Re}(\, \exp(-i\lambda)\,[\exp(i\eta) - \epsilon\,]\,) \;>\; 0\,,$$

1 Under the stated assumptions on c_i, s_i, c_f, s_f and ϕ, this factor is always non–zero. The same is true of the term $\exp(i\eta) - \epsilon$, for all values of η.

by the parameters η and λ, and consequently

$$\exp(-i\lambda) \;=\; \mu_0(\eta) \qquad \text{with} \qquad \mu_0(\eta) \;=\; \frac{\exp(-i\eta) - \overline{\epsilon}}{|\exp(-i\eta) - \overline{\epsilon}|}\,. \tag{9.2.11}$$

Substituting from (9.2.11) into (9.2.10), we obtain

$$|\alpha_1|^2 \;=\; \rho\,\gamma^2 f_1(\eta) \qquad \text{with} \qquad f_1(\eta) \;=\; \frac{\frac{1}{2}\,|\,s_f \exp(i\tfrac{1}{2}\phi) - s_i \exp(i\eta)\,|^2}{|\exp(i\eta) - \epsilon\,|}\,. \tag{9.2.12}$$

Assuming that[2] $3\overline{\alpha}_0 + 4\overline{\alpha}_1 + 3\overline{\alpha}_2 \neq 0$, equation (9.1.8) allows β_1 to be expressed in terms of α_1 as

$$\beta_1 \;=\; -\,\frac{(6\beta_0 + \beta_2)\,\overline{\alpha}_0 + 3(\beta_0 + \beta_2)\,\overline{\alpha}_1 + (\beta_0 + 6\beta_2)\,\overline{\alpha}_2}{3\overline{\alpha}_0 + 4\overline{\alpha}_1 + 3\overline{\alpha}_2}\,.$$

Equating this expression for β_1 with (9.2.9) and cancelling γ from both sides gives the equation

$$\delta_0(\eta,\rho)\,\alpha_1 \;+\; \delta_1(\eta,\rho)\,\overline{\alpha}_1 \;=\; \gamma\,\delta_2(\eta,\rho)\,, \tag{9.2.13}$$

for α_1, with coefficients

$$\begin{aligned}
\delta_0(\eta,\rho) \;&=\; 3\,[\,c_i + \rho\,c_f\mu_0 \exp(-i\tfrac{1}{2}\phi)\,]\,\mu_1\,,\\
\delta_1(\eta,\rho) \;&=\; 3\,[\,s_i + \rho\,s_f\overline{\mu}_0 \exp(-i\tfrac{1}{2}\phi)\,]\,,\\
\delta_2(\eta,\rho) \;&=\; -6\,[\,c_i s_i + \rho^2 c_f s_f \exp(-i\phi)\,] - 4\,\rho\,f_1\,\mu_1\\
&\qquad -\rho\,\exp(-i\tfrac{1}{2}\phi)[\,c_i s_f\,\overline{\mu}_0 + c_f s_i\,\mu_0\,]\,,
\end{aligned} \tag{9.2.14}$$

where we define

$$\mu_1(\eta) \;=\; \frac{c_i \exp(i\eta) - c_f \exp(-i\tfrac{1}{2}\phi)}{s_f \exp(i\tfrac{1}{2}\phi) - s_i \exp(i\eta)}\,. \tag{9.2.15}$$

Now the pairs of (ρ,η) values such that $|\delta_0|^2 = |\delta_1|^2$ and $\mathrm{Re}((\delta_0 - \delta_1)\overline{\delta}_2) \neq 0$ or $\mathrm{Im}((\delta_0 + \delta_1)\overline{\delta}_2) \neq 0$ are unacceptable, because equation (9.2.13) has no solution. On the other hand, if there exist pairs such that $|\delta_0|^2 = |\delta_1|^2$ and $\mathrm{Re}((\delta_0 - \delta_1)\overline{\delta}_2) = \mathrm{Im}((\delta_0 + \delta_1)\overline{\delta}_2) = 0$, equation (9.2.13) corresponds to only one scalar condition. In this special case, we also need equation (9.2.12) to determine α_1.

In general, we can assume that $|\delta_0|^2 \neq |\delta_1|^2$ and derive α_1 from (9.2.13) as

$$\alpha_1 \;=\; \gamma\,\frac{\overline{\delta}_0\delta_2 - \delta_1\overline{\delta}_2}{|\delta_0|^2 - |\delta_1|^2}\,.$$

2 This incurs no loss of generality: the condition $\alpha_1 = -\frac{3}{4}\,(\alpha_0 + \alpha_2)$ imposes two more scalar constraints on η and ρ, so no degrees of freedom remain for satisfying (9.2.10).

Once η is chosen, the correct ρ value is identified via (9.2.12) by the positive real roots of the equation

$$|\,\overline{\delta}_0\delta_2 - \delta_1\overline{\delta}_2\,|^2 \;-\; \rho\, f_1(\eta)\,(|\delta_0|^2 - |\delta_1|^2)^2 \;=\; 0\,, \tag{9.2.16}$$

which is a polynomial equation of degree 6 with real coefficients. We may write

$$\overline{\delta}_0\delta_2 - \delta_1\overline{\delta}_2 \;=\; \sum_{k=0}^{3} \mathbf{z}_k\,\rho^k\,,$$

with

$$\begin{aligned}
\mathbf{z}_0 &= 18\,c_i s_i (s_i - c_i\overline{\mu}_1)\,,\\
\mathbf{z}_1 &= 18\,c_i s_i\overline{\mu}_0[s_f\exp(-i\tfrac{1}{2}\phi) - c_f\overline{\mu}_1\exp(i\tfrac{1}{2}\phi)]\\
&\quad + 3\,s_i\exp(i\tfrac{1}{2}\phi)(c_i s_f\mu_0 + c_f s_i\overline{\mu}_0) + 12\,f_1\overline{\mu}_1(s_i - c_i\mu_1)\\
&\quad - 3\,c_i\overline{\mu}_1\exp(-i\tfrac{1}{2}\phi)(c_i s_f\overline{\mu}_0 + c_f s_i\mu_0)\,,\\
\mathbf{z}_2 &= 18\,c_f s_f[s_i\exp(i\phi) - c_i\overline{\mu}_1\exp(-i\phi)] + 3\,s_f\overline{\mu}_0(c_i s_f\mu_0 + c_f s_i\overline{\mu}_0))\\
&\quad + 12\,f_1\overline{\mu}_0\overline{\mu}_1[s_f\exp(-i\tfrac{1}{2}\phi) - c_f\mu_1\exp(i\tfrac{1}{2}\phi)]\\
&\quad - 3\,c_f\overline{\mu}_1\overline{\mu}_0(c_i s_f\overline{\mu}_0 + c_f s_i\mu_0)\,,\\
\mathbf{z}_3 &= 18\,c_f s_f\overline{\mu}_0[s_f\exp(i\tfrac{1}{2}\phi) - c_f\overline{\mu}_1\exp(-i\tfrac{1}{2}\phi)]\,,
\end{aligned}$$

while

$$|\delta_0|^2 \;=\; \sum_{k=0}^{2} d_{0k}\rho^k \qquad \text{and} \qquad |\delta_1|^2 \;=\; \sum_{k=0}^{2} d_{1k}\rho^k\,,$$

with

$$\begin{aligned}
d_{00} &= 9\,|\mu_1|^2 c_i^2\,,\\
d_{01} &= 9\,|\mu_1|^2 c_i c_f\,[\,\mu_0\exp(-i\tfrac{1}{2}\phi) + \overline{\mu}_0\exp(i\tfrac{1}{2}\phi)\,]\,,\\
d_{02} &= 9\,|\mu_1|^2 c_f^2\,,
\end{aligned}$$

$$\begin{aligned}
d_{10} &= 9\,s_i^2\,,\\
d_{11} &= 9\,s_i s_f\,[\,\overline{\mu}_0\exp(-i\tfrac{1}{2}\phi) + \mu_0\exp(i\tfrac{1}{2}\phi)\,]\,,\\
d_{12} &= 9\,s_f^2\,.
\end{aligned}$$

Hence, setting

$$|\,\overline{\delta}_0\delta_2 - \delta_1\overline{\delta}_2\,|^2 \;=\; \sum_{k=0}^{6} c_k\rho^k\,,$$

where

$$\begin{aligned} c_0 &= |\mathbf{z}_0|^2\,, \\ c_1 &= 2\,\mathrm{Re}(\mathbf{z}_1\bar{\mathbf{z}}_0)\,, \\ c_2 &= 2\,\mathrm{Re}(\mathbf{z}_2\bar{\mathbf{z}}_0) + |\mathbf{z}_1|^2\,, \\ c_3 &= 2\,\mathrm{Re}(\mathbf{z}_3\bar{\mathbf{z}}_0) + 2\,\mathrm{Re}(\mathbf{z}_2\bar{\mathbf{z}}_1)\,, \\ c_4 &= 2\,\mathrm{Re}(\mathbf{z}_3\bar{\mathbf{z}}_1) + |\mathbf{z}_2|^2\,, \\ c_5 &= 2\,\mathrm{Re}(\mathbf{z}_3\bar{\mathbf{z}}_2)\,, \\ c_6 &= |\mathbf{z}_3|^2\,, \end{aligned} \tag{9.2.17}$$

equation (9.2.16) reduces to

$$c_6\,\rho^6 + \sum_{j=1}^{5}(c_j - e_{j-1}f_1)\rho^j + c_0 = 0\,, \tag{9.2.18}$$

with

$$\begin{aligned} e_0 &= (d_{00} - d_{10})^2\,, \\ e_1 &= 2\,(d_{00} - d_{10})(d_{01} - d_{11})\,, \\ e_2 &= (d_{01} - d_{11})^2 + 2\,(d_{00} - d_{10})(d_{02} - d_{12})\,, \\ e_3 &= 2\,(d_{01} - d_{11})(d_{02} - d_{12})\,, \\ e_4 &= (d_{02} - d_{12})^2\,. \end{aligned}$$

Equation (9.2.18) must possess at least one positive real root, for some value of the angular parameter η, if an RRMF quintic G^1 Hermite interpolant is to exist. Since the coefficients of (9.2.18) have a complicated, non–linear dependence on the Hermite data and on the parameter η, a thorough investigation of the existence (and number) of interpolants is a challenging task, beyond our present scope.

From (9.2.4)–(9.2.5) and (9.2.9)–(9.2.10) we observe that the coefficients of $\boldsymbol{\alpha}(t)$, $\boldsymbol{\beta}(t)$ are all proportional to γ. Hence, we may write

$$\boldsymbol{\alpha}_k = \gamma\,\mathbf{a}_k \qquad \text{and} \qquad \boldsymbol{\beta}_k = \gamma\,\mathbf{b}_k \tag{9.2.19}$$

for $k = 0, 1, 2$, where

$$\mathbf{a}_0 = c_i\,, \qquad \mathbf{a}_1 = \frac{\bar{\delta}_0\delta_2 - \delta_1\bar{\delta}_2}{|\delta_0|^2 - |\delta_1|^2}\,, \qquad \mathbf{a}_2 = \rho\,c_f\,\bar{\mu}_0\exp(i\tfrac{1}{2}\phi)\,, \tag{9.2.20}$$

$$\mathbf{b}_0 = s_i\,, \qquad \mathbf{b}_1 = \mu_1\mathbf{a}_1\,, \qquad \mathbf{b}_2 = \rho\,s_f\,\bar{\mu}_0\exp(-i\tfrac{1}{2}\phi)\,. \tag{9.2.21}$$

Substituting (9.2.19) into (9.1.7), the γ value corresponding to a positive real root of (9.2.18) can be computed as

$$\gamma = \sqrt{\frac{5X}{f_2(\eta)}}, \tag{9.2.22}$$

where $f_2(\eta)$ is defined by

$$\begin{aligned} f_2(\eta) \;=\; & |\mathbf{a}_0|^2 - |\mathbf{b}_0|^2 + \mathrm{Re}(\mathbf{a}_0\bar{\mathbf{a}}_1 - \mathbf{b}_0\bar{\mathbf{b}}_1) \\ & + \tfrac{1}{3}\,\mathrm{Re}(\mathbf{a}_0\bar{\mathbf{a}}_2 - \mathbf{b}_0\bar{\mathbf{b}}_2) + \tfrac{2}{3}\,(|\mathbf{a}_1|^2 - |\mathbf{b}_1|^2) \\ & + \mathrm{Re}(\mathbf{a}_1\bar{\mathbf{a}}_2 - \mathbf{b}_1\bar{\mathbf{b}}_2) + |\mathbf{a}_2|^2 - |\mathbf{b}_2|^2\,. \end{aligned} \tag{9.2.23}$$

Of course, we must require $f_2(\eta) > 0$ for (9.2.22) to yield a real γ value. Again, due to the complicated dependence of (9.2.23) on η and the prescribed Hermite data, a detailed study of the conditions under which this holds is deferred to a future study. For the present, we only observe from experience with experimental tests that there are infinitely many admissible choices for η in the case of sufficiently dense data sampled from a smooth analytic curve, some of which produce very reasonable shapes. On the other hand, as shown in the examples of the following section, we have also been able to identify admissible fair–shaped RRMF quintic interpolants for many other data sets.

We conclude by summarizing the computation of RRMF quintic interpolants to spatial G^1 Hermite data as follows (for brevity, we exclude the cases $\eta = \frac{1}{2}\phi$ when $s_f = s_i$, and $\eta = \frac{1}{2}\phi + \pi$ when $s_f = -s_i$). The procedure employs N_η uniformly–sampled values of the η parameter.

Algorithm

Input: $\mathbf{p}_i, \mathbf{p}_f, \mathbf{t}_i, \mathbf{t}_f, N_\eta$

1. transform the Hermite data to canonical form;
2. determine θ_i, θ_f, $\phi = \phi_f$ from expressions (9.1.4)–(9.1.5);
3. compute c_i, s_i and c_f, s_f from (9.1.6);
4. compute $\epsilon = c_i c_f \exp(-i\frac{1}{2}\phi) + s_i s_f \exp(i\frac{1}{2}\phi)$;
5. for $\eta = 2\pi k/N_\eta$ with $k = 0, \ldots, N_\eta - 1$:
   a) compute μ_0, μ_1, f_1 from (9.2.11), (9.2.15), (9.2.12);
   b) compute $c_0, \ldots, c_6$ from (9.2.17);
   c) find a positive real root ρ of equation (9.2.18);
   if no positive real root exists, return to step 5;
   d) compute $\delta_0, \delta_1, \delta_2$ from (9.2.14);
   e) compute $\mathbf{a}_0, \mathbf{a}_1, \mathbf{a}_2$ and $\mathbf{b}_0, \mathbf{b}_1, \mathbf{b}_2$ from (9.2.20) and (9.2.21);

f) compute f_2 from (9.2.23) — if $f_2 \leqslant 0$ return to step 5;

g) determine γ from expression (9.2.22);

h) compute $\alpha_0, \alpha_1, \alpha_2$ and $\beta_0, \beta_1, \beta_2$ from (9.2.19)–(9.2.21);

i) construct the hodograph (3.2.2) from $\boldsymbol{\alpha}(t)$ and $\boldsymbol{\beta}(t)$;

j) transform to original coordinates by inverting step 1.

Output: a set of RRMF quintics interpolating the Hermite data, corresponding to the chosen η values.

9.3 NUMERICAL RESULTS

The numerical results show that the η, ρ values can significantly influence the shape of the resulting RRMF interpolant. In computing the following examples, we used the MATLAB function `roots` to solve (9.2.18). The Bernstein coefficients of the polynomials $\boldsymbol{\alpha}(t)$, $\boldsymbol{\beta}(t)$, $\mathbf{w}(t)$ are quoted to five significant digits.

Example 9.1. Figure 9.2 shows two RRMF quintic interpolants to the data

$$\mathbf{p}_0 = (0,0,0), \qquad \mathbf{p}_1 = (1,1,1), \qquad \mathbf{t}_0 = \frac{(1,0,1)}{\sqrt{2}}, \qquad \mathbf{t}_1 = \frac{(0,1,1)}{\sqrt{2}},$$

together with their Bézier control polygons. After transforming this data to canonical form, the coefficients of the $\boldsymbol{\alpha}(t)$, $\boldsymbol{\beta}(t)$, $\mathbf{w}(t)$ polynomials are

$$\begin{aligned}
&\alpha_0 = 1.4194, \quad &&\alpha_1 = -0.7920 + 0.4058\,i, \quad &&\alpha_2 = -0.9158 + 2.5605\,i,\\
&\beta_0 = 0.4512, \quad &&\beta_1 = 1.1392 + 0.7361\,i, \quad &&\beta_2 = -0.5593 - 0.6590\,i,\\
&w_0 = 1.0, \quad &&w_1 = -0.2751 + 0.4094\,i, \quad &&w_2 = 1.1863 + 1.5044\,i,
\end{aligned}$$

for the curve on the left with $(\eta, \rho) = (5.2000, 1.9158)$, and

$$\begin{aligned}
&\alpha_0 = 1.5363, \quad &&\alpha_1 = 1.1372 + 0.4334\,i, \quad &&\alpha_2 = 0.7595 + 1.2735\,i,\\
&\beta_0 = 0.4883, \quad &&\beta_1 = -0.0461 - 0.2865\,i, \quad &&\beta_2 = -0.4712 + 0.0067\,i,\\
&w_0 = 1.0, \quad &&w_1 = 0.6637 + 0.2024\,i, \quad &&w_2 = 0.6024 + 0.7542\,i,
\end{aligned}$$

for the curve on the right with $(\eta, \rho) = (4.3250, 0.9652)$. Both cases satisfy (6.2.2). The corresponding values of the shape integrals (8.6.1) introduced in the previous chapter are

$$L = 2.3259, \quad E = 44.509, \quad E_{RMF} = 22.856,$$

for the curve on the left, and

$$L = 1.9070, \quad E = 5.7495, \quad E_{RMF} = 1.4641,$$

for the curve on the right. Figure 9.3 shows the variation of the ERF and RMF along the RRMF quintic on the right in Figure 9.2.

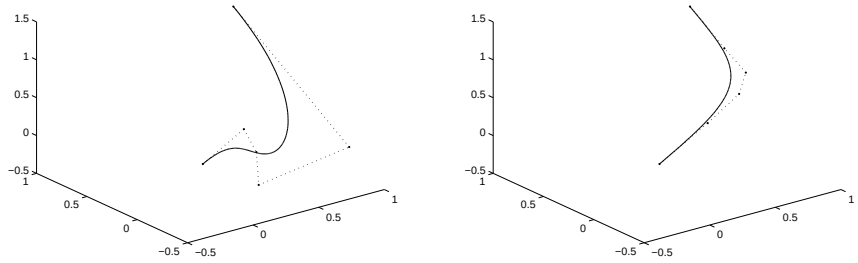

Figure 9.2: The RRMF quintic interpolants of Example 1, with Bézier control polygons.

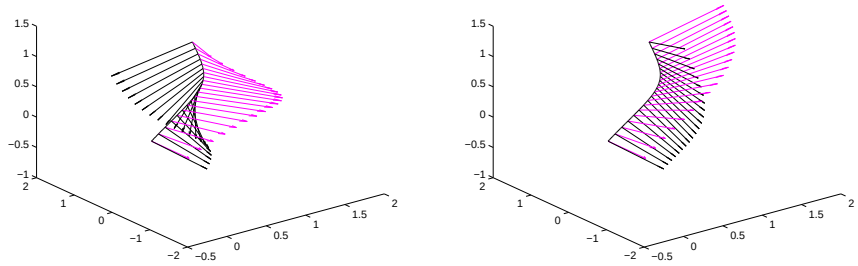

Figure 9.3: Comparison of the ERF (left) and RMF (right) along the RRMF quintic shown on the right in Figure 9.2. For clarity, the unit tangent vector is omitted from the plots.

Example 9.2. Figure 9.4 shows two RRMF quintic interpolants to the data

$$\mathbf{p}_0 = (0,0,0), \qquad \mathbf{p}_1 = (1,0,0), \qquad \mathbf{t}_0 = \frac{(1,1,0)}{\sqrt{2}}, \qquad \mathbf{t}_1 = \frac{\mathbf{d}_1}{|\mathbf{d}_1|},$$

where $\mathbf{d}_1 = (0.2, 0.2, 0.4057)$, together with their Bézier control polygons. In this case, the coefficients of the $\boldsymbol{\alpha}(t)$, $\boldsymbol{\beta}(t)$, $\mathbf{w}(t)$ polynomials are

$$\begin{aligned}
\boldsymbol{\alpha}_0 &= 1.9240, & \boldsymbol{\alpha}_1 &= 0.3403 - 0.9857\,\mathrm{i}, & \boldsymbol{\alpha}_2 &= -0.8882 - 1.2811\,\mathrm{i},\\
\boldsymbol{\beta}_0 &= 0.7970, & \boldsymbol{\beta}_1 &= 0.1805 + 1.4013\,\mathrm{i}, & \boldsymbol{\beta}_2 &= -1.0041 + 0.1499\,\mathrm{i},\\
\mathbf{w}_0 &= 1.0, & \mathbf{w}_1 &= 0.1841 - 0.1798\,\mathrm{i}, & \mathbf{w}_2 &= 0.7110 - 0.5408\,\mathrm{i},
\end{aligned}$$

for the curve on the left with $(\eta, \rho) = (4.2000, 0.8933)$, and

$$\begin{aligned}
\boldsymbol{\alpha}_0 &= 2.0292, & \boldsymbol{\alpha}_1 &= 0.8559 - 0.4150\,\mathrm{i}, & \boldsymbol{\alpha}_2 &= -0.7008 - 1.0107\,\mathrm{i},\\
\boldsymbol{\beta}_0 &= 0.8405, & \boldsymbol{\beta}_1 &= -0.7890 + 1.0190\,\mathrm{i}, & \boldsymbol{\beta}_2 &= -0.7921 + 0.1183\,\mathrm{i},\\
\mathbf{w}_0 &= 1.0, & \mathbf{w}_1 &= 0.2226 + 0.0030\,\mathrm{i}, & \mathbf{w}_2 &= 0.5319 - 0.4045\,\mathrm{i},
\end{aligned}$$

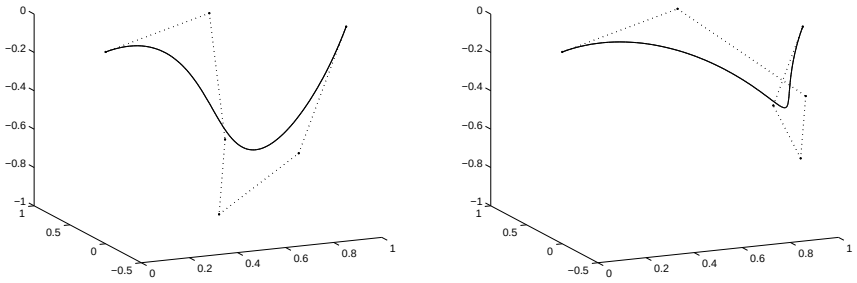

Figure 9.4: The RRMF quintic interpolants of Example 2, with Bézier control polygons.

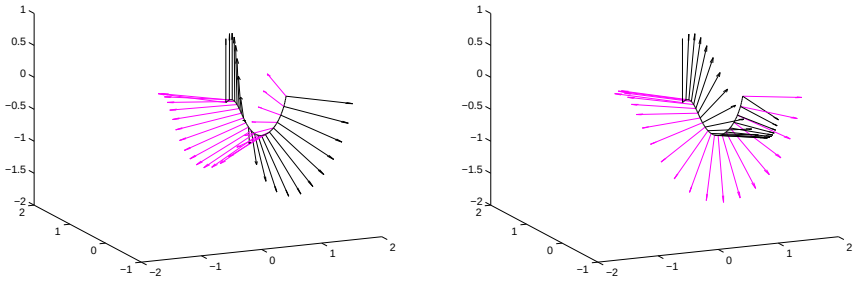

Figure 9.5: Comparison of the ERF (left) and RMF (right) along the RRMF quintic shown on the left in Figure 9.4. For clarity, the unit tangent vector is omitted in these plots.

for the curve on the right with $(\eta, \rho) = (4.2000, 0.6682)$. Both curves satisfy (6.2.2). The values of the shape integrals are

$$L = 2.1610\,, \quad E = 15.806\,, \quad E_{RMF} = 12.807$$

for the curve on the left, and

$$L = 1.9263\,, \quad E = 19.945\,, \quad E_{RMF} = 15.998\,,$$

for the curve on the right. Figure 9.5 shows the variation of the ERF and RMF along the RRMF quintic on the left in Figure 9.4.

Example 9.3. In the final example, we consider data obtained by sampling the circular helix $\mathbf{r}(t) = (\sin(t), \cos(t), t)$ at ten equidistant points on $t \in [0, \frac{9}{2}\pi]$. The resulting G^1 RRMF quintic interpolants are illustrated in Figure 9.6.

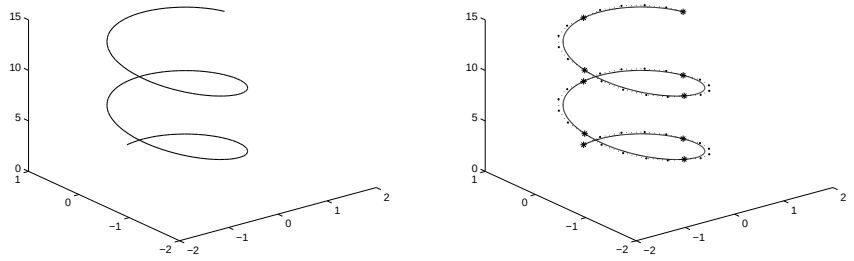

Figure 9.6: A piecewise G^1 RRMF quintic interpolant (right) to Hermite data sampled from the circular helix (left). For each spline segment (delimited by the * symbols) the RRMF quintic Hermite interpolant is shown together with its Bézier control polygon.

9.4 GEOMETRICAL SIGNIFICANCE OF THE FREE ANGULAR PARAMETER

The rational RMAF $(\mathbf{a}_1(t), \mathbf{a}_2(t), \mathbf{a}_3(t))$ can be expressed according to (6.1.2) in terms of the ERF (6.1.1) and the complex polynomial $\mathbf{w}(t)$ defined in (9.1.1) as follows

$$\begin{aligned}
\mathbf{a}_1(t) &= \mathbf{e}_1(t)\,, \\
\mathbf{a}_2(t) &= \frac{1}{|\mathbf{w}(t)|^2}\,\left[\mathrm{Re}\,(\mathbf{w}^2(t))\,\mathbf{e}_2(t) - \mathrm{Im}\,(\mathbf{w}^2(t))\,\mathbf{e}_3(t)\right]\,, \\
\mathbf{a}_3(t) &= \frac{1}{|\mathbf{w}(t)|^2}\,\left[\mathrm{Im}\,(\mathbf{w}^2(t))\,\mathbf{e}_2(t) + \mathrm{Re}\,(\mathbf{w}^2(t))\,\mathbf{e}_3(t)\right]\,.
\end{aligned} \tag{9.4.1}$$

Hence, from (6.1.1) and (9.4.1), we can write the ERAF and RMAF vectors at the two end-point as

$$\begin{aligned}
\mathbf{e}_1(t_j) &= \frac{(\,|\boldsymbol{\alpha}_j|^2 - |\boldsymbol{\beta}_j|^2\,,\, 2\,\mathrm{Re}\,(\boldsymbol{\alpha}_j\overline{\boldsymbol{\beta}}_j)\,,\, 2\,\mathrm{Im}\,(\boldsymbol{\alpha}_j\,\overline{\boldsymbol{\beta}}_j)\,)}{|\boldsymbol{\alpha}_j|^2 + |\boldsymbol{\beta}_j|^2}\,, \\
\mathbf{e}_2(t_j) &= \frac{(-2\,\mathrm{Re}\,(\boldsymbol{\alpha}_j\,\boldsymbol{\beta}_j)\,,\, \mathrm{Re}\,(\boldsymbol{\alpha}_j^2 - \boldsymbol{\beta}_j^2)\,,\, \mathrm{Im}\,(\boldsymbol{\alpha}_j^2 + \boldsymbol{\beta}_j^2)\,)}{|\boldsymbol{\alpha}_j|^2 + |\boldsymbol{\beta}_j|^2}\,, \\
\mathbf{e}_3(t_j) &= \frac{(\,2\,\mathrm{Im}\,(\boldsymbol{\alpha}_j\,\boldsymbol{\beta}_j)\,,\, -\mathrm{Im}\,(\boldsymbol{\alpha}_j^2 - \boldsymbol{\beta}_j^2)\,,\, \mathrm{Re}\,(\boldsymbol{\alpha}_j^2 + \boldsymbol{\beta}_j^2)\,)}{|\boldsymbol{\alpha}_j|^2 + |\boldsymbol{\beta}_j|^2}\,,
\end{aligned} \tag{9.4.2}$$

and

$$\begin{aligned}
\mathbf{a}_1(t_j) &= \mathbf{e}_1(t_j)\,, \\
\mathbf{a}_2(t_j) &= \frac{1}{|\mathbf{w}_j|^2}\,\left[\mathrm{Re}\,(\mathbf{w}_j^2)\,\mathbf{e}_2(t_j) - \mathrm{Im}\,(\mathbf{w}_j^2)\,\mathbf{e}_3(t_j)\right]\,, \\
\mathbf{a}_3(t_j) &= \frac{1}{|\mathbf{w}_j|^2}\,\left[\mathrm{Im}\,(\mathbf{w}_j^2)\,\mathbf{e}_2(t_j) + \mathrm{Re}\,(\mathbf{w}_j^2)\,\mathbf{e}_3(t_j)\right]\,,
\end{aligned} \tag{9.4.3}$$

with $j = 0$ or $j = 2$ and $t_0 = 0$, $t_2 = 1$.

When $j = 0$, setting $\mathbf{w}_0 = 1$ as in (9.1.2) and substituting $\boldsymbol{\alpha}_0, \boldsymbol{\beta}_0$, as defined in equations (9.2.19) into the above relations yields

$$\mathbf{e}_1(0) = (c_i^2 - s_i^2,\, 2\,c_i s_i, 0)\,, \quad \mathbf{e}_2(0) = (-2\,c_i s_i,\, c_i^2 - s_i^2,\, 0)\,, \quad \mathbf{e}_3(0) = (0,\, 0,\, 1)$$

and

$$\mathbf{a}_1(0) = \mathbf{e}_1(0)\,, \qquad \mathbf{a}_2(0) = \mathbf{e}_2(0)\,, \qquad \mathbf{a}_3(0) = \mathbf{e}_3(0)\,.$$

This means that for the parameter value $t = 0$ the RMF coincides with the ERF and does not depend on the free angular parameter η. On the other side, when $j = 2$, setting

$$\mathbf{z} = \frac{\mathbf{w}_2^2}{|\mathbf{w}_2|^2}\,,$$

and substituting equations (9.4.2) into (9.4.3) yields

$$\begin{aligned}
\mathbf{a}_1(1) &= \frac{(\,|\boldsymbol{\alpha}_2|^2 - |\boldsymbol{\beta}_2|^2\,,\, 2\,\mathrm{Re}\,(\boldsymbol{\alpha}_2\overline{\boldsymbol{\beta}}_2)\,,\, 2\,\mathrm{Im}\,(\boldsymbol{\alpha}_2\,\overline{\boldsymbol{\beta}}_2)\,)}{|\boldsymbol{\alpha}_2|^2 + |\boldsymbol{\beta}_2|^2}\,,\\
\mathbf{a}_2(1) &= \frac{(-2\,\mathrm{Re}\,(\overline{\mathbf{z}}\,\boldsymbol{\alpha}_2\,\boldsymbol{\beta}_2)\,,\, \mathrm{Re}\,(\overline{\mathbf{z}}\,(\boldsymbol{\alpha}_2^2 - \boldsymbol{\beta}_2^2))\,,\, \mathrm{Im}\,(\overline{\mathbf{z}}\,(\boldsymbol{\alpha}_2^2 + \boldsymbol{\beta}_2^2))\,)}{|\boldsymbol{\alpha}_2|^2 + |\boldsymbol{\beta}_2|^2}\,,\\
\mathbf{a}_3(1) &= \frac{(\,2\,\mathrm{Im}\,(\overline{\mathbf{z}}\,\boldsymbol{\alpha}_2\,\boldsymbol{\beta}_2)\,,\, -\mathrm{Im}\,(\overline{\mathbf{z}}\,(\boldsymbol{\alpha}_2^2 - \boldsymbol{\beta}_2^2))\,,\, \mathrm{Re}\,(\overline{\mathbf{z}}\,(\boldsymbol{\alpha}_2^2 + \boldsymbol{\beta}_2^2))\,)}{|\boldsymbol{\alpha}_2|^2 + |\boldsymbol{\beta}_2|^2}\,.
\end{aligned} \tag{9.4.4}$$

Now, substituting $\boldsymbol{\alpha}_2, \boldsymbol{\beta}_2$ as defined in equations (9.2.19) into the expression for $\mathbf{w}_2$ reported in (9.1.2), gives

$$\mathbf{w}_2 = \rho\,\overline{\mu}_0\,\exp(-\mathrm{i}\,\eta),$$

and consequently

$$\mathbf{z} = \frac{\mathbf{w}_2^2}{|\mathbf{w}_2|^2} = \overline{\mu}_0^2\,\exp(-\mathrm{i}\,2\eta)\,.$$

Hence equations (9.4.4) becomes

$$\begin{aligned}
\mathbf{a}_1(1) &= \big(c_f^2 - s_f^2,\, 2\,c_f s_f\,\cos\phi,\, 2\,c_f s_f\,\sin\phi\big)\,,\\
\mathbf{a}_2(1) &= \big(-2\,c_f s_f\,\cos 2\eta\,,\, (c_f^2 - s_f^2)\,\cos\phi\cos 2\eta - \sin\phi\sin 2\eta\,,\\
&\qquad (c_f^2 - s_f^2)\,\sin\phi\cos 2\eta + \cos\phi\sin 2\eta\big)\,,\\
\mathbf{a}_3(1) &= \big(2\,c_f s_f\,\sin 2\eta\,, -(c_f^2 - s_f^2)\,\cos\phi\sin 2\eta - \sin\phi\cos 2\eta,\\
&\qquad -(c_f^2 - s_f^2)\,\sin\phi\sin 2\eta + \cos\phi\cos 2\eta\big)\,.
\end{aligned} \tag{9.4.5}$$

Hence, the residual angular degree of freedom that characterizes G^1 quintic Hermite interpolants is related to the orientation of both the ERF and the RMF corresponding to the parameter value $t = 1$.

Given a unit vector $\mathbf{v} = (v_x, v_y, v_z)$ in the plane orthogonal to $\mathbf{t}_f$, it is possible to find the G^1 RRMF quintic interpolant whose RMF vector $\mathbf{a}_2$ coincides with $\mathbf{v}$ for the parameter value $t = 1$, by choosing the free angular parameter η as follows

$$\eta = \tfrac{1}{2}\arccos\left(-\frac{v_x}{2\,c_f s_f}\right) \qquad \text{or} \qquad \eta = \pi - \tfrac{1}{2}\arccos\left(-\frac{v_x}{2\,c_f s_f}\right).$$

CLOSURE

MOVING FRAMES ON SPACE CURVES

Adapted and *directed* orthonormal frames on space curves are characterized by the fact that one frame vector corresponds to a fixed unit direction while the other two frame vectors span the *normal* and *image* plane, respectively. Adapted frames — whose fixed direction coincides with the curve unit tangent at each curve point — are a natural choice in, for example, specifying the motion of a rigid body, in which a principal axis of the object remains aligned with its trajectory, or in constructing a swept surface through the motion of a profile curve along a three–dimensional path. Directed frames — whose fixed direction corresponds to the unit polar vector from the origin to each curve point — may offer a useful camera orientation control strategy in applications such as the navigation of virtual environments, interactive computer games, and endoscopic surgery imaging, as an alternative to the usual maintenance of vertical orientation.

To introduce the idea of directed frames (Chapter 2), it is shown that the basic theory is equivalent to the established theory for adapted frames (Chapter 1) if one replaces the given space curve by its anti–hodograph (i.e., indefinite integral). A special instance, the Frenet directed frame, is identified by analogy with the most familiar adapted frame — the classical Frenet frame — and motivates the introduction of the polar curvature and polar torsion of space curves.

To avoid an undesirable rotation of the basis vector in the normal or image plane, the construction of rotation–minimizing frames (RMFs), whose angular velocity vector maintains a vanishing component along the curve tangent or polar vector, is of practical interest. Since, on replacing a curve by its anti–hodograph, the theory of rotation–minimizing directed frames (RMDFs) coincides with that of rotation–minimizing adapted frames (RMAFs), the RMDF was shown to be related to the Frenet directed frame, through an angular displacement function specified by the integral of the polar torsion multiplied for the radial distance of each curve point from the origin. For general polynomial or rational curves, the torsion of a curve and its anti–hodograph are both rational in the curve parameter, but since the corresponding parametric speeds are *square roots* of polynomials, we cannot, in general, obtain a closed form reduction of this integral. For the special family of *Pythagorean–hodograph* (PH) curves (Chapter 3), the integral which defines RMAFs admits a closed–form evaluation by the partial fraction expansion of a rational function. By analogy, we introduced the class of *Pythagorean* (P) curves (Chapter 7), for which the polar parametric speed is a polynomial in the curve parameter and the integral defining RMDFs is thus rational, allowing their exact computation.

CURVES WITH RATIONAL MOVING FRAMES

Rational forms are always preferred in computer–aided geometric design whenever possible, since they are exactly compatible with the representation schemes of most CAD systems and permit efficient computations. In general, however, both Frenet frames and rotation–minimizing frames are not rational — even for PH and P curves. These facts have motivated recent interest in two special class of polynomial space curves — curves with rational Frenet frames and the set of polynomial curves with rational RMFs.

A comprehensive treatment of the theory of "double" PH curves and of helical polynomial curves, in terms of the complementary quaternion and Hopf map representations, has been presented. Such DPH curves possess the attractive distinguishing property that their Frenet adapted frames, and curvature and torsion functions, have a rational dependence on the curve parameter, and they incorporate all *helical* polynomial curves. A complete categorization of *double* Pythagorean–hodograph (DPH) curves of degree 3, 5, and 7 has been presented, together with algorithms for their construction and a representative selection of computed examples (Chapter 4). All spatial PH cubics are DPH curves — they are also helical, and admit simple characterizations in terms of the Bézier control polygon geometry [43]. As noted in [4], the DPH curves of degree 5 correspond to the *helical* spatial PH quintics, discussed in [4, 37]. We therefore focused on the degree 7 DPH curves, which admit both helical and non–helical instances [4]. In particular, the Hopf map formulation of the DPH condition — specified in terms of two complex polynomials — was invoked to categorize the degree 7 DPH curves in terms of the possible combinations of the degrees for the real polynomial and the complex polynomial which appear. For each category of the degree 7 DPH curves, a system of equations and compatibility constraints was derived, whose solutions facilitate construction of representative curves.

For the helical DPH curves, a more intuitive construction — based on the approach of Monterde [70] that uses inverse stereographic projection of a line/-circle to generate a circular tangent indicatrix — was also described (Chapter 5). Starting from lines/circles parameterized in terms of rational linear complex functions, all higher–order representations are generated by multiplying the numerator and denominator by a complex polynomial, by a (real) non–linear rational re–parameterization, or by a combination of these schemes. Moreover, simple criteria were formulated to distinguish between helical and non–helical degree 7 DPH curves in each category.

We note that the construction algorithms for degree 7 DPH curves described herein are mostly algebraic in character, and hence do not offer much insight into the shape properties of the resulting curves. For geometric design applications, it would be desirable to formulate more geometrically–intuitive constructions, such as Hermite interpolation — such algorithms are a fruitful topic for further research.

The existence of polynomial space curves with rational RMAFs (for brevity, RRMF curves) is investigated, using the Hopf map representation for PH space curves (Chapter 6). The known result that all RRMF cubics are degenerate (linear or planar) curves is easily deduced in this representation. The existence of non–degenerate RRMF quintics is newly demonstrated through a constructive process, involving simple algebraic constraints on the coefficients of two complex polynomials that are sufficient and necessary for any PH quintics to admit a rational RMAF. The approach to characterizing RRMF quintics presented herein permits extensions to the characterization of RRMF curves of degree 7 or higher.

In view of the above mentioned *adapted–directed* analogy of a curve with its anti–hodograph, much of the established theory for the PH curves can be adapted to the construction and analysis of P curves. Similarly, the theory of double PH curves, can be modified to define double P curve, having rational Frenet directed frames and polar curvature and torsion functions, or curves with rational RMDFs (Chapter 7).

APPLICATION ALGORITHMS

Several criteria have been proposed for determining the two free parameters inherent in the spatial PH quintic Hermite interpolation problem, and their performance has been tested through some computed examples (Chapter 8). Conditions on the Hermite data for the existence of PH cubic interpolants were identified, and the selection criteria were designed to yield such cubics when possible. Furthermore, it was proved that four helical PH quintic Hermite interpolants always exist, and that they represent extrema of the arc length (dependent on only one of the free parameters).

A method for computing quintic RRMF curves that interpolate spatial G^1 Hermite data has been presented in Chapter 9. Such curves are useful in applications such as motion control, animation, and swept surface constructions. The method involves one free angular parameter, that can strongly influence the curve shape. A possible geometrical significance of this angular parameter is also given. Numerical experiments show that, for many Hermite data sets, interpolants of good shape can be obtained by the method, but the formulation of an automatic and efficient procedure for their selection is an open problem. Further open problems concern the existence and multiplicity of the interpolants to arbitrary Hermite data, and the identification of reasonable data conditions which may ensure the existence of solutions. Because they are highly non–linear, this problems are non–trivial: we hope to address them more carefully in future studies.

Based on the second RRMF quintics characterization [25], the geometrical construction of PH quintics with rational rotation–minimizing adapted frames via geometric Hermite interpolation can be simplified. Moreover, the G^1 RRMF

interpolation algorithm is modifiable to permit geometric design of rigid body motions using RRMF quintics, through an end–frame interpolation scheme. Some recent progress on this issues is reported in [31].

The basic outlines of two methods for the geometric construction of P curves have also been presented (Chapter 7), but without addressing the problem of optimal choices for the free parameters, since it is non–trivial and beyond our present scope. Starting from [31], the problem of constructing quartic space curves that possess rational rotation–minimizing directed frames by interpolation of initial/final positions and orientations of the associated RMDF could be considered. Noting that P quartics with rational RMDFs form a proper subset of the spatial Pythagoran quartics, characterized by a vector constraint on their coefficient in the quaternion representation, and that C^0 spatial P quartic interpolants possess six free scalar parameters, by fixing two of them with the interpolation of initial/final frame orientations and other three with the vector RRMF condition, we obtain a one–parameter family of solutions. The analysis of this problem could be the subject of future research.

Part IV

APPENDICES

A

20 YEARS OF PYTHAGOREAN–HODOGRAPH CURVES

The idea of incorporating a special algebraic structure in the Cartesian components of the curve first derivative in order to let their sum of squares be the perfect square of a polynomial was introduced in [42]. Starting from this first study a broad research activity has been devoted to the theory of Pythagorean–hodograph curves and their consequent application for the solution of several geometric design problems.

This appendix briefly summarizes the most important results related to *planar* and *spatial* PH curves in Section A.1 and A.2, respectively. A glance to the generalization of the Pythagorean condition in the Minkowski space is given in Section A.3. Finally, Section A.4 briefly reviews the main results related to some possible extension of these concepts.

A.1 PLANAR PH CURVES

Planar polynomial curves $\mathbf{r}(t) = (x(t), y(t))$ that satisfy

$$|\,\mathbf{r}'(t)\,|^2 \;=\; x'^2(t) + y'^2(t) \;=\; \sigma^2(t)\,, \tag{A.1.1}$$

for some polynomial $\sigma(t)$ are known as Pythagorean–hodograph curves. In order to satisfy condition (A.1.1), Farouki and Sakkalis noted in [42] that the three polynomials $x'(t)$, $y'(t)$ and $\sigma(t)$ must comprise a Pythagorean triple. Hence, according to the result of Kubota [66], these polynomials must be expressible in terms of other real polynomials $u(t)$, $v(t)$ and $h(t)$ in the form

$$x'(t) \;=\; h(t)\left[u^2(t) - v^2(t)\right], \qquad y'(t) \;=\; 2\,h(t)\,u(t)\,v(t)\,, \tag{A.1.2}$$

with corresponding polynomial parametric speed

$$\sigma(t) \;=\; h(t)\left[u^2(t) + v^2(t)\right]. \tag{A.1.3}$$

If $u(t), v(t)$ have a common factor, this can be included into $h(t)$, so we may assume without loss of generality that the two polynomials $u(t)$ and $v(t)$ are relatively prime. Moreover, if $u(t)$ and $v(t)$ are of degree m at most and $p = \deg h(t)$, the PH curve $\mathbf{r}(t)$ obtained by integrating the hodograph components (A.1.2) is of degree $n = p + 2m + 1$. In the case of *primitive* hodograph, characterized by the fact $\gcd(x'(t), y'(t)) = \text{constant}$, which necessarily implies $\deg h(t) = 0$, PH curves are always of *odd* degree $n = 2m + 1$. In order to avoid irregular curve points where the hodograph vanishes, primitive hodographs are usually considered in all the application algorithms.

Planar Pythagorean–hodographs admit [20] a compact description using the algebra of complex numbers. The PH condition is equivalent to the requirement that the hodograph $\mathbf{r}'(t)$ can be expressed in terms of the square of the complex polynomial $\mathbf{w}(t) = u(t) + i\,v(t)$ as follows

$$\mathbf{r}'(t) \;=\; h(t)\,\mathbf{w}^2(t) \;=\; h(t)\left[u^2(t) - v^2(t) + i\,2\,u(t)v(t)\right] .$$

By using this form is easy to verify the *rotation invariance* of the PH property (A.1.1). If $\exp(i\,\theta) = \cos(\theta) + i\sin\theta$ is any unit complex number, the hodograph (A.1.2) after a rotation through angle θ is given by

$$\begin{aligned}\mathbf{r}'(t) = \exp(i\,\theta)\,h(t)\,\mathbf{w}^2(t) \;&=\; h(t)\left[\cos\theta(u^2 - v^2) - \sin\theta\,2\,uv\right] \\ &+ i\,h(t)\left[\cos\theta\,2\,uv + \sin\theta(u^2 - v^2)\right] ,\end{aligned}$$

and condition (A.1.1) is still verified.

Although PH curves of degree n have just $n+3$ degrees of freedom[1] (compared to $2n+2$ for general degree–n polynomial curves), the Pythagorean condition (A.1.1) ensures that PH plane curves have the following distinctive properties:

- polynomial arc–length functions $s(t) = \int_0^t |\,\mathbf{r}'(t)\,|$;
- unit tangent $\mathbf{t}$, normal unit vector $\mathbf{n}$, and signed curvature κ all rational;
- rational offset curves $\mathbf{r}_d(t) = \mathbf{r}(t) + d\,\mathbf{n}(t)$, $d \in \mathbb{R}$;
- closed–form expression for the bending energy [21], given by the integral of the curvature with respect to arc length and commonly used as "fairness" measure.

Obviously, working in floating point arithmetic, we necessarily need to reduce the intrinsic numerical propagation errors of any computation at a minimimum level. Hence, the choice of the Bézier form, which gives rise to algorithms formulated in the Bernstein basis [41], accomplishes not only the representation CAGD standard but also an optimal numerical stability [35]. This preserves the Pythagorean structure of the hodograph components during the execution of the arithmetic operations involved in the several algorithmic procedures, and minimize the error influence on the arc–length or offset functions computation.

Focusing on primitive curves with $h(t) = 1$ and $\gcd(u, v) =$ constant the parametric speed (A.1.3) reduces to $\sigma(t) = u^2(t) + v^2(t)$ and, not having real roots, does not change its sign. By expressing $\sigma(t)$ in the Bernstein basis, the arc length function

$$s(t) \;=\; \int_0^t \sigma(\tau)\,d\tau \quad \text{with} \quad \sigma(t) \;=\; |\mathbf{r}'(t)| \;=\; \sum_{i=0}^{n-1} \sigma_i\, b_i^{n-1}(t)$$

1 Of these $n+3$ degrees of freedom, three can be fixed by choosing the reference coordinate system, and two can be used to select the desired parameterization — see [42] for more detailed comments. Hence, a planar PH curve of degree n exhibits $n-2$ effective degrees of freedom.

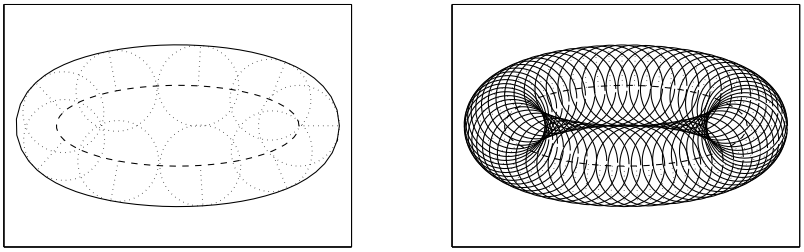

Figure A.1: Left: offset (solid line) at $d = 1$ to an ellipse (dashed line). The offset is tangent to every circle centered on a point along the ellipse. Right: offset at $d = 1$ as the *envelope* of circles whose centers are on the ellipse (dashed line).

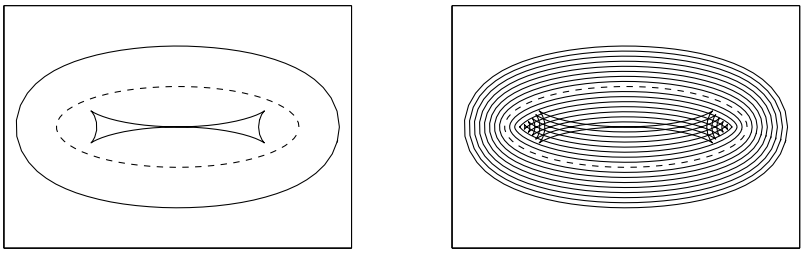

Figure A.2: Left: interior ($d = -1$) and exterior ($d = 1$) offset to an ellipse (dashed line). Right: offset curves to an ellipse (dashed line) at difference distances.

reduces to the polynomial form

$$s(t) = \sum_{i=0}^{n} s_i b_i^n(t), \quad \text{where} \quad s_i = \frac{1}{n} \sum_{j=0}^{i-1} \sigma_i, \quad i = 1, \ldots, n,$$

and $s_0 = 0$, while the total arc–length $L = s(1)$ can be expressed simply as

$$L = \frac{1}{n} \sum_{i=0}^{n-1} \sigma_i .$$

The offset (or parallel) curve (see Figures A.1 and A.2) is the locus of points at a fixed signed distance d from the curve $\mathbf{r}(t) = (x(t), y(t))$ in the direction of the unit normal vector

$$\mathbf{n}(t) = \frac{(y'(t), -x'(t))}{\sqrt{x'^2(t) + y'^2(t)}} .$$

Offset curves are commonly used in computer numerical controlled (CNC) machining to describe the cutter trajectory with respect to the cut shape on the working piece, and serve as an effective tool in many computer graphics applications which require tolerance analysis tecniques. The problem is that their construction is a real computational challenge. Even the offset of a simple polynomial curve may result in complicated equations, which preclude efficient numerical computations systematically required in computer aided design context. Hence, several schemes have been proposed to approximate offsets of a given curve in terms of piecewise polynomial or rational functions, see for example [50, 60, 61, 82] or the more recent works [1, 83, 91].

In the case of Pythagorean–hodograph curves, the unit normal vector simply reduces to $\mathbf{n}(t) = (y'(t), -x'(t))/\sigma(t)$, and consequently offset curves $\mathbf{r}_d(t) = (x_d(t), y_d(t))$ are precisely expressable in terms of rational functions of the representation parameter as

$$x_d(t) = x(t) + \frac{dy'(t)}{\sigma(t)}, \qquad y_d(t) = y(t) - \frac{dx'(t)}{\sigma(t)},$$

meeting the standard form of representation of modern CAD systems and avoiding the need of approximation schemes. Application of the PH curves in the CNC context have been studied in many papers, see for example [45, 95, 98, 101].

The algebraic characterization of the simplest example of primitive planar PH curves — the cubic case — was given in [42] together with a geometrical description of the corresponding Bézier control polygon. The double point of any planar PH cubic, which can not exhibit any real inflection point, is always a *crunode*, i.e., a self–intersection of the curve so that the two branches of the planar path have distinct real tangents. Once the coordinate system is fixed so that the crunode is placed at the origin and the two parametric equations for the x and y components share the factor $(t^2 - 1)$, any planar PH cubic can be simply defined by the parametric form

$$x(t) = r\,(t^2 - 1), \qquad y(t) = \pm \tfrac{1}{\sqrt{3}}\, r\, t\, (t^2 - 1) \tag{A.1.4}$$

which describes the *Tschirnhausen cubic* — also known as *l'Hopital's cubic* or *trisectrix of Catalan* [67] (see Figure A.3). Now, since planar PH cubics show only one effective degree of freedom (see the last footnote), which simply corresponds to different choices of the factor r in (A.1.4), as compared to the three free parameters of general polynomial cubics, they inherently preclude sufficient flexibility for free–form design application algorithms. Consequently, already from the beginning of the PH research activity, the investigation on higher–order PH curves revealed itself to be essential. In particular, the role played by standard cubics for the solution of practical interpolation algorithm is here re–covered by PH quintics. These two different classes of polynomial planar curves exhibit similar degree of freedom to modify the curve shape

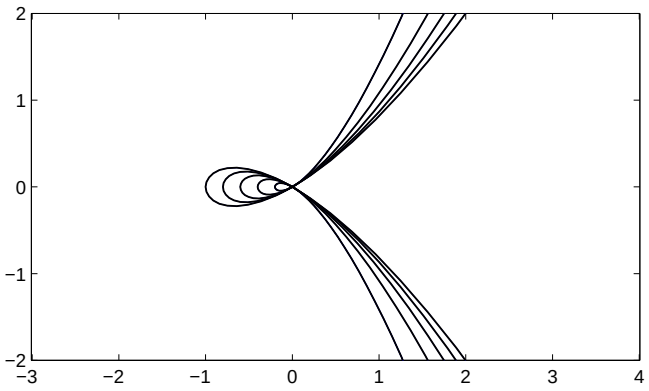

Figure A.3: The Tschirnhausen cubic (A.1.4) for the parameter r values $0.2, 0.4, 0.6, 0.8, 1$.

or satisfy prescribed geometrical constraints. Nevertheless, if there exists a unique "ordinary" cubic interpolant to given Hermite planar data, the problem of Hermite interpolation by PH curves inherently admits a *multiplicity* of formal solution, and the issue of selecting a "good" or "best" interpolant among the complete set of nominal solutions must be addressed.

Preliminary results on the solution of the first order Hermite interpolation with planar PH quintics were presented in the application–oriented survey [19]. Subsequently [40] introduced a more detailed analysis of the problem. Interpolation of planar first–order Hermite data by PH quintics generically incurs four distinct solutions [40], and a number of method are available to identify the "good" interpolant [9, 40, 74]. These are based upon absolute shape measures, or a comparison with the unique "ordinary" cubic interpolant, and include an *a priori* method for constructing the "good" solution alone, under mild constraints on the Hermite data. These analysis on the construction of PH quintic interpolants show how they succeed in identifying *fair* interpolants with more even curvature profiles when compared with ordinary polynomial curves.

The construction of C^2 PH spline were addressed in [3, 38], while possible solutions of the local G^1 and G^2 Hermite interpolation problems were given in [55] and [54], respectively. Shape-preserving interpolation techniques by G^1 and G^2 PH quintic splines were introduced in [39]. By analogy with the standard B-spline form, a different approach to construct PH spline curves through a control polygon scheme was recently presented in [78].

A.2 SPATIAL PH CURVES

Pythagorean–hodograph space curves were first introduced in [43] as polynomial parametric curves $\mathbf{r}(t)$ whose hodographs $\mathbf{r}'(t) = (x'(t), y'(t), z'(t))$ satisfy the Pythagorean condition

$$|\mathbf{r}'(t)|^2 = x'^2(t) + y'^2(t) + z'^2(t) = \sigma^2(t), \tag{A.2.1}$$

for some polynomial $\sigma(t)$ together with a first sufficient but not necessary characterization. The sufficient and necessary condition analogous of (A.1.2) for planar PH curves was then given in [16] in terms of real polynomials $u(t)$, $v(t)$, $p(t)$, $q(t)$ in the form

$$\begin{aligned} x'(t) &= h(t)\left[u^2(t) + v^2(t) - p^2(t) - q^2(t)\right], \\ y'(t) &= 2\,h(t)\left[u(t)q(t) + v(t)p(t)\right], \\ z'(t) &= 2\,h(t)\left[v(t)q(t) - u(t)p(t)\right], \end{aligned} \tag{A.2.2}$$

with corresponding *polynomial* parametric speed

$$\sigma(t) = h(t)\left[u^2(t) + v^2(t) + p^2(t) + q^2(t)\right].$$

Note that the form (A.2.2) — which is similar to the characterization for Pythagorean quartuples of integers [8] — was given in [16] in a different context, not in the study of PH space curves. A proof of (A.2.2) over more general domains than $\mathbb{R}[t]$ was recently given in [97]. To avoid the possibility of undesirable inflection points, we focus on the odd–degree spatial PH curves of the form (3.0.2) defined by taking $\deg(h(t)) = 0$.

Choi et al. [13] introduced two algebraic characterizations of solutions to condition (A.2.1), based on *quaternions* (see Appendix B) and the *Hopf map* (see Appendix C), that are extremely useful in the construction and analysis of spatial PH curves. The definitions and properties of these representations, and conversions between them, are presented in Chapter 3. The structural invariance of the characterization (A.2.2) for spatial Pythagorean hodographs with respect to spatial rotations was demonstrated in [27].

PH space curves inherit the classical property of planar PH curves of having a polynomial arc length function. Since the spatial Pythagorean condition is necessary for a rational unit tangent, this class of curves includes as proper subset all the spatial polynomial curves with rational adapted frames. Moreover, *pipe* surfaces[2] — the generalization of offset curves to planar loci — based on spatial PH curves as spines, admit rational parameterizations [43].

Geometric Hermite interpolation by spatial PH cubics was addressed in [77]. As in the planar case, a geometrical description of the Bézier control polygon of PH space cubics and their identification as polynomial helical curves were

2 See Section 1.4.

introduced in the original paper [43]. A *helix* is characterized by the fact that its tangent maintains a constant inclination with respect to a fixed unit vector. All spatial PH cubics are helical, but not all PH quintics. As noted in [37], the satisfaction of the helical condition implies that every helical polynomial curve must be a PH curve. It was also implicitly noted in [37] — and more explicitly emphasized in [4] — that for a helical polynomial curve the quantity $|\mathbf{r}'(t) \times \mathbf{r}(t)|$ must be a *polynomial* in t. Thus all helical polynomial curves must exhibit a "double" PH structure (see Chapter 4). However, the sets of helical polynomial curves and of double Pythagorean–hodograph (DPH) curves are not coincident: all helical PH curves are DPH curves, which encompass all PH cubics and all helical PH quintics, although non–helical double PH curves of higher order exist. Hence, the DPH curves encompass all helical polynomial curves as a proper subset.

Monterde recently identified [71] a special subclass of Salkowski curves[3] with rational Frenet adapted frame and, hence, a double Pythagorean–hodograph structure. Even if this novel class of DPH curves is characterized by interesting geometric properties — as in the case of helices — being a one–parameter family of curves defined by a parameter which varies in $\mathbb{Z}$, its practical use in application algorithms could be restrictive.

Interpolation of first–order spatial Hermite data by PH quintics is a non–trivial problem [26], involving a two–parameter family of solutions rather than a finite multiplicity as in the planar case. In this context, the quaternion representation is typically used — although an alternative approach in terms of the Clifford algebra *geometric product* is described in [79]. The two free parameters that characterize spatial PH quintic Hermite interpolants are angular variables and the identification of "good" or "optimal" values for them is a challenging open problem that must be addressed, since the shape of the PH quintic interpolants may depend sensitively on these parameters (see Chapter 8). One approach to specifying the two free angular parameters is to require the PH quintic Hermite interpolant to be a helical curve [37]. As noted in [37], when the tangents at the start and end points are not parallel, the helical quintics can be divided into two (non–disjoint) classes, the *general helices* and *monotone helices*. The monotone helical quintics are not sufficiently flexible to interpolate arbitrary Hermite data [37]. The formal proof for the existence of general helical PH quintic interpolants to arbitrary data is given in [29] (see again Chapter 8). A different approach is proposed in [99] where the asymptotic order of approximation to an analytic curve, from which the data is presumed to have been sampled, is used to select these parameters. The same idea is used in [100] which is concerned with interpolation of second–order Hermite data by spatial PH curves of degree 9 involving a four–parameter family of solutions.

3 A family of curves introduced at the beginning of the 20–th century by E. Salkowski and characterized by constant curvature and non–constant torsion.

A.3 MPH CURVES

The generalization of the PH property within the Minkowski metric led Moon toward the definition of *Minkowski Pythagorean–hodographs* (MPH) which allow precise reconstructions of planar shapes from their *medial–axis transform* (MAT) [72, 73]. The medial axis of a planar domain collects all the centers (x, y) of the circles of maximum radius r which are tangent to the contour in two or more points. The MAT is then constructed by combining the (x, y) coordinates of the medial axis with the corresponding radius value r.

Polynomial curves $(x(t), y(t), r(t))$ in the Minkowski space $\mathbb{R}^{2,1}$ that satisfy

$$x'^2(t) + y'^2(t) - r'^2(t) = \sigma^2(t),$$

for some polynomial $\sigma(t)$ are known as MPH curves. The sufficient and necessary condition analogous to (A.1.2) and (A.2.2) for planar and spatial PH curves, respectively, in terms of four other polynomials was given in [73]. The computation of MAT and offset curves by MPH curves was presented in [11]. The G^1 Hermite interpolation problem by MPH cubics was addressed in [63], while the C^1 Hermite interpolation problem by MPH quintics was recently studied in [64].

As a point (x, y, r) in the Minkowski space $\mathbb{R}^{2,1}$ with two space–like and one time–like coordinates can be mapped to a circle in $\mathbb{R}^2$ with center (x, y) and radius r, a point (x, y, z, r) in the Minkowski space $\mathbb{R}^{3,1}$ with three space–like and one time–like coordinates can be mapped to a sphere in $\mathbb{R}^3$ with center (x, y, z) and radius r. Hence if an MPH curve in $\mathbb{R}^{2,1}$ identifies a one–parameter family of circles, an MPH curve in $\mathbb{R}^{3,1}$ identifies a one–parameter family of spheres whose envelope is a canal surface, see for example [12, 13].

A.4 GENERALIZATIONS

The generalization of the PH property to the *rational* case allows to determine all rational curves whose parametric speed $\sigma(t)$ is a rational function of the parameter [2, 84] and also all the rational surfaces $S(u, v)$ whose normal vector $\mathbf{n}(u, v) = S_u \times S_v / |S_u \times S_v|$, where S_u, S_v denote partial derivatives with respect to u and v, is a rational function of the two parameters [85]. An alternative to these *Pythagorean normal* approaches for identifying surfaces with rational offsets are the patches with a linear field of normal vectors, generally indicated as *LN surfaces*, originally proposed by Jüttler [53] and then further investigated in [57, 88]. Recent related works concern the connection between two-parameter families of spheres and rational offset surfaces [80, 81].

B

QUATERNION DIVISION ALGEBRA

The *algebra of quaternion* is an algebraic system, first invented by William R. Hamilton (1805–1865) in the 19th century, which finds natural applications in different fields of mathematics and physics. Just as planar geometry can be described by means of complex numbers, three–dimensional geometric transformations can be represented with *quaternions*. This effective algebraic tool, necessarily closely connected with animation techniques, is widely used in computer graphics and scientific visualization [48, 92].

In order to properly define the quaternion division algebra, we begin in Section B.1 by briefly reviewing some basic algebra concepts. Section B.2 summarizes basic ideas from the algebra of quaternions, and presents some identities of technical nature that are required in Chapter 8. The relationship between unit quaternions and 3D rotations is then described in Section B.3.

B.1 ALGEBRAIC SYSTEMS OVERVIEW

In abstract algebra, a *field* comprises a set S and two binary operations $+$ and $\cdot$ on S, usually called addition and multiplication, respectively, such that the following axioms hold for all $a, b, c \in S$.

(i) *Associativity*: $(a + b) + c = a + (b + c)$ and $(a \cdot b) \cdot c = a \cdot (b \cdot c)$.

(ii) *Commutativity*: $a + b = b + a$ and $a \cdot b = b \cdot a$.

(iii) *Distributivity of multiplication over addition*: $a \cdot (b + c) = a \cdot b + a \cdot c$.

(iv) *Identity*: there exist two elements $0, 1 \in S$ such that $a + 0 = a \cdot 1 = a$.

(v) *Additive inverse*: for all $a \in S$, there exists $b \in S$ such that $a + b = 0$.

(vi) *Multiplicative inverse*: for all $a \in S$, $a \neq 0$, there exists $c \in S$ such that $a \cdot c = 1$.

The best known fields are the rational numbers $\mathbb{Q}$, real numbers $\mathbb{R}$, complex numbers $\mathbb{C}$, and the field of rational functions, i.e., the field of fractions of polynomials in one indeterminate with coefficients in any given field.

By assuming only part of the above axioms, different algebraic structures arise. For example, if we do not require both the multiplicative identity and the multiplicative inverse, we obtain a *commutative ring* and, if we relax also the commutativity of multiplication, just a *ring*. Obviously any field is also a

commutative ring. Other commutative ring examples are the integers $\mathbb{Z}$ and the polynomial ring in one or more variables with coefficients in another ring. A special class of commutative rings are the *integral domains*, commutative rings without zero divisors and with a multiplicative identity 1 not equal to 0, the additive identity. Again, every field is an integral domain and even the integer $\mathbb{Z}$ or a polynomial ring with coefficients in an integral domain are integral domains.

If we remove the requirement of commutativity of multiplication from the above mentioned properties characterizing the algebraic structure of a field, we obtain a *division ring*, also called a *division algebra* or a *skew field* or even a *non–commutative field*. Quaternions, denoted by the letter $\mathbb{H}$ which stands for Hamilton, are an example of division ring and constitute a non–commutative real normed division algebra[1].

B.2 BASIC QUATERNION ALGEBRA RESULTS

Originally born as extension of complex numbers by the lack of possibility of using only three basis elements to define a division algebra (see for example Section 5.2 in [24]), quaternions are "four–dimensional numbers" of the form

$$\mathcal{A} = a + a_x \mathbf{i} + a_y \mathbf{j} + a_z \mathbf{k}, \tag{B.2.1}$$

where the four coefficients a, a_x, a_y, a_z are real numbers and the *basis elements* 1, $\mathbf{i}$, $\mathbf{j}$, $\mathbf{k}$ satisfy the relations

$$\mathbf{i}^2 = \mathbf{j}^2 = \mathbf{k}^2 = \mathbf{i}\,\mathbf{j}\,\mathbf{k} = -1\,.$$

Here 1 is the usual real unit: its product with $\mathbf{i}$, $\mathbf{j}$, $\mathbf{k}$ leaves them unchanged. Preserving the order of terms in products, we infer from the above that

$$\mathbf{i}\,\mathbf{j} = -\mathbf{j}\,\mathbf{i} = \mathbf{k}, \qquad \mathbf{j}\,\mathbf{k} = -\mathbf{k}\,\mathbf{j} = \mathbf{i}, \qquad \mathbf{k}\,\mathbf{i} = -\mathbf{i}\,\mathbf{k} = \mathbf{j}\,. \tag{B.2.2}$$

Since the products of the basis elements are non–commutative, we have $\mathcal{A}\,\mathcal{B} \neq \mathcal{B}\mathcal{A}$ in general, for any two quaternions $\mathcal{A}$, $\mathcal{B}$. Quaternion multiplication is associative, however, so that $(\mathcal{A}\,\mathcal{B})\mathcal{C} = \mathcal{A}(\mathcal{B}\,\mathcal{C})$ for any three quaternions $\mathcal{A}$,$\mathcal{B}$, $\mathcal{C}$, and each non–zero element has a multiplicative inverse. Thus, Hamilton obtained a skew field and a four–dimensional division algebra over the reals.

The sum of the two elements

$$\mathcal{A} = a + a_x \mathbf{i} + a_y \mathbf{j} + a_z \mathbf{k} \qquad \text{and} \qquad \mathcal{B} = b + b_x \mathbf{i} + b_y \mathbf{j} + b_z \mathbf{k},$$

of $\mathbb{H}$ is simply defined as the sum of the corresponding quaternion components,

$$\mathcal{A} + \mathcal{B} = (a + b) + (a_x + b_x)\,\mathbf{i} + (a_y + b_y)\,\mathbf{j} + (a_z + b_z)\,\mathbf{k}, \tag{B.2.3}$$

1 A division algebra over the reals is a real normed division algebra if it is also a normed vector space $\mathbb{R}^n$, with norm such that: $\|xy\| = \|x\| \cdot \|y\|$ for all x and y in $\mathbb{R}^n$.

and using the basis elements relations (B.2.2) together with the distributivity of addition over multiplication, the quaternion product is given by

$$\begin{aligned}\mathcal{A}\,\mathcal{B} =& (ab - a_x b_x - a_y b_y - a_z b_z) + (a b_x + b a_x + a_y b_z - a_z b_y)\,\mathbf{i} \\ &+ (a b_y + b a_y + a_z b_x - a_x b_z)\,\mathbf{j} + (a b_z + b a_z + a_x b_y - a_y b_x)\,\mathbf{k}\,.\end{aligned} \tag{B.2.4}$$

Regarding $\mathbf{i}$, $\mathbf{j}$, $\mathbf{k}$ as unit vectors in Cartesian coordinates, we may regard $\mathcal{A}$ as comprising "scalar" and "vector" parts, a and $\mathbf{a} = a_x\mathbf{i} + a_y\mathbf{j} + a_z\mathbf{k}$. We write $\mathcal{A} = (a, \mathbf{a})$ — conversely,

$$a \;=\; \mathrm{scal}(\mathcal{A}) \qquad \text{and} \qquad \mathbf{a} \;=\; \mathrm{vect}(\mathcal{A})\,. \tag{B.2.5}$$

Thus, all real numbers and three–dimensional vectors are subsumed as "pure scalar" and "pure vector" quaternions, of the form $(a, \mathbf{0})$ and $(0, \mathbf{a})$, respectively. For brevity, we often denote such quaternions by simply a and $\mathbf{a}$.

The sum and product of the two quaternions $\mathcal{A} = (a, \mathbf{a})$ and $\mathcal{B} = (b, \mathbf{b})$ may be concisely expressed [87] in terms of the familiar vector dot and cross products as

$$\mathcal{A} + \mathcal{B} \;=\; (\,a + b\,,\, \mathbf{a} + \mathbf{b}\,)\,, \tag{B.2.6}$$

$$\mathcal{A}\,\mathcal{B} \;=\; (\,ab - \mathbf{a}\cdot\mathbf{b}\,,\, a\,\mathbf{b} + b\,\mathbf{a} + \mathbf{a}\times\mathbf{b})\,. \tag{B.2.7}$$

The scalar and vector parts are also known as the "real" and "imaginary" parts,

$$a \;=\; \mathrm{Re}(\mathcal{A})\,, \qquad \text{and} \qquad \mathbf{a} = \mathrm{Im}(\mathcal{A})$$

since the square of a "pure imaginary" quaternion $(0, \mathbf{a})$ is always the negative real number $-|\,\mathbf{a}\,|^2$. Obviously, if we may identify $\mathbb{H}$ with $\mathbb{R}^4$, quaternions imaginary parts $\mathbf{a}$ could be seen as elements of $\mathbb{R}^3$, namely $\mathrm{Im}(\mathbb{H}) = \mathbb{R}^3$.

Every quaternion $\mathcal{A} = (a, \mathbf{a})$ has a *conjugate*, $\mathcal{A}^* = (a, -\mathbf{a})$, and a *magnitude* equal to the non–negative real number $|\mathcal{A}|$ defined by

$$|\mathcal{A}|^2 \;=\; \mathcal{A}^*\mathcal{A} \;=\; \mathcal{A}\mathcal{A}^* \;=\; a^2 + |\,\mathbf{a}\,|^2\,. \tag{B.2.8}$$

One can readily verify that the conjugates of products satisfy the rule

$$(\mathcal{A}\,\mathcal{B})^* \;=\; \mathcal{B}^*\mathcal{A}^*\,, \tag{B.2.9}$$

and, consequently,

$$|\mathcal{A}\mathcal{B}| = |\mathcal{A}||\mathcal{B}|\,. \tag{B.2.10}$$

Equation (B.2.8) allows to define *inverse* of any quaternion $\mathcal{A} \neq 0$ as

$$\mathcal{A}^{-1} \;=\; \frac{\mathcal{A}^*}{|\mathcal{A}|^2}\,,$$

so that $\mathcal{A}^{-1}\mathcal{A} = \mathcal{A}\mathcal{A}^{-1} = 1$, and hence the corresponding division operation that characterizes the quaternion ring. Since the product of two quaternions is in general non–commutative, we can distinguish between *left* and *right* division, namely $\mathcal{A}^{-1}\mathcal{B}$ versus $\mathcal{B}\mathcal{A}^{-1}$.

As a direct consequence of the above mentioned quaternion multiplication properties, we quote from [6] the following Lemma.

Lemma B.1. *For any two quaternions* $\mathcal{A} = (a, \mathbf{a})$ *and* $\mathcal{B} = (b, \mathbf{b})$*, we have*

- $\mathcal{A}\mathcal{B} = \mathcal{B}\mathcal{A}$ *if and only if the two real vectors* $\mathbf{a}$ *and* $\mathbf{b}$ *are linearly dependent, i.e.,* $\mathbf{a} \times \mathbf{b} = 0$*. In particular, the reals are the only quaternions that commute with all others.*
- $\mathcal{A}^2 = -1$ *if and only if* $|\mathcal{A}| = 1$ *and* $\mathcal{A} = \mathbf{a}$*. Note that the set of all such* $\mathcal{A}$ *is the usual two–sphere* $S^2 \subset \mathbb{R}^3 = \mathrm{Im}(\mathbb{H})$*.*

B.2.1 *Solutions of the quaternion equation*

Consider the quaternion equation

$$\mathcal{A}\,\mathbf{u}\,\mathcal{A}^* \;=\; \mathbf{d}\,, \tag{B.2.11}$$

where $\mathbf{u}$ is a unit vector, and $\mathbf{d}$ is any non–zero vector not aligned with $-\mathbf{u}$. The quaternion solutions of (B.2.11) comprise a one–parameter family [26], which can be conveniently described in terms of the unit vectors

$$\delta \;=\; \frac{\mathbf{d}}{|\mathbf{d}|} \qquad \text{and} \qquad \mathbf{n} \;=\; \frac{\mathbf{u}+\delta}{|\mathbf{u}+\delta|}\,.$$

Here δ is a unit vector in the direction of $\mathbf{d}$, while $\mathbf{n}$ is the (unit) *bisector* of δ and $\mathbf{u}$. The solutions to (B.2.11) can then be written as

$$\mathcal{A} \;=\; \sqrt{|\mathbf{d}|}\,\mathbf{n}\,\exp(\phi\,\mathbf{u})\,, \tag{B.2.12}$$

where ϕ is a free angular variable, and we invoke the short–hand notation

$$\exp(\phi\,\mathbf{u}) \;=\; \cos\phi \;+\; \sin\phi\,\mathbf{u}\,.$$

Note that, in expression (B.2.12), $\sqrt{|\mathbf{d}|}$ is a scalar, $\mathbf{n}$ is a pure vector quaternion, and $\exp(\phi\,\mathbf{u})$ is a unit quaternion with vector part in the direction of $\mathbf{u}$ (note also that, when a combination of scalars, vectors, and quaternions is simply written in juxtaposition, the *quaternion* product is implied).

For completeness we remark that if $\delta = -\mathbf{u}$ the general solution of (B.2.11) is

$$\mathcal{A} \;=\; \sqrt{|\mathbf{d}|}\;(\delta_1^{\perp}\cos\phi + \delta_2^{\perp}\sin\phi)\,,$$

where the vectors δ, $\delta_1^{\perp}$, $\delta_2^{\perp}$ comprise an orthonormal basis for $\mathbb{R}^3$.

B.2.2 *Some special quaternion identities*

Because they are rather long, the proofs of the following two propositions are presented here. These results are used in the analysis of Chapter 8.

Proposition B.1. *Let* $\mathbf{u}$ *be a unit vector, and* $\mathcal{A}$ *and* $\mathcal{B}$ *be quaternions such that* $\mathbf{d}_{\mathcal{A}} = \mathcal{A}\,\mathbf{u}\,\mathcal{A}^*$ *and* $\mathbf{d}_{\mathcal{B}} = \mathcal{B}\,\mathbf{u}\,\mathcal{B}^*$ *satisfy* $\mathbf{d}_{\mathcal{A}} \times \mathbf{d}_{\mathcal{B}} \neq \mathbf{0}$. *Then the quaternions* $\mathcal{A}$, $\mathcal{B}$, $\mathcal{A}\,\mathbf{u}$, $\mathcal{B}\,\mathbf{u}$ *are linearly independent.*

Proof : We argue by contradiction. First, from the quaternion product rules, one can easily verify that $\mathcal{A}$ and $\mathcal{A}\mathbf{u}$ are linearly independent. Now suppose scalars λ, μ with $\lambda^2 + \mu^2 > 0$ exist, such that $\mathcal{B} = \lambda\mathcal{A} + \mu\mathcal{A}\mathbf{u}$. Then we would have

$$\mathcal{B}\,\mathbf{u}\,\mathcal{B}^* \;=\; (\lambda\mathcal{A} + \mu\mathcal{A}\mathbf{u})\,\mathbf{u}\,(\lambda\mathcal{A}^* - \mu\mathbf{u}\mathcal{A}^*) \;=\; (\lambda^2 + \mu^2)\mathcal{A}\,\mathbf{u}\,\mathcal{A}^*\,,$$

which contradicts the assumption that $\mathbf{d}_{\mathcal{A}} = \mathcal{A}\,\mathbf{u}\,\mathcal{A}^*$ and $\mathbf{d}_{\mathcal{B}} = \mathcal{B}\,\mathbf{u}\,\mathcal{B}^*$ satisfy $\mathbf{d}_{\mathcal{A}} \times \mathbf{d}_{\mathcal{B}} \neq \mathbf{0}$. Therefore, $\mathcal{A}$, $\mathcal{A}\mathbf{u}$, $\mathcal{B}$ must be linearly independent. Likewise, if we assume $\mathcal{B}\mathbf{u} = \lambda\mathcal{A} + \mu\mathcal{A}\mathbf{u}$, we would have $\mathcal{B} = -\lambda\mathcal{A}\mathbf{u} + \mu\mathcal{A}$, and by the preceding argument we infer that $\mathcal{A}$, $\mathcal{A}\mathbf{u}$, $\mathcal{B}\mathbf{u}$ are also linearly independent.

Finally, suppose scalars λ, μ, ν exist, such that $\mathcal{B} = \lambda\mathcal{A} + \mu\mathcal{A}\mathbf{u} + \nu\mathcal{B}\mathbf{u}$. Then we would have $\mathcal{B}\mathbf{u} = \lambda\mathcal{A}\mathbf{u} - \mu\mathcal{A} - \nu\mathcal{B}$, and hence

$$\mathcal{B} \;=\; (\lambda - \mu\nu)\mathcal{A} \;+\; (\mu + \lambda\nu)\mathcal{A}\mathbf{u} \;-\; \nu^2\mathcal{B}\,.$$

But this implies that

$$\mathcal{B} \;=\; \frac{\lambda - \mu\nu}{1+\nu^2}\,\mathcal{A} \;+\; \frac{\mu + \lambda\nu}{1+\nu^2}\,\mathcal{A}\mathbf{u}\,,$$

in contradiction to the conclusion that $\mathcal{A}$, $\mathcal{A}\mathbf{u}$, $\mathcal{B}$ are linearly independent. This completes the proof. ∎

Also, given the unit vector $\mathbf{u}$ and quaternions $\mathcal{A}$, $\mathcal{B}$ we introduce the following four quaternions:

$$\begin{aligned}
\mathcal{Q}_{\mathcal{A}} \;&=\; (q_{\mathcal{A}}, \mathbf{q}_{\mathcal{A}}) \;=\; (\mathcal{A}\mathcal{A}^*\,,\, \mathcal{A}\,\mathbf{u}\,\mathcal{A}^*)\,,\\
\mathcal{Q}_{\mathcal{B}} \;&=\; (q_{\mathcal{B}}, \mathbf{q}_{\mathcal{B}}) \;=\; (\mathcal{B}\mathcal{B}^*\,,\, \mathcal{B}\,\mathbf{u}\,\mathcal{B}^*)\,,\\
\mathcal{V} \;&=\; (\nu, \mathbf{v}) \;=\; (\mathcal{A}\mathcal{B}^* + \mathcal{B}\mathcal{A}^*\,,\, \mathcal{A}\,\mathbf{u}\,\mathcal{B}^* + \mathcal{B}\,\mathbf{u}\,\mathcal{A}^*)\,,\\
\mathcal{S} \;&=\; (s, \mathbf{s}) \;=\; (-\mathcal{A}\,\mathbf{u}\,\mathcal{B}^* + \mathcal{B}\,\mathbf{u}\,\mathcal{A}^*\,,\, \mathcal{A}\mathcal{B}^* - \mathcal{B}\mathcal{A}^*)\,.
\end{aligned} \tag{B.2.13}$$

For these quaternions, the following relations can be verified.

Proposition B.2. *Let* $(q, \mathbf{q})$ *be either* $\mathcal{Q}_{\mathcal{A}}$ *or* $\mathcal{Q}_{\mathcal{B}}$. *Then we have*

$$\mathbf{v}\cdot\mathbf{s} = \nu\,s\,, \quad |\mathbf{v}|^2 - \nu^2 = |\mathbf{s}|^2 - s^2\,, \quad \mathbf{v}\cdot\mathbf{q} = \nu\,q\,, \quad \mathbf{s}\cdot\mathbf{q} = s\,q\,. \tag{B.2.14}$$

Proof : From (B.2.7) the scalar product $\mathbf{v}\cdot\mathbf{s}$ can be written as the quaternion expression $-\frac{1}{2}(\mathbf{vs}+\mathbf{sv})$. Then the first relation in (B.2.14) becomes $\mathbf{vs}+\mathbf{sv} = -(vs+sv)$. Now we have

$$\begin{aligned}\mathbf{vs}+\mathbf{sv} &= (\mathcal{A}\mathbf{u}\mathcal{B}^*\mathcal{A}\mathcal{B}^* - \mathcal{A}\mathbf{u}\mathcal{B}^*\mathcal{B}\mathcal{A}^* + \mathcal{B}\mathbf{u}\mathcal{A}^*\mathcal{A}\mathcal{B}^* - \mathcal{B}\mathbf{u}\mathcal{A}^*\mathcal{B}\mathcal{A}^*)\\ &+ (\mathcal{A}\mathcal{B}^*\mathcal{A}\mathbf{u}\mathcal{B}^* + \mathcal{A}\mathcal{B}^*\mathcal{B}\mathbf{u}\mathcal{A}^* - \mathcal{B}\mathcal{A}^*\mathcal{A}\mathbf{u}\mathcal{B}^* - \mathcal{B}\mathcal{A}^*\mathcal{B}\mathbf{u}\mathcal{A}^*)\\ &= \mathcal{A}\mathbf{u}\mathcal{B}^*\mathcal{A}\mathcal{B}^* - \mathcal{B}\mathbf{u}\mathcal{A}^*\mathcal{B}\mathcal{A}^* + \mathcal{A}\mathcal{B}^*\mathcal{A}\mathbf{u}\mathcal{B}^* - \mathcal{B}\mathcal{A}^*\mathcal{B}\mathbf{u}\mathcal{A}^*.\end{aligned}$$

On the other hand, we also have

$$\begin{aligned}-(vs+sv) &= (\mathcal{A}\mathcal{B}^*\mathcal{A}\mathbf{u}\mathcal{B}^* - \mathcal{A}\mathcal{B}^*\mathcal{B}\mathbf{u}\mathcal{A}^* + \mathcal{B}\mathcal{A}^*\mathcal{A}\mathbf{u}\mathcal{B}^* - \mathcal{B}\mathcal{A}^*\mathcal{B}\mathbf{u}\mathcal{A}^*)\\ &+ (\mathcal{A}\mathbf{u}\mathcal{B}^*\mathcal{A}\mathcal{B}^* + \mathcal{A}\mathbf{u}\mathcal{B}^*\mathcal{B}\mathcal{A}^* - \mathcal{B}\mathbf{u}\mathcal{A}^*\mathcal{A}\mathcal{B}^* - \mathcal{B}\mathbf{u}\mathcal{A}^*\mathcal{B}\mathcal{A}^*)\\ &= \mathcal{A}\mathcal{B}^*\mathcal{A}\mathbf{u}\mathcal{B}^* - \mathcal{B}\mathcal{A}^*\mathcal{B}\mathbf{u}\mathcal{A}^* + \mathcal{A}\mathbf{u}\mathcal{B}^*\mathcal{A}\mathcal{B}^* - \mathcal{B}\mathbf{u}\mathcal{A}^*\mathcal{B}\mathcal{A}^*.\end{aligned}$$

Thus, the first relation in (B.2.14) holds.

Consider now the second relation in (B.2.14). Noting that $|\mathbf{v}|^2$ and $|\mathbf{s}|^2$ amount to the quaternion expressions $-\mathbf{vv}$ and $-\mathbf{ss}$, this relation becomes $-\mathbf{vv}+\mathbf{ss} = v^2 - s^2$. Now we have

$$\begin{aligned}-\mathbf{vv}+\mathbf{ss} &= -(\mathcal{A}\mathbf{u}\mathcal{B}^*\mathcal{A}\mathbf{u}\mathcal{B}^* + \mathcal{A}\mathbf{u}\mathcal{B}^*\mathcal{B}\mathbf{u}\mathcal{A}^* + \mathcal{B}\mathbf{u}\mathcal{A}^*\mathcal{A}\mathbf{u}\mathcal{B}^* + \mathcal{B}\mathbf{u}\mathcal{A}^*\mathcal{B}\mathbf{u}\mathcal{A}^*)\\ &+ (\mathcal{A}\mathcal{B}^*\mathcal{A}\mathcal{B}^* - \mathcal{A}\mathcal{B}^*\mathcal{B}\mathcal{A}^* - \mathcal{B}\mathcal{A}^*\mathcal{A}\mathcal{B}^* + \mathcal{B}\mathcal{A}^*\mathcal{B}\mathcal{A}^*)\\ &= -\mathcal{A}\mathbf{u}\mathcal{B}^*\mathcal{A}\mathbf{u}\mathcal{B}^* - \mathcal{B}\mathbf{u}\mathcal{A}^*\mathcal{B}\mathbf{u}\mathcal{A}^* + \mathcal{A}\mathcal{B}^*\mathcal{A}\mathcal{B}^* + \mathcal{B}\mathcal{A}^*\mathcal{B}\mathcal{A}^*.\end{aligned}$$

On the other hand, we also have

$$\begin{aligned}v^2 - s^2 &= (\mathcal{A}\mathcal{B}^*\mathcal{A}\mathcal{B}^* + \mathcal{A}\mathcal{B}^*\mathcal{B}\mathcal{A}^* + \mathcal{B}\mathcal{A}^*\mathcal{A}\mathcal{B}^* + \mathcal{B}\mathcal{A}^*\mathcal{B}\mathcal{A}^*)\\ &- (\mathcal{A}\mathbf{u}\mathcal{B}^*\mathcal{A}\mathbf{u}\mathcal{B}^* - \mathcal{A}\mathbf{u}\mathcal{B}^*\mathcal{B}\mathbf{u}\mathcal{A}^* - \mathcal{B}\mathbf{u}\mathcal{A}^*\mathcal{A}\mathbf{u}\mathcal{B}^* + \mathcal{B}\mathbf{u}\mathcal{A}^*\mathcal{B}\mathbf{u}\mathcal{A}^*)\\ &= \mathcal{A}\mathcal{B}^*\mathcal{A}\mathcal{B}^* + \mathcal{B}\mathcal{A}^*\mathcal{B}\mathcal{A}^* - \mathcal{A}\mathbf{u}\mathcal{B}^*\mathcal{A}\mathbf{u}\mathcal{B}^* - \mathcal{B}\mathbf{u}\mathcal{A}^*\mathcal{B}\mathbf{u}\mathcal{A}^*.\end{aligned}$$

This establishes the second relation in (B.2.14).

Now consider the remaining two relations in (B.2.14) where, for example, we take $\mathcal{Q} = \mathcal{Q}_{\mathcal{A}}$. Again, we have $\mathbf{v}\cdot\mathbf{q} = -\frac{1}{2}(\mathbf{vq}+\mathbf{qv})$. Thus, the third relation becomes $\mathbf{vq}+\mathbf{qv} = -2vq$. Now, we have

$$\begin{aligned}\mathbf{vq}+\mathbf{qv} &= (\mathcal{A}\mathbf{u}\mathcal{B}^*\mathcal{A}\mathbf{u}\mathcal{A}^* + \mathcal{B}\mathbf{u}\mathcal{A}^*\mathcal{A}\mathbf{u}\mathcal{A}^*) + (\mathcal{A}\mathbf{u}\mathcal{A}^*\mathcal{A}\mathbf{u}\mathcal{B}^* + \mathcal{A}\mathbf{u}\mathcal{A}^*\mathcal{B}\mathbf{u}\mathcal{A}^*)\\ &= \mathcal{A}\mathbf{u}(\mathcal{B}^*\mathcal{A} + \mathcal{A}^*\mathcal{B})\mathbf{u}\mathcal{A}^* - \mathcal{A}\mathcal{A}^*(\mathcal{B}\mathcal{A}^* + \mathcal{A}\mathcal{B}^*)\\ &= -\mathcal{A}\mathcal{A}^*(\mathcal{B}^*\mathcal{A} + \mathcal{A}^*\mathcal{B}) - \mathcal{A}\mathcal{A}^*(\mathcal{B}\mathcal{A}^* + \mathcal{A}\mathcal{B}^*)\\ &= -2\mathcal{A}\mathcal{A}^*\,\mathrm{scal}(\mathcal{B}^*\mathcal{A}) - 2\mathcal{A}\mathcal{A}^*\,\mathrm{scal}(\mathcal{A}\mathcal{B}^*) = -4\mathcal{A}\mathcal{A}^*\,\mathrm{scal}(\mathcal{A}\mathcal{B}^*).\end{aligned}$$

On the other hand, we also have

$$vq = (\mathcal{A}\mathcal{B}^* + \mathcal{B}\mathcal{A}^*)\,\mathcal{A}\mathcal{A}^* = 2\mathcal{A}\mathcal{A}^*\mathrm{scal}(\mathcal{A}\mathcal{B}^*).$$

This establishes the third relation in (B.2.14). Finally, the fourth relation in (B.2.14) can be written as $\mathbf{sq} + \mathbf{qs} = -2sq$. Now we have

$$\begin{aligned}\mathbf{sq} + \mathbf{qs} &= (\mathcal{A}\mathcal{B}^*\mathcal{A}\mathbf{u}\mathcal{A}^* - \mathcal{B}\mathcal{A}^*\mathcal{A}\mathbf{u}\mathcal{A}^*) + (\mathcal{A}\mathbf{u}\mathcal{A}^*\mathcal{A}\mathcal{B}^* - \mathcal{A}\mathbf{u}\mathcal{A}^*\mathcal{B}\mathcal{A}^*)\\ &= \mathcal{A}(\mathcal{B}^*\mathcal{A}\mathbf{u} - \mathbf{u}\mathcal{A}^*\mathcal{B})\mathcal{A}^* - \mathcal{A}\mathcal{A}^*(\mathcal{B}\mathbf{u}\mathcal{A}^* - \mathcal{A}\mathbf{u}\mathcal{B}^*)\\ &= 2\mathcal{A}\mathcal{A}^*\mathrm{scal}(\mathcal{B}^*\mathcal{A}\mathbf{u}) - 2\mathcal{A}\mathcal{A}^*\mathrm{scal}(\mathcal{B}\mathbf{u}\mathcal{A}^*) = 4\mathcal{A}\mathcal{A}^*\mathrm{scal}(\mathcal{A}\mathbf{u}\mathcal{B}^*)\,.\end{aligned}$$

On the other hand, we also have

$$sq = (-\mathcal{A}\mathbf{u}\mathcal{B}^* + \mathcal{B}\mathbf{u}\mathcal{A}^*)\,\mathcal{A}\mathcal{A}^* = -2\mathcal{A}\mathcal{A}^*\mathrm{scal}(\mathcal{A}\mathbf{u}\mathcal{B}^*)\,.$$

Hence, the fourth relation in (B.2.14) is established. ∎

B.3 UNIT QUATERNIONS AND 3D ROTATIONS

If $|\mathcal{A}| = 1$, we say that $\mathcal{A}$ is a *unit* quaternion. Since the product of two unit quaternions is always a unit quaternion, the set of unit quaternions, necessarily of the form

$$\mathcal{U} = (\cos\tfrac{1}{2}\theta, \sin\tfrac{1}{2}\theta\,\mathbf{n})$$

for some angle θ and unit vector $\mathbf{n}$, defines a (non–commutative) *group* under multiplication,

Now, as stated by the Euler's rotation theorem, any 3D rotation may be described by three degrees of freedom. One of them specifies the rotation angle θ, while the remaining two identify the axis of rotation $\mathbf{n}$. Obviously, any rotation can be represented in different forms: the pair $(\theta + 2k\pi, \mathbf{n})$ for any integer k, as well as $(2k\pi - \theta, -\mathbf{n})$, specify the same rotation of $(\theta, \mathbf{n})$. For any pure vector quaternion $\mathbf{q}$ and unit quaternion $\mathcal{U}$, the product $\mathcal{U}\,\mathbf{q}\,\mathcal{U}^*$ always yields a pure vector quaternion. By (B.2.10) the map

$$\mathbf{q} \;\to\; \mathcal{U}\,\mathbf{q}\,\mathcal{U}^* \tag{B.3.1}$$

leave the norm unchanged and, hence preserves the Euclidean scalar product. Moreover by a simple and straightforward calculation, the vector $\mathbf{q}$, regarded as sum of two vectors, the first given by the component of $\mathbf{q}$ along $\mathbf{n}$ and the second by the remaining vector part of $\mathbf{q}$ in the plane orthogonal to $\mathbf{n}$, namely

$$\mathbf{q} = (\mathbf{n}\cdot\mathbf{q})\mathbf{n} + (\mathbf{n}\times\mathbf{q})\times\mathbf{n}\,,$$

is rotated into the vector

$$\mathcal{U}\,\mathbf{q}\,\mathcal{U}^* = (\mathbf{n}\cdot\mathbf{q})\mathbf{n} + \sin\theta\,\mathbf{n}\times\mathbf{q} + \cos\theta\,(\mathbf{n}\times\mathbf{q})\times\mathbf{n}\,,$$

where the component along $\mathbf{n}$ is unchanged and the others move according to $\sin\theta$ and $\cos\theta$ as for planar rotations. This corresponds to a rotation of $\mathbf{q}$ through

PLANAR CASE	SPATIAL CASE
complex numbers	quaternions
$\mathbf{a} = a + ia_x$	$\mathcal{A} = a + a_x\mathbf{i} + a_y\mathbf{j} + a_z\mathbf{k}$
Euler's formula	unit quaternion
$\exp(i\theta) = \cos\theta + i\sin\theta$	$\exp(\theta\,\mathbf{n}) = \cos\theta + \sin\theta\mathbf{n}\,.$
2D rotation of $\mathbf{p}$ through θ	3D rotation of $\mathbf{q}$ through θ about $\mathbf{n}$
$\exp(i\theta)\,\mathbf{p}$	$\exp(\frac{1}{2}\theta\,\mathbf{n})\,\mathbf{q}\;\exp(-\frac{1}{2}\theta\,\mathbf{n})$

Table B.1: Planar and three-dimensional geometry in terms of complex numbers and quaternions. With $\mathbf{p}$ and $\mathbf{q}$ any given 2D or 3D vector — identified with a complex number and a pure vector quaternion, respectively — is indicated.

angle θ about the axis defined by $\mathbf{n}$ [87]. Note also that the unit quaternion $-\mathcal{U} = (-\cos\frac{1}{2}\theta, -\sin\frac{1}{2}\theta\,\mathbf{n})$ specifies a rotation through $2\pi - \theta$ about $-\mathbf{n}$, and thus has exactly the same effect as $\mathcal{U} = (\cos\frac{1}{2}\theta, \sin\frac{1}{2}\theta\,\mathbf{n})$. Finally, we may observe that $\mathcal{U}\mathbf{q}\mathcal{U}^* = \mathbf{q}$ for any $\mathbf{q} \in \operatorname{Im}\mathbb{H}$ if and only if $\mathcal{U} \in \mathbb{R}$, i.e. if $\mathcal{U} = \pm 1$. The quaternion rotation operator may be used in several rotation sequences applications.

There is an intimate connection between quaternions and complex numbers in view of their geometric meaning. As shown in Table B.1, if complex multiplication represent rotations matrices in two dimensions and hence planar rotations, quaternion multiplication represent three-dimension rotations matrices and hence spatial rotations. This geometrical aspect was just the motivation which drove Hamilton to extend the classical complex number theory to quaternions.

C

THE HOPF FIBRATION

The *Hopf map*, discovered by Heinz Hopf (1894–1971) in 1931, is a particular mathematical function which associates each circle of points on the four–dimensional sphere with exactly one point on the ordinary three-dimensional sphere. The set of these circles form the *Hopf* (fiber) *bundle*, also called the *Hopf fibration*[1]. If, in virtue of its geometric and algebraic properties, the map plays, beyond doubt, a fundamental role in both differential geometry and algebraic topology, it arises also as basic geometrical element in many different physical subject areas [68, 96].

As initial step, we introduce the formal Hopf map definition in Section C.1. The intimate connection between the Hopf map, unit quaternions and, consequently, spatial rotations is then analyzed in Section C.2. As ancillary tool, an overview of the stereographic projection, which allows to visualize and better understand the Hopf fibration in practice, is given in Section C.3.

C.1 THE MAPPING

The Hopf map $H : \mathbb{R}^4 \to \mathbb{R}^3$, defined by

$$H(u, v, p, q) = (u^2 + v^2 - p^2 - q^2, 2(uq + vp), 2(vq - up)), \tag{C.1.1}$$

can be regarded as associating complex number pairs

$$(\alpha, \beta) = (u + iv, q + ip) \in \mathbb{C} \times \mathbb{C}$$

with points $\mathbf{p} = (x, y, z) \in \mathbb{R}^3$ according to

$$\mathbf{p} = H(\alpha, \beta) = (|\alpha|^2 - |\beta|^2, 2\,\mathrm{Re}(\alpha\overline{\beta}), 2\,\mathrm{Im}(\alpha\overline{\beta})). \tag{C.1.2}$$

Now, the unit n–sphere S^n is the set of points in $(n+1)$–dimensional Euclidean space which are at unit distance from a central point, namely

$$S^n = \left\{(x_0, x_1, \ldots, x_n) \in \mathbb{R}^{n+1} : \textstyle\sum_{i=0}^{n} x_i^2 = 1\right\}.$$

An overview of standard n–dimensional unit spheres for $n \leqslant 3$ is showed in Table C.1. Spheres in more than three dimensions are generally called *hyperspheres*. When we restrict (C.1.2) to complex numbers satisfying $|\alpha|^2 + |\beta|^2 = 1$, it can be

1 In topology, bundles (or fiber bundles) and their generalizations to fibrations are well–known concepts related to surjective continuous maps between topological spaces that satisfy specific properties within the homotopy theory context.

DIMENSION	DEFINITION
0–sphere	$S^0 = \{x_0 \in \mathbb{R} : x_0^2 = 1\}$
1–sphere	$S^1 = \{(x_0, x_1) \in \mathbb{R}^2 : x_0^2 + x_1^2 = 1\}$
2–sphere	$S^2 = \{(x_0, x_1, x_2) \in \mathbb{R}^3 : x_0^2 + x_1^2 + x_2^2 = 1\}$
3–sphere	$S^3 = \{(x_0, x_1, x_2, x_3) \in \mathbb{R}^4 : x_0^2 + x_1^2 + x_2^2 + x_3^2 = 1\}$
⋮	⋮
n–sphere	$S^n = \{(x_0, x_1, \ldots, x_n) \in \mathbb{R}^{n+1} : x_0^2 + x_1^2 + \ldots + x_n^2 = 1\}$

Table C.1: Unit n–spheres. For $n = 0, 1, 2, 3$ we have the pair of points $(-1, 1)$ on the real line, the unit circle in the plane, the standard unit sphere in three-dimensional space and the so–called *glomes* in four-dimensional space, respectively.

interpreted as a map $S^3 \to S^2$ between the "3–sphere" $S^3 : u^2 + v^2 + p^2 + q^2 = 1$ in the space $\mathbb{R}^4$ spanned by coordinates (u, v, p, q), and the familiar "2–sphere" $S^2 : x^2 + y^2 + z^2 = 1$ in $\mathbb{R}^3$ with (x, y, z) as coordinates. Thus, for example, the *great circles* of S^3 are mapped to *points* of S^2 by (C.1.2). According to Section B.3, the group S^3 may also be regarded as the set of unit quaternions

$$S^3 = \left\{\mathcal{U} \in \mathbb{H} : |\mathcal{U}|^2 = 1\right\},$$

which forms a group under quaternion multiplication.

C.2 HOPF MAP AND 3D ROTATIONS

The Hopf map model (C.1.2) and the quaternion product $\mathcal{A}\mathbf{u}\mathcal{A}^*$, where $\mathcal{A} = \boldsymbol{\alpha} + \mathbf{k}\boldsymbol{\beta} = u + v\mathbf{i} + p\mathbf{j} + q\mathbf{k}$ and $\mathbf{u}$ is any unit vector, are just different notation to express the coordinates on the right hand–side of (3.0.2) that identify a specific point in the Euclidean three-dimensional space. As seen in Section B.3, when we restrict $\mathcal{A}$ to the set of unit quaternions $|\mathcal{A}|^2 = |\boldsymbol{\alpha}|^2 + |\boldsymbol{\beta}|^2 = 1$ we define the group $SO(3)$ of three–dimensional rotations with respect to the composition operator. In this case, the map $S^3 \to SO(3)$ can also be seen as a *group homomorphism*.

C.3 STEREOGRAPHIC PROJECTION

In complex analysis, the *stereographic projection* maps each point (x, y, z) on the unit sphere S^2 to the point $\mathbf{z}$ of the complex plane $\mathbb{C}$ according to the formulas

$$\mathrm{Re}(\mathbf{z}) = \frac{y}{1-x}, \qquad \mathrm{Im}(\mathbf{z}) = \frac{z}{1-x}. \tag{C.3.1}$$

The intersection of the ray from the north pole $(1, 0, 0)$ of S^2, chosen as point of projection, through each point $\mathbf{z} \in \mathbb{C}$ with the sphere, gives the corresponding

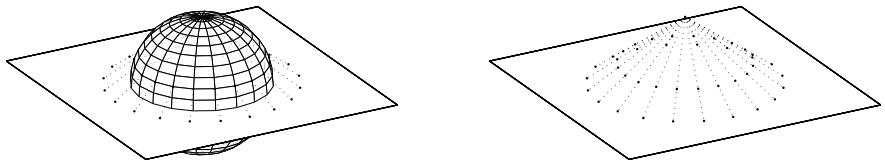

Figure C.1: Stereographic projection $S^2 \to \mathbb{C}$: all the circle on the sphere that do not pass through the north pole are projected to circles on the complex plane.

point (x, y, z) on the sphere. Circles on the sphere are mapped to either circles or lines on the complex plane, depending on whether or not the circle on the sphere passes through the point of projection, see Figure C.1 and C.2.

The inverse of the stereographic projection (C.3.1) which associates to each point $\mathbf{z}$ of the complex plane the point (x, y, z) on the unit sphere according to

$$(x, y, z) = \frac{(|\mathbf{z}|^2 - 1, 2\,\mathrm{Re}(\mathbf{z}), 2\,\mathrm{Im}(\mathbf{z}))}{|\mathbf{z}|^2 + 1}, \tag{C.3.2}$$

may be regarded in terms of the Hopf map as $H(\mathbf{z}, 1)/(|\mathbf{z}|^2 + 1)$. Lines in the complex plane mapped to circles on the sphere by (C.3.2) intersect each other at infinity.

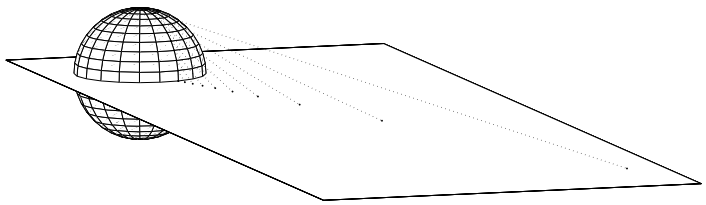

Figure C.2: Stereographic projection $S^2 \to \mathbb{C}$: all the circle on the sphere that do pass through the north pole are projected to lines on the complex plane. These lines may also be regarded as circles of infinite radius.

BIBLIOGRAPHY

[1] Y. J. Ahn, Y. s. Kim, and Y. Shin, Approximation of circular arcs and offset curves by Bézier curves of high degree, *Journal of Computational and Applied Mathematics*, **167** (2004), pp. 405–416. (Cited on page 182.)

[2] R. Ait Haddou and L. Biard, G^2 approximation of an offset curve by Tschirnhausen quartics, in *Mathematical Methods for Curves and Surfaces*, M. Daehelen, T. Lyche, and L. L. Schumaker, eds., Vanderbilt University Press, (1995), pp. 1–10. (Cited on page 186.)

[3] G. Albrecht and R. T. Farouki, Construction of C^2 Pythagorean–hodograph interpolating splines by the homotopy method, *Advances in Computational Mathematics*, **5** (1996), pp. 417–442. (Cited on page 183.)

[4] J. V. Beltran and J. Monterde, A characterization of quintic helices, *Journal of Computational and Applied Mathematics*, **206** (2007), pp. 116–121. (Cited on pages 22, 23, 68, 74, 85, 86, 90, 91, 106, 174, and 185.)

[5] R. L. Bishop, There is more than one way to frame a curve, *American Mathematical Monthly*, **82** (1975), pp. 246–251. (Cited on pages 29 and 37.)

[6] F. E. Burstall, F. Pedit, D. Ferus, K. Leschke, and U. Pinkall, Quaternions, in *Conformal geometry of surfaces in* S^4 *and quaternions*, vol. 1772 of *Lecture Notes in Mathematics*, Springer, (2002), pp. 1–4. (Cited on page 190.)

[7] C. G. L. Cao, Guiding navigation in colonoscopy, *Surgical Endoscopy*, **21** (2007), pp. 408–484. (Cited on page 46.)

[8] R. D. Carmichael, *Diophantine analysis*, Cornell University Library, Ithaca, New York, (1915). (Cited on page 184.)

[9] H. I. Choi, R. T. Farouki, S. H. Kwon, and H. P. Moon, Topological criterion for selection of quintic Pythagorean–hodograph Hermite interpolants, *Computer Aided Geometric Design*, **25** (2008), pp. 411–433. (Cited on page 183.)

[10] H. I. Choi and C. Y. Han, Euler–Rodrigues frames on spatial Pythagorean–hodograph curves, *Computer Aided Geometric Design*, **19** (2002), pp. 603–620. (Cited on pages 22, 23, 109, and 111.)

[11] H. I. Choi, C. Y. Han, H. P. Moon, K. H. Roh, and N.-S. Wee, Medial axis transform and offset curves by Minkowski Pythagorean hodograph curves, *Computer Aided Design*, **31** (1999), pp. 59–72. (Cited on page 186.)

[12] H. I. Choi and D. S. Lee, Rational parametrization of canal surface by 4 dimensional Minkowski Pythagorean hodograph curves, in *Geometric Modeling and Processing*, IEEE Computer Society, (2000), pp. 301–309. (Cited on page 186.)

[13] H. I. Choi, D. S. Lee, and H. P. Moon, Clifford algebra, spin representation, and rational parameterization of curves and surfaces, *Advances in Computational Mathematics*, **17** (2002), pp. 5–48. (Cited on pages 60, 63, 125, 184, and 186.)

[14] M. Christie, R. Machap, J.-M. Normand, P. Olivier, and J. Pickering, Virtual camera planning: a survey, in *Proceedings of Smart Graphics 2005*, vol. 3638 of *Lecture Notes in Computer Science*, Springer, (2005), pp. 40–52. (Cited on page 45.)

[15] H. G. Colt, S. W. Crawford, and O. G. III, Virtual reality bronchoscopy simulation: a revolution in procedural training, *Chest*, **120** (2001), pp. 1333–1339. (Cited on page 46.)

[16] R. Dietz, J. Hoschek, and B. Jüttler, An algebraic approach to curves and surfaces on the sphere and on other quadrics, *Computer Aided Geometric Design*, **10** (1993), pp. 211–229. (Cited on page 184.)

[17] M. P. do Carmo, *Differential Geometry of Curves and Surfaces*, Prentice–Hall, Englewood Cliffs, N.J., (1976). (Cited on pages 29, 33, 34, and 83.)

[18] G. Farin, *Curves and Surfaces for Computer Aided Geometric Design*, 4th edition, Academic Press, San Diego, (1997). (Cited on pages 30, 31, 33, and 59.)

[19] R. T. Farouki, Pythagorean–hodograph curves in practical use, in *Geometry Processing for design and Manufacturing*, R. E. Barnhill, ed., SIAM, Philadelphia, (1992), pp. 3–33. (Cited on page 183.)

[20] ——, The conformal map $z \to z^2$ of the hodograph plane, *Computer Aided Geometric Design*, **11** (1994), pp. 363–390. (Cited on pages 71 and 180.)

[21] ——, The elastic bending energy of Pythagorean–hodograph curves, *Computer Aided Geometric Design*, **13** (1996), pp. 227–241. (Cited on page 180.)

[22] ——, Exact rotation–minimizing frames for spatial Pythagorean–hodograph curves, *Graphical Models*, **64** (2002), pp. 382–395. (Cited on pages 41, 52, and 65.)

[23] ——, Pythagorean–hodograph curves, in *Handbook of Computer Aided Geometric Design*, G. Farin, J. Hoschek, and M.-S. Kim, eds., Elsevier, (2002), pp. 405–427. (Cited on page 59.)

[24] ——, *Pythagorean–Hodograph Curves: Algebra and Geometry Inseparable*, Springer, Berlin, (2008). (Cited on pages 21, 59, 65, 67, and 188.)

[25] ——, Quaternion and Hopf map characterizations for the existence of rational rotation-minimizing frames on quintic space curves, *Advances in Computational Mathematics*, to appear (2009). (Cited on pages 23, 109, 122, and 175.)

[26] R. T. Farouki, M. al Kandari, and T. Sakkalis, Hermite interpolation by rotation–invariant spatial Pythagorean–hodograph curves, *Advances in Computational Mathematics*, **17** (2002), pp. 369–383. (Cited on pages 24, 119, 126, 127, 140, 150, 185, and 190.)

[27] ——, Structural invariance of spatial Pythagorean hodographs, *Computer Aided Geometric Design*, **19** (2002), pp. 395–407. (Cited on pages 60, 62, and 184.)

[28] R. T. Farouki and C. Giannelli, Spatial camera orientation control by rotation–minimizing directed frames, *Computer Animation and Virtual Worlds*, **20** (2009), pp. 457–472. (Cited on pages 19 and 23.)

[29] R. T. Farouki, C. Giannelli, C. Manni, and A. Sestini, Identification of spatial PH quintic Hermite interpolants with near–optimal shape measures, *Computer Aided Geometric Design*, **25** (2008), pp. 274–297. (Cited on pages 24 and 185.)

[30] ——, Quintic space curves with rational rotation–minimizing frames, *Computer Aided Geometric Design*, **26** (2009), pp. 580–592. (Cited on pages 22, 23, 111, and 122.)

[31] ——, Design of rational rotation–minimizing rigid body motions by Hermite interpolation, preprint, (2010). (Cited on page 176.)

[32] R. T. Farouki, C. Giannelli, and A. Sestini, Helical polynomial curves and double Pythagorean hodographs II. Enumeration of low–degree curves, *Journal of Symbolic Computation*, **44** (2009), pp. 307–332. (Cited on page 22.)

[33] ——, Helical polynomial curves and double Pythagorean hodographs I. Quaternion and Hopf map representations, *Journal of Symbolic Computation*, **44** (2009), pp. 161–179. (Cited on pages 22 and 160.)

[34] ——, Geometric design using space curves with rational rotation–minimizing frames, in *Mathematical Methods for Curves and Surfaces*, M. Daehlen et al., ed., vol. 5862 of *Lecture Notes in Computer Science*, Springer, 2010, pp. 194–208. (Cited on page 25.)

[35] R. T. Farouki and T. N. T. Goodman, On the optimal stability of the Bernstein basis, *Mathematics of Computation*, **65** (1996), pp. 1553–1566. (Cited on pages 31 and 180.)

[36] R. T. Farouki and C. Y. Han, Rational approximation schemes for rotation–minimizing frames on Pythagorean–hodograph curves, *Computer Aided Geometric Design*, **20** (2003), pp. 435–454. (Cited on pages 20, 43, 50, and 150.)

[37] R. T. Farouki, C. Y. Han, C. Manni, and A. Sestini, Characterization and construction of helical polynomial space curves, *Journal of Computational and Applied Mathematics*, **162** (2004), pp. 365–392. (Cited on pages 23, 62, 65, 68, 84, 85, 86, 90, 91, 96, 136, 138, 139, 144, 174, and 185.)

[38] R. T. Farouki, B. K. Kuspa, C. Manni, and A. Sestini, Efficient solution of the complex quadratic tridiagonal system for C^2 PH quintic splines, *Numerical Algorithms*, **27** (2001), pp. 35–60. (Cited on page 183.)

[39] R. T. Farouki, C. Manni, and A. Sestini, Shape-preserving interpolation by G^1 and G^2 PH quintic splines, *IMA Journal of Numerical Analysis*, **23** (2003), pp. 175–195. (Cited on page 183.)

[40] R. T. Farouki and C. A. Neff, Hermite interpolation by Pythagorean hodograph quintics, *Mathematics of Computation*, **64** (1995), pp. 1589–1609. (Cited on page 183.)

[41] R. T. Farouki and V. T. Rajan, Algorithms for polynomials in Bernstein form, *Computer Aided Geometric Design*, **5** (1988), pp. 1–26. (Cited on pages 32 and 180.)

[42] R. T. Farouki and T. Sakkalis, Pythagorean hodographs, *IBM Journal of Research and Development*, **34** (1990), pp. 736–752. (Cited on pages 22, 73, 179, 180, and 182.)

[43] ——, Pythagorean–hodograph space curves, *Advances in Computational Mathematics*, **2** (1994), pp. 41–66. (Cited on pages 74, 85, 136, 174, 184, and 185.)

[44] ——, Rational rotation–minimizing frames on polynomial space curves of arbitrary degree, *Journal of Symbolic Computation*, to appear (2010). (Cited on pages 66, 71, 111, and 112.)

[45] R. T. Farouki and S. Shah, Real–time CNC interpolators for Pythagorean–hodograph curves, *Computer Aided Geometric Design*, **13** (1996), pp. 583–600. (Cited on page 182.)

[46] H. Guggenheimer, Computing frames along a trajectory, *Computer Aided Geometric Design*, **6** (1989), pp. 77–78. (Cited on pages 20, 29, and 41.)

[47] C. Y. Han, Nonexistence of rational rotation–minimizing frames on cubic curves, *Computer Aided Geometric Design*, **25** (2008), pp. 298–304. (Cited on pages 22, 23, 110, 112, and 122.)

[48] A. Hanson, Visualizing quaternions: course notes for Siggraph 2007, in *SIGGRAPH '07: ACM SIGGRAPH 2007 courses*, New York, (2007), ACM. (Cited on page 187.)

[49] J. G. Holden, J. M. Flach, and Y. Donchin, Perceptual–motor coordination in an endoscopic surgery simulation, *Surgical Endoscopy*, **13** (1999), pp. 127–132. (Cited on page 46.)

[50] J. Hoschek, Spline approximation of offset curves, *Computer Aided Geometric Design*, **5** (1988), pp. 33–40. (Cited on page 182.)

[51] J. Hoschek and D. Lasser, *Fundamentals of Computer Aided Geometric Design*, A. K. Peters, Ltd., Natick, MA, USA, (1993). Translator–L. L. Schumaker. (Cited on pages 30, 31, 33, 42, and 59.)

[52] B. Jüttler, Generating rational frames of space curves via Hermite interpolation with Pythagorean hodograph cubic splines, in *Geometric Modeling and Processing '98*, Bookplus Press, (1998), pp. 83–106. (Cited on pages 20, 41, and 109.)

[53] ——, Triangular Bézier surface patches with a linear normal vector field, in *The mathematics of surfaces VIII*, R. Cripps, ed., Information Geometers, Winchester, (1998), pp. 431–446. (Cited on page 186.)

[54] ——, Hermite interpolation by Pythagorean hodograph curves of degree seven, *Mathematics of Computation*, **70** (2001), pp. 1089–1111. (Cited on page 183.)

[55] B. Jüttler and C. Mäurer, Cubic Pythagorean hodograph spline curves and applications to sweep surface modeling, *Computer Aided Design*, **31** (1999), pp. 73–83. (Cited on pages 20, 41, 43, and 183.)

[56] ——, Rational approximation of rotation minimizing frames using Pythagorean–hodograph cubics, *Journal for Geometry and Graphics*, **3** (1999), pp. 141–159. (Cited on pages 20, 41, and 43.)

[57] B. Jüttler and M. L. Sampoli, Hermite interpolation by piecewise polynomial surfaces with rational offsets, *Computer Aided Geometric Design*, **17** (2000), pp. 361–385. (Cited on page 186.)

[58] B. Jüttler and M. G. Wagner, Rational motion–based surface generation, *Computer Aided Design*, **31** (1999), pp. 203–213. (Cited on page 43.)

[59] M.-S. Kim, E.-J. Park, and H.-Y. Lee, Modeling and animation of generalized cylinders with variable radius offset space curves, *The Journal of Visualization and Computer Animation*, **5** (1994), pp. 189–207. (Cited on page 42.)

[60] M.-S. Kim, E.-J. Park, and S.-B. Lims, Approximation of variable-radius offset curves and its application to Bézier brush-stroke design, *Computer Aided Design*, **25** (1993), pp. 684–698. (Cited on page 182.)

[61] R. Klass, An offset spline approximation for plane cubic splines, *Computer Aided Design*, **15** (1983), pp. 297–299. (Cited on page 182.)

[62] F. Klok, Two moving coordinate frames for sweeping along a 3D trajectory, *Computer Aided Geometric Design*, **3** (1986), pp. 217–229. (Cited on pages 20, 29, 37, 41, and 43.)

[63] J. Kosinka and B. Jüttler, G^1 Hermite interpolation by Minkowski Pythagorean hodograph cubics, *Computer Aided Geometric Design*, **23** (2006), pp. 401–418. (Cited on page 186.)

[64] ——, C^1 Hermite interpolation by Pythagorean hodograph quintics in Minkowski space, *Advances in Computational Mathematics*, **30** (2009), pp. 123–140. (Cited on page 186.)

[65] E. Kreyszig, *Differential Geometry*, University of Toronto Press, (1959). (Cited on pages 29, 33, 34, 35, 83, and 150.)

[66] K. K. Kubota, Pythagorean triples in unique factorization domains, *American Mathematical Monthly*, **79** (1972), pp. 503–505. (Cited on pages 68, 70, 110, and 179.)

[67] J. D. Lawrence, *A Catalog of Special Plane Curves*, Dover, New York, (1972). (Cited on page 182.)

[68] D. W. Lyons, An Elementary Introduction to the Hopf Fibration, *Mathematics Magazine*, **76** (2003), pp. 87–98. (Cited on page 195.)

[69] D. Mattsson-Boze and D. Chatenever, Image orientation for endoscopic video displays, *United States Patent 6097423*, (2000). (Cited on page 45.)

[70] J. Monterde, A characterization of helical polynomial curves of any degree, *Advances in Computational Mathematics*, **30** (2009), pp. 61–78. (Cited on pages 23, 74, 83, 85, 86, 87, 96, and 174.)

[71] ——, Salkowski curves revisited: a family of curves with constant curvature and non–constant torsion, *Computer Aided Geometric Design*, **26** (2009), pp. 271–278. (Cited on page 185.)

[72] H. P. Moon, Computing rational offsets via medial axis transform using polynomial speed curves in $\mathbb{R}^{2,1}$, in *Geometric Modeling and Processing '98*, Bookplus Press, (1998), pp. 187–203. (Cited on page 186.)

[73] ——, Minkowski Pythagorean hodographs, *Computer Aided Geometric Design*, **16** (1999), pp. 739–753. (Cited on page 186.)

[74] H. P. Moon, R. T. Farouki, and H. I. Choi, Construction and shape analysis of PH quintic Hermite interpolants, *Computer Aided Geometric Design*, **18** (2001), pp. 93–115. (Cited on page 183.)

[75] T. Needham, *Visual Complex Analysis*, Oxford University Press, (1997). (Cited on page 87.)

[76] D. Nieuwenhuisen and M. H. Overmars, Motion planning for camera movements, in *Proceedings of the 2004 IEEE International Conference on Robotics and Automation*, New Orleans, LA, (2004), pp. 3870–3876. (Cited on page 45.)

[77] F. Pelosi, R. T. Farouki, C. Manni, and A. Sestini, Geometric Hermite interpolation by spatial Pythagorean-hodograph cubics, *Advances in Computational Mathematics*, **22** (2005), pp. 325–352. (Cited on page 184.)

[78] F. Pelosi, M. L. Sampoli, R. T. Farouki, and C. Manni, A control polygon scheme for design of planar C^2 PH quintic spline curves, *Computer Aided Geometric Design*, **24** (2007), pp. 28–52. (Cited on page 183.)

[79] C. Perwass, R. T. Farouki, and L. Noakes, A geometric product formulation for spatial Pythagorean hodograph curves with applications to Hermite interpolation, *Computer Aided Geometric Design*, **24** (2007), pp. 220–237. (Cited on page 185.)

[80] M. Peternell, Rational two-parameter families of spheres and rational offset surfaces, *Journal of Symbolic Computation*, **45** (2010), pp. 1–18. (Cited on page 186.)

[81] M. Peternell, B. Odehnal, and M. L. Sampoli, On quadratic two-parameter families of spheres and their envelopes, *Computer Aided Geometric Design*, **25** (2008), pp. 342–355. (Cited on page 186.)

[82] B. Pham, Offset approximation of uniform B-splines, *Computer Aided Design*, **20** (1988), pp. 471–474. (Cited on page 182.)

[83] L. A. Piegl and W. Tiller, Computing offsets of NURBS curves and surfaces, *Computer Aided Design*, **31** (1999), pp. 147–156. (Cited on page 182.)

[84] H. Pottmann, Curve design with rational Pythagorean–hodograph curves, *Advances in Computational Mathematics*, **3** (1995), pp. 147–170. (Cited on page 186.)

[85] ——, Rational curves and surfaces with rational offsets, *Computer Aided Geometric Design*, **12** (1995), pp. 175–192. (Cited on page 186.)

[86] A. G. Requicha, Representations for rigid solids: theory, methods, and systems, *ACM Computing surveys*, **12** (1980), pp. 437–464. (Cited on page 42.)

[87] J. Roe, *Elementary Geometry*, Oxford University Press, (1993). (Cited on pages 189 and 194.)

[88] M. L. Sampoli, M. Peternell, and B. Jüttler, Rational surfaces with linear normals and their convolutions with rational surfaces, *Computer Aided Geometric Design*, **23** (2006), pp. 179–192. (Cited on page 186.)

[89] J. N. Schara, H. D. Hoeg, and E. L. Hale, Gravity referenced endoscopic image orientation, *United States Patent 7134992*, (2006). (Cited on page 45.)

[90] H. Schwerdtfeger, *Geometry of Complex Numbers*, Dover Publications (reprint), New York, (1979). (Cited on page 87.)

[91] J.-L. Shih and S.-H. Frank Chuang, One–sided offset approximation of freeform curves for interference–free NURBS machining, *Computer Aided Design*, **40** (2008), pp. 931–937. (Cited on page 182.)

[92] K. Shoemake, Animating rotation with quaternion curves, in *SIGGRAPH '85: Proceedings of the 12th annual conference on Computer graphics and interactive techniques*, New York, NY, USA, (1985), ACM, pp. 245–254. (Cited on page 187.)

[93] S. B. Solomon, P. White, Jr., C. M. Wiener, J. B. Orens, and K. P. Wang, Three–dimensional CT–guided bronchoscopy with a real–time electromagnetic position sensor: a comparison of two image registration methods, *Chest*, **118** (2000), pp. 1783–1787. (Cited on page 46.)

[94] D. J. Struik, *Lectures on Classical Differential Geometry*, Dover Publications (reprint), New York, (1961). (Cited on pages 83 and 84.)

[95] Y.-F. Tsai, R. T. Farouki, and B. Feldman, Performance analysis of CNC interpolators for time–dependent feedrates along PH curves, *Computer Aided Geometric Design*, **18** (2001), pp. 245–265. (Cited on page 182.)

[96] H. K. Urbantke, The Hopf fibration–seven times in physics, *Journal of Geometry and Physics*, **46** (2003), pp. 125–150. (Cited on page 195.)

[97] L. Vaserstein, T. Sakkalis, and S. Frisch, Polynomial parametrization of Pythagorean tuples, *International Journal of Number Theory*, to appear (2010). (Cited on page 184.)

[98] Z. Šír, R. Feichtinger, and B. Jüttler, Approximating curves and their offsets using biarcs and Pythagorean hodograph quintics, *Computer Aided Design*, **38** (2006), pp. 608–618. (Cited on page 182.)

[99] Z. Šír and B. Jüttler, Spatial Pythagorean hodograph quintics and the approximation of pipe surfaces, in *The Mathematics of Surfaces XI*, R. Martin, H. Bez, and M. Sabin, eds., Berlin, (2005), Springer, pp. 364–380. (Cited on pages 24, 152, and 185.)

[100] ——, C^2 Hermite interpolation by Pythagorean hodograph space curves, *Mathematics of Computation*, **76** (2007), pp. 1373–1391. (Cited on pages 127 and 185.)

[101] Z. Šír, E. Wings, and B. Jüttler, Rounding spatial G-code tool paths using Pythagorean hodograph curves, *Trans. of the ASME, Journal of Computing and Information Science in Engineering* , **7** (2007), pp. 186–191. (Cited on page 182.)

[102] M. G. Wagner and B. Ravani, Curves with rational Frenet–Serret motion, *Computer Aided Geometric Design*, **15** (1997), pp. 79–101. (Cited on page 68.)

[103] W. Wang and B. Joe, Robust computation of the rotation minimizing frame for sweep surface modelling, *Computer Aided Design*, **29** (1997), pp. 379–391. (Cited on pages 41 and 43.)

[104] W. Wang, B. Jüttler, D. Zheng, and Y. Liu, Computation of rotation minimizing frames, *ACM Transactions on Graphics*, **27**, No. 1, Article 2 (2008), pp. 1–18. (Cited on pages 20 and 43.)